

**From:** Rick Ennis  
**To:** Cheng-Ih Wu; Christopher Boyd; George Thomas; Harold Walker; Thomas Scarbrough  
**Date:** 8/2/05 4:33PM  
**Subject:** VY EPU Supplement 30, Attachment 11

As followup to the email I sent earlier today transmitting portions of Vermont Yankee EPU Supplement 30, the licensee sent me Attachment 11 to Supplement 30 which contains 10 exhibits (files are attached). The exhibits relate to the following RAIs:

SRXB-A-18 (1 exhibit)  
SPSB-C-52 (6 exhibits)  
EMEB-138 (3 exhibits)

Please let me know if you have any questions. Thanks,

Rick  
415-1420

**Mail Envelope Properties (42EFD87D.BEF : 11 : 372)**

**Subject:** VY EPU Supplement 30, Attachment 11  
**Creation Date:** 8/2/05 4:33PM  
**From:** Rick Ennis

**Created By:** RXE@nrc.gov

<b>Recipients</b>	<b>Action</b>	<b>Date &amp; Time</b>
TWGWPO02.HQGWDO01 HXW (Harold Walker)	Delivered	08/02/05 4:33 PM
owf2_po.OWFN_DO CIW1 (Cheng-Ih Wu) GXT (George Thomas) TGS (Thomas Scarbrough)	Delivered	08/02/05 4:33 PM
twf5_po.TWFN_DO CXB5 (Christopher Boyd)	Delivered	08/02/05 4:33 PM

<b>Post Office</b>	<b>Delivered</b>	<b>Route</b>
TWGWPO02.HQGWDO01	08/02/05 4:33 PM	
owf2_po.OWFN_DO	08/02/05 4:33 PM	
twf5_po.TWFN_DO	08/02/05 4:33 PM	

<b>Files</b>	<b>Size</b>	<b>Date &amp; Time</b>
MESSAGE	1065	08/02/05 04:33PM
BVY 05-072 Ex.SRXB-A-18-1.pdf	600742	08/02/05 03:21PM
BVY 05-072 Ex. SPSB-C-52-1.pdf	591203	08/02/05 03:17PM
BVY 05-072 Ex. SPSB-C-52-2.pdf	1159854	08/02/05 03:17PM
BVY 05-072 Ex. SPSB-C-52-3.pdf	5083648	08/02/05 03:18PM
BVY 05-072 Ex. SPSB-C-52-4.pdf	3401670	08/02/05 03:20PM
BVY 05-072 Ex. SPSB-C-52-5.pdf	725499	08/02/05 03:20PM
BVY 05-072 Ex. SPSB-C-52-6.pdf	282378	08/02/05 03:19PM
BVY 05-072 Ex.EMEB-B-138-1.pdf	832848	08/02/05 03:21PM
BVY 05-072 Ex.EMEB-B-138-2.pdf	972271	08/02/05 03:21PM
BVY 05-072 Ex.EMEB-B-138-3.pdf	1256329	08/02/05 03:21PM

**Options**

**Auto Delete:** No  
**Expiration Date:** None  
**Notify Recipients:** Yes  
**Priority:** Standard  
**Reply Requested:** No  
**Return Notification:** None

**Concealed Subject:**  
**Security:**

No  
Standard

**To Be Delivered:**  
**Status Tracking:**

Immediate  
Delivered & Opened

**Exhibit SRXB-A-18-1**

**Vermont Yankee Nuclear Power Station**

**Proposed Technical Specification Change No. 263 – Supplement No. 30**

**Extended Power Uprate**

**Response to Request for Additional Information**

**"RS-001, BWR Template SE"**

Total number of pages in this Exhibit  
(excluding this cover sheet) is 8.

(2) draft GDC-9, insofar as it requires that the reactor coolant pressure boundary shall be designed and constructed so as to have an exceedingly low probability of gross rupture or significant leakage throughout its design lifetime;

## **2.8.5 Accident and Transient Analyses**

### **2.8.5.1 Decrease in Feedwater Temperature, Increase in Feedwater Flow, Increase in Steam Flow, and Inadvertent Opening of a Main Steam Relief or Safety Valve**

#### **Regulatory Evaluation**

Excessive heat removal causes a decrease in moderator temperature which increases core reactivity and can lead to a power level increase and a decrease in shutdown margin. Any unplanned power level increase may result in fuel damage or excessive reactor system pressure. Reactor protection and safety systems are actuated to mitigate the transient. The NRC staff's review covered (1) postulated initial core and reactor conditions, (2) methods of thermal and hydraulic analyses, (3) the sequence of events, (4) assumed reactions of reactor system components, (5) functional and operational characteristics of the reactor protection system, (6) operator actions, and (7) the results of the transient analyses. The NRC's acceptance criteria are based on (1) draft GDC-6, insofar as it requires that the reactor core be designed to function throughout its design lifetime without exceeding acceptable fuel damage limits; (2) draft GDC-14 and 15, insofar as they require that the core protection system be designed to act automatically to prevent or suppress conditions that could result in exceeding acceptable fuel damage limits and that protection systems be provided for sensing accident situations and initiating the operation of necessary ESFs; and (3) draft GDC-27 and 28, insofar as they require that at least two reactivity control systems be provided and be capable of making and holding the core subcritical from any hot standby or hot operating condition sufficiently fast to prevent exceeding acceptable fuel damage limits. Specific review criteria are contained in SRP Section 15.1.1-4 and other guidance provided in Matrix 8 of RS-001.

#### **Technical Evaluation**

[Insert technical evaluation. The technical evaluation should (1) clearly explain why the proposed changes satisfy each of the requirements in the regulatory evaluation and (2) provide a clear link to the conclusions reached by the NRC staff, as documented in the conclusion section.]

#### **Conclusion**

The NRC staff has reviewed the licensee's analyses of the excess heat removal events described above and concludes that the licensee's analyses have adequately accounted for operation of the plant at the proposed power level and were performed using acceptable analytical models. The NRC staff further concludes that the licensee has demonstrated that the reactor protection and safety systems will continue to ensure that the SAFDLs and the RCPB pressure limits will not be exceeded as a result of these events. Based on this, the NRC staff concludes that the plant will continue to meet the requirements of draft GDC-6, 14, 15, 27, and 28 following implementation of the proposed EPU. Therefore, the NRC staff finds the proposed EPU acceptable with respect to the events stated. 9

(2) draft GDC-9, insofar as it requires that the reactor coolant pressure boundary shall be designed and constructed so as to have an exceedingly low probability of gross rupture or significant leakage throughout its design lifetime;

## 2.8.5.2 Decrease in Heat Removal by the Secondary System

### 2.8.5.2.1 Loss of External Load; Turbine Trip; Loss of Condenser Vacuum; Closure of Main Steam Isolation Valve; and Steam Pressure Regulator Failure (Closed)

#### Regulatory Evaluation

A number of initiating events may result in unplanned decreases in heat removal by the secondary system. These events result in a sudden reduction in steam flow and, consequently, result in pressurization events. Reactor protection and safety systems are actuated to mitigate the transient. The NRC staff's review covered the sequence of events, the analytical models used for analyses, the values of parameters used in the analytical models, and the results of the transient analyses. The NRC's acceptance criteria are based on (1) draft GDC-6, insofar as it requires that the reactor core be designed to function throughout its design lifetime without exceeding acceptable fuel damage limits; and (2) draft GDC-27 and 28, insofar as they require that at least two reactivity control systems be provided and be capable of making and holding the core subcritical from any hot standby or hot operating condition sufficiently fast to prevent exceeding acceptable fuel damage limits. Specific review criteria are contained in SRP Section 15.2.1-5 and other guidance provided in Matrix 8 of RS-001.

#### Technical Evaluation

[Insert technical evaluation. The technical evaluation should (1) clearly explain why the proposed changes satisfy each of the requirements in the regulatory evaluation and (2) provide a clear link to the conclusions reached by the NRC staff, as documented in the conclusion section.]

#### Conclusion

The NRC staff has reviewed the licensee's analyses of the decrease in heat removal events described above and concludes that the licensee's analyses have adequately accounted for operation of the plant at the proposed power level and were performed using acceptable analytical models. The NRC staff further concludes that the licensee has demonstrated that the reactor protection and safety systems will continue to ensure that the SAFDLs and the RCPB pressure limits will not be exceeded as a result of these events. Based on this, the NRC staff concludes that the plant will continue to meet the requirements of draft GDC-6, 27, and 28 following implementation of the proposed EPU. Therefore, the NRC staff finds the proposed EPU acceptable with respect to the events stated.

9,

(2) draft GDC-9, insofar as it requires that the reactor coolant pressure boundary shall be designed and constructed so as to have an exceedingly low probability of gross rupture or significant leakage throughout its design lifetime;

### 2.8.5.2.2 Loss of Nonemergency AC Power to the Station Auxiliaries

#### Regulatory Evaluation

The loss of nonemergency ac power is assumed to result in the loss of all power to the station auxiliaries and the simultaneous tripping of all reactor coolant circulation pumps. This causes a flow coastdown as well as a decrease in heat removal by the secondary system, a turbine trip, an increase in pressure and temperature of the coolant, and a reactor trip. Reactor protection and safety systems are actuated to mitigate the transient. The NRC staff's review covered (1) the sequence of events, (2) the analytical model used for analyses, (3) the values of parameters used in the analytical model, and (4) the results of the transient analyses. The NRC's acceptance criteria are based on (1) draft GDC-6, insofar as it requires that the reactor core be designed to function throughout its design lifetime without exceeding acceptable fuel damage limits, and (2) draft GDC-27 and 28, insofar as they require that at least two reactivity control systems be provided and be capable of making and holding the core subcritical from any hot standby or hot operating condition sufficiently fast to prevent exceeding acceptable fuel damage limits. Specific review criteria are contained in SRP Section 15.2.6 and other guidance provided in Matrix 8 of RS-001.

#### Technical Evaluation

[Insert technical evaluation. The technical evaluation should (1) clearly explain why the proposed changes satisfy each of the requirements in the regulatory evaluation and (2) provide a clear link to the conclusions reached by the NRC staff, as documented in the conclusion section.]

#### Conclusion

The NRC staff has reviewed the licensee's analyses of the loss of nonemergency ac power to station auxiliaries event and concludes that the licensee's analyses have adequately accounted for operation of the plant at the proposed power level and were performed using acceptable analytical models. The NRC staff further concludes that the licensee has demonstrated that the reactor protection and safety systems will continue to ensure that the SAFDLs and the RCPB pressure limits will not be exceeded as a result of this event. Based on this, the NRC staff concludes that the plant will continue to meet the requirements of draft GDC-6, 27, and 28 following implementation of the proposed EPU. Therefore, the NRC staff finds the proposed EPU acceptable with respect to the loss of nonemergency ac power to station auxiliaries event.

9,

(2) draft GDC-9, insofar as it requires that the reactor coolant pressure boundary shall be designed and constructed so as to have an exceedingly low probability of gross rupture or significant leakage throughout its design lifetime;

### 2.8.5.2.3 Loss of Normal Feedwater Flow

#### Regulatory Evaluation

A loss of normal feedwater flow could occur from pump failures, valve malfunctions, or a LOOP. Loss of feedwater flow results in an increase in reactor coolant temperature and pressure which eventually requires a reactor trip to prevent fuel damage. Decay heat must be transferred from fuel following a loss of normal feedwater flow. Reactor protection and safety systems are actuated to provide this function and mitigate other aspects of the transient. The NRC staff's review covered (1) the sequence of events, (2) the analytical model used for analyses, (3) the values of parameters used in the analytical model, and (4) the results of the transient analyses. The NRC's acceptance criteria are based on (1) draft GDC-6, insofar as it requires that the reactor core be designed to function throughout its design lifetime without exceeding acceptable fuel damage limits, and (2) draft GDC-27 and 28, insofar as they require that at least two reactivity control systems be provided and be capable of making and holding the core subcritical from any hot standby or hot operating condition sufficiently fast to prevent exceeding acceptable fuel damage limits. Specific review criteria are contained in SRP Section 15.2.7 and other guidance provided in Matrix 8 of RS-001.

#### Technical Evaluation

[Insert technical evaluation. The technical evaluation should (1) clearly explain why the proposed changes satisfy each of the requirements in the regulatory evaluation and (2) provide a clear link to the conclusions reached by the NRC staff, as documented in the conclusion section.]

#### Conclusion

The NRC staff has reviewed the licensee's analyses of the loss of normal feedwater flow event and concludes that the licensee's analyses have adequately accounted for operation of the plant at the proposed power level and were performed using acceptable analytical models. The NRC staff further concludes that the licensee has demonstrated that the reactor protection and safety systems will continue to ensure that the SAFDLs and the RCPB pressure limits will not be exceeded as a result of the loss of normal feedwater flow. Based on this, the NRC staff concludes that the plant will continue to meet the requirements of draft GDC-6, 27, and 28 following implementation of the proposed EPU. Therefore, the NRC staff finds the proposed EPU acceptable with respect to the loss of normal feedwater flow event.

9



(2) draft GDC-9, insofar as it requires that the reactor coolant pressure boundary shall be designed and constructed so as to have an exceedingly low probability of gross rupture or significant leakage throughout its design lifetime;

### 2.8.5.3 Decrease in Reactor Coolant System Flow

#### 2.8.5.3.1 Loss of Forced Reactor Coolant Flow

##### Regulatory Evaluation

A decrease in reactor coolant flow occurring while the plant is at power could result in a degradation of core heat transfer. An increase in fuel temperature and accompanying fuel damage could then result if SAFDLs are exceeded during the transient. Reactor protection and safety systems are actuated to mitigate the transient. The NRC staff's review covered (1) the postulated initial core and reactor conditions, (2) the methods of thermal and hydraulic analyses, (3) the sequence of events, (4) assumed reactions of reactor systems components, (5) the functional and operational characteristics of the reactor protection system, (6) operator actions, and (7) the results of the transient analyses. The NRC's acceptance criteria are based on (1) draft GDC-6, insofar as it requires that the reactor core be designed to function throughout its design lifetime without exceeding acceptable fuel damage limits, and (2) draft GDC-27 and 28, insofar as they require that at least two reactivity control systems be provided and be capable of making and holding the core subcritical from any hot standby or hot operating condition sufficiently fast to prevent exceeding acceptable fuel damage limits. Specific review criteria are contained in SRP Section 15.3.1-2 and other guidance provided in Matrix 8 of RS-001.

##### Technical Evaluation

[Insert technical evaluation. The technical evaluation should (1) clearly explain why the proposed changes satisfy each of the requirements in the regulatory evaluation and (2) provide a clear link to the conclusions reached by the NRC staff, as documented in the conclusion section.]

##### Conclusion

The NRC staff has reviewed the licensee's analyses of the decrease in reactor coolant flow event and concludes that the licensee's analyses have adequately accounted for operation of the plant at the proposed power level and were performed using acceptable analytical models. The NRC staff further concludes that the licensee has demonstrated that the reactor protection and safety systems will continue to ensure that the SAFDLs and the RCPB pressure limits will not be exceeded as a result of this event. Based on this, the NRC staff concludes that the plant will continue to meet the requirements of draft GDC-6, 27, and 28 following implementation of the proposed EPU. Therefore, the NRC staff finds the proposed EPU acceptable with respect to the decrease in reactor coolant flow event. 9

(2) draft GDC-9, insofar as it requires that the reactor coolant pressure boundary shall be designed and constructed so as to have an exceedingly low probability of gross rupture or significant leakage throughout its design lifetime;

### 2.8.5.5 Inadvertent Operation of ECCS or Malfunction that Increases Reactor Coolant Inventory

#### Regulatory Evaluation

Equipment malfunctions, operator errors, and abnormal occurrences could cause unplanned increases in reactor coolant inventory. Depending on the temperature of the injected water and the response of the automatic control systems, a power level increase may result and, without adequate controls, could lead to fuel damage or overpressurization of the RCS. Alternatively, a power level decrease and depressurization may result. Reactor protection and safety systems are actuated to mitigate these events. The NRC staff's review covered (1) the sequence of events, (2) the analytical model used for analyses, (3) the values of parameters used in the analytical model, and (4) the results of the transient analyses. The NRC's acceptance criteria are based on (1) draft GDC-6, insofar as it requires that the reactor core be designed to function throughout its design lifetime without exceeding acceptable fuel damage limits, and (2) draft GDC-27 and 28, insofar as they require that at least two reactivity control systems be provided and be capable of making and holding the core subcritical from any hot standby or hot operating condition sufficiently fast to prevent exceeding acceptable fuel damage limits. Specific review criteria are contained in SRP Section 15.5.1-2 and other guidance provided in Matrix 8 of RS-001.

#### Technical Evaluation

[Insert technical evaluation. The technical evaluation should (1) clearly explain why the proposed changes satisfy each of the requirements in the regulatory evaluation and (2) provide a clear link to the conclusions reached by the NRC staff, as documented in the conclusion section.]

#### Conclusion

The NRC staff has reviewed the licensee's analyses of the inadvertent operation of ECCS or malfunction that increases reactor coolant inventory and concludes that the licensee's analyses have adequately accounted for operation of the plant at the proposed power level and were performed using acceptable analytical models. The NRC staff further concludes that the licensee has demonstrated that the reactor protection and safety systems will continue to ensure that the SAFDLs and the RCPB pressure limits will not be exceeded as a result of this event. Based on this, the NRC staff concludes that the plant will continue to meet the requirements of draft GDC-6, 27, and 28 following implementation of the proposed EPU. Therefore, the NRC staff finds the proposed EPU acceptable with respect to the inadvertent operation of ECCS or malfunction that increases reactor coolant inventory.

(2) draft GDC-9, insofar as it requires that the reactor coolant pressure boundary shall be designed and constructed so as to have an exceedingly low probability of gross rupture or significant leakage throughout its design lifetime;

#### 2.8.5.4.3 Startup of a Recirculation Loop at an Incorrect Temperature and Flow Controller Malfunction Causing an Increase in Core Flow Rate

##### Regulatory Evaluation

A startup of an inactive loop transient may result in either an increased core flow or the introduction of cooler water into the core. This event causes an increase in core reactivity due to decreased moderator temperature and core void fraction. The NRC staff's review covered (1) the sequence of events, (2) the analytical model, (3) the values of parameters used in the analytical model, and (4) the results of the transient analyses. The NRC's acceptance criteria are based on (1) draft GDC-6, insofar as it requires that the reactor core be designed to function throughout its design lifetime without exceeding acceptable fuel damage limits; (2) draft GDC-14 and 15, insofar as they require that the core protection systems be designed to act automatically to prevent or suppress conditions that could result in exceeding acceptable fuel damage limits and that protection systems be provided for sensing accident situations and initiating the operation of necessary ESFs; (3) draft GDC-32, insofar as it requires that limits, which include considerable margin, be placed on the maximum reactivity worth of control rods or elements and on rates at which reactivity can be increased to ensure that the potential effects of a sudden or large change of reactivity cannot (a) rupture the reactor coolant pressure boundary or (b) disrupt the core, its support structures, or other vessel internals sufficiently to impair the effectiveness of emergency core cooling; and (4) draft GDC-27 and 28, insofar as they require that at least two reactivity control systems be provided and be capable of making and holding the core subcritical from any hot standby or hot operating condition sufficiently fast to prevent exceeding acceptable fuel damage limits. Specific review criteria are contained in SRP Section 15.4.4-5 and other guidance provided in Matrix 8 of RS-001.

##### Technical Evaluation

[Insert technical evaluation. The technical evaluation should (1) clearly explain why the proposed changes satisfy each of the requirements in the regulatory evaluation and (2) provide a clear link to the conclusions reached by the NRC staff, as documented in the conclusion section.]

##### Conclusion

The NRC staff has reviewed the licensee's analyses of the increase in core flow event and concludes that the licensee's analyses have adequately accounted for operation of the plant at the proposed power level and were performed using acceptable analytical models. The NRC staff further concludes that the licensee has demonstrated that the reactor protection and safety systems will continue to ensure that the SAFDLs and the RCPB pressure limits will not be exceeded as a result of this event. Based on this, the NRC staff concludes that the plant will continue to meet the requirements of draft GDC-6, 14, 15, 27, 28, and 32 following implementation of the proposed EPU. Therefore, the NRC staff finds the proposed EPU acceptable with respect to the increase in core flow event. (9)

(2) draft GDC-9, insofar as it requires that the reactor coolant pressure boundary shall be designed and constructed so as to have an exceedingly low probability of gross rupture or significant leakage throughout its design lifetime;

## 2.8.5.6 Decrease in Reactor Coolant Inventory

### 2.8.5.6.1 Inadvertent Opening of a Pressure Relief Valve

#### Regulatory Evaluation

The inadvertent opening of a pressure relief valve results in a reactor coolant inventory decrease and a decrease in RCS pressure. The pressure relief valve discharges into the suppression pool. Normally there is no reactor trip. The pressure regulator senses the RCS pressure decrease and partially closes the turbine control valves (TCVs) to stabilize the reactor at a lower pressure. The reactor power settles out at nearly the initial power level. The coolant inventory is maintained by the feedwater control system using water from the condensate storage tank via the condenser hotwell. The NRC staff's review covered (1) the sequence of events, (2) the analytical model used for analyses, (3) the values of parameters used in the analytical model, and (4) the results of the transient analyses. The NRC's acceptance criteria are based on (1) draft GDC-6, insofar as it requires that the reactor core be designed to function throughout its design lifetime without exceeding acceptable fuel damage limits, and (2) draft GDC-27 and 28, insofar as they require that at least two reactivity control systems be provided and be capable of making and holding the core subcritical from any hot standby or hot operating condition sufficiently fast to prevent exceeding acceptable fuel damage limits. Specific review criteria are contained in SRP Section 15.6.1 and other guidance provided in Matrix 8 of RS-001.

#### Technical Evaluation

[Insert technical evaluation. The technical evaluation should (1) clearly explain why the proposed changes satisfy each of the requirements in the regulatory evaluation and (2) provide a clear link to the conclusions reached by the NRC staff, as documented in the conclusion section.]

#### Conclusion

The NRC staff has reviewed the licensee's analyses of the inadvertent opening of a pressure relief valve event and concludes that the licensee's analyses have adequately accounted for operation of the plant at the proposed power level and were performed using acceptable analytical models. The NRC staff further concludes that the licensee has demonstrated that the reactor protection and safety systems will continue to ensure that the SAFDLs and the RCPB pressure limits will not be exceeded as a result of this event. Based on this, the NRC staff concludes that the plant will continue to meet the requirements of draft GDC-6, 27, and 28 following implementation of the proposed EPU. Therefore, the NRC staff finds the proposed EPU acceptable with respect to the inadvertent opening of a pressure relief valve event. (9)

BVY 05-072  
Docket No. 50-271

**Exhibit SPSB-C-52-1**

**Vermont Yankee Nuclear Power Station**

**Proposed Technical Specification Change No. 263 – Supplement No. 30**

**Extended Power Uprate**

**Response to Request for Additional Information**

**Calculation VYC-0886, Rev. 2**

**Total number of pages in this Exhibit  
(excluding this cover sheet) is 13.**

VY CALCULATION CHANGE NOTICE (CCN)

CCN Number: 04 Calculation Number: VYC-0886 Rev. No. 2

Calculation Title: Station Blackout Documentation Analysis

Initiating Document: EPU  
 VYDC/MM/TM/Spec. No./ other

Safety Evaluation Number: N/A

Superseded Calculation: N/A Superseded by N/A

Implementation Required:  Yes  No

Computer Codes: N/A

Reason for Change: The VYC-0886 Rev 2 is updated to assess the effect of Extended Power Uprate (EPU) on this calculation.
Description of Change: This CCN updates VYC-886 Rev 2, for EPU.
Technical Justification for Change: See Attachment A
Conclusions: The results of Reference 1 were addressed at EPU conditions. The effect of EPU on VYC-886Rev2 are summarized in Attachment A.

Are there any open items in this CCN?  Yes  No

Prepared By/Date	Interdiscipline Review By/Date	Independent Review By/Date	Approved By/Date
<i>Liliane Schor</i> 02/18/2004 Liliane Schor	<i>N/A</i>	<i>Alan L. Robertshaw</i> 18 February 2004 Alan L. Robertshaw	<i>James G. Rogers</i> 2-19-04 James G. Rogers

Final Turnover to DCC (Section 2):

- 1) All open items, if any, have been closed.
- 2) Implementation Confirmation (Section 2.3.4)
  - Calculation accurately reflects existing plant configuration,  
(confirmation method indicated below)
  - Walkdown  As-Build input review  Discussion with \_\_\_\_\_  
OR (print name)
  - N/A, calculation does not reflect existing plant configuration
- 3) Resolution of documents identified in the Design Output Documents Section of VYAPF 0017.07 has been initiated as required (Section 2.3.6, 2.3.7)

\_\_\_\_\_/\_\_\_\_\_/\_\_\_\_\_  
 Print Name Signature Date

Total number of pages in package including all attachments: 13 pages

VY CALCULATION DATABASE INPUT FORM

Place this form in the calculation package immediately following the Title page or CCN form.

VYC-0886/CCN04                      2                      N/A                      N/A  
 VY Calculation/CCN Number      Revision Number      Vendor Calculation Number      Revision Number  
 Vendor Name: N/A                      PO Number: N/A

Originating Department: Design Engineering

Critical References Impacted:  UFSAR  DBD  Reload. "Check" the appropriate box if any critical document is identified in the tables below.

EMPAC Asset/Equipment ID Number(s): N/A

EMPAC Asset/System ID Number(s): N/A

Keywords: Decay Heat, SBO, Torus Temperature, Condensate Storage Tank, Ventilation

For Revision/CCN only: Are deletions to General References, Design Input Documents or Design Output Documents required?  Yes†  No

Design Input Documents and General References - The following documents provide design input or supporting information to this calculation. (Refer to Appendix A, sections 3.2.7 and section 4)

* Reference #	** DOC #	REV #	***Document Title (including Date, if applicable)	Significant Difference Review ††	**** Affected Program	Critical Reference (✓)
1	VYC-0886	2	Station Blackout Documentation Analysis, 01/03/2001			
2	TE 2003-064		Station Blackout PUSAR Input			
3	GE-VYNPS-AEP-146	N/A	Letter, Michael Dick (GE) to Craig Nichols (ENOI), VYNPS EPU Task T0400: Decay Heat for Containment Analysis dated March 10,2003.			
4	VYC-2282	0	Vessel Stored Energy with GE14 Fuel at 20% Power Uprate, dated 5/9/03			
5	NUMARC 87-00	N/A	NUMARC 87-00, dated 11/20/87, including NRC accepted errata and Q & A's from MUMARC seminars and Topical Report F.			
6	NAVY 91-98	N/A	Letter, USNRC to VYNPC, NAVY 91-98, "Vermont Yankee Station Blackout Analysis," June 5, 1991			
7		N/A	ASME Steam Tables			
8		N/A	VY Technical Specification			
9	VYC-2270	0	VY GE 14 Appendix R at 20% Power Uprate, dated 05/09/2003			
10	VYC-415	0	Appendix R/RCIC, HPCI & ECCS Room Cooling, dated 4/29/1986			
11	VYC-415 CCN 01	0	Appendix R/RCIC, HPCI & ECCS Room Cooling, dated 9/04/2002			

* Reference #	** DOC #	REV #	***Document Title (including Date, if applicable)	Significant Difference Review ††	**** Affected Program	Critical Reference (✓)
12	VYC-888 CCN3	2	Station Blackout Documentation Analysis, dated 9/04/2002			
13	VYC-2279	0	Evaluation of EPU Impact on Ambient Space Temperatures During Normal Operation, dated 04/11/2003			
14	VYC-1347	0	Main Steam Tunnel Heatup Calculation, dated 11/1/96			
15	OT-3122	19	Loss of Normal Power, 04/18/00			
16	VYC-1628D CCN02	0	Torus Temperature Response to Appendix R and Station Blackout Scenarios, dated			

VYC-0886 Rev 2 CCN04, Page 3 of 7



VY CALCULATION DATABASE INPUT FORM (Continued)

Design Output Documents - This calculation provides output to the following documents. (Refer to Appendix A, section 5)

* Reference #	** DOC #	REV #	Document Title (including Date, if applicable)	**** Affected Program	†††Critical Reference (✓)
	VYC-1432	4	VY Vessel Level for Appendix R, 05/17/1996		
	VYC-1458	0	Station Blackout Load Capacity Analysis, 10/15/1996		
	VYC-1628	0 CCN3	Torus Temperature and Pressure Response to Large Break LOCA and MSLB Accident Scenarios, 3/21/2002		
	VYC-1628D	0	Torus Temperature Response to Appendix R and Station Blackout Scenarios-dated November 5, 1998.		
	VYC-2159	0	VY-Cycle Independent Decay Heat-Comparison Between ORIGEN-2 and ANSI/ANS 5.1-1979 Standard, 2/27/2001		
	VYC-2314	0	Minimum Containment Overpressure for Non-LOCA Events, 9/03/2003		
			DBD SADBD	DBD	✓
			DBD CPS	DBD	✓
			DBD HPCI	DBD	✓
			DBD HVAC	DBD	✓
			DBD MS	DBD	✓
			DBD NBVI	DBD	✓
			DBD RCIC	DBD	✓
			DBD RHR	DBD	✓
			SSCA Vol 1	Appendix R	✓

VYC-0886 Rev 2 CCN04, Page 4 of 7

VYAPF0017.07  
 AP 0017 Rev. 8  
 Page 3 of 4  
 LPC#6

VY CALCULATION DATABASE INPUT FORM (Continued)

- \* Reference # - Assigned by preparer to identify the reference in the body of the calculation.
- \*\* Doc # - Identifying number on the document, if any (e.g., 5920-0264, G191172, VYC-1286)
- \*\*\* Document Title - List the specific documentation in this column. "See attached list" is not acceptable. Design Input/Output Documents should identify the specific design input document used in the calculation or the specific document affected by the calculation and not simply reference the document (e.g., VYDC, MM) that the calculation was written to support.
- \*\*\*\* Affected Program - List the affected program or the program that reference is related to or part of.
- † If "yes," attach a copy of "VY Calculation Data" marked-up to reflect deletion (See Section 3.1.8 for Revision and 5.2.3.18 for CCNs).
- †† If the listed input is a calculation listed in the calculation database that is not a calculation of record (see definition), place a check mark in this space to indicate completion of the required significant difference review. (see Appendix A, section 4.1.4.4.3). Otherwise, enter "N/A."
- ††† If the reference is UFSAR, DBD or Reload (IASD or OPL), check Critical Reference column and check UFSAR, DBD or Reload, as appropriate, on this form (above).

**Note: All calculations in the Design Output list were reviewed. No revision required.**

**Other Design Output were reviewed. The following revisions are required:**

- 1) DBDs referencing VYC-886 Rev2 need to be addressed.
- 2) Calculation VYC-1347 should be addressed for EPU.

VYC-0886 Rev 2 CCN04, Page 5 of 7

VYAPF0017.07  
AP 0017 Rev. 8  
Page 4 of 4  
LPC#6

VY CALCULATION REVIEW FORM

Calculation Number: VYC-0886 Revision Number: 2 CCN Number: 04

Title: Station Blackout Documentatlon Analysis

Reviewer Assigned: Alan Robertshaw

Required Date: February 2004

Interdiscipline Review  Independent Review

Comments\*

Resolution

1. Assumptions on page 1 of Att. A need Reference.

1. Added

2. Need Reference for Table 1 in Att. A.

2. Done

3. On page 5 of Att. A please state the TS CST Inventory.

3. Added TS CST inventory

Alan Z Robertshaw 18 February 2004  
Reviewer Signature Date

[Signature] 02/18/2004  
Calculation Preparer (Comments Resolved) Date

Method of Review:  Calculation/Analysis Review  
 Alternative Calculation  
 Qualification Testing

Alan Z Robertshaw 18 February 2004  
Reviewer Signature (Comments Resolved) Date

\*Comments shall be specific, not general. Do not list questions or suggestions unless suggesting wording to ensure the correct interpretation of issues. Questions should be asked of the preparer directly.

VY CALCULATION OPEN ITEM LIST

Calculation Number: VYC-886

Revision Number: 2

CCN Number: 4

Open Item	Resolution	Method of OI Tracking or Date Closed
<u>DBDs referencing VYC-886 Rev2 need to</u> <u>be verified for changes to torus temperatures.</u> <u>VYC-1347 needs to be CCN for EPU</u>		

## Attachment A

### Reason for Revision

Revision 2 of VYC-0886 is updated to incorporate the EPU changes

This CCN incorporates:

- 1) Condensate Inventory Requirements at EPU incorporating:
  - The decay heat at EPU from Reference 3.
  - Vessel stored energy at EPU from Reference 4 (VYC-2282).
- 2) Loss of ventilation
- 3) Torus Temperature

### Assumptions (same as in reference 1)

1. No off-site power available (SBO)
2. The reactor depressurizes from 1095 psia to 100 psia during the SBO scenario. The 1095 psia is assumed to be an average SRV setpoint. The 100 psia is assumed a low pressure setpoint where RHR system is deployed for shutdown cooling.
3. It is assumed that at about 8 hours, the vessel pressure decreased to about 100 psia.
4. It is assumed that at 100 psia the fluid and solids in the reactor vessel are at the same temperature. This is a reasonable assumption, since at 8 hours, most of the metal in the vessel will be at the fluid saturation temperature.

### Condensate Inventory Requirements

The inventory required for decay heat removal will be calculated using a formula given in NUMARC 87-00 and also using the decay heat calculated in Reference 3.

#### Condensate Inventory to Remove Decay Heat

From Reference 5

$$V = 35.55 \text{ gal/MWt} = 35.55 * 1912 * 1.02 = 69331 \text{ gallons for 8 hours}$$

From the decay heat calculation

Q decay at 8 hours (interpolated in the integrated decay heat table -- Table 1, Reference 3, next page)

20000	4.68951E+08
28800	6.11079E+08
40000	7.91978E+08

Attachment A

Table 1 – Integrated Decay Heat for 20% power Uprate

Time (sec)	GE 2 sigma P/Po	Integrated	Integrated Kwsec	Integrated, BTU
0.00000	1.00000	0.00000	0.00000	0.00000
0.10000	0.99210	0.09961	1.94254E+05	1.89980E+05
0.15000	0.96250	0.14847	2.89552E+05	2.83182E+05
0.20000	0.93280	0.19585	3.81959E+05	3.73556E+05
0.40000	0.74710	0.36384	7.09580E+05	6.93969E+05
0.60000	0.59080	0.49763	9.70503E+05	9.49152E+05
0.80000	0.49380	0.60609	1.18203E+06	1.15602E+06
1.00000	0.33880	0.68935	1.34440E+06	1.31483E+06
2.00000	0.15480	0.93615	1.82572E+06	1.78556E+06
4.00000	0.06073	1.15168	2.24606E+06	2.19664E+06
10.00000	0.05234	1.49089	2.90760E+06	2.84363E+06
20.00000	0.04546	1.97989	3.86127E+06	3.77632E+06
40.00000	0.03986	2.83309	5.52521E+06	5.40366E+06
60.00000	0.03687	3.60039	7.02163E+06	6.86715E+06
80.00000	0.03466	4.31569	8.41664E+06	8.23147E+06
100.00000	0.03321	4.99439	9.74026E+06	9.52598E+06
150.00000	0.03073	6.59289	1.28577E+07	1.25749E+07
200.00000	0.02909	8.08839	1.57743E+07	1.54273E+07
400.00000	0.02550	13.54739	2.64207E+07	2.58394E+07
600.00000	0.02346	18.44339	3.59690E+07	3.51777E+07
800.00000	0.02197	22.98639	4.48290E+07	4.38427E+07
1000.00000	0.02079	27.26239	5.31682E+07	5.19985E+07
1500.00000	0.01861	37.11239	7.23781E+07	7.07858E+07
2000.00000	0.01707	46.03239	8.97742E+07	8.77992E+07
4000.00000	0.01370	76.80239	1.49783E+08	1.46488E+08
6000.00000	0.01209	102.59239	2.00080E+08	1.95678E+08
8000.00000	0.01114	125.82239	2.45384E+08	2.39985E+08
10000.00000	0.01047	147.43239	2.87529E+08	2.81203E+08
15000.00000	0.00986	198.25739	3.86649E+08	3.78143E+08
20000.00000	0.00918	245.86739	4.79500E+08	4.68951E+08
40000.00000	0.00775	415.22739	8.09793E+08	7.91978E+08
60000.00000	0.00699	562.63739	1.09728E+09	1.07314E+09
80000.00000	0.00647	697.19739	1.35970E+09	1.32979E+09
86400.00000	0.00633	738.15099	1.43957E+09	1.40790E+09
100000.00000	0.00608	822.54579	1.60416E+09	1.56887E+09
150000.00000	0.00539	1109.27079	2.16334E+09	2.11575E+09
172800.00000	0.00515	1229.46099	2.39774E+09	2.34499E+09
200000.00000	0.00492	1366.41299	2.66483E+09	2.60621E+09
259200.00000	0.00451	1645.27459	3.20868E+09	3.13809E+09
345600.00000	0.00406	2015.28259	3.93028E+09	3.84382E+09
400000.00000	0.00384	2230.16259	4.34935E+09	4.25367E+09
432000.00000	0.00373	2351.26659	4.58553E+09	4.48465E+09
600000.00000	0.00327	2939.18259	5.73211E+09	5.60601E+09
800000.00000	0.00290	3556.48259	6.93599E+09	6.78340E+09
864000.00000	0.00281	3739.39459	7.29272E+09	7.13228E+09
1000000.00000	0.00265	4110.81059	8.01707E+09	7.84069E+09

**Attachment A**

$Q = M (h(g) - h(l))$  to calculate the inventory requirement

Where:

$h(g)$  (Reference 1) = 1187 Btu/lbm (average between 1095 and 100 psia) [see note on page 22 of Reference 1]

$h(l)$  = 118 Btu/lbm (150 °F conservative temperature of CST)

$v(l)$  = 0.01634 ft<sup>3</sup>/lbm @ 150°F

All properties are from Reference 7.

$$M = \frac{6.11079 \text{ E}8 * 0.01634 * 7.48}{(1187 - 118)} = 69867 \text{ gal}$$

This inventory matches very well the NUMARC formula and it will be used. Therefore the inventory requirement for 8 hours of decay heat is 69867 gallons.

Condensate needed to remove the vessel stored energy to depressurize from 1095 psia to 100 psia.

Stored Energy in Fluid

The fluid energy at full power (EPU conditions is) (Reference 4)

Fluid (EPU, t=0.0)	Mass (lbm)	Enthalpy (Btu/lbm)	Total Energy (BTU)
Liquid	386,971	525.54	2.03369E8
Steam	13,186.12	1191.05	0.15705E8
Total			2.19074E8

The fluid energy at 100 psia is not changed from Reference 4. The level will be the same after depressurization for current licensed power (CLP) as for EPU. Hence the volumes of steam and liquid will be the same, as well as the enthalpy.

Fluid (depressurized at 100 psia)	Mass (lbm)	Enthalpy (Btu/lbm)	Total Energy (BTU)
Liquid	510322.4	298.4	1.5228E8
Steam	703.13	1187.2	0.008E8
Total			1.5311E8

Thus, the difference in fluid energy:  $\Delta E_{\text{fluid}} = 2.19074\text{e}8 - 1.5311\text{E}8 = 0.65964\text{E}8$  Btu

## Attachment A

Stored Energy in Solid (From Reference 4)

Solid (EPU, time= 0.0)	Total Solid Energy (BTU)	Heat Conductor Effective Temperature (°F)
Liquid Exposed	0.9604399E8	601.24
Steam Exposed	0.25155507E8	609.18
Total	1.211995E8	602.83

$$Q = MC_p \Delta T = MC_p (602.83 - 32) = MC_p 570.83$$

$$MC_p = 1.211995E8 / 570.83 = 212321.53 \text{ Btu /}^\circ\text{F}$$

$$T_{\text{sat}} @ P= 100 \text{ psia} = 328^\circ\text{F (ASME Steam Tables- Reference 7)}$$

At 100 psia:

$$Q = 212321.53 * (328-32) = 0.628472E8 \text{ Btu}$$

$$\text{Total Energy removed from structures: } \Delta E_{\text{structures}} = 1.211995E8 - 0.628472E8 = 0.58352E8 \text{ Btu}$$

$$\text{Total energy removed from the vessel during depressurization} = \Delta E_{\text{fluid}} + \Delta E_{\text{structures}} = 0.65964E8 + 0.58352E8 = 1.24316E8 \text{ Btu}$$

The inventory needed to remove this heat =

$$V = \frac{1.24316E8 * (.01634) * 7.48}{(1187 - 118)} = 14,214 \text{ gallons}$$

$$\text{Hence, the total inventory requirements} = 69867 \text{ gallons} + 14,214 \text{ gallons} = 84081 \text{ gallons}$$



## Attachment A

For the CLP (Reference 1) the total CST inventory requirements for removing the decay heat and vessel stored energy = 75,837 gallons.

The TS (Reference 8) CST inventory of 75000 gallons is exceeded at both EPU and CLP for the 8 hours coping duration.

The HPCI/RCIC taking suction from CST has to make up for the vessel leakage (TS allowable and pump seal leakage of 61 gpm – Reference 6, page 17 of TER, also used in both Appendix R analysis (Reference 9, VYC-2270) and in Reference 1. The leakage amount does not change for EPU.

The needed CST inventory to account for leakage;  
 $V = 61 \text{ gpm} * 8 \text{ hours} * 60 \text{ min/hour} = 29,280 \text{ gallons.}$

This inventory, added to that already calculated for decay heat and depressurization would total:

$V = 29280 + 84081 = 113361$  gallons, which would normally be available from CST but, if not could easily be made available from the torus. Therefore, the conclusions of VYC-886 Rev2 that the Technical Specifications CST inventory requirement of 75000 gallons is not adequate for an 8 hour duration is valid at EPU. However, with Alternate AC (Vernon Tie) and low pressure systems available, sufficient inventory is available from the torus for the required 8 hours.

The power uprate results in a need for more inventory, 113361 gallons versus 105117 gallons at CLP.

### Reactor Coolant Inventory

The depletion of the available inventory in CST will not jeopardize reactor coolant inventory because makeup inventory can be provided from the torus. When the torus temperature exceeds 140 °F and RCIC and HPCI can not be used with suction from the torus, reactor inventory can be provided from the torus via low pressure pumps. Since VY is an Alternate AC plant, crediting use of the low pressure pumps is acceptable. This conclusion is unaffected by power uprate.

### Loss of Ventilation

The heat-up due to the loss of ventilation due to an SBO event for RCIC Room, HPCI Room, Main Steam Tunnel, Control Room, Switchgear Room, and Intake Structure is addressed in Reference 1.

### RCIC Room

The heat-up calculation is based on VYC-415 Rev0 (Reference 10 modified by CCN 1 (Reference 11)). The heatup is based on the piping temperature, RCIC turbine and Switch Heat Loss. The RCIC Room Temperature calculated in Reference 12 is unaffected by EPU.

## Attachment A

### HPCI Room

The heat-up calculation is based on heat loads from VYC-0415 Rev 0 (Reference 10). The heat loads are from the piping and the HPCI turbine. The heat loads are unaffected by power uprate. Therefore the calculation for HPCI room heat-up is not affected by EPU.

### Main Steam Tunnel

The issue is isolation of HPCI and RCIC on high steam tunnel temperature.

Reference 13 calculated an increase of 0.6 °F in the normal temperature of the steam tunnel, at EPU. The conclusion of VYC-886 Rev 2, that the main steam tunnel heat-up is slow on loss of ventilation and the reactor will already be in the process of cool-down, is valid at EPU.

Furthermore, Reference 14 (VYC-1347) concluded that the heat-up in the main steam tunnel is less than that required to isolate HPCI and RCIC. For the case when the feedwater and main steam isolates (SBO conditions), the peak room temperature from Reference 14 is 174°F (isolation temperature assuming loop accuracy) at approximately 18 hours. Based on the results of Reference 13, the change in Main Steam Tunnel Heatup will be very small at EPU. Furthermore, procedure OT-3122 (Reference 15) limits HPCI & RCIC operation to 2 hours; hence the reactor pressure after 2 hours should be low enough to permit operation of the Low Pressure Pumps (CS and RHR).

Therefore the impact of power uprate on heatup of the Main Steam Tunnel is negligible. It is recommended that calculation VYC-1347 be updated for EPU conditions.

### Control Room

Restoration of ventilation in the Control Room is governed by Procedure OT-3122 and is unaffected by Power Uprate. Control Room Heatup for loss of ventilation is unaffected by power uprate.

### Switchgear Room

The heat loads in the switchgear room are unaffected by the power uprate.

### Intake Structure

The heatup of the Intake structure on loss of ventilation with only 2 Service Water available is unaffected by the power uprate since the heat loads in the intake structure are unaffected by power uprate.

### Torus Temperature

The Torus Temperature calculation for SBO at power uprate was performed in Reference 16 (VYC-1628D CCN02). The peak suppression pool temperature is 187.9 °F.

**Exhibit SPSB-C-52-2**

Vermont Yankee Nuclear Power Station

Proposed Technical Specification Change No. 263 – Supplement No. 30

Extended Power Uprate

Response to Request for Additional Information

Calculation VYC-1347, Rev.0

Total number of pages in this Exhibit  
(excluding this cover sheet) is 29.

Text 117  
+ Total

ORIGINAL: PAGE 1 of 117 PAGES  
 Rev. 1: PAGE 1 of      PAGES  
 Rev. 2: PAGE 1 of      PAGES  
 Rev. 3: PAGE 1 of      PAGES

QA RECORD?

IMS NO. M02.01.05

YES

RECORD TYPE 09.C16.004

NO

W.O./P.O. NO. 4055

YANKEE NUCLEAR SERVICES DIVISION  
 CALCULATION/ANALYSIS FOR

TITLE Main Steam Tunnel Heatup Calculation

PLANT Vermont Yankee CYCLE N/A

CALCULATION NUMBER VYC-1347

	PREPARED BY /DATE	REVIEWED BY /DATE	APPROVED BY /DATE	SUPERSEDES CALC/REV. NO.
ORIGINAL	<i>J. Pap</i> 11-1-96	<i>[Signature]</i> 11-1-96	<i>[Signature]</i> 1/10/97	N/A JP 10-30-97
REVISION 1				
REVISION 2				
REVISION 3				

KEYWORDS GOTHIC: Room: Heat-up: RRU



NUCLEAR SERVICES DIVISION  
 OF  
 YANKEE ATOMIC ELECTRIC COMPANY  
 580 MAIN STREET  
 BOLTON, MASSACHUSETTS 01740

TABLE OF CONTENTS

<u>Section</u>	<u>Description</u>	<u>Page</u>
	LIST OF TABLES .....	3
	LIST OF FIGURES .....	4
1.0	PROBLEM DESCRIPTION .....	5
1.1	Objective .....	5
1.2	Method of Solution .....	6
1.3	Design Inputs.....	6
1.4	Assumptions .....	9
2.0	PROBLEM ANALYSIS.....	10
2.1	GOTHIC Model Input.....	10
2.1.1	Control Volumes .....	10
2.1.2	Thermal Conductors.....	11
2.1.3	Heaters: Main Steam Isolation Valves .....	11
2.2	GOTHIC Runs .....	20
2.2.1	Run MST1.....	20
2.2.2	Run MST2.....	24
3.0	CONCLUSION.....	29
4.0	REFERENCES .....	30
	Appendices	
A	GOTHIC Run MST1 .....	35
B	GOTHIC Run MST2 .....	81
C	Computer Code Evaluation .....	112
D	Reviewer's Comments .....	114

LIST OF TABLES

<u>Table No.</u>	<u>Description</u>	<u>Page</u>
1.3-1	Thermo-Physical Properties .....	7
1.3-2	Outer Environment Temperatures .....	8
2.1-1a	MST2 Dimensional Data.....	15
2.1-1b	West Wall Dimensional Data.....	16
2.1-2a	Piping Design Data.....	17
2.1-2b	Piping Heat Transfer Surface Areas.....	18

LIST OF FIGURES

<u>Figure No.</u>	<u>Description</u>	<u>Page</u>
2.1.3-1	MSIV Valve Outline Drawing.....	19
2.2-1a	MST1 Schematic .....	22
2.2-1b	MST1 Temperature Profile .....	23
2.2-2a	MST2 Schematic .....	26
2.2-2b	MST2 Temperature Profile to Seven Days .....	27
2.2-2c	MST2 Temperature Profile to Four Hours .....	28
A-1	MST1 Schematic .....	38
A-2	MST1 Input Tables .....	39
A-3	MST1 Graphical Results.....	55
A-4	MST1 Output Verifying the MSIV Model.....	70
A-5	MST1 Output Showing Condensation Heat Transfer Fluctuations.....	73
A-1	MST2 Schematic .....	82
A-2	MST2 Input Tables .....	83
A-3	MST2 Graphical Results.....	98

## 1.0 PROBLEM DESCRIPTION

This calculation determines the temperature rise in the main steam tunnel with a loss of HVAC to document whether this rise will result in an automatic isolation of the HPCI and RCIC systems. The HPCI/RCIC excess air temperature switches, within the main steam tunnel, provide automatic isolation of the HPCI and RCIC lines if a temperature of  $185^{\circ}\text{F} \pm 5^{\circ}\text{F}$  is sustained for longer than 30 minutes (References 23 and 24). The loop accuracy is  $6^{\circ}\text{F}$  (Reference 36). Therefore HPCI and RCIC isolation can occur at a steam tunnel temperature as low as  $174^{\circ}\text{F}$ . This high temperature isolation scheme is for line break protection and it is not intended for non-line break events, such as loss of main steam tunnel cooling under loss of normal power.

Normal ventilation in the main steam tunnel is supplied by the Reactor Building Ventilation System and by RRUs 17A and 17B, located in the tunnel. A Reactor Transfer Fan (RTF-1A/1B) exhausts air from the main steam tunnel at approximately 4200 cfm. Each fan has a total capacity of 14,400 cfm and takes inlet air from various locations in the Reactor Building. The RRUs circulate and cool air inside the main steam tunnel. The fan capacity of each RRU is 5000 cfm and service water, supplied to coils within the RRUs, provides the cooling.

RTF-1A and both RRUs are powered from 480v MCC 6A. This MCC is NNS and is supplied from 4160v Bus 1. RTF-1B is powered from 480v MCC 7A, which is also NNS, and is supplied from 4160v Bus 2.

Controls are located on the Turbine Building HVAC control panel, with auxiliary indications on the Control Room 9-25 panel. Typically, one fan and both RRUs are operating, with the second fan in stand-by. The operating fan and the RRUs maintain the main steam tunnel environment temperature at a yearly average of  $125^{\circ}\text{F}$ , as described in the Vermont Yankee Environmental Qualification Program (Reference 25). A review of temperature data for the main steam tunnel indicates that the air temperature can peak at about  $150^{\circ}\text{F}$  during the summer months (Reference 30).

### 1.1 Objective

The objective of this calculation is to determine the temperature rise of the air in the main steam tunnel, during a loss of normal power and under the following conditions:

- Loss of HVAC in the main steam tunnel.
- Summer peak temperature for initial and boundary conditions.
- Main steam and feedwater lines in the tunnel are:
  - Isolated (steam and water are not flowing, GOTHIC run MST1).
  - Not isolated (steam and water are flowing, GOTHIC run MST2).



1.2 Method of Solution

A lumped parameter GOTHIC model of the main steam tunnel is used to calculate the air temperature rise on loss of HVAC. GOTHIC<sup>(33,34)</sup> is a general purpose thermal-hydraulic computer program for design, licensing, safety, and operating analysis of nuclear power plant containment and other confinement buildings. See Appendix C for verification of the GOTHIC version used.

The models consist of *volumes, flow paths, & thermal conductors* arranged and connected to represent the thermal-hydraulic response of the main steam tunnel. The thermal mass of each conductor is included in the GOTHIC computation.

1.3 Design Inputs

1.3.1 The thermo-physical properties for the materials used are shown in Table 1.3-1.

1.3.2 The boundary temperatures for spaces surrounding the main steam tunnel are shown in Table 1.3-2.

TITLE Main Steam Tunnel Heatup CalculationPREPARED BY Jim Pappas

REVIEWED BY \_\_\_\_\_

PAGE 7 OF \_\_\_\_\_

Table 1.3-1  
Thermo-Physical Properties

Material	Temperature (°F)	Thermal Conductivity (Btu/hr/ft/F)	Density (lbm/ft <sup>3</sup> )	Specific Heat (Btu/lbm/°F)
Concrete <sup>(3)</sup>	75	1.05	142	0.156
Steel Pipe <sup>(3)</sup>	68	25.0	487	0.11
Insulation <sup>(3)</sup>	1000	0.073	15 <sup>(b)</sup>	0.10 <sup>(b)</sup>
	900	0.067		
	800	0.060		
	700	0.055		
	600	0.050		
	500	0.046		
	400	0.042		
	300	0.038		
	200	0.036		
	100	0.033		

Notes

a) Superscript numbers refer to References in Section 4.0.

b) Assumed.

Table 1.3-2  
Outer Environment Temperatures

Condition	East Wall Ref. 25, pp. 7-12 Drywell Below 270	West Wall Ref. 25, pp. 7-13 Heater Bay	North/South Walls Ref. 25, pp. 7-11 Non-Occupied Area	Ceiling Outside
Normal Operation	150°F	125°F	100°F	83°F <sup>(a)</sup>
Peak Summer	160°F	130°F	120°F	90°F <sup>(b)</sup>

Notes

- a) Vermont Yankee FSAR (Reference 32), Table 2.3.2, Highest mean daily maximum for summer months.
- b) Vermont Yankee FSAR (Reference 32), Section 10.12, Summer design temperature.

#### 1.4 Assumptions

The critical assumptions used in the GOTHIC models are as follows:

- 1.4.1 Initial main steam tunnel air temperature is 150°F. This is based on Reference 30 and is considered conservative. Reference 30, describes that this value is derived from a temperature element that is close to hot process lines. Therefore, the corresponding ambient room temperature should be lower.
- 1.4.2 Initial main steam thermodynamic statepoint is saturated steam at 985 psia based on the heat balance shown on Figure 1.6-1 in the FSAR (Reference 32). Therefore, the temperature is 543°F.
- 1.4.3 Initial feedwater thermodynamic statepoint is saturated water at 373°F based on the heat balance shown on Figure 1.6-1 in the FSAR (Reference 32). Therefore, the pressure is 179.8 psia.
- 1.4.4 HPCI and RCIC turbine steam supply temperatures are 543°F.
- 1.4.5 Both RRUs are inoperative for the analysis.
- 1.4.6 The air temperatures in the spaces surrounding the main steam tunnel are listed in Table 1.3-2 and are assumed to be constant throughout the transients.
- 1.4.7 In model MST1, where the main steam lines are isolated and the feedwater pumps are off, the four main steam lines (MS-1A through D) and the feedwater lines (FDW-14/15/16/17) dissipate the heat in the line volume, cooling down as they do so. All other lines contain fluid at their respective constant temperatures, as listed in Table 2.1-2a.
- 1.4.8 In model MST2, where the main steam lines do not isolate, all lines contain fluid at their respective constant temperatures, as listed in Table 2.1-2a.
- 1.4.9 Miscellaneous piping, steel, and equipment are left out of the models.
- 1.4.10 The floor is left out of the models to add conservatism to the room heat-up.
- 1.4.11 The west wall contains a metal section through which the main steam lines pass and which two blowout panels are installed. This metal section is modeled in the GOTHIC runs. However, other non-concrete wall sections are not. They include:
  - a) ventilation duct with blowout damper in the north wall,
  - b) a blowout panel and a blowout door in the south wall, and
  - c) various duct work and pipe sleeves.

This is assumed to be conservative since it inhibits natural circulation that would normally exist in the room.

2.0 PROBLEM ANALYSIS

2.1 GOTHIC Model Input

The following sections describe the major input that was calculated for the GOTHIC models.

2.1.1 Control Volumes

Main Steam Tunnel

The main steam tunnel is Volume 1 in the models. The relevant dimensional data of the main steam tunnel for construction of the models are shown in Table 2.1-1. From these data, the wall surface areas and the room overall volume are obtained. The volume of the steam tunnel is:

$$V_{MST} = (\text{North Wall}) \times (\text{East Wall}) \times (\text{Height})$$

$$V_{MST} = 36.25' \times 24' \times 25.5' = 22,185 \text{ ft}^3$$

The hydraulic diameter is:

$$D_h = \frac{4A}{P_w}$$

where A is the cross sectional area of the volume (i.e., the ceiling or floor area) and  $P_w$  is the wetted perimeter.  $P_w$  is defined by GOTHIC as  $S/h$  or the surface area of all structures divided by the height of the volume. S would, therefore, be the total surface area of all the walls and the ceiling. The floor is not modeled.

$$D_h = \frac{4Ah}{S}$$

$$D_h = \frac{4(A_{\text{ceiling}})h}{A_{\text{north}} + A_{\text{south}} + A_{\text{east}} + A_{\text{west}} + A_{\text{ceiling}}}$$

$$D_h = \frac{4(870)(25.5)}{924.38 + 924.38 + 612 + 612 + 870}$$

$$D_h = 225 \text{ ft}$$

In the run where the main steam and feedwater lines are isolated, those lines are modeled as separate control volumes. The four main steam lines are lumped into one volume as are the two feedwater

lines. The volumes are obtained from the pipe data in Table 2.1-2b, and follow. The hydraulic diameters are simply the pipe diameters.

#### Main Steam Lines

$$V_{MSL} = 4 \times \pi (L R)^2 \times L$$

$$V_{MSL} = 4 \times \pi (8.062 / 12)^2 \times 46.5$$

$$V_{MSL} = 263.75 \text{ ft}^3$$

#### Feedwater Lines

$$V_{FDW} = \pi (L R)^2 (L_{14/16} + L_{15/17})$$

$$V_{FDW} = \pi (6.781 / 12)^2 (45.7 + 47.9)$$

$$V_{FDW} = 93.90 \text{ ft}^3$$

#### 2.1.2 Thermal Conductors

The input for the thermal conductors that represent the steam tunnel walls and ceiling is taken from Table 2.1-1. The floor is left out of the model to add conservatism. Typically there is little heat transfer through the floor of a heated room.

The thermally significant piping found in the main steam tunnel are described in Table 2.1-2. The GOTHIC input for these conductors is also shown in the table.

#### 2.1.3 Heaters: Main Steam Isolation Valves

The main steam isolation valves (MSIV) in the steam tunnel have a substantial amount of un-insulated structure that makes up the yoke and actuator. Figure 2.1.3-1 (Reference 39) shows the outline of the valve. Heat will conduct through and out of this structure into the main steam tunnel. There are four such valves in the tunnel.

The yoke of each MSIV consists of four 3" solid rods attached to the bonnet (Reference 40). The yoke acts as a support for the actuator and as a spring guide. Through the center of the yoke, the valve stem travels.

The method of modeling the heat transferred to the main steam tunnel by this assembly will be to treat each 3" yoke rod and the stem as a fin. The stem will be modeled as though it were a fifth yoke rod. Therefore, each MSIV will be modeled as having five 3" solid rod fins heated at one end. The heated end is that attached to the body of the valve. It is assumed that the actuator is far enough away from the valve body that any heat conducted to it is negligible.

GOTHIC cannot model this situation because it involves two-dimensional conductive heat transfer. GOTHIC can only model one-dimensional conduction. Therefore, a formulation of the heat rate provided by the yokes will be derived here and input into GOTHIC as a "heater".

The general equation for such a fin is (Reference 29):

$$q = \sqrt{hPkA}(T_s - T_\infty) \tanh(mL)$$

where:

$q$  = heat rate (Btu/hr)

$h$  = convective heat transfer coefficient (Btu/hr-ft<sup>2</sup>-°F)

$P$  = perimeter of the fin ( $\pi d$ ) (ft)

$d$  = diameter of the rod (ft)

$k$  = thermal conductivity of the rod material (Btu/hr-ft-°F)

$A$  = cross sectional area of the fin (ft<sup>2</sup>)

$T_s$  = temperature of the heated end (°F)

$T_\infty$  = ambient room temperature (°F)

$$m = \sqrt{\frac{hP}{kA}} \text{ (ft}^{-1}\text{)}$$

$L$  = length of the fin (ft)

The values in the following table will be used. The value for  $h$  is taken from Reference 38 and is considered to be conservative. In a transient calculation, it would be expected to vary around a value of 0.5 Btu/hr-ft<sup>2</sup>-°F to 1.0 Btu/hr-ft<sup>2</sup>-°F. The length,  $L$ , is taken as the "AC" dimension from Figure 2.1.3-1. This is clearly much longer than the actual length of the yoke. However, the yoke dimension is not given. So, the more conservative, longer length is arbitrarily used. This presents hardly any penalty in heat rate to the room because the value is used in the  $\tanh()$  function which is barely sensitive to the length. For example, using the 9 ft value  $\tanh(9) = 0.9999$  and using half that value  $\tanh(4.5) = 0.9998$ .

Variable	Value	Remarks
h	1.65 Btu/hrft <sup>2</sup> *F	Reference 38
d	= 3 in = 0.25 ft	Reference 40
P	= $\pi d$ = $\pi (0.25)$ = 0.785 ft	
k	25 Btu/hrft*F	Table 1.3-1
A	= $\frac{\pi d^2}{4}$ = $\frac{\pi (0.25)^2}{4}$ = 0.049 ft <sup>2</sup>	
m	= $\sqrt{\frac{hP}{kA}}$ = $\sqrt{\frac{165 \times 0.785}{25 \times 0.049}}$ = 1.028 ft <sup>-1</sup>	
L	= 108 in = 9 ft	Figure 2.1.3-1 (See discussion above)

The temperatures will be taken from the GOTHIC run using control variables. This will allow the temperature difference to vary with time to more accurately represent the changing heat transfer rate.

The source temperature,  $T_s$ , will be taken as the temperature inside the main steam line. This is highly conservative since the more appropriate value would be that of the bonnet. Calculation VYC-660 (Reference 40) is a state-point calculation of the heat conduction through the same MSIV structure. For the state-point modeled in VYC-660, the steam inside the pipe is modeled at 545°F and the bonnet temperature is calculated to be about 375°F. So, as expected, the bonnet is cooler than the steam inside the pipe. However, the assumptions in VYC-660 are not all consistent with those of the present calculation and a definitive correlation between these two temperatures is not readily derivable. Therefore, using the steam temperature is certainly conservative since it is clearly bounding - the bonnet can never be hotter than the steam.



The ambient temperature,  $T_{\infty}$ , is the bulk room temperature calculated by GOTHIC.

So, the heat rate generated by a single yoke rod is:

$$q = \sqrt{(165 \times 0.785 \times 25 \times 0.049)} (T_s - T_{\infty}) \tanh(1028 \times 9)$$
$$q = 126(T_s - T_{\infty}) \text{ Btu/hr}$$

Each of the four MSIVs is to be modeled as having five such rods, and GOTHIC requires input in units of Btu/sec. So, the final input to GOTHIC is:

$$q = 4 \text{ MSIVs} \times 5 \text{ Rods} \times \frac{1 \text{ hr}}{3600 \text{ sec}} \times 126(T_s - T_{\infty})$$
$$q = 0.007(T_s - T_{\infty}) \text{ Btu/s}$$

In GOTHIC this will be represented as a heater with a heat rate of 0.007 Btu/s multiplied by a forcing function. The forcing function is in turn equated to a control variable. And, the control variable represents the temperature difference between the main steam line and the room average of the tunnel.

**Table 2.1-1a**  
**Main Steam Tunnel Dimensional Data**

	North Wall	South Wall	East Wall	Ceiling
Length (ft)	36.25 <sup>(11)</sup>	36.25 <sup>(11)</sup>	24 <sup>(10)</sup>	36.25 <sup>(11)</sup>
Height / Width (ft)	25.5 <sup>(12)</sup>	25.5 <sup>(12)</sup>	25.5 <sup>(12)</sup>	24 <sup>(10)</sup>
Area (ft <sup>2</sup> )	924.38	924.38	612.0	870.0
Thickness (ft)	4.0 <sup>(10)</sup>	4.0 <sup>(10)</sup>	4.0 <sup>(13)</sup>	4.0 <sup>(11)</sup>

Notes \_\_\_\_\_

Superscript numbers refer to References in Section 4.0.

**Table 2.1-1b**  
**West Wall Dimensional Data**

	West Wall Overall	Total Section Containing Buried Pipes	Remaining Concrete
Length (ft)	24 <sup>(10)</sup>	24.0 <sup>(12)</sup>	24
Height / Width (ft)	25.5 <sup>(12)</sup>	8.0 <sup>(12)</sup>	25.5
Area (ft <sup>2</sup> )	612.0	192	420
Thickness (ft)	3.0 <sup>(10)</sup>	0.25 in <sup>(17)</sup>	3.0

Notes \_\_\_\_\_

Superscript numbers refer to References in Section 4.0.

Table 2.1-2a  
Piping Design Data

Pipe Number	Nominal Diameter (in)	Schedule	Insulation Thickness (in)	Operating Temperature (°F)
MS-1A	18 <sup>(25)</sup>	80	3.5 <sup>(27)</sup>	543 <sup>(f)</sup>
MS-1B	18 <sup>(25)</sup>	80	3.5 <sup>(27)</sup>	543 <sup>(f)</sup>
MS-1C	18 <sup>(25)</sup>	80	3.5 <sup>(27)</sup>	543 <sup>(f)</sup>
MS-1D	18 <sup>(25)</sup>	80	3.5 <sup>(27)</sup>	543 <sup>(f)</sup>
MS-4A <sup>(b)</sup>	10 <sup>(19)</sup>	80	3.5 <sup>(19)</sup>	543 <sup>(f)</sup>
MS-4B <sup>(b)</sup>	10 <sup>(19)</sup>	80	2.0 <sup>(19)</sup>	543 <sup>(f)</sup>
FDW-14/16	16 <sup>(18)</sup>	120	2.0 <sup>(18)(e)</sup>	373 <sup>(d)</sup>
FDW-15/17	16 <sup>(18)</sup>	120	2.0 <sup>(40)(e)</sup>	373 <sup>(d)</sup>
MS-5A <sup>(c)</sup>	3 <sup>(22)</sup>	160	2.0 <sup>(22)</sup>	543 <sup>(f)</sup>
RCIC-1 <sup>(f)</sup>	4 <sup>(21)</sup>	120	None <sup>(21)</sup>	140 <sup>(h)</sup>
RCIC-2 <sup>(f)</sup>	4 <sup>(21)</sup>	120	None <sup>(21)</sup>	140 <sup>(h)</sup>
RCIC-8B <sup>(f)</sup>	4 <sup>(21)</sup>	120	2.0 <sup>(21)</sup>	140 <sup>(h)</sup>
RCIC-8A <sup>(f)</sup>	4 <sup>(21)</sup>	120	2.0 <sup>(21)</sup>	140 <sup>(h)</sup>
HPCI-15B <sup>(g)</sup>	14 <sup>(20)</sup>	120	2.5 <sup>(27)</sup>	140 <sup>(d)</sup>
HPCI-15A <sup>(g)</sup>	14 <sup>(20)</sup>	120	2.5 <sup>(27)</sup>	140 <sup>(d)</sup>

## Notes \_\_\_\_\_

- a) Reference 27 says 2.5"
- b) HPCI Steam Supply
- c) RCIC Steam Supply
- d) FSAR (Reference 32), Figure 6.4-1 (Highest temperature at Location 2)
- e) Superscript numbers refer to References in Section 4.0.
- f) RCIC Discharge
- g) HPCI Discharge
- h) FSAR (Reference 32), Figure 4.7-3 (Highest temperature at Location 3)
- i) Assumption 1.4.2
- j) Assumption 1.4.3

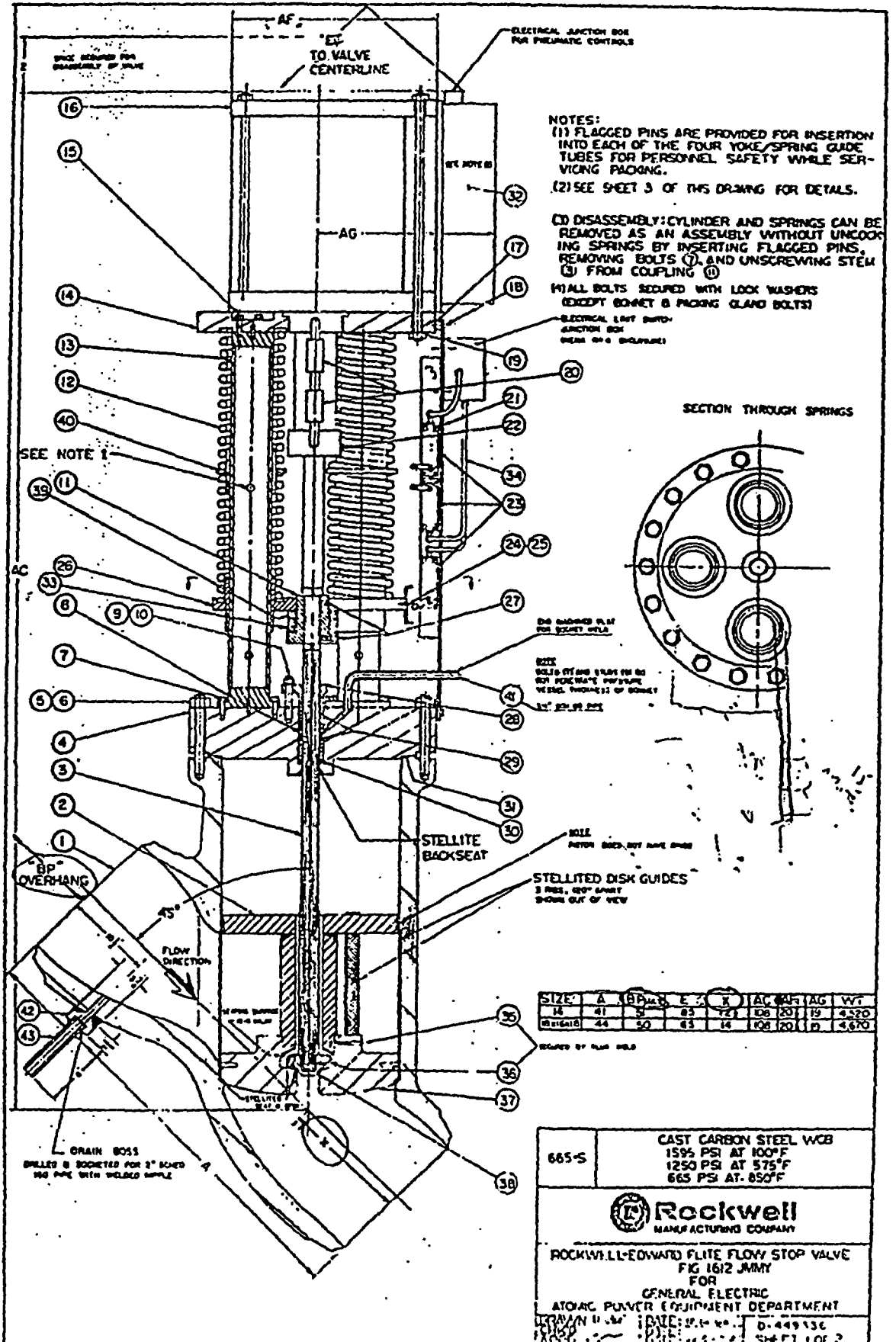
**Table 2.1-2b**  
**Piping Heat Transfer Surface Areas**

Line Number	Inner Radius <sup>(f)</sup> (in)	Outer Radius <sup>(f)</sup> (in)	Length (ft)	Heat Transfer Surface Area <sup>(g)</sup> (ft <sup>2</sup> )
MS-1A	8.062	9.000	46.5 <sup>(6,7)</sup>	304.3
MS-1B	8.062	9.000	46.5 <sup>(6,7)</sup>	304.3
MS-1C	8.062	9.000	46.5 <sup>(6,7)</sup>	304.3
MS-1D	8.062	9.000	46.5 <sup>(6,7)</sup>	304.3
MS-4A <sup>(b)</sup>	4.781	5.375	17.6 <sup>(19)</sup>	81.8
MS-4B <sup>(b)</sup>	4.781	5.375	35.2 <sup>(19)</sup>	135.9
FDW-14/16	6.781	8.000	45.7 <sup>(18)</sup>	239.3
FDW-15/17	6.781	8.000	47.9 <sup>(35)</sup>	250.8
MS-5A <sup>(c)</sup>	1.312	1.750	46.7 <sup>(22)</sup>	91.7
RCIC-1 <sup>(f)</sup>	1.812	2.250	28.7 <sup>(21)</sup>	33.8
RCIC-2 <sup>(f)</sup>	1.812	2.250	29.7 <sup>(21)</sup>	35.0
RCIC-3B <sup>(f)</sup>	1.812	2.250	6.5 <sup>(21)</sup>	14.5
RCIC-3A <sup>(f)</sup>	1.812	2.250	11.4 <sup>(21)</sup>	25.4
HPCI-15B <sup>(g)</sup>	5.906	7.000	40.6 <sup>(20)</sup>	202.0
HPCI-15A <sup>(g)</sup>	5.906	7.000	9.2 <sup>(20)</sup>	45.8

**Notes**

- a) Area =  $2\pi(\text{Outer Radius} + \text{Insulation}) \times (1 \text{ ft}/12 \text{ in}) \times \text{Length}$
- b) HPCI Steam Supply
- c) RCIC Steam Supply
- e) Superscript numbers refer to References in Section 4.0.
- f) RCIC Discharge
- g) HPCI Discharge

Figure 2.1.3-1



Page 19

YANKEE ATOMIC ELECTRIC COMPANY  
 CALCULATION NO VYC-1347  
 ATTACHMENT PAGE OF

10-31-76

## 2.2 GOTHIC Runs

### 2.2.1 Run MST1

This run of the main steam tunnel heat-up represents a typical loss-of-normal power event. On a loss-of-power, the HVAC system trips and the MSIVs and feedwater pumps isolate. The room then heats up because of the heat gain from the pipes within it. However, the major loads are from the main steam and feedwater lines and the fluids in those lines are not flowing. Therefore, their heat gain to the room diminishes as the transient progresses and the room eventually peaks out and then begins to drop in temperature.

This run represents a typical heat-up of the tunnel following loss of ventilation, however many conservatisms are included so that the results are assured to bound a true event. These conservatisms include:

- The initial main steam tunnel temperature of 150°F is based on the Reference 30 data and represents a peak room temperature as opposed to an average room temperature. A more representative average (initial) room temperature would be something lower.
- Miscellaneous structures and equipment in the room are not modeled. They would act as heat sinks resulting in a temperature rise that is slower than that predicted by GOTHIC.
- Miscellaneous "cold" piping, such as service water piping, is not modeled as heat sinks.
- Wall openings such as ventilation ducts/dampers or pipe sleeves are not modeled inhibiting cooling by natural circulation.
- Natural circulation through the RRUs is not modeled. The RRUs trip on loss of power however they continue to receive cool service water and would contribute a small amount of cooling.
- On a loss of power, HPCI and RCIC would automatically start resulting in flushing some of the 373°F water from the feedwater lines and replacing it with 140°F water. This is not accounted for.
- The MSIV heat gain is conservative as described in Section 2.1.3. Most notably, the source temperature of the yoke, modeled as a series of fins, is the steam temperature itself as opposed to the bonnet temperature of the valve.
- The floor as a heat sink is not modeled.

The non-conservatisms in the model are:

- Main steam line drains are not modeled. They would add heat to the room but only a small amount because the lines are about 2½" NPS. This is believed to be counteracted by the lack of "cold" piping being modeled as well.
- There is no account for MSIV leakage that would continuously add a slight heat load to the main steam lines. (Run MST2 in Section 2.2.2 accounts for this).

- There is no spatial definition in the model, therefore an axial temperature gradient is not calculated. Because the HPCI/RCIC temperature switches are in the upper, ceiling, area they may experience a higher temperature than that of the bulk room. This is believed to be counteracted by the initial room temperature of 150°F which represents a temperature from a hot area of the steam tunnel. (See Assumption 1.4.1).

It is believed that the conservatisms listed above far outweigh the non-conservatisms. Therefore, it can be assured that the true heat-up profile of the main steam tunnel will be a curve that is below - and therefore bounded by - the GOTHIC result.

The GOTHIC model MST1 is shown schematically in Figure 2.2-1a. It consists of the following :

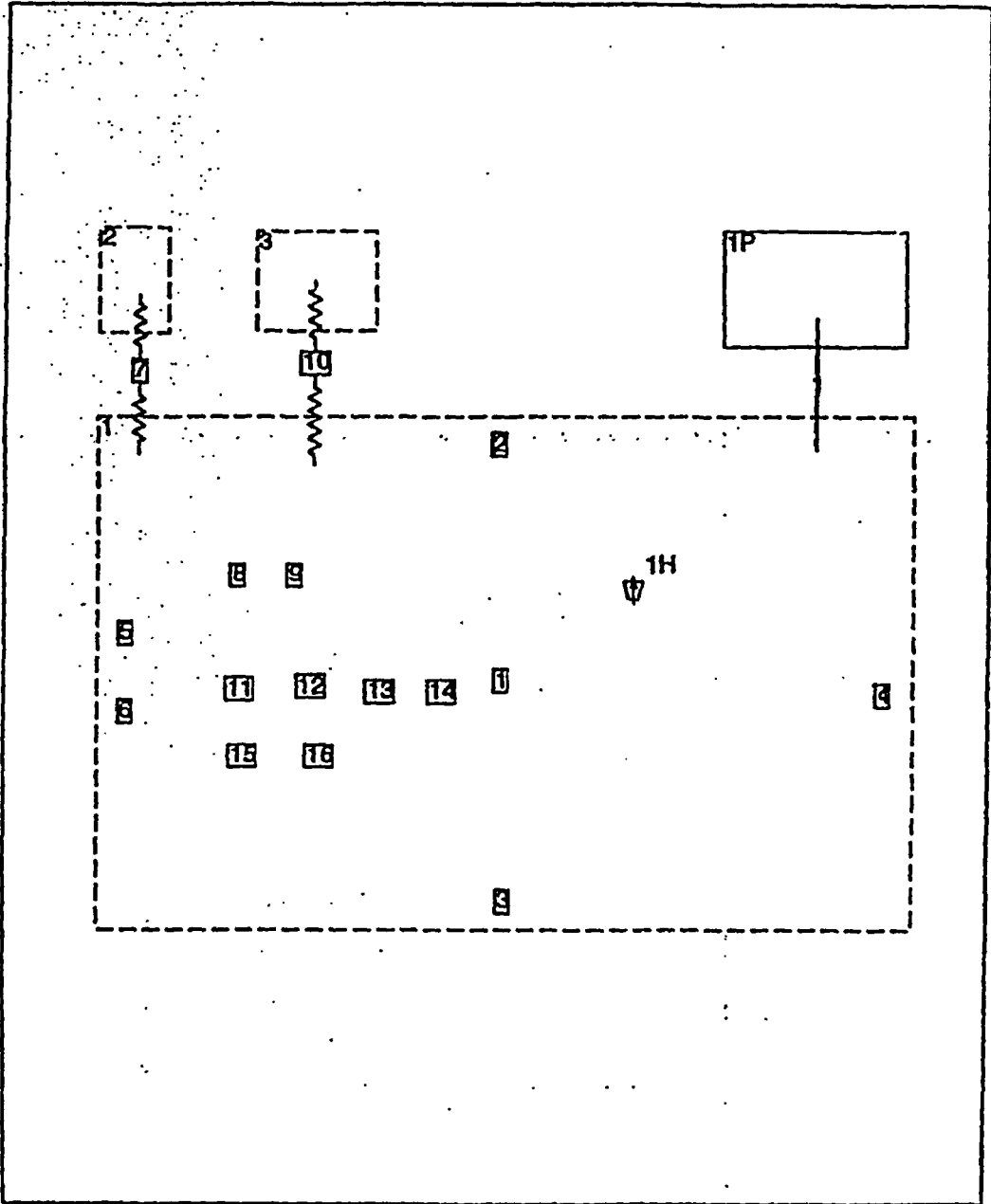
- Volume 1 representing the main steam tunnel.
- Volume 2 representing the main steam lines isolated at  $t = 0$  seconds.
- Volume 3 representing the feedwater lines with pumps off and no flow at  $t = 0$  seconds.
- Flow path 1 connecting Volume 1 with a pressure boundary condition 1P. This flow path and boundary condition are used to maintain the pressure within the main steam tunnel at 14.7 psia as the air heats up.
- Thermal Conductors 1-6, 8, 9, 11-16 connecting the heat sources and sinks to Volume 1.
- Thermal Conductor 7 connecting Volume 2 to Volume 1.
- Thermal Conductor 10 connects Volume 3 to Volume 1.
- Heater 1 representing the MSIVs.

Appendix A contains the detailed listing of the GOTHIC input for this run. Included are graphical results and calculations validating the run. The model is run for 7 days to determine the temperature rise profile of the air in the main steam tunnel. The heat-up of the main steam tunnel is shown in Figure 2.2-1b for the full 7 days.

The graph shows that the steam tunnel reaches a peak average temperature of 174°F after approximately  $\frac{1}{4}$  of a day. It then drops during the remainder of the transient. The peak is considered to bound the actual peak that would result during a true loss-of-ventilation scenario because of the conservatisms discussed above.



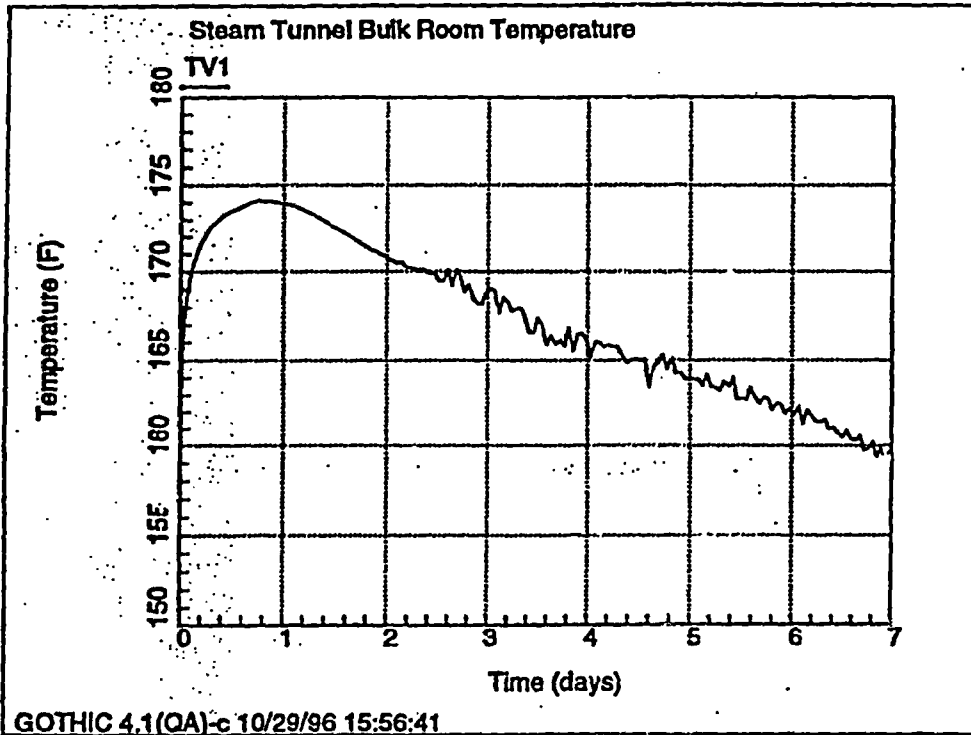
Figure 2.2-1a



YANKEE ATOMIC ELECTRIC COMPANY  
CALCULATION NO VYc-1347  
ATTACHMENT \_\_\_\_\_ PAGE \_\_\_\_\_ OF \_\_\_\_\_

10-31-96  
Page 22

Figure 2.2-1b



YANKEE ATOMIC ELECTRIC COMPANY  
CALCULATION NO VYC-1347  
ATTACHMENT \_\_\_\_\_ PAGE \_\_\_\_\_ OF \_\_\_\_\_

10-31-96  
Page 23

### 2.2.2 Run MST2

This run of the main steam tunnel heat-up represents an extreme loss-of-normal power event. As stated in Section 2.2.1, on a loss-of-power, the MSIVs and feedwater pumps normally isolate. However, the possibility exists that one or more isolation function fails - such as a MSIV not closing. Furthermore, as stated in the non-conservatisms of run MST1, it is more than likely that some leakage would exist past the MSIVs.

Justifiably quantifying such conditions is not straight forward. However, the situation can be bounded. The most bounding scenario is that none of the main steam and feedwater lines isolate and the steam/water continues to flow. The initial temperature of the fluids within these lines is, therefore, constant throughout the transient resulting in a much higher heat gain to the room. This modeling technique also clearly bounds any postulated leakage past isolated MSIVs.

The model, itself, is identical to MST1 except:

- the volumes representing the main steam and feedwater lines are removed.
- the conductors (7 and 10) that connected those volumes are moved into the main steam tunnel volume as internal conductors.
- the boundary heat transfer coefficients on conductors 7 and 10 are fixed temperatures representing the steam and feedwater temperatures.

All other conservatisms and non-conservatisms listed for run MST1 remain in this run.

The GOTHIC model MST2 is shown schematically in Figure 2.2-2a. It consists of the following :

- Volume 1 representing the main steam tunnel.
- Flow Path 1 connecting Volume 1 with a pressure boundary condition 1P. This flow path and boundary condition are used to maintain the pressure within the main steam tunnel at 14.7 psia as the air heats up.
- Thermal Conductors 1 - 16 connecting the heat sources and sinks to Volume 1.
- Heater 1 representing the MSIVs.

Appendix B contains the detailed listing of the GOTHIC input for this run and graphical results. The model is run for 7 days to determine the temperature rise profile of the air in the main steam tunnel. The heat-up of the main steam tunnel is shown in Figures 2.2-2b for the full 7 days and 2.2-2c for the first four hours. The first four hours is of particular interest for Appendix R scenarios.

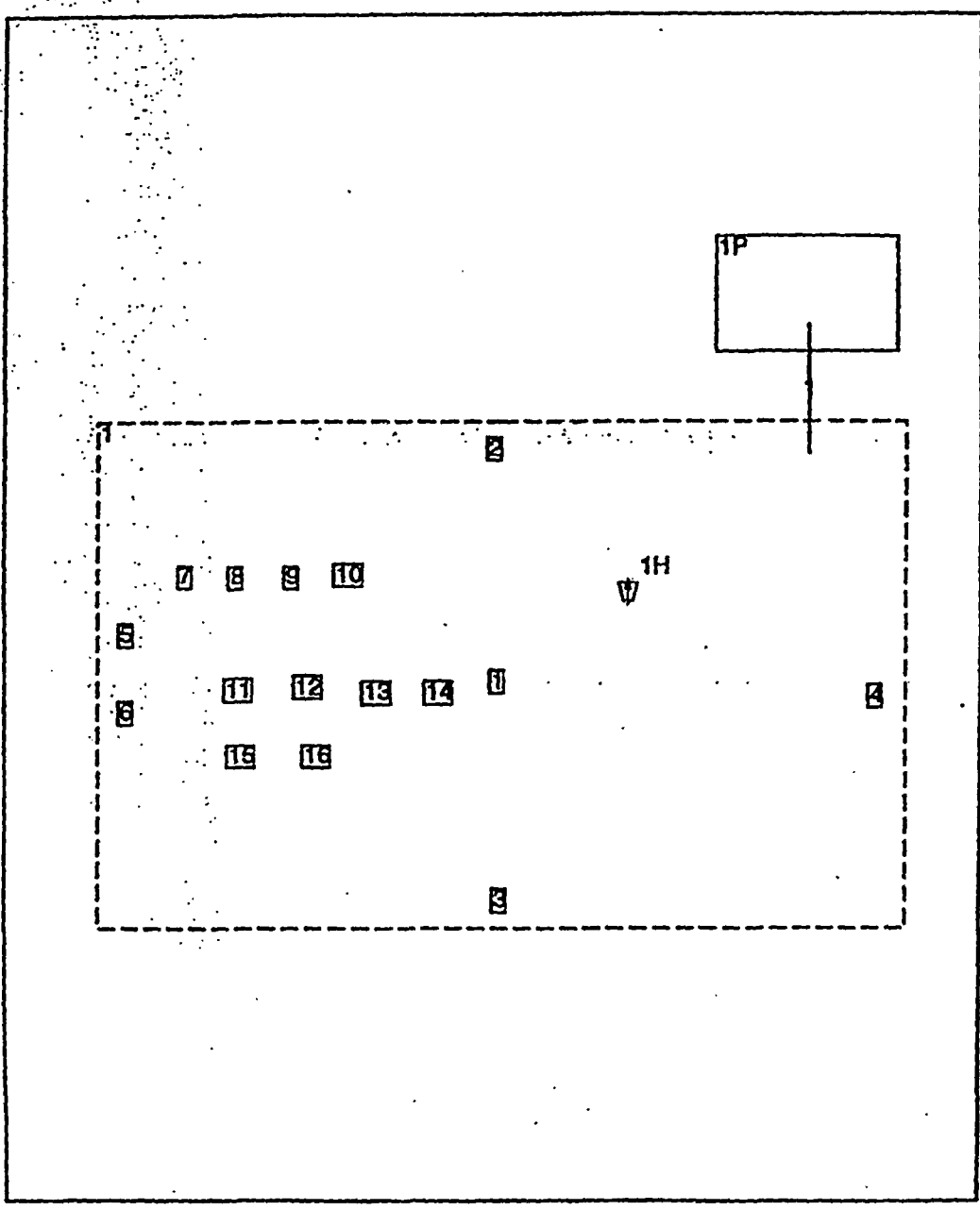
YANKEE NUCLEAR SERVICES DIVISION      CALC. NO. VYC-1347      REV. \_\_\_\_\_      DATE 11-1-96  
TITLE Main Steam Tunnel Heatup Calculation  
PREPARED BY Jim Pappas      REVIEWED BY \_\_\_\_\_      PAGE 25 OF \_\_\_\_\_

---

The graphs show that the steam tunnel reaches an average temperature of 172°F after four hours. It continues to rise until it is about 207°F at 7 days and still rising.

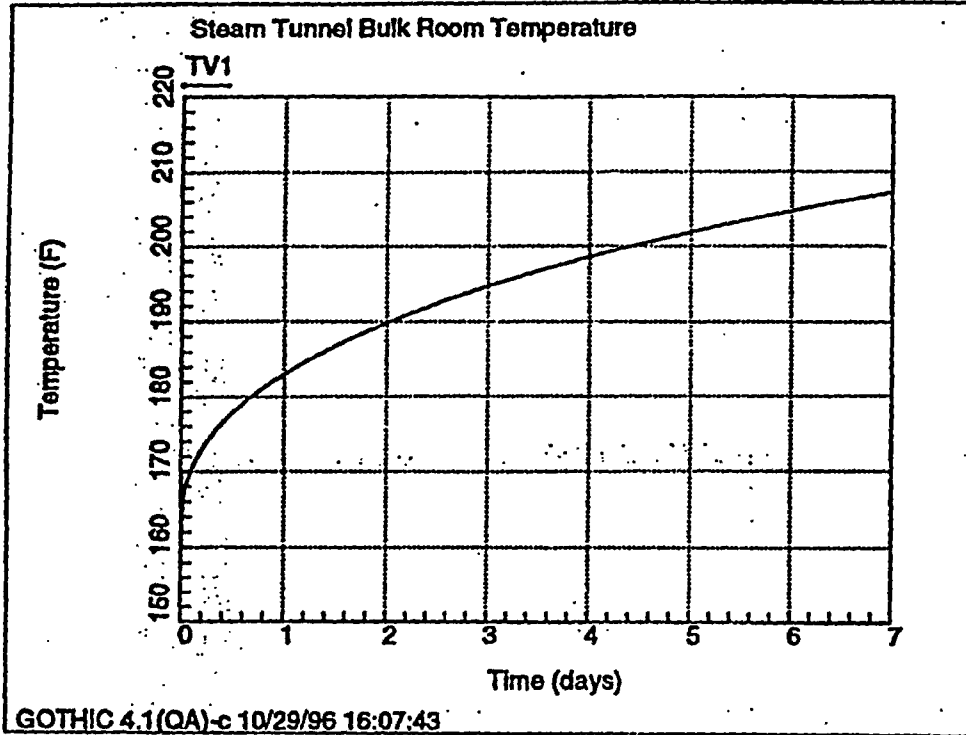
As with MST1, these results are considered to bound the actual temperature rise that would result during such a scenario. Furthermore, because the scenario itself is extreme by nature, the results greatly bound any possible steam tunnel heat rise that may be postulated.

Figure 2.2-2a



YANKEE ATOMIC ELECTRIC COMPANY  
CALCULATION NO. UYC-1347  
ATTACHMENT \_\_\_\_\_ PAGE 26 OF \_\_\_\_\_  
10-31-96

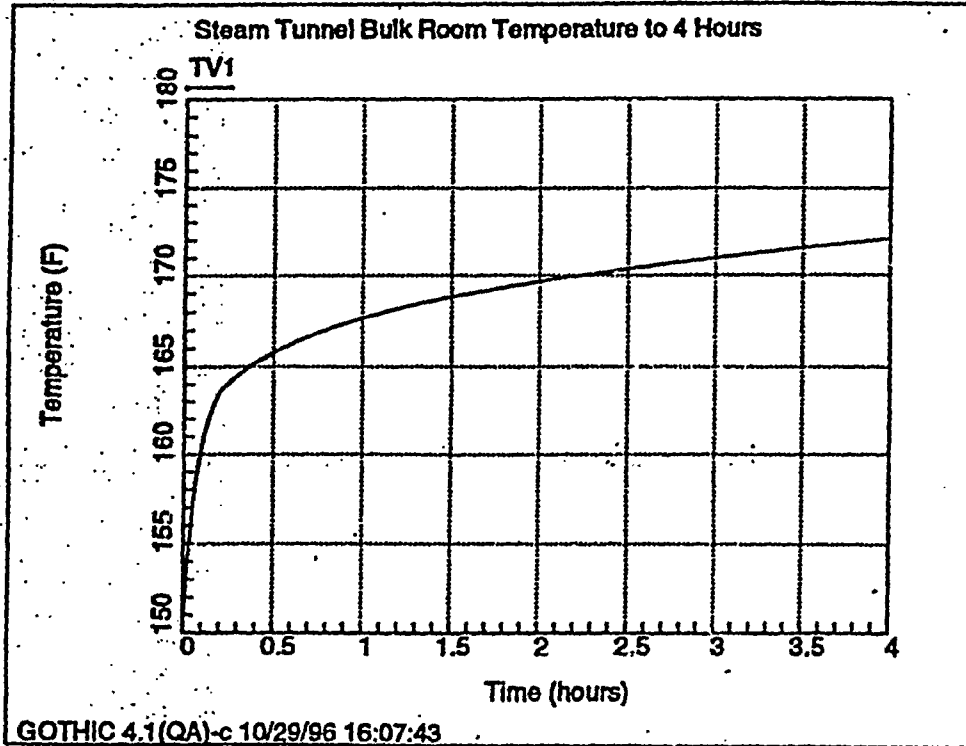
Figure 2.2-zb



YANKEE ATOMIC ELECTRIC COMPANY  
CALCULATION NO VYC-1347  
ATTACHMENT \_\_\_\_\_ PAGE 27 OF \_\_\_\_\_

10-31-96

Figure 2.2-2c



YANKEE ATOMIC ELECTRIC COMPANY  
CALCULATION NO VYC-1347  
ATTACHMENT \_\_\_\_\_ PAGE 28 OF \_\_\_\_\_

10-31-96

### 3.0 CONCLUSION

The results of the two GOTHIC runs show the air temperature in the steam tunnel to approach about 172°F in the first four hours of each transient. Both transients show almost the same profile for that time frame because the cooldown of the main steam and feedwater lines is not large enough in the first four hours to have a significant effect on the room temperature rise.

In the case where the main steam lines and feedwater lines isolate, the peak room temperature is about 174°F at approximately 18 hours. In the case where these lines do not isolate, the room temperature rises to 174°F at about 6¼ hours. It continues to rise and is about 207°F at the end of the seven day transient and still rising.

As discussed in Section 2.2, the many conservatism included in the model offer a high degree of confidence that the GOTHIC results envelop any true heat-up profile of the steam tunnel. Therefore, the actual room heat-up is expected to be something less and it is concluded that HPCI and RCIC would not isolate under the conditions modeled.

The results of this calculation do not affect the FSAR, Technical Specifications, Technical Programs, or controlled drawings.



**Exhibit SPSB-C-52-3**

Vermont Yankee Nuclear Power Station

Proposed Technical Specification Change No. 263 – Supplement No. 30

Extended Power Uprate

Response to Request for Additional Information

Calculation VYC-1502, Rev.0

Total number of pages in this Exhibit  
(excluding this cover sheet) is 43.

ORIGINAL: PAGE 1 OF 140 PAGES  
 REV. 1: PAGE 1 OF      PAGES  
 REV. 2: PAGE 1 OF      PAGES  
 REV. 3: PAGE 1 OF      PAGES

QA RECORD?  
 YES  
 NO

IMS NO. M08.01.04  
 RECORD TYPE 13.C16.036, 13.C09.001  
 W.O./P.O. NO. 4055

YANKEE NUCLEAR SERVICES DIVISION  
 CALCULATION/ANALYSIS FOR

TITLE Control Room Heatup due to Loss of HVAC  
 PLANT Vermont Yankee CYCLE NA

CALCULATION NUMBER VYC-1502

	PREPARED BY DATE	REVIEWED BY DATE	APPROVED BY DATE	SUPERSEDES CALC/REV NO.
ORIGINAL	<i>Calderon</i> C.D.F. 8/30	<i>Furth</i> 8-30-96	<i>Abinlaram</i> 8/30/96	N/A
REVISION 1				
REVISION 2				
REVISION 3				

KEYWORDS GOETHIC 02, Control Room, Appendix E, HVAC, Loss of Ventilation, Heatup

## TABLE OF CONTENTS

1.0	Objective	3
2.0	Method	3
2.1	Heat Sources	4
2.2	Heat Sinks	5
2.3	Review of Results	5
3.0	Input and Assumptions	7
3.1	Generic Control Room GOTHIC Model	7
3.2	Assumptions	21
3.2.1	GOTHIC Model Assumptions	21
3.2.2	Control Room Heat Load Calculation Assumptions	21
4.0	Calculation	23
4.1	Control Room Heat Load Calculation	23
4.1.1	Heat Load Test 1	23
4.1.2	Heat Load Test 2	26
4.1.3	Determination of Limiting Control Room Heat Load	29
4.2	Characterization of Abstract Heat Conductor	30
4.3	Control Room Heatup During App. R Event	38
4.4	Control Room Heatup Mitigation Options	40
5.0	Conclusions	43
6.0	References	44
7.0	Microfilm Index	45
Appendix A	Control Room Heatup Test GOTHIC Input Model	46
Appendix B	Control Room Appendix R Heatup GOTHIC Input Model	61
Appendix C	Control Room Heat Load Test Data	77
Appendix D	Control Room Heatup Test Data	82
Appendix E	Control Room Appendix R Heatup Option 1 GOTHIC Input Model	98
Appendix F	Control Room Appendix R Heatup Option 2 GOTHIC Input Model	115
	Evaluation of Computer Code Use	132
	Calculation/Analysis Review	133

## 1.0 Objective

The objective of this calculation is to determine the temperature of the control room as a function of time as a result of a loss of ventilation of the control room due to an Appendix R fire scenario. The success criteria for this analysis is to have the control room maintained in a habitable condition and one which ensures equipment operability. Based on published guidelines, both are satisfied by maintaining control room temperature at or below 120°F [1]

## 2.0 Method

The control room is an enclosed room with concrete walls, floor and roof. The roof, north and east wall are exposed to the outdoor environment while the west wall is a common wall with the turbine building and the south wall is a common wall with the reactor building. There is a suspended ceiling below the control room roof above which ventilation ducting is routed. Acoustic ceiling tiles and lighting panels are held by the suspended ceiling structure.

The control room, as expected, has many control panels and cabinets with a variety of electrical components such as relays, indicating lights, power supplies and control systems. These electrical components, as well as other amenities (computers, refrigerator, copy machine, printers, etc), produce heat. This heat is normally removed by an HVAC system. But it is postulated that an Appendix R event in specific locations may render the HVAC system inoperable resulting in a heatup of the control room.

The heatup of an enclosed room is dependent on a couple of key parameters. The first key parameter is the heat input into the room. This heat input must be removed by convection, conduction or mass transfer. Given a loss of ventilation mass transfer is not available to remove the heat. Thus, convection and conduction are required to remove the heat through the surrounding walls to the outside environment. Since heat removal by convection and conduction are roughly proportional to the temperature difference across the walls, given a fixed outside air temperature, the higher the heat input the higher the inside air temperature.

Heat in an enclosed space with no ventilation is removed through the surrounding walls to the outside environment. The rate of heat removal is dependent on the thermal conductivity of the wall material and the convection of heat from the air in the room to the inside wall surface and from the outside wall surface to the outside air. These three factors make up the thermal resistance of the wall. This thermal resistance is the second key parameter and the higher the thermal resistance, the higher the required differential temperature between the outside air and the inside air.

The third key parameter is internal thermal conductors and affects only the transient heatup of an enclosed room. The first two parameters, heat rate and thermal resistance, can be used to predict the steady state temperature in the room since in steady state heat input equals heat removal. However, internal thermal conductors can serve to change the transient temperature

response by acting as a heat sink (as the room heats up, some of the heat is absorbed by the internal conductor as it heats up) or a heat source (if the heat sink started out hotter than the surrounding air, it will give up its heat to the surroundings.)

In this problem, all three key parameters need to be determined in order to solve the transient heatup of the control room following a loss of ventilation. These parameters were determined using a combination of test and analysis. The physical configuration of the outer walls of the control room can be determined from drawings and allows for determining the heat removal due to convection and conduction. The internal configuration of the room with respect to internal heat sources and sinks is more problematic and the method of determining these two parameters is explained in the subsequent sections.

The transient control room heatup will be calculated using the GOTHIC computer code [2]. A bounding scenario is determined in order to provide conservative input for the code. In addition, conservative boundary and initial conditions are chosen. The GOTHIC code produces a curve of control room temperature versus time which can then be used in assessing any necessary operator actions in the case of loss of ventilation to the control room.

The GOTHIC computer code is capable of solving general thermo-hydraulic problems and has many useful tools (internal conductors, heat sources, control mechanisms, air properties as a function of pressure and temperature, etc). GOTHIC has been validated for this type of application [2].

## 2.1 Heat Sources

The heat sources in the control room can be classified as follows:

**Electrical** - sources of heat due to I<sup>2</sup>R losses in electrical equipment. A variety of electrical equipment is contained in the control room (computers, monitors, relays, ambient lighting, controls and indications, conveniences such as refrigerators, copy machines, microwave ovens, etc.)

**Ambient** - if the outside air temperature is higher than the inside air temperature, heat is conducted through the walls and convected into the room.

**Personnel** - people generate heat and that heat is given off to the surroundings. The total heat generated by people depends on the number of people in the control room at any one time and the type of activity being performed (the more strenuous the activity, the greater the heat rejected by the body.)

The latter two heat sources can be calculated and/or estimated to a fair degree of accuracy. The former is much more problematic in that no complete inventory of electrical heat sources has been compiled. Reviews of HVAC documents reveal at least one source of information

with the data necessary to calculate the total heat generation in the control room. This data consists of data taken on the HVAC system including chill water flows and temperature. In addition, a test was performed part of which measured the air flow through the control room and the inlet and outlet air temperatures. This data can be used to calculate the total heat rate in the control room.

Using this combination of test data and analysis an adequate heat source can be determined for use in transient heatup calculations.

## 2.2 Heat Sinks

Heat sinks can absorb heat or transfer heat from the inside air to the outside ambient air. The contribution latter can be determined by calculation from information on drawings. However, the transient heat sinks, those that absorb or give off heat to the room and do not transmit heat to the outside air are more difficult to determine. These heat sinks can be in many forms: metal control panels, interior walls, chairs, tables, miscellaneous cabinets, etc. Determining the heat sinks and their characteristics is as difficult as determining the individual heat sources. Thus, a test was conducted to allow acquisition of data that can be used to determine the heat sink contribution.

The test conducted was a simple room heatup test. During a planned outage of the HVAC system, the ambient air temperature in the control room was recorded in several different locations. Given this temperature data and the heat source, an equivalent heat sink can be modeled. This equivalent heat sink model was constructed so that a control room heatup model, which mimicked the control room conditions at the time of the test, resulted in the calculated temperature transient matching the transient temperature data as closely as possible.

This equivalent heat sink can then be used in the control room model for examining the transient control room temperature given different initial conditions.

## 2.3 Review of Results

Four GOTHIC models were used in performing this calculation. The first model helped to quantify the control room internal heat sinks. The second model assessed the control room heatup transient for a period of four hours after the loss of HVAC to the control room. The third and fourth models assessed the effectiveness of two possible options that can mitigate the temperature rise after the initial four hour transient.

Model results show that the control room temperature will stay below 120°F for the first four hours after the loss of HVAC. Operator action is required to remove sufficient acoustic ceiling tiles (ten or more) before the control room temperature reaches 110°F (this occurs around 2.5 to 3 hours into the transient.) The removal of the acoustic tiles allows a larger

surface area for heat removal from the control room. It is expected that shortly after four hours that the control room temperature will reach and exceed 120 °F.

It was seen that long term corrective action can ensure that the control room remains habitable beyond the first four hours. Two effective methods of mitigating the room heatup are temporary ventilation and/or reducing the heat load in the control room. It was found that about 6600 cfm of outside air is required to ensure that the control room long-term temperature stays at or below 120 °F (with no reduction in control room heat load.) It was also found that 3600 cfm of outside air is required in conjunction with a control room heat load reduction by at least 52 percent will ensure that the control room long-term temperature stays at or below 120 °F.

There are some conservatisms in this calculation. These include:

- control room heat rate determined by test is increased by 10 percent to account for uncertainties
- control room internal heat sink area determined by test is decreased by 10 percent to account for uncertainties
- all of the heat rate determined by test plus margin is put into the control room (as opposed to into the drop ceiling space; some heat from the light fixtures could be argued to go into the drop ceiling space as opposed to in the control room space)
- all adjacent rooms are taken to be at higher than normal temperatures
- the event is assumed to occur on the hottest possible day with days prior and after to be equally hot
- thermal radiation from the hot air is not accounted for (this would increase the heat transfer to the walls resulting in a lower internal air temperature)

### 3.0 Input and Assumptions

The input and assumptions used for the GOTHIC model will be addressed step by step based upon the GOTHIC input tables. This section will describe and address the physical configuration of the control room model. Section 4 will address how the model was used and possibly any modifications to the model that were made in order to address specific variations or calculations for the purpose of calculating the transient control room heat up. For instance, the model that attempts to duplicate the control room heatup test will have specific initial conditions. The model that attempts to calculate the transient temperature during an Appendix R fire will have different initial conditions. This section describes the commonalities between the two models. A listing of the GOTHIC input tables for the control room heatup test model is included as Appendix A. The input tables for the control room transient heatup is included as Appendix B.

Figure 1 [3][4][5][6] provides a schematic plan view of the control room envelope.

#### 3.1 Generic Control Room GOTHIC Model

The Control Room is modeled as a two lumped-parameter volumes. The GOTHIC model is shown schematically in Figure 2. While the Control Room has a more complicated three-dimensional geometry than allowed by two lumped-parameter volumes, some variations on the geometry can be taken into account.

##### Control Volumes

From Figure 1 the room inside plan dimensions are: 80.063 feet (east/west walls) x 48.573 feet (north/south walls). However, the Control Room has five separate, smaller rooms along the north wall. From investigation it was found that the doors to these rooms are normally open. For this calculation, it is assumed that the doors to these rooms are open and the volume of these rooms will heat up at the same rate as the rest of the Control Room. Thus, the floor area for the Control Room is simply the product of the two side dimensions mentioned above.

The floor elevation for the Control Room is 272.5 ft and the roof elevation is 290.0 ft [3]. The roof thickness is 1.667 ft for a total inside net ht of 15.833'. However, the Control Room has a more complicated ceiling geometry due to an installed drop ceiling. From observation, it is apparent that the drop ceilings are fairly efficient in preventing commingling of air below the drop ceiling with air above the drop ceiling. Therefore, the air space between the drop ceiling and the roof will be modeled as a separate lumped-parameter volume. There are two separate sections of drop ceiling. The first is a 34 ft x 32 ft (8 x 17 panels) raised ceiling which is approximately 38 inches above the rest of the ceiling [7]. The second results in a ceiling level of 10 ft above the Control Room floor and represents the balance of the Control Room ceiling level. In the five office/utility spaces the drop ceiling



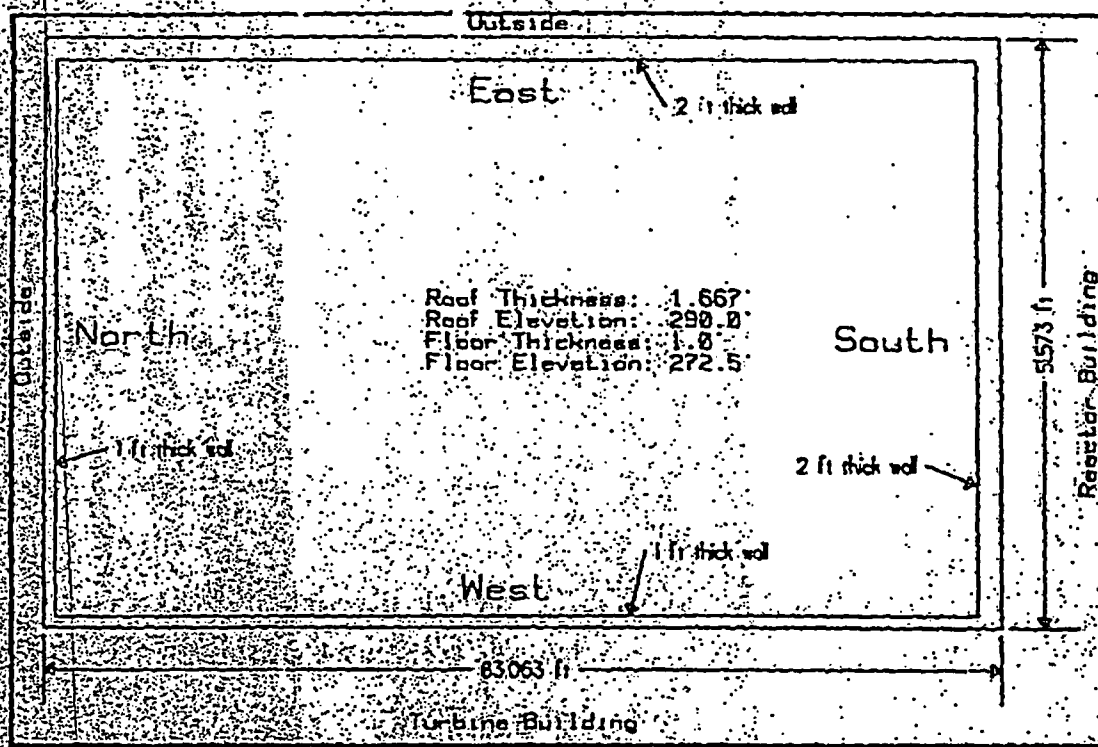


Figure 1: Control Room Schematic, Plan View

was determined to be 8 ft above the Control Room floor by inspection. Because any variations in the height of the ceilings in the office/utility spaces will have such a minor effect on the total Control Room volume, inspection was deemed sufficient for determining ceiling height.

The Control Room total volume is found by summing the individual volumes calculated from the three different ceiling heights. (The floor area of the office/utility region was determined by scaling from the drawing [4], the low drop ceiling area is the balance of the control room floor area.)

High drop ceiling region:  $34 \text{ ft} \times 32 \text{ ft} \times 13.167 \text{ ft} = 14325.7 \text{ ft}^3$

Office/Utility region:  $10.9 \text{ ft} \times 36.737 \text{ ft} \times 8 \text{ ft} = 3204.05 \text{ ft}^3$

Low drop ceiling region:  $[80.063 \text{ ft} \times 48.573 \text{ ft} - (34 \text{ ft} \times 32 \text{ ft} + 10.9 \text{ ft} \times 36.7437 \text{ ft})] \times 10 \text{ ft} = 24004.0 \text{ ft}^3$

Total volume (sum):  $41533.75 \text{ ft}^3$

Elevation = 272.5 ft (floor elevation)

Height = 10.0 ft (rough average ceiling height)

VY Control Room Heating Test Model  
Mon Aug 28 14:08:15 1996  
GOTHIC Version 5.0(QA) - April 1996

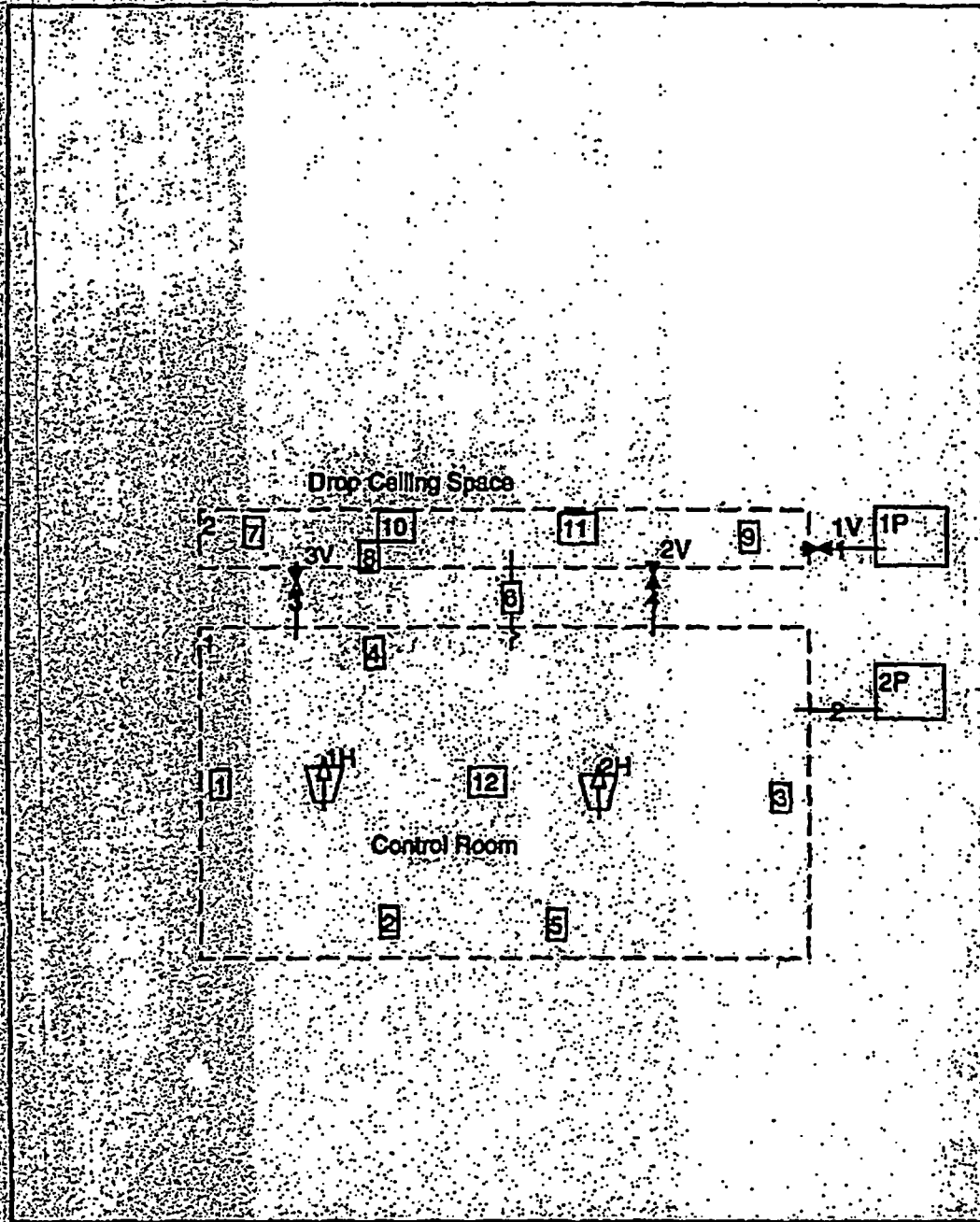


Figure 2 GOTHIC Model Schematic of VY Control Room

It should be noted that the control room has large arrays of cabinets and control panels. Most of the cabinets are open-backed and not fully enclosed. Thus, the free volume of the control room is not reduced for the cabinets. For the control cabinets that are enclosed, it is conservative with respect to the average room temperature, that the cabinets do not reduce the free air space since the heat loads in the control room are, in general, contained within the control cabinets.

The hydraulic diameter is calculated from  $4 \cdot \text{Area} / \text{Wetted Perimeter}$ :

$$4 \cdot (80.063 \cdot 48.573) / (2 \cdot 80.063 + 2 \cdot 48.573) = 60.46 \text{ ft}$$

The volume above the drop ceilings can be found by calculating the total volume of the space enclosed by the concrete walls and subtracting the volume below the drop ceiling, calculated above.

$$\text{Volume Above Drop Ceiling} = 80.063' \cdot 48.753' \cdot 15.833' - 41533.75 \text{ ft}^3 = 20267.4 \text{ ft}^3$$

The elevation of the drop ceiling volume is the elevation of the ceiling in the control room volume:  $272.5 \text{ ft} + 10.0 \text{ ft} = 282.5 \text{ ft}$ .

The height of the drop ceiling volume is the difference between the ceiling elevation (roof elevation minus roof thickness) and the drop ceiling volume elevation:

$$\text{Height} = 290.0 \text{ ft} - 1.667 \text{ ft} - 282.5 \text{ ft} = 5.833 \text{ ft}$$

The hydraulic diameter of this volume is the same as the hydraulic diameter of the control room volume since they share common walls and have the same plan dimensions.

The L/V IA (liquid to vapor interface area) is used to determine condensation or evaporation from any liquid pool to/from any water vapor. No liquid pool or steam is expected to be present in this model (other than the minute quantities of water imposed by the code and the humidity in the air) this value is left to DEFAULT and the actual value calculated by the code is of no real concern.

#### Fluid Boundary Conditions, Tables 1 through 4

Two fluid boundary conditions are included in the model. They are pressure boundary conditions set to atmospheric pressure in order to maintain the control room and drop ceiling volumes at constant, atmospheric, pressure.

The pressure is set to outside, ambient conditions of 14.7 psia and 90°F in accordance with FSAR Section 10.12 (8).

It is expected that the control room model will undergo only heating, no cooling, and will try to pressurize as a result. Since the boundary condition is set to maintain a constant pressure, mass will flow from the control room to the boundary condition to maintain the constant pressure. Since there will be no inflow from the boundary condition, the temperature of the boundary condition is of no consequence.

### Flow Paths, Tables 1 through 3

Four flow paths are specified in the model. Two of these flow paths connect the control room and drop ceiling volumes to their respective fluid boundary condition and the other two connect the drop ceiling volume with the control room volume.<sup>1</sup>

For the flow paths connecting the volumes to the boundary conditions, the connection elevations are set arbitrarily but within the volumes specified. The connection height is set relatively arbitrarily at 2 feet. The flow area is set to a sufficiently large area to ensure that undue pressurization of the model volumes does not occur. Likewise, the hydraulic diameter, inertia length and friction lengths are set to ensure no pressurization. The loss coefficients are set to provide some frictional loss but not sufficient to pressurize the model volumes.

The flow paths connecting the control room volume and the drop ceiling volume are modeled based on about 10 drop ceiling panels being removed to allow air circulation with the drop ceiling volume. Two flow paths are used to model the openings as it allows bidirectional flow through the openings. GOTHIC allows only unidirectional flow through a junction so multiple junctions allow bidirectional flow.

Since hot air rises and the majority of the heat source in the control room is in the control room volume, opening the panels will allow the hot air to rise and the nominally cooler air in the drop ceiling volume to fall. The end connections are at elevations and heights to allow the top of the control room volume to communicate with the bottom of the drop ceiling volume:

Vol A: Elev. = 282 ft; Height = 0.01 ft  
Vol B: Elev. = 283 ft; Height = 0.01 ft

The flow area is 40 ft<sup>2</sup> each based on about 10 panels being removed and the panels are on the order of 2 ft x 4 ft [7].

The hydraulic diameter is based on the individual 2 ft x 4 ft opening:

<sup>1</sup> While the drop ceiling essentially prevents the two volumes from communicating by other than conduction, it will be postulated later that the operators may want to open the drop ceiling panels to allow mixing of air between the control room and the volume above the drop ceiling. Thus, these flow paths are included in the model but will be controlled as appropriate to the scenario.

$$D_h = 4 \cdot A / P_w = 4 \cdot 2 \text{ ft} \cdot 4 \text{ ft} / (2 \cdot 2 \text{ ft} + 2 \cdot 4 \text{ ft}) = 2.667 \text{ ft.}$$

The inertia length is taken to be the vertical distance between the center of the control room volume and the center of the drop ceiling volume:

$$\text{Inertia Length} = 10 \text{ ft} / 2 + 5.833 \text{ ft} / 2 = 7.92 \text{ ft}$$

The friction length is nominally the thickness of the ceiling tile, about 5/8-inch (assumed based on examples of ceiling tile.)

$$\text{Friction Length} = 0.052 \text{ ft}$$

Each flow path (with the exception of the flow paths to the boundary conditions (1 & 4)) has a forward and reverse loss coefficient of 1.5.

This loss coefficient is derived from a sharp-edged exit loss coefficient of 1.0 and a sharp-edged entrance loss coefficient of 0.5. [9]

The flow paths connecting the boundary conditions are given zero loss coefficients so as to minimize the pressure drop from the boundary condition to its connected volume.

### Thermal Conductors

Twelve thermal conductors are modeled:

1. represents the east wall of the control room volume,
2. represents the south wall of the control room volume,
3. represents the west wall of the control room volume,
4. represents the north wall of the control room volume,
5. represents the floor of the control room volume,
6. represents the ceiling tiles of the drop ceiling,
7. represents the east wall of the drop ceiling volume,
8. represents the south wall of the drop ceiling volume,
9. represents the west wall of the drop ceiling volume,

- 10. represents the north wall of the drop ceiling volume,
- 11. represents the roof of the control room volume,
- 12. represents the abstract internal room heat sinks.

The surface areas are calculated

$$\#1 \& \#3 \text{ East/West Wall: } 80.063 \text{ ft} * 10.0 \text{ ft} = 800.63 \text{ ft}^2$$

$$\#2 \& \#4 \text{ North/South Wall: } 48.573 \text{ ft} * 10.0 \text{ ft} = 485.73 \text{ ft}^2$$

$$\#5, \#6 \& \#11 \text{ Floor, Ceiling Tile, Roof: } 48.573 \text{ ft} * 80.063 \text{ ft} = 3888.9 \text{ ft}^2$$

$$\#7 \& \#9 \text{ East/West Wall: } 80.063 \text{ ft} * 5.833 \text{ ft} = 467.0 \text{ ft}^2$$

$$\#8 \& \#10 \text{ South/North Wall: } 48.573 \text{ ft} * 5.833 \text{ ft} = 283.3 \text{ ft}^2$$

The area for the abstract internal room heat sink is used as a variable to match the test data with model results. This process was alluded to in the method description and details of the test and this process will be described in a later section.

These thermal conductors are initialized to the initial control room ambient air temperature, 78°F [Ref. 8 Section 10.12.3]. The conductor temperatures are further initialized to the appropriate linear temperature profile represented by the initial temperatures of the surroundings on either side of the conductor. This is accomplished by the appropriate setting of the DT Ratio in the Run Control Parameters table discussed later. In essence, a large number of conduction equation iterations are performed for each iteration of the hydrodynamic equations. This has the effect of forcing the thermal conductors to an equilibrium with the fluid and boundary conditions surroundings without affecting the transient hydrodynamic solution.

For the heat transfer coefficients, for those thermal conductors that are considered internal conductors, the Volume A connection is considered the "outside" surface and the Volume B connection is the interior surface. The heat transfer coefficients for the control room inside surfaces are natural convection correlation coefficients. For the walls (#1 - #4 & #7 - #10) these are the correlations for vertical surfaces. For the ceiling regions (#6 on Volume A side and #11) the correlation for face down horizontal surfaces is used. The floor (#5) and the top of the drop ceiling tiles (#6 on Volume B side) uses the correlation for face up horizontal surfaces. The abstract internal room heat sink uses a vertical surface natural convection coefficient correlation as it is assumed that the most likely orientation for the internal room heat sinks is vertical.

The exterior surfaces (Volume A connections for thermal conductors #1 - #5 & #7 - #11) use an assumed natural convection heat transfer coefficient representative of their orientation coupled with a specified temperature boundary condition based on the expected temperatures of the adjoining spaces be they the reactor building, turbine building or outside air.

The specific values used for the heat transfer coefficients are explained further in the next section.

#### Heat Transfer Coefficients, Tables 1 through 4

Heat transfer coefficients 1, 2 & 3 are the natural convection correlation coefficients corresponding to a vertical, face up or face down surface, respectively. These are used with no modification.

Heat transfer coefficient 4, 5 & 6 are general natural convection heat transfer coefficients. These coefficients are used in the description of the outside surface heat transfer coefficients for which specified ambient temperatures are included. GOHIC does not allow one to choose a correlation coefficient when using a specified temperature. The values of these coefficients were based on a general 10°F temperature difference between the wall surface and the ambient air. The heat transfer coefficient correlations of interest are given by [10]:

$$h = 0.19 (\Delta T)^{0.33} \quad \text{for vertical plates in the turbulent range,}$$

$$h = 0.22 (\Delta T)^{0.33} \quad \text{for horizontal plates facing upward when heated in the turbulent range}$$

$$h = 0.12 (\Delta T/L)^{0.25} \quad \text{for horizontal plates facing downward when heated in the turbulent range}$$

where  $h$  is in units of BTU/hr-ft<sup>2</sup>-°F,  $\Delta T$  is in units of °F and  $L$  is in units of feet.

Given the specified  $\Delta T$  (10°F):

$$\text{vertical plates:} \quad h = 0.406 \text{ BTU/hr-ft}^2\text{-°F}$$

$$\text{horizontal plates facing upward:} \quad h = 0.470 \text{ BTU/hr-ft}^2\text{-°F}$$

$$\text{horizontal plates facing downward:} \quad h = 0.071 \text{ BTU/hr-ft}^2\text{-°F}$$

Due to the thickness of the concrete wall structures, the heat transfer coefficients chosen have little to no effect on the short transient results. In addition, conservatively high outer exposure ambient temperatures are chosen.

Use as "L" of 80.063 ft, the longest length of the control room.

The boundary conditions for the outside wall (and roof and floor) surfaces consist of specified heat transfer coefficients with a constant ambient temperature. For those walls with outdoor exposure, an average temperature was chosen based on the SOLAIR method of taking into account solar heating of the walls and long-wave radiation from the surroundings. [10] The SOLAIR method and temperatures for the north wall, east wall and roof have been calculated previously [11]. Table 1 provides the 24 hour transient SOLAIR temperature for the three surfaces. The last value in the temperature columns is the average temperature.

Table 1 - 24 Hour SOLAIR Temperatures

Time of Day	North Wall Temp.	East Wall Temp.	Roof Temp.
1500	90.00	90.00	172.8
1600	89.28	89.28	146.8
1700	87.60	87.60	117.7
1800	84.96	84.96	91.3
1900	81.84	81.84	81.84
2000	78.72	78.72	78.72
2100	76.08	76.08	76.08
2200	73.68	73.68	73.68
2300	71.76	71.76	71.76
2400	70.32	70.32	70.32
0100	69.12	69.12	69.12
0200	67.92	67.92	67.92
0300	66.96	66.96	66.96
0400	66.24	66.24	66.24
0500	66.00	77.5	66.00
0600	66.48	110.9	71.5
0700	67.68	142.0	97.3
0800	69.84	155.9	127.6
0900	72.96	151.2	156.0
1000	76.56	132.7	178.8
1100	80.64	107.1	194.5

An implicit assumption by using these SOLAIR temperature values is that the control room building has a similar color ("light" as opposed to "dark") as the reactor building.

These values, as stated previously, were developed for the reactor building. Since the control room building is north of the reactor building and the reactor building is much taller than the control room building, it is expected that the roof temperatures would be much lower if shading were taken into account. Thus, the roof temperatures are highly conservative as they will result in less heat removal from the control room and thus, a higher control room temperature.



Time of Day	North Wall Temp.	East Wall Temp.	Roof Temp.
1200	84.48	84.48	202.3
1300	87.36	87.36	201.2
1400	89.28	89.28	191.3
Average	76.49	92.2	114.1

The average SOLAIR temperature was used rather than the transient temperature for ease of analysis. Due to the thick concrete (low thermal conductivity) of the walls and roof the effect of any transient temperature is sufficiently damped that the control room space is, in essence, seeing the effects of an average temperature.

The west wall of the control room is adjacent to the turbine building. From the FSAR, the maximum design temperature of the turbine building is 105°F. However, the hallway immediately outside the control room is an office hallway and as such will not be subject to the same temperature as the turbine deck. For conservatism, the hallway outside the control room is set to the control room temperature (the implicit assumption is that the outside hallway loses ventilation at the same time as the control room and heats up in a manner similar to the control room.) This minimizes heat loss from the control room resulting in a conservative calculation.

The south wall of the control room is adjacent to the reactor building. From the FSAR, the maximum design temperature of the reactor building is 100°F. Thus, the temperature boundary condition heat transfer coefficient is 11 in 100°F [Ref. 8 Section 10.12.3].

Below the control room floor is the cable vault and battery room. The air temperature in these areas is maintained by the same HVAC system as the control room. Thus, when the control room experiences a loss of HVAC, the cable vault and battery room lose HVAC. The temperature of the floor surface external to the control room is taken to be the temperature of the control room. As with the turbine building wall, the assumption is that the cable vault and battery room heat up at the same rate as the control room.

#### Thermal Conductor Types

There are six thermal conductor types required for this model:

1. 1 ft thick concrete slab (North & West walls and Floor)
2. 2 ft thick concrete slab (East Wall)
3. 1.667 ft thick concrete slab (Roof)

4. 4 ft thick concrete slab (South Wall)
5. 5/8" thick ceiling tile
6. 12 gage steel for abstract internal thermal conductor

The GOTHIC automatic subdivision routine is described in the GOTHIC User Manual. It automatically generates mesh points in a thermal conductor given constraints (starting and ending point, i.e. slab edges, and material boundaries) and qualitative assessments of the slab side heat transfer coefficients. For all slab sides the qualitative assessment of the heat transfer coefficient is VERY LOW. Each region is divided into 10 subregions.

The south wall represents both the control room south wall, 2 feet thick [7] and the adjacent reactor building north wall, also 2 feet thick [12]. This results in a total thickness of 4 feet.

### Materials

Three materials are used in the GOTHIC model: concrete, acoustic tile and abstract thermal conductor material.

For all three materials they are assumed to have constant physical properties and for the range of expected temperatures (65°F to < 200°F) this is a good assumption.

Concrete is Material Type 1.

Density = 142 lbm/ft<sup>3</sup> [13] Table 4.4.3  
 Thermal Conductivity = 1.05 BTU/hr-ft-°F [13] Table 4.4.3  
 Specific Heat = 0.156 BTU/lbm-°F [13] Table 4.2.25

Acoustic Tile is Material Type 2. [10] Chapter 22, Table 4, Mineral fiberboard, wet felted acoustical tile<sup>3</sup>

Density = 18.0 lbm/ft<sup>3</sup>  
 Thermal Conductivity = 0.0292 BTU/hr-ft-°F  
 Specific Heat = 0.19 BTU/lbm-°F

<sup>3</sup> This acoustical tile was chosen because specific information on the tile in the control room was not available and this tile represented the worst case in terms of thermal conductivity.

Abstract Thermal Conductor is Material Type 3 (steel was used as the basis for this thermal conductor since a visual inspection of the control room gives the impression that the majority of the internal conductor is steel in the form of thick cabinets.)  
[13, pg 6-11, Steel, AISI C1020]

Density = 490.1 lbm/ft<sup>3</sup>  
Thermal Conductivity = 27 BTU/hr-ft-°F  
Specific Heat = 0.10 BTU/lbm-°F

### Coolers/Heaters

Two different heaters are modeled. These are:

1. Electrical Heat Load
2. Occupants; 1833 BTU/sec

The electrical heat load is determined and justified in Section 4.2.

The average number of occupants in the control room during the transient in question is assumed to be 12. The heat load per person is taken as 550 BTU/hr.  
[10] (Chapter 26, Table 3)

### Volumetric Fans

A volumetric fan component is included in the model. This fan component does not represent an actual installed fan but is used to simulate the effects of the operators removing the ceiling tile panels allowing the air in the drop ceiling space to intermix with the air in the balance of the control room. As such, the input values in the volumetric fan tables are chosen arbitrarily but with sufficient air flow to ensure that the air in the two volumes is mixed thoroughly.

### Valves & Doors

Three valves are included in the model. They are used to model the opening of the ceiling tiles by the operators. Trips are used to control the time that this occurs. When the ceiling tiles are postulated to be removed, the quick open valves are opened to allow the exchange of air between the two volumes.

One valve, quick close type, is included to prevent more than one pressure boundary condition from being active at any one time. When the flow paths between the control room volume and the ceiling tile volume are opened, the flow path to one of the boundary conditions is shut off to prevent the boundary conditions from interacting.

No loss in any of the valves is included as the desired losses are included in the flow paths. The flow area is taken to be large so as not to provide any more restrictive an opening than the valve's associated flow path.

### Component Trips

Trips are used to control the valves and the volumetric fan. It is postulated that the operators will take action to open the ceiling tiles when the control room temperature reaches 110°F.

### Functions

One function is defined which converts the control variable into a form which can be used as a forcing function for the components described previously.

### Control Variables

The defined control variable is used to get the control room temperature so that it can be passed to a function to be used as a forcing function for the components described previously.

### Volume Initial Conditions

All volumes are set to 78°F initially but can be modified based upon the given scenario requirements. The humidity is not expected to have any significant effect but is set to the design value of 50% RH [Ref. 8 Section 10.12.3].

### Run Control Parameters

Four time intervals are defined. The first time interval is very short with respect to the rest of the transient and is used to set the initial temperature profile in the thermal conductors. By setting the DT Ratio to a large value (10<sup>6</sup>), the conduction equation is solved to convergence within a very short time (with respect to the transient.)

The second and third time intervals define the transient period for determining the temperature profile in the room. They were chosen to bound the period of interest (the first ten minutes) of the scenarios.

The fourth time interval is used to determine a pseudo steady-state temperature for the scenario. It uses the large DT Ratio to drive the conduction equations to convergence and a long transient time allows the hydrodynamic equations to reach equilibrium sooner. While the solution during this time interval is not accurate in the time domain, it results in a steady-state temperature within a reasonable calculation time.

### 3.2 Assumptions

The assumptions used in this calculation are presented in separate sections as there are some explicit and implicit assumptions that apply to the GOTHIC model and those that apply to the test data interpretations and calculations associated with the test data.

#### 3.2.1 GOTHIC Model Assumptions

In describing the basic control room model GOTHIC input several explicit assumptions were made. They are listed here for reference.

1. The hallway outside the control room and the cable vault/battery room lose HVAC at the same time as the control room and experience the same temperature transient as the control room.
2. When the temperature in the control room reaches 110°F the operators have removed sufficient acoustic tiles in the ceiling such that the two model volumes are now the equivalent of one volume.

#### 3.2.2 Control Room Heat Load Calculation Assumptions

In the calculation of control room heat load that follows, there are several explicit and implicit assumptions. They are listed here for reference.

1. Infiltration, exfiltration and heat losses through the ducting are negligible or ignored. This assumption is necessitated by the lack of information available to assess the degree of infiltration, exfiltration or ducting losses. Infiltration is considered negligible since the control room HVAC system is designed to be able to provide adequate ventilation during various accident conditions where excessive infiltration would lead to excessive radiation doses to the operators. Since the paths for exfiltration are the same as the paths for infiltration and infiltration is assumed to be negligible, the same conclusion can be made for exfiltration. Ducting heat losses are ignored as the temperature differences between the air in the ducts and the external air during the tests were low.

However, a 10 percent increase in control room heat load will be taken to account for any non-conservatism present due to this assumption. [14]

2. When the temperature in the control room reaches 110°F, the operators take action to remove sufficient acoustic ceiling tiles (10 or more is assumed in this calculation) to allow air in the drop ceiling space to mix with the control room air and vice versa.

3. At four hours after the loss of HVAC, action is taken to mitigate the temperature rise. Two possibilities are postulated:

- a. temporary ventilation is provided that brings in at least 6600 cfm of outside air (90°F).
- b. temporary ventilation is provided that brings in at least 3000 cfm of outside air (90°F) and heat load in the control room is reduced by 52 percent.

These conditions were chosen based on their ability to maintain the control room at or less than 120°F.

## 4.0 Calculation

The calculation is divided into several sections. The objective of the calculation is to calculate the control room transient temperature following a loss of ventilation due to an Appendix R event. The physical configuration and model of the control room has been described in Section 3.1. Two other pieces of information are required to complete the model: control room heat load and control room internal heat sink characterization. Tests were conducted on the HVAC system and the data that was taken can be used to characterize both the heat load and the internal heat sinks.

Section 4.1 gives a detailed description of the data used to calculate the control room heat load and the actual calculation of that heat load. Section 4.2 uses the heat load information as well as the control room GOTHIC model and test data to characterize the control room internal heat sinks. Section 4.3 uses both pieces of information to assess the control room heatup transient following an a loss of ventilation due to an Appendix R event. Section 4.4 provides two additional analyses given postulated long-term corrective actions to mitigate the loss of HVAC transient.

### 4.1 Control Room Heat Load Calculation

Two independent tests were conducted that obtained data that can be used to characterize the control room heat load. Both tests took temperature measurements at the inlet and outlet of the control room ventilation ductwork and an air flow measurement in the HVAC ductwork. This information can be used to calculate the control room heat load.

Neither test was performed using instruments in a calibration program nor were they performed using a properly QA'ed test procedure. However, they were performed by qualified personnel and using standard instruments. In addition, they were performed completely independently. In combination, they provide a sufficient basis for judging the control room heat load.

#### 4.1.1 Heat Load Test 1

This test data was taken in response to the necessity to characterize the heat load and heatup characteristics of the control room [14]. Data was taken with the control room HVAC system in recirculation mode. The air flow measurement was taken on the inlet side of the control room. Only drybulb temperatures were taken at the supply and return points so for the calculation of heat load, some humidity will have to be assumed.



The following data was obtained for air flow through the control room :

Air Flow = 8597 cfm +/- 10%  
 Supply Air Temperature = 55 °F db  
 Return Air Temperature = 73 °F db

The following equations are the result of simple mass and energy balance relations. They are conveniently outlined in ASHRAE Fundamentals. [10]

The heat input from the control room is given by:  $q = m_a(h_2 - h_1)$

where  $q$  = heat added to moist air between points 1 and 2  
 $m_a$  = mass flow of dry air per unit time  
 $h_2$  = enthalpy of moist air at point 2, BTU/lb dry air  
 $h_1$  = enthalpy of moist air at point 1, BTU/lb dry air

Assuming the incoming air was at 60% RH (from test data), the enthalpies are given by:

$$\phi = \frac{p_v}{p_{ws}}$$

$$W = 0.62198 \frac{p_v}{p - p_v}$$

$$h = 0.240t + W(1061 + 0.44t)$$

where  $\phi$  = relative humidity, dimensionless  
 $p_v$  = partial pressure of water vapor in moist air, psia  
 $p_{ws}$  = pressure of saturated water  
 $W$  = humidity ratio  
 $p$  = total pressure of moist air  
 $h$  = enthalpy of moist air, BTU/lb dry air  
 $t$  = dry bulb temperature, °F

For  $h_2$ 

$$\phi = 0.60$$

$$p_{ws} = 0.0217 \text{ psia (at } t = 73 \text{ F)}$$

$$p_v = \phi p_{ws} = 0.241302 \text{ psia}$$

$$p = 14.7 \text{ psia}$$

$$W = 0.62198 \frac{0.241302}{14.7 - 0.241302} = 0.01038$$

$$h_2 = 28.87 \text{ BTU/lb dry air}$$

During this test it will be assumed that the vapor load on the control room is negligible. Thus the mole fraction of water in the air stream is constant so the humidity ratio would be constant and  $h_1$  can be calculated.

$$W = 0.01038$$

$$h_1 = 0.240 \cdot 55 + 0.01038(1061 + 0.444 \cdot 55)$$

$$h_1 = 24.47 \text{ BTU/lb dry air}$$

Thus, the energy added to the air from heat sources in the control room is given by:

$$q = m_a (h_2 - h_1)$$

$$m_a = \frac{V}{v}$$

$$v = 12.970 \frac{\text{ft}^3}{\text{lb dry air}}$$

$$V = 8597 \frac{\text{ft}^3}{\text{min}}$$

$$q = \frac{8597}{12.970} (28.87 - 24.47) = 2916.6 \text{ BTU/min or } 175,000 \text{ BTU/hr or } 48.61 \text{ BTU/sec}$$

This value for the control room heat load could be at least +/- 10% based on the uncertainty in the air flow measurement.

#### 4.1.2 Heat Load Test 2

To help confirm the heat load that was calculated in the previous section the control room heat load is calculated from data included in a memorandum that reported a control room HVAC reliability study [15]. Attachment 5 of the reference includes data taken on the HVAC system. The data sheets are included in Appendix C.

The data on the HVAC system is more complex than the data taken for and used in the previous section. Some explanation of the control room HVAC system is in order.

Figure 3 gives a schematic view of the control room HVAC system [Ref. 8, Figure 10.12-2][16]. The data from the HVAC reliability study gives enough information to determine the conditions of the air around the system and to determine the heat load of the control room.

Return air flow,  $V_7 = 8681$  cfm

Exhaust air flow,  $V_{\text{exhaust}} = 300$  cfm from exhaust fans [Ref. 8, Figure 10.12-2]

Control Room return air dry bulb temperature,  $T_{\text{db}} = 73.1$  °F

Control Room return air wet bulb temperature,  $T_{\text{wb}} = 60.3$  °F

Control Room supply air dry bulb temperature,  $T_{\text{db}} = 54.4$  °F

Control Room supply air wet bulb temperature,  $T_{\text{wb}} = 51.6$  °F

The control room heat load can be determined from this information. First, calculate the mass of air flowing through the control room:

$$V_7 = 8681 \text{ cfm}$$

$$V_6 = V_7$$

$$V_6 = V_7 + V_{\text{exhaust}}$$

$$= 8681 \text{ cfm} + 300 \text{ cfm} = 8981 \text{ cfm}$$

$$v_6 = 13.4275 \frac{\text{ft}^3}{\text{lb dry air}}$$

$$\dot{m}_a = \frac{V_6}{v_6}$$

$$= \frac{8981}{13.4275} = 668.85 \text{ lb dry air/minute}$$

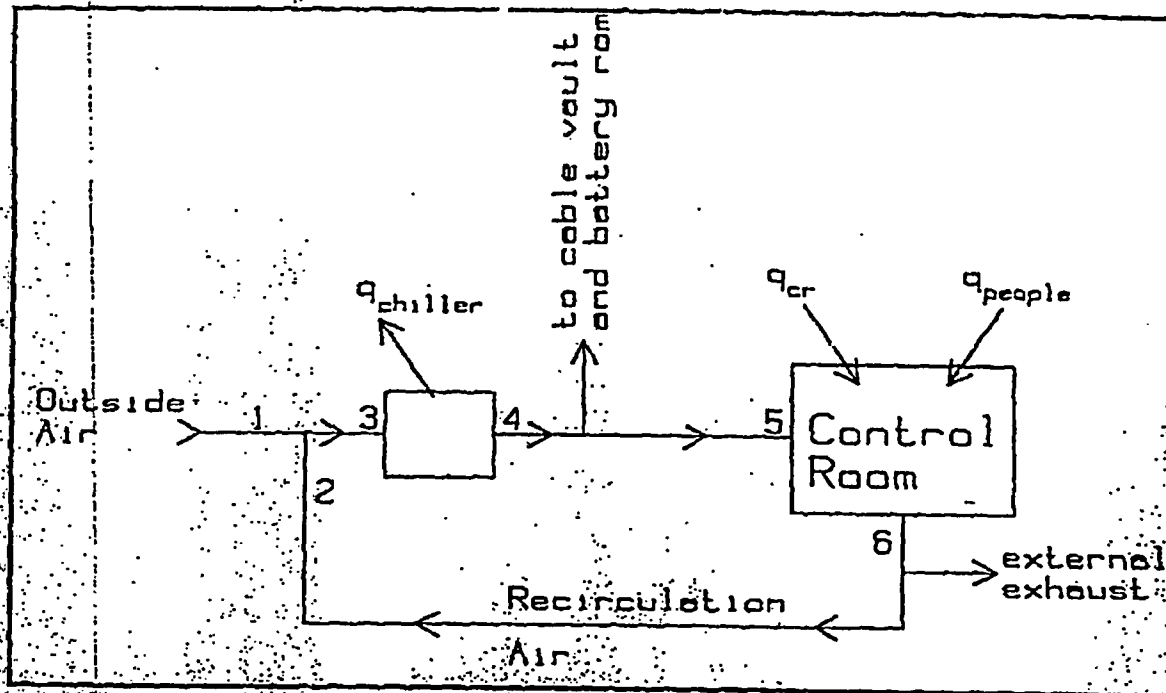


Figure 3 Control Room HVAC Schematic

Then, determine the enthalpies and humidity ratio of the entering and leaving air:

$$h = 0.240t + W(1061 + 0.444t)$$

$$W = \frac{(1093 - 0.556t) W_s - 0.240(t - t^*)}{1093 + 0.444t - t^*}$$

where  $t^*$  = thermodynamic wet-bulb temperature, °F

$W_s$  = humidity ratio at saturation based on wet-bulb temperature  
(from ASHRAE table.)

specifically, at the inlet:

$$\begin{aligned}t &= 54.4^{\circ}\text{F} \\t^* &= 51.6^{\circ}\text{F} \\W_s^* &= 0.0081374\end{aligned}$$

$$\begin{aligned}W &= \frac{(1093 - 0.556t^*)W_s^* - 0.240(t - t^*)}{1093 + 0.444t - t^*} \\&= \frac{(1093 - 0.556 \cdot 51.6) \cdot 0.0081374 - 0.240 \cdot (54.4 - 51.6)}{1093 + 0.444 \cdot 54.4 - 51.6} \\&= 7.8533 \cdot 10^{-3}\end{aligned}$$

$$\begin{aligned}h_s &= 0.240t + W(1061 + 0.444t) \\&= 0.240 \cdot 54.4 + 7.8533 \cdot 10^{-3} \cdot (1061 + 0.444 \cdot 54.4) \\&= 21.578 \text{ BTU/lb dry air}\end{aligned}$$

and at the outlet:

$$\begin{aligned}t &= 73.1^{\circ}\text{F} \\t^* &= 60.3^{\circ}\text{F} \\W_s^* &= 0.0112097\end{aligned}$$

$$\begin{aligned}W &= \frac{(1093 - 0.556t^*)W_s^* - 0.240(t - t^*)}{1093 + 0.444t - t^*} \\&= \frac{(1093 - 0.556 \cdot 60.3) \cdot 0.0112097 - 0.240 \cdot (73.1 - 60.3)}{1093 + 0.444 \cdot 73.1 - 60.3} \\&= 8.2658 \cdot 10^{-3}\end{aligned}$$

$$\begin{aligned}h_o &= 0.240t + W(1061 + 0.444t) \\&= 0.240 \cdot 73.1 + 8.2658 \cdot 10^{-3} \cdot (1061 + 0.444 \cdot 73.1) \\&= 26.582 \text{ BTU/lb dry air}\end{aligned}$$

and the total heat addition to the air stream from the control room is:

$$q_{cr} = m_a (h_6 - h_5)$$

$$m_a = 668.85 \text{ lb dry air/minute}$$

$$h_6 = 26.582 \text{ BTU/lb dry air}$$

$$h_5 = 21.578 \text{ BTU/lb dry air}$$

$$q = 668.85 (26.582 - 21.578) = 3346.9 \text{ BTU/min or } 200,815 \text{ BTU/hr or } 55.78 \text{ BTU/sec}$$

The uncertainties in this value of control room heat load are not entirely known since uncertainty values are not directly attributable to the instruments used.

#### 4.1.3 Determination of Limiting Control Room Heat Load

Two values for control room heat load have been calculated using independent methods, instrumentation and personnel. The values obtained are: 175,000 BTU/hr and 200,815 BTU/hr. The latter value was determined with data taken on a warm day in mid-July. The former value was obtained on a cool day in late May. Variations in solar heat load, electrical load, occupancy and instrument accuracy can account for this difference. Each of these values includes heat load from conduction into or out of the control room through the control room walls and occupancy heat load. Thus, there is an inherent conservatism in these values since their use in GOTHIC models will be as electrical loads (conduction and occupancy being explicit inputs in the GOTHIC model input.)

Therefore, to ensure a bounding value for control room heat load is used, the average of the two values + 10 % will be the control room heat load used for determining the control room transient temperature response to a loss of HVAC due to an Appendix R fire event. This is considered bounding based on the information received regarding the potential electrical loads in the control room: (14)

$$q_{cr} = (175000 + 200815) / 2 * 1.1 = 206,700 \text{ BTU/hr or } 57.42 \text{ BTU/sec}$$

#### 4.2 Characterization of Abstract Heat Conductor

As mentioned previously, the transient temperature of the control room due to a loss of HVAC depends on two important factors: the heat load in the control room and the internal heat absorbing structures. This section attempts to characterize the internal heat absorbing structures as a GOTHIC heat conductor using test data obtained during a control room heatup test.

In a heated room, the transient temperature rise is predicated on two major factors: the heat load and the heat absorbing structures. For the control room, the previous sections have identified the heat load. Thus, to be able to predict the transient temperature profile, the heat absorbing structures must be able to be modeled. However, the control room has a very complex array of heat absorbing structures (cabinets, panels, etc.) making it difficult to model with accuracy. Thus, a test was performed to gather data (temperature rise versus time and heat load) that can be used to characterize the heat absorbing structures.

In the previous sections, the control room heat load during the test is characterized. Given this heat load and known ambient conditions, it is possible to modify the GOTHIC model developed previously to attempt to model the test conditions. An abstract internal heat conductor can be included in the GOTHIC model of the test. By varying the surface area of the abstract heat conductor it is possible to match the transient test data and thus have a fairly good representative internal conductor model for use in later control room heatup analyses.

The test data is a series of temperatures at different locations within the control room taken over a period of about 35 minutes. Because the control room is a three-dimensional structure with air currents and localized heat sources (lights, relays, power supplies, etc.) but the GOTHIC representation of the control room is one dimensional (a lumped parameter volume) it is not expected that the GOTHIC model will match the test results exactly. However, to adequately characterize the internal heat conductors, matching the slope of the temperature rise will be sufficient. It was found that the slope of the temperature rise was fairly constant over the different locations of the temperature readings. In fact, it was much more constant than the absolute temperatures between locations.

The test data is included in Appendix D. The test data is plotted in Figure 4, Figure 5 and Figure 6 along with lines showing the least squares linear data fit for each of the data sets. The following equations are used to obtain the least squares fit. Note that since the slope is the only variable of concern, only the slope is calculated.

### Vermont Yankee Control Room Heatup Test

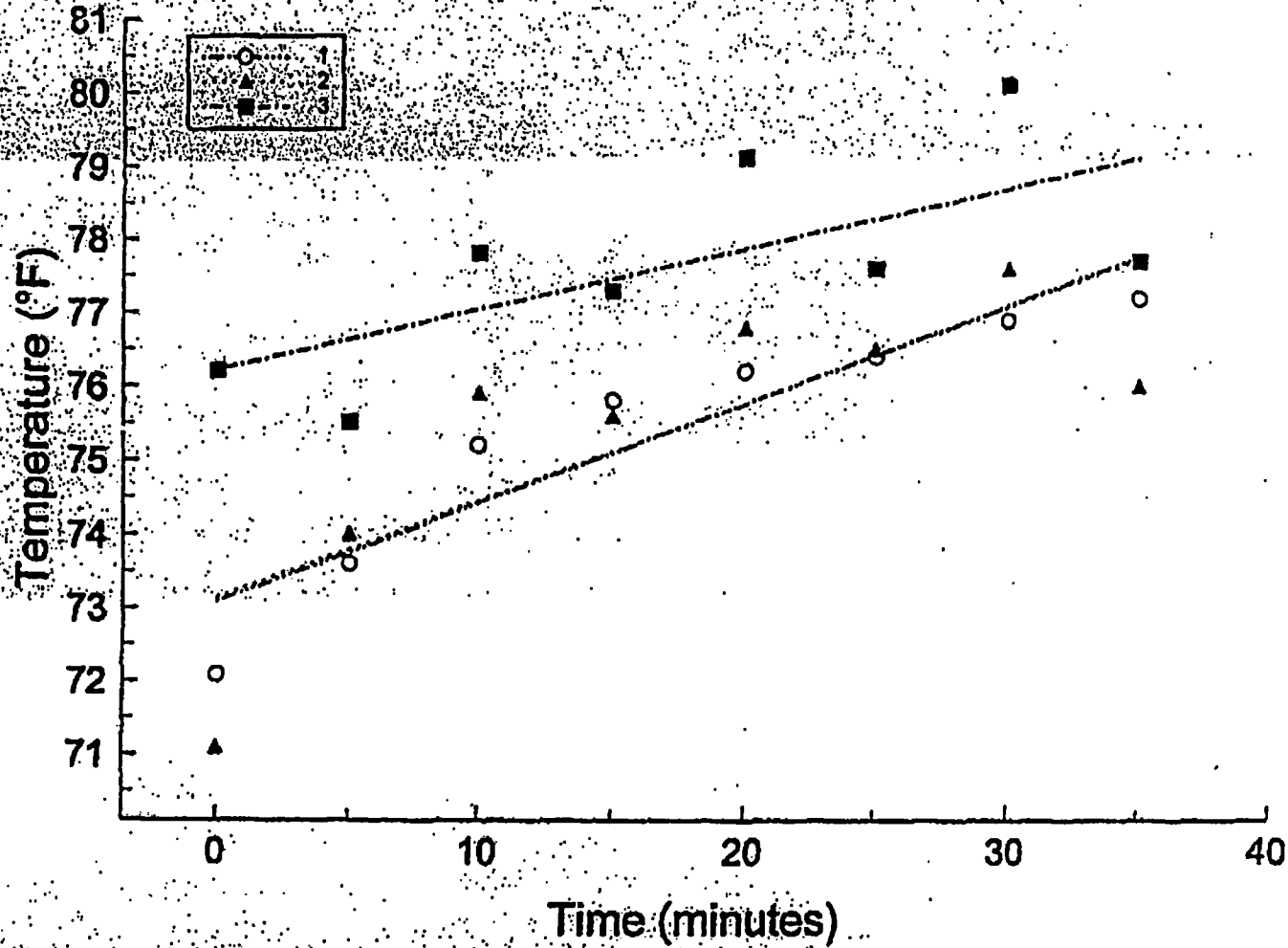


Figure 4 Control Room Heat Up Test, Data Sets 1, 2 & 3



Cell D: Page: Vermont Atomic Electric Co. Aug. 24, 1959, 1242-1174

### Vermont Yankee Control Room Heatup Test

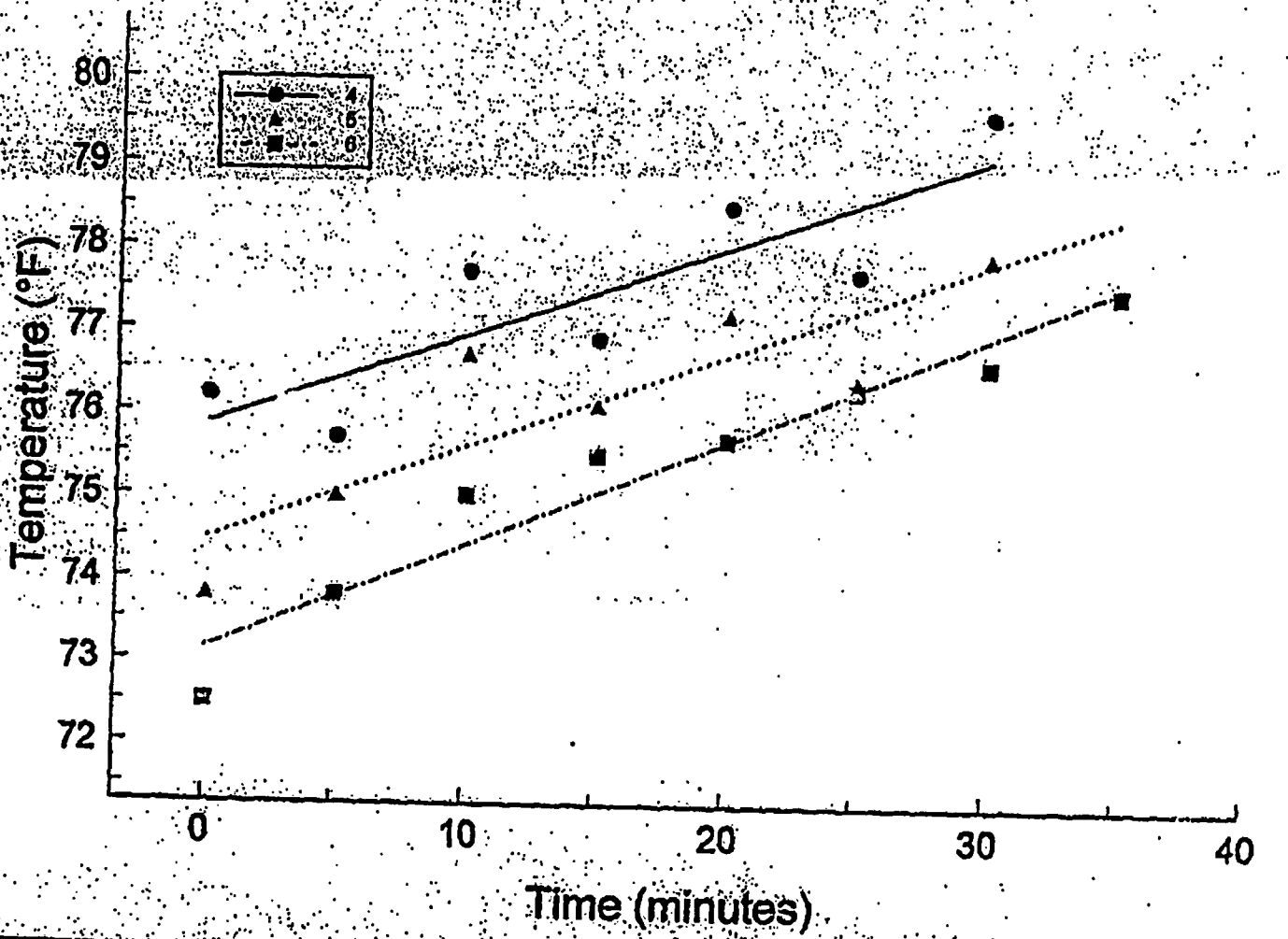
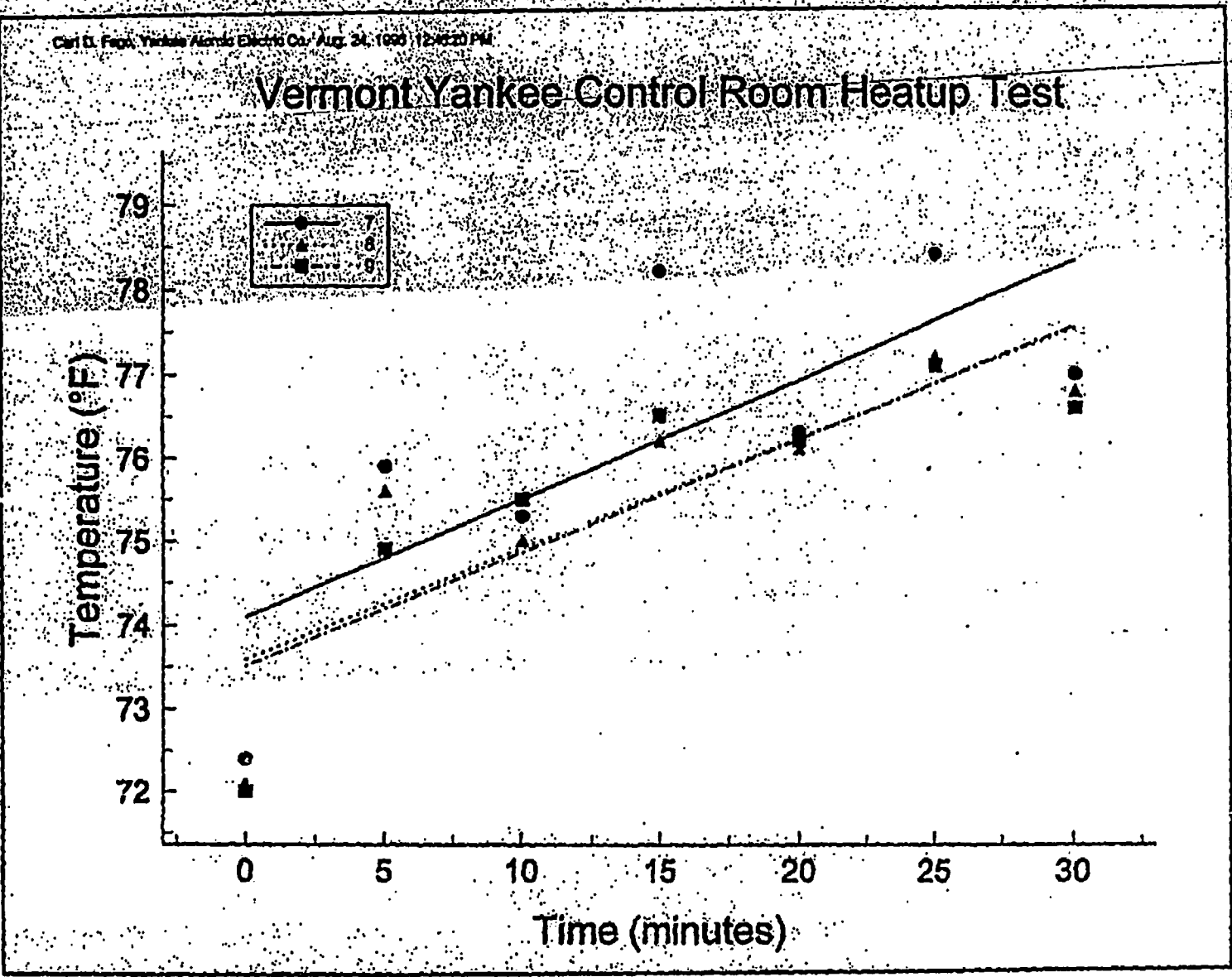


Figure 5 Control Room Heat Up Test, T ma Sets 4, 5 & 6

Control Room Heatup due to Loss of HVAC; VYC-1502 Rev. 0

Figure 6 Control Room Heat Up Test, Data Sets 7, 8 & 9



$$y = mx + b$$

$$\text{where } m = \frac{N \sum_{i=1}^N x_i y_i - \left( \sum_{i=1}^N x_i \right) \left( \sum_{i=1}^N y_i \right)}{N \sum_{i=1}^N x_i^2 - \left( \sum_{i=1}^N x_i \right)^2}$$

$$b = \frac{\left( \sum_{i=1}^N x_i^2 \right) \left( \sum_{i=1}^N y_i \right) - \left( \sum_{i=1}^N x_i y_i \right) \left( \sum_{i=1}^N x_i \right)}{N \sum_{i=1}^N x_i^2 - \left( \sum_{i=1}^N x_i \right)^2}$$

Putting the data for the first data set in the equation for m gives:

i	x	y	x <sup>2</sup>	xy
1	0	72.1	0	0
2	5	73.6	25	368
3	10	75.2	100	752
4	15	75.8	225	1137
5	20	76.2	400	1524
6	25	76.4	625	1910
7	30	76.9	900	2307
8	35	77.2	1225	2702
Sums	140	603.4	3500	10700

$$m_1 = \frac{8 \cdot 10700 \text{ } ^\circ\text{F} \cdot \text{min} - 140 \text{ } ^\circ\text{F} \cdot 603.4 \text{ min}}{8 \cdot 3500 \text{ min}^2 - (140 \text{ min})^2}$$

$$= 0.1338 \text{ } ^\circ\text{F}/\text{min}$$

The balance of the data can be similarly manipulated and the results are:

Data Set	Slope
1	0.1338 °F/min
2	0.1317 °F/min
3	0.08262 °F/min
4	0.1057 °F/min
5	0.1114 °F/min
6	0.1264 °F/min
7	0.1414 °F/min
8	0.1314 °F/min
9	0.1350 °F/min

Each slope represents rate of temperature increase in a local region in the control room. As such, it is determined in part by the heat load and the internal heat conductors in that local region. Since other test data has given the average heat load in the control room during the test (Section 4.1.1), the average of these slopes will give a representation of the combined average effect of all the heat conductors in the control room.

Average slope = 0.12216 °F/min

This, then is the target slope of the transient temperature curve for the GOTHIC model. The modifications and additions to the initial input model are:

- Thermal Conductors - #12 abstract heat sin :: Area = 25,000 ft<sup>2</sup>
- Thermal Conductors - all initial temperatures at 73.16 °F<sup>6</sup>
- Heat Transfer Coefficients - all temperature boundary conditions set to 70°F to represent the relatively mild conditions in the rooms adjacent to the control room and the outdoor air temperature (partly cloudy day based on the test data.)<sup>7</sup>
- Coolers/Heaters - Heater #1 (electrical load) set to 48.61 BTU/sec based on results from Section 4.1.1; Heater #2 (occupants) set to 3.25 BTU/sec based on 30 seated occupants at 390 BTU/hr [14][10].
- Volumetric Fan - On trip set to 10<sup>6</sup> seconds, off trip set to 0 seconds (no opening of ceiling tiles.)
- Valves & Doors - On trip set to 10<sup>6</sup> seconds, off trip set to 0 seconds (no opening of ceiling tiles.)
- Volume Initial Conditions - Volume 1 (Control Room) set to 73.16 °F<sup>6</sup>, Volume 2 (Drop Ceiling Space) set to 72.1 °F to match Time 0 test data.

<sup>6</sup> Average Time 0 air temperature from the test data.

<sup>7</sup> The outside wall temperatures have little effect on the calculation of transient temperature with a transient of only an hour. The only effect that outside temperatures would have is on the initial temperature profile through the wall which would affect the wall heating at the inside surface. For any reasonable range of wall temperature profiles that could be postulated given the test conditions, the effect on room heat up is negligible.

- Run Control Parameters - the test lasted for 35 minutes; the GOTHIC problem will run for 60 minutes to be able to cover the test period and see any short term trends.

The GOTHIC input tables for this model are included in Appendix A. The GOTHIC output results are included on microfiche under the filename "CONTROL.SOT".

The results from this run are shown in Figure 7 and Figure 8. The temperature plot shows an initial sharp increase in temperature followed by a shallower but steady increase. The initial sharp increase in temperature is not readily seen in the test data but can be explained by the behavior of the heat transfer coefficients in the code. Initially, the differential temperature across boundary layers on all the heat conductors is very small. This leads to a very small heat transfer coefficient which is based on differential temperature (the correlation heat transfer coefficients). Thus, initially, very little heat is removed from the vapor phase in the model. Thus, this initial heatup is very similar to an adiabatic heatup of the room.

As the room heats up, the heat transfer coefficient on the heat conductor surfaces increases as shown in the heat transfer coefficient plot. Shortly, the conductance of the heat structures dominates the heat transfer phenomena and mitigates the control room temperature rise. The slope of this controlled temperature rise is calculated from GOTHIC output information:

At 1105 seconds,  $T = 82.55$  °F. At 3600 seconds,  $T = 87.67$  °F.

Slope =  $(87.67$  °F -  $82.55$  °F) / (3600 sec - 1105 sec) \* 60 sec/min =  $0.1231$  °F/min

Compared with the test slope of  $0.12216$  °F/min, the result is within 1% of the desired slope.

Thus, an abstract internal heat conductor with an exposed area of  $25,000$  ft<sup>2</sup> on a side will adequately model the internal heat conductors within the control room. However, for conservatism, this area is reduced by 10% (to  $22,500$  ft<sup>2</sup>) for use in subsequent analyses.

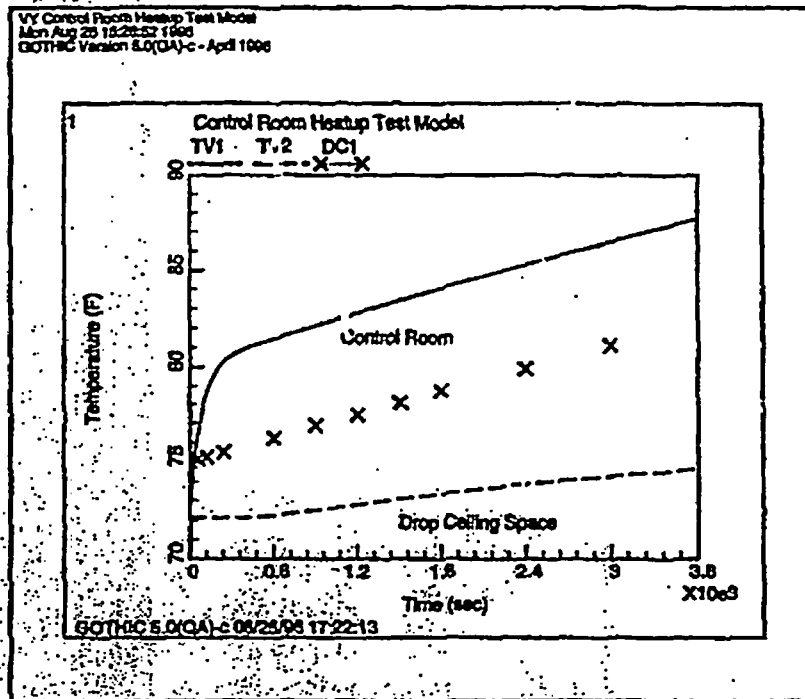


Figure 7 Control Room Heatup Test Model, Volume Vapor Temperatures

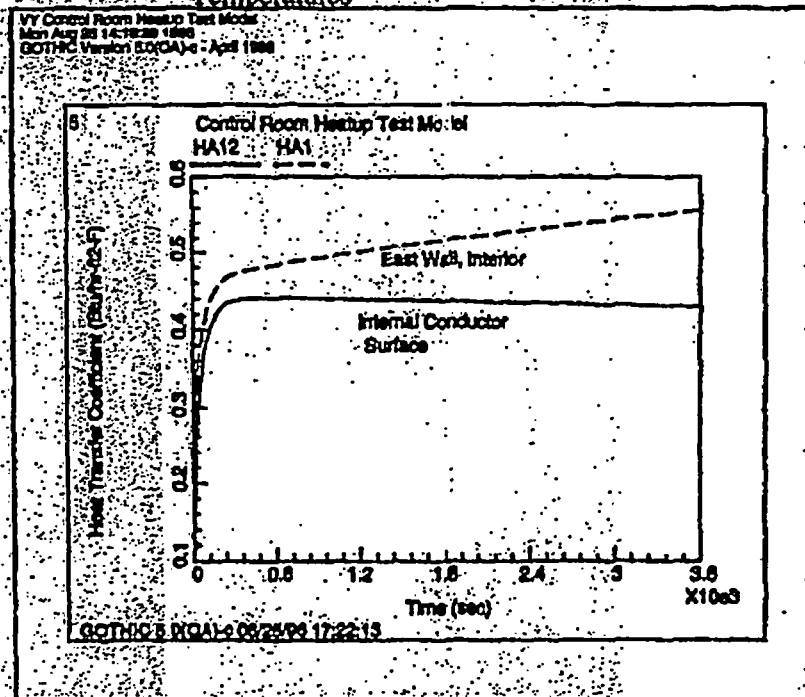


Figure 8 Control Room Heatup Test Model, Selected Wall Heat Transfer Coefficients

### 4.3 Control Room Heatup During App. R Event

Given the information available from the test data, it is now possible to adequately model the control room during a loss of HVAC following an Appendix R event. The generic control room GOTHIC input model described previously is used with modifications to the model made on the basis of the test results described in previous sections.

The modifications and additions to the initial input model are:

- Thermal Conductors - #12 abstract heat sink: Area = 22,500 ft<sup>2</sup>
- Thermal Conductors - all initial temperatures at 78 °F
- Heat Transfer Coefficients - for walls exposed to outside conditions, the temperature boundary conditions set to respective average SOLAIR temperatures
- Coolers/Heaters - Heater #1 (electrical load) set to 57.42 BTU/sec based on results from Section 4.1.3
- Volumetric Fan - On trip set to 110°F control room temperature in accordance with the assumptions previously discussed
- Valves & Doors - On trip set to 110°F control room temperature in accordance with the assumptions previously discussed
- Volume Initial Conditions - Volumes 1 and 2 are set to 78 °F;
- Run Control Parameters - the GOTHIC problem will run for a four hour transient (14400 seconds)

The GOTHIC input tables for this model are included in Appendix B. The GOTHIC output results are included on microfiche under the filename "HEATUP.SOT".

The temperature results are shown on Figure 9. The results clearly show that the control room temperature does not exceed 120 °F during the entire period of the transient. It is also clear that 120 °F would be exceeded if taken beyond 4 hours which would necessitate some action not included in this model. The effect of the opening of the ceiling tiles can clearly be seen as the control room temperature reaches 110 °F. The drop ceiling space remains cooler than the rest of the control room since the heat sources are in the control room.

It could reasonably be expected that the temperature seen by the operators and equipment would be less than shown by the results due to the heat rising to the ceiling. Common experience shows that there is a noticeable difference in the temperature at floor level and the temperature at ceiling level in a heated room.

VY Control Room Heatup, Loss of HVAC  
Mon Aug 29 14:18:28 1996  
GOTHIC Version 5.0(QA)-c - April 1996

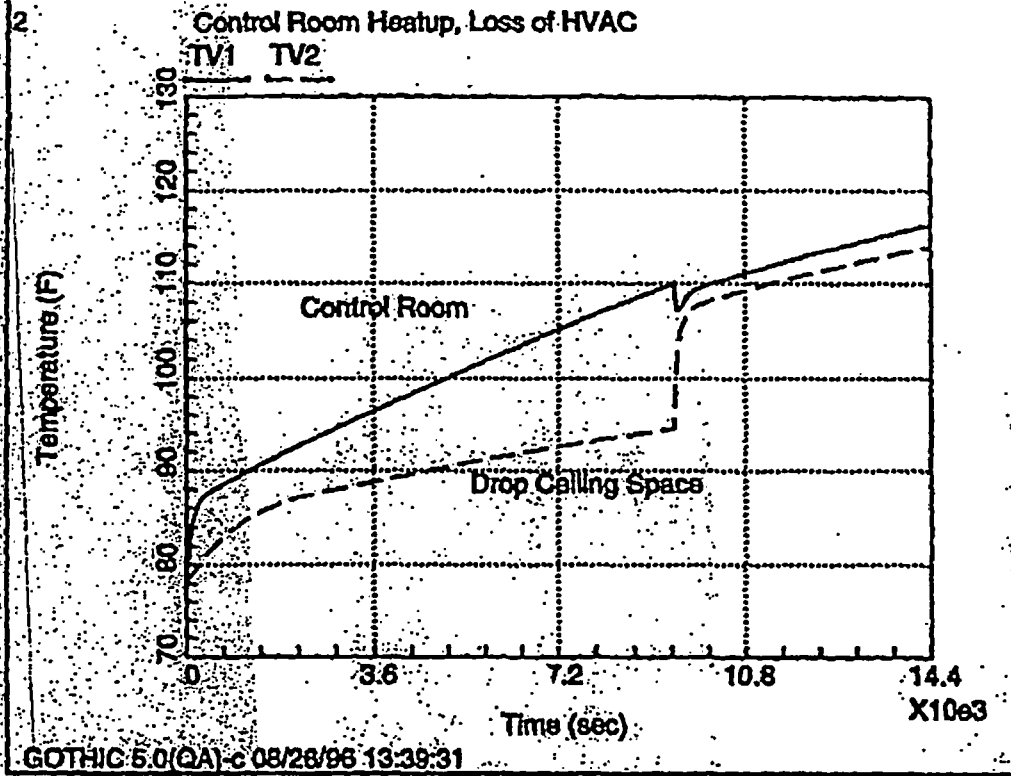


Figure 9 Control Room Heatup, Loss of HVAC Temperature Transient



#### 4.4 Control Room Heatup Mitigation Options

As seen by the results in Section 4.3, during the first four hours of the control room loss of HVAC transient the temperature in the control room stays under 120 °F. However, due to the heat load in the room and the insulating effect of the thick concrete walls, the steady state temperature is expected to be well above 120 °F. To mitigate this temperature rise, two possible options are explored. Any option chosen will have to do one of two things, either singly or in combination. Either the heat load will have to be reduced or some alternate ventilation/cooling will have to be provided.

The first option explored was to provide a means of alternate ventilation. Given some temporary ventilation using outside air the control room temperature can be maintained at or below 120°F. A GOTHIC model was used to determine the amount of air flow required. The second option was to reduce the heat load and provide some means of alternate ventilation (at some reduced level from the first option.)

The basic GOTHIC control room model developed previously was used with some minor modifications. A schematic of the new GOTHIC model is shown in Figure 10. As seen on the schematic, an additional flow boundary condition and a flow path to that boundary condition were added. Details of the modifications are outlined below for each option.

Option 1 - The input tables for this option are included as Appendix E. The output for this run is included on microfiche under the filename "OPTION1.SOT".

Option 2 - The input tables for this option are included as Appendix F. The output for this run is included on microfiche under the filename "OPTION2.SOT".

- **Fluid Boundary Conditions** - a flow boundary condition was added to simulate a constant ventilation air flow; in this case, the flow was set to a function which had zero flow up to 14400 seconds (four hours) and 110 cfs (6600 cfm for Option 1) or 50 cfs (3000 cfm for Option 2) thereafter (the flow is actually negative, into the boundary condition, allowing the control room pressure boundary condition to provide the inlet air)
- **Flow Paths** - a flow path was modeled connecting the new fluid boundary condition with the control room; the flow path is not intended to model any particular ventilation connection and for simplicity was set to the same parameters as the other control room boundary condition connecting flow path;
- **Coolers/Heaters** - a forcing function was assigned to the electrical heat load; for Option 1, this forcing function was unity (no change in heat load) but for Option 2, this forcing function was set to 0.48 at four hours to represent a reduction in heat load

The temperature transient results of these models are shown in Figure 11 and Figure 12.

VY Control Room Heatup: Loss of HVAC, Option 1  
Mon Aug 28 14:20:20 1996  
GOTHIC Version 5.0(QA)-c - April 1996

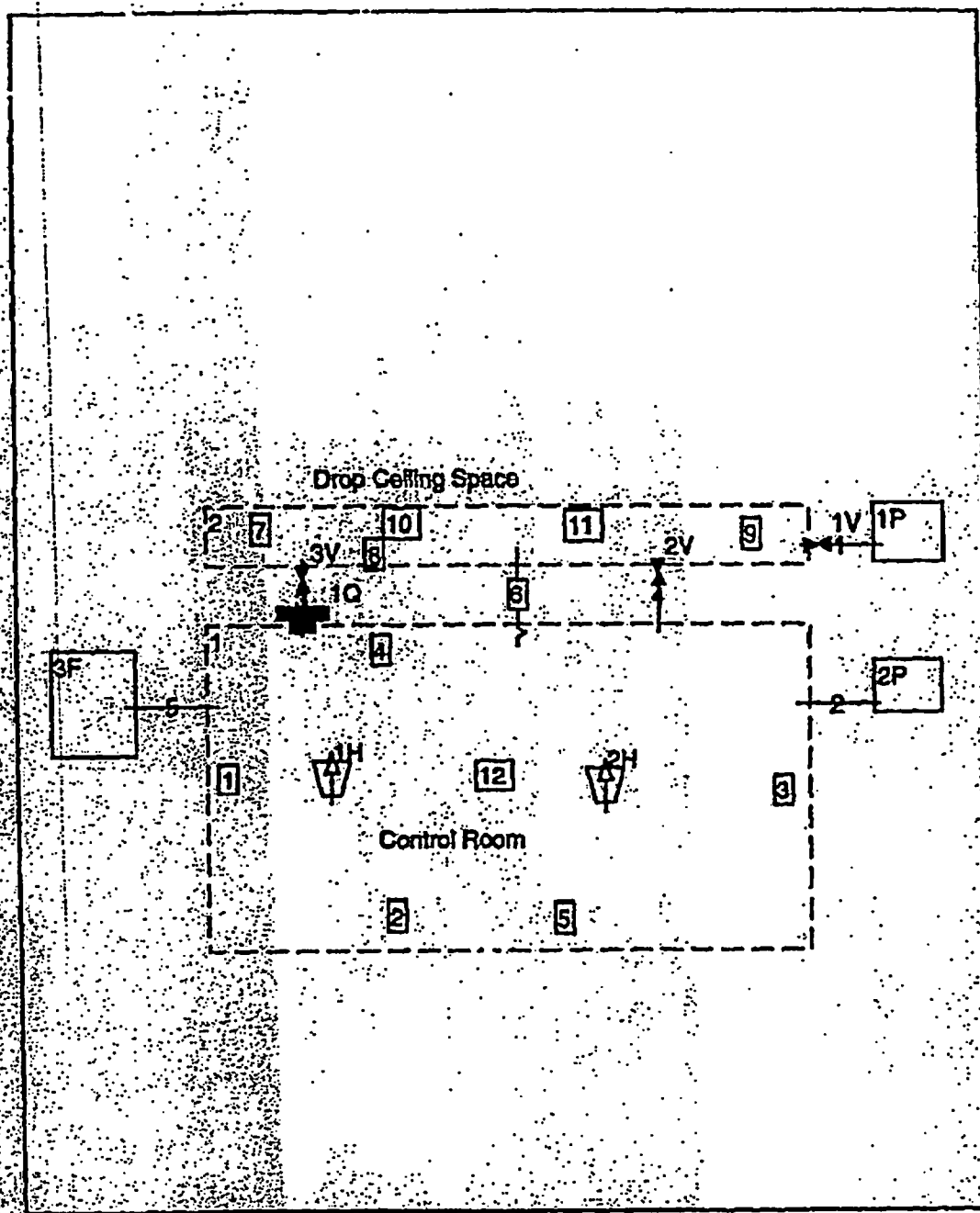


Figure 10 GOTHIC Model Schematic for Option 1 and Option 2 Models

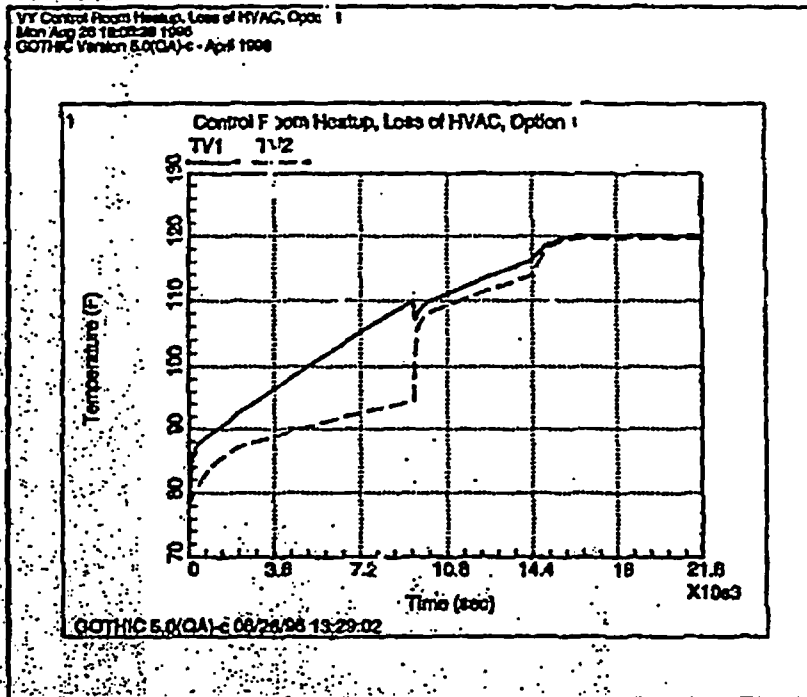


Figure 11 Control Room Heatup Results, Option 1 - Temporary Ventilation

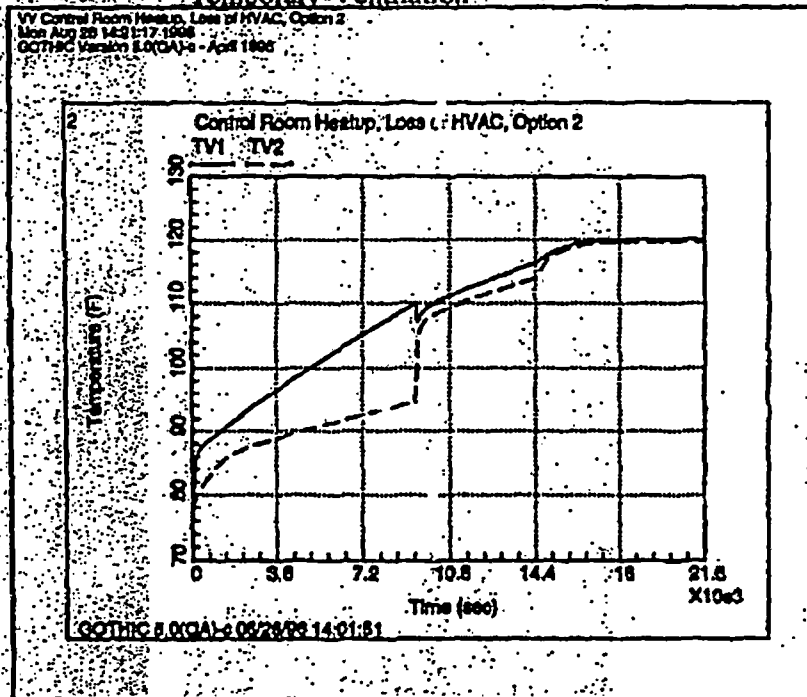


Figure 12 Control Room Heatup Results, Option 2 - Temporary Ventilation and Reduce Heat Load

## 5.0 Conclusions

It has been shown that for the first four hours after a control room loss of HVAC transient, the temperature in the control room does not exceed 120 °F given operator action to remove sufficient ceiling tiles when room temperature reaches 110 °F. To prevent the control room temperature from exceeding 120 °F after four hours, some action is required to mitigate the temperature rise. Two possible options have been identified which ensure control room temperature does not exceed 120 °F in a long term transient:

- a. temporary ventilation providing at least 6600 cfm of outside air, or
- b. heat load reduction by at least 52% accompanied by at least 3000 cfm of outside air.

BVY 05-072  
Docket No. 50-271

**Exhibit SPSB-C-52-4**

**Vermont Yankee Nuclear Power Station**

**Proposed Technical Specification Change No. 263 – Supplement No. 30**

**Extended Power Uprate**

**Response to Request for Additional Information**

**Calculation VYC-2405, Rev.0**

**Total number of pages in this Exhibit  
(excluding this cover sheet) is 85.**

**CALCULATION COVER PAGE**

<input type="checkbox"/> IP-2 <input type="checkbox"/> IP-3 <input type="checkbox"/> JAF <input type="checkbox"/> PNPS <input checked="" type="checkbox"/> VY						
Calculation No. <b>VYC-2405 Rev. 0</b>	This revision incorporates the following MERLIN DRNs or Minor Calc Changes:	Sheet <u>1</u> of <u>85</u>				
Title: <b>Drywell Temperature Calculation for a Station Blackout Event at Extended Power Upate.</b>		<input checked="" type="checkbox"/> QR <input type="checkbox"/> NQR				
Discipline: Fluid Systems Design Engineering		Design Basis Calculation? <input checked="" type="checkbox"/> Yes <input type="checkbox"/> No				
This calculation supersedes/voids calculation: N/A						
Modification No./Task No./ER No: <b>EPU</b>						
<input type="checkbox"/> No software used <input checked="" type="checkbox"/> Software used and filed separately (Include Computer Run Summary Sheet). If "YES", Code: <b>GOTHIC V7.0p2</b> <input type="checkbox"/> Software used and filed with this calculation. If "YES", Code:						
System No./Name: _____ Component No./Name: _____ (Attach additional pages if necessary)						
<b>Print/Sign</b>						
REV #	STATUS (Prel, Pend, A, V, S)	PREPARER	REVIEWER/ DESIGN VERIFIER	OTHER REVIEWER/ DESIGN VERIFIER	APPROVER	DATE
0	Prelim	Liliane Schor <i>Liliane Schor</i> 3/17/05	Alan L. Robertshaw <i>Alan Robertshaw</i> 3/17/05	NA	James G. Rogers <i>James G. Rogers</i>	3-17-05



**CALCULATION SUMMARY PAGE**Calculation No. VYC-2405Revision No. 0**Drywell Temperature Calculation for a Station Blackout Event at Extended Power Uprate.****CALCULATION OBJECTIVE:**

This calculation will address the VY drywell temperature for Station Blackout (SBO) at Extended Power Uprate (EPU) Conditions. The calculation will look into means to mitigate the drywell temperature for this event, such that there will be no need for Emergency Depressurization.

**CONCLUSIONS:**

See Section 7.0

**ASSUMPTIONS:**

See Assumption in Section 4.0. (see also list of open items – assumptions which need verification or implementation - Section 4.1)

**DESIGN INPUT DOCUMENTS:**

See Design Input Documents identified in References Section 8.0

**AFFECTED DOCUMENTS:**

See Assumption Section, Section 4.2

**METHODOLOGY:**

See Section 3.0





## TABLE OF CONTENTS

Cover Sheet (ENN-DC-126 Attachment 9.2).....	1
Record of Revisions (ENN-DC-126 Attachment 9.6).....	2
Calculation Summary Page (ENN-DC-126 Attachment 9.4).....	3
Table of Contents.....	4
List of Effective Pages (ENN-DC-126 Attachment 9.15).....	5
1.0 Background.....	6
2.0 Purpose.....	6
3.0 Method of Analysis.....	7
4.0 Inputs and Assumptions.....	7
5.0 Input and Design Criteria.....	15
6.0 Calculation / Analyses.....	26
7.0 Results and Conclusions.....	67
8.0 References.....	68
Computer Run Summary Sheet (ENN-DC-126 Attachment 9.10).....	71
Calculation Impact Review Page (ENN-DC-126 Attachment 9.7).....	72
Calculation Design Verification and Review (ENN-DC-134).....	77
Files on CD.....	85
Attachments	
Attachment A.....	A1 – A39
TOTAL NUMBER OF PAGE (Including Attachments).....	124



---

**ATTACHMENT 9.15****LIST OF EFFECTIVE PAGES**

---

**LIST OF EFFECTIVE PAGES**Calculation Number: VYC-2405 Revision Number: 0 Page 5 of 85**Torus Temperature Calculation for a Station Blackout Event at Extended Power Uprate.**

PAGE	REV.	PAGE	REV.	PAGE	REV.
All	0				



## **1.0 Background**

The Station Blackout (SBO) torus temperature calculation (Reference 1) accommodated a higher coping time of 2 hours versus 10 minutes previously assumed. In addition to an increased coping time, Reference 1 also eliminated the potential need for Containment Overpressure (COP) for the SBO event. In the process, it was determined that in order to implement coping strategies for the two hours, two additional parameters need to be analyzed:

- Drywell temperature and the coping strategy to accommodate an expected higher drywell temperature, and
- Procedural direction for the operators (if needed) to limit the drywell temperature while ensuring capability of HPCI/RCIC to maintain vessel level

## **2.0 Purpose**

This calculation will address the VY drywell temperature for Station Blackout (SBO) at Extended Power Uprate (EPU) Conditions. The calculation will look into means to reduce the drywell temperature for this event, such that there will be no need for Reactor Pressure Vessel Emergency Depressurization (RPVED – Reference 30).

This analysis will address control of the drywell temperature by controlled depressurization (cooldown) and will show that RCIC/HPCI injection is maintained until power is restored and the low pressure pumps (RHR and CS) are available.

As indicated in Section 1.0 of Reference 1, for the SBO event, the Alternate AC (AAC) power source is restored at 2 hours into the event. After the restoration of power, torus cooling and drywell spray will become available.

### **2.1 Acceptance Criteria**

To evaluate the results the following criteria are applied:

1. The maximum allowable drywell bulk average temperature should remain below the EQ temperature (340°F for the first 30 minutes and 325°F for the next 270 minutes) (Reference 19).
2. The maximum allowable drywell surface temperature is 281 °F (Reference 20).
3. The maximum allowable drywell air pressure is 56 psig, (Reference 27).
4. Maintain the torus pressure below PSP curve (Reference 30) during the 2 hour coping duration and the 10 minutes of low pressure pumps restoration period.
5. The analyses should provide assurance that there is no need to spray the drywell in the unsafe region of the DWSIL curve (Reference 30).



### 3.0 Method of Analysis

The model developed in Reference 1 is modified to accommodate changes related to the purpose described in Section 2.

The GOTHIC code (Reference 7), Version 7.0p2 has been selected for use in this analysis. This code was used in the original suppression pool temperature calculation (Reference 6) and in the analysis for SBO at EPU conditions, Reference 1. This specific version of the code has been installed and complies with the ENVY SQA procedures ENN-IT-104 (it replaced VY procedure AP-6030) as documented in calculation VYC-2208 (Reference 8).

The following changes to the input *SBO-NoLeak-80* to produce *SBO-drywell2* are being added:

- drywell heat load
- drywell heat slabs
- leakage from drywell to wetwell
- modifications to the vacuum breaker modeling

The GOTHIC input file for the case *SBO-drywell2* is presented in attachment A.

### 4.0 Inputs and Assumptions

The inputs and assumptions for the SBO event were developed in Reference 1. For completeness, they are added to this calculation. The more important modifications to the model have been made, for this analysis, by the addition of the Drywell Heat Loads and Drywell Heat Slabs (see Section 5.0 for details).

The SBO scenario postulates a complete loss of onsite and offsite AC power. The vessel is assumed to be isolated at the start of the event.

The scenario is modeled as follows:

- 1) Scram occurs at time zero.
- 2) The MSIVs are isolated at time zero (this is a conservative assumption for the drywell temperature calculation since the energy transferred to the condenser while the MSIVs are opened will remain in the vessel).
- 3) The Reactor Vessel level is maintained with HPCI or RCIC in a band between 127-177 inches above Top of Active Fuel (TAF). Level is maintained with HPCI at a nominal flow of 4250 gpm. In reality HPCI flow will be adjusted to keep level in the band and to prevent excessive start/stop cycles. The HPCI (or RCIC) modeling in the GOTHIC input as a continuous flow (lower flow) or as intermittent flow has no effect on the drywell temperature analysis results. The choice of RCIC or HPCI or the flow capacity has no effect on the analysis since HPCI injects intermittently to maintain inventory or can be throttled as required to maintain level. If RCIC were used, it would inject more often.



- 4) HPCI takes suction from CST at 135°F. The CST inventory available for injection is 75000 gal.

The GOTHIC input value in lbm = 75000 gals \* 1 ft<sup>3</sup>/7.48 gals /0.01627 lbm/ft<sup>3</sup>  
(Reference 31 for the density at 135 °F) = 616271.7 lbm

- 5) Power is restored at 2 hours. Torus cooling is initiated at 2 hours and 10 minutes. Two RHR Service Water pumps are available at 2 hours and 10 minutes, delivering 4700 gpm. The second RHRSW pump is discontinued at 16 hours in the transient to maintain the Corner Room temperatures below the EQ limit (Reference 1, Attachment B). The drywell temperature analysis is performed for only 25000 seconds for the base case and for 14400 (4 hours) seconds for the sensitivity cases since, after 2 hours and 10 minutes (7800 seconds), the low pressure pumps are available to spray the drywell, if needed, hence there is no need to analyze the drywell temperature for a longer duration.
- 6) An orderly reactor cooldown is initiated at one hour in order to maintain the drywell temperature below the EQ limit (Reference 19) and the drywell shell metal below 281 °F (Reference 20). Two cooldown rates will be analyzed: 80°F/hr and 45°F/hr.
- 7) The RPV level is controlled by HPCI until the CST is depleted or HPCI shutoff pressure is reached. When the pressure permissive is reached, one Core Spray pump starts (after 2 hours and 10 minutes) to inject into the vessel. After the level is recovered in the normal range, the Core Spray system is used to maintain the level with the vessel pressure being controlled by an SRV cycling between 50 and 100 psig. The suppression pool is cooled continuously by the RHR system. The reactor vessel is maintained in this configuration. The RHR pump in torus cooling is also available for drywell spray after 2 hour and 10 minutes.
- 8) The HPCI turbine takes steam from the vessel to provide its motive power. It returns the exhaust steam to the torus. The steam to the turbine is not modeled since the model assumes SRV opening and closing to maintain pressure. Any steam not removed by the HPCI turbine will be removed through the SRV to maintain a certain pressure. The total flow through the SRV is increased, but the details of SRV flow are not important for this applications and the two (SRV flow and HPCI turbine) can be combined for model simplicity.
- 9) The liquid leak is modeled as a fixed flow of 8.4585 lb/sec (61 gpm, Reference 3) [(61 gpm /60 s/min /7.4805 gal/ft<sup>3</sup> /0.0161 ft<sup>3</sup>/lb = 8.4585 lb/sec)] and it stays on for the entire transient. (Analyses will be performed with and without leak for one depressurization (cooldown) rate: 80 °F/hour). In reality, the leak is variable depending on pressure. Assuming a density of 62 lb/ft<sup>3</sup> and fixed flow is conservative for the drywell temperature analysis.

Analysis of drywell temperature for a 45 °F/hour cooldown with no RPV leakage was not performed because for the case with 80 °F/hr cooldown, for the period of interest the drywell temperature stays below 300 °F for both cases (with and without RPV Leakage). For the 45 °F/hour cooldown, the temperature in the drywell for the no-leak case is expected to remain below 300 °F as in the 45 °F/hour cooldown case with RPV leakage for the analysis duration.



- 10) The analysis will assume a fouling of 0.0018 in the tubes and 0.0005 in the shell. This corresponds to an overall RHR Heat Exchanger (RHRHX) fouling of:

$$R_f = R_{fi} \left( \frac{d_o}{d_i} \right) + R_{fo}$$

where:

$R_{fi}$  and  $R_{fo}$  = tube and shell fouling factors, respectively (hr-ft<sup>2</sup>-°F/Btu)

$d_o$  = outside tube diameter (in)

$d_i$  = inside tube diameter (in)

$d_o$  = 0.625 in (Reference 22)

$d_i$  = 0.527 in (Reference 22)

$R_{fo}$  = 0.0005 hr-ft<sup>2</sup>-°F/Btu (Reference 22)

$R_{fi}$  = 0.0018 hr-ft<sup>2</sup>-°F/Btu (from 0.0020)

Overall RHRHX fouling

$$R_f = 0.0018 * \left( \frac{0.625}{0.527} \right) + 0.0005 = 0.0026$$

This number compares well with the maximum fouling calculated in Reference 23 of 0.002307 and 0.002445 for the RHR HX E14-1A and RHR HX E-14-1B, respectively.

- 11) A variable SW temperature is used, consistent with Reference 1. Since this change of depressurization (cooldown) function of service water temperature requires procedure changes, it is added in Section 4.1 as an unverified Assumption.
- For SW > 75°F, depressurize the vessel at 80°F/hr or higher.
  - For lower SW temperature (SW ≤ 75°F no restrictions on depressurization) rates.
- 12) - Various assumptions made concerning the added Heat Conductors:
- The heat load decreases linearly when the temperature difference between RPV and drywell becomes smaller.
  - For all conductors, only heat conduction is conservatively assumed in the air and concrete layers.
  - The outer surface boundary condition is conservatively assumed to be adiabatic (i.e., the heat transfer coefficient is set to zero)


**Table 1 – Vessel and Core Initial Conditions and Parameters, Primary Variables**

Parameter	Nominal Value	Analysis Value	Basis
Initial Reactor Power	1912 Mwth	1950 MWth	100% power +2 % uncertainty (per NEI-87-001, SBO can be performed at 100% power, however this analysis used 102% power, consistent with CLTP and the Reference 1 analysis).
Core Decay Heat	ANS 5.1	ANS 5.1 +2 $\sigma$	ANS 5.1 1979 standard+2 $\sigma$ uncertainty -(Reference 24)
MSIV closure time	3.0-5.0 sec	0.0 sec (MSIVs not modeled)	Minimum value allowed retains the maximum energy in the vessel.
RPV Pressure	1015-1025 psia (Reference 28)	1045.2 psia	Higher value, conservative, maximizes the vessel energy.
Initial Vessel Level	162 inches	172 inches	Analysis value conservatively accounts for 3 inches increase above normal (uncertainty and operational fluctuations) and 7 inches for dimensional uncertainties. These assumptions are LOCA assumptions and are judged conservative for SBO.
Core Flow Rate	48.0E6 lb/hr	51.36e6 lb/hr	Includes ICF of 7%.
Initial Feedwater Flowrate	7.876e6 lb/hr	8.076e6 lb/hr	Reference 25 (TE 2003-20)
Initial feedwater temperature	393.5-393.6 °F	393.9 °F	See discussion in Reference 25. Feedwater is tripped at time 0, due to SBO. The feedwater is used only for the steady state initialization.
SRV Cycling	1080-1047.6 psi (between RPV and Drywell)	1080-1047.6 psi (between RPV and Drywell)	The setpoints for the SRVs are nominal. No additional as found allowable of 3% is added since it will have no effect on the drywell temperature since the SRVs open to remove the decay heat and, until the depressurization starts, indifferent of setpoints, the SRVs will cycle to remove the decay heat. The operators will take manual control of the SRV and will cycle between 800 and 1000 psig (EOP-1- Reference 37) to reduce the numbers of times the valves cycle. There is no effect on the calculation since the valves in any operational mode will open to remove decay heat.
Vessel Leak	61 gpm	61 gpm	A constant 61 gpm leakage is assumed; (Reference 3). The analysis will be performed with & without leakage, since the drywell temperature will have a different profile for the cases with no leakage.

**Table 2- ECCS Initial Conditions and Parameters**

Parameter	Nominal	Analysis Value	Basis	Comments
HPCI flow rate	4250 gpm	4250 gpm	Tech Spec Flow (Reference 2)	Since the flow is intermittent there is no need to use the min flow of 3570 gpm (uncertainty added) (References 2 and 5). In reality the HPCI flow will be adjusted to maintain level to prevent excessive pump stop/start.
HPCI pressure range	1135-165 psia		1135-165 psia	Reference 5 and 27. HPCI is shut off if vessel pressure drops below 165 psia.
CST Temperature	120 °F	135 °F		<b>OPEN Item</b>
CST available inventory	75000 gallons (VY Tech Spec -- Reference 2)	75000 gallons	Available CST inventory for HPCI injection	Per Reference 3, the Tech Spec value can be used. An administrative limit for the CST level of 25% is required.
Core Spray Flow	Curve of flow vs. vessel-torus ΔP.	Same as nominal.	The core spray flow rate used in the SBO analysis of Reference 1 will be used. The flow rate is determined as a function of the vessel-torus ΔP. (consistent with the LOCA analysis)	The Core Spray System will be used for level control only after the CST is depleted and/or the low pressure is reached.  OPL4 --Reference 5
RHR Flow (t=7800 seconds)	7000 gpm	6400gpm	6400gpm used in analyses	Consistent with Reference 1 limiting case and Reference 5.
RHR Hx Fouling	0.0005 shell, 0.0018 tube	0.0005 shell, 0.0018 tube		Assumption input #10, supported by Reference 23.
RHR Hx Tube Plugging	N/A	5%	Allowable plugging margin	Design value providing margin above the current plugging value of 3.6%
RHR SW Flow	4700	4700 gpm (2 RHR SW pumps) 4700 gpm = 650.98 lb/sec (at 85 °F)	4700 gpm	(Reference 4)
RHR SW Inlet Temperature	32-85 °F	Variable, see assumptions, based on depressurization (cooldown) rate	If SW is > 75 °F, depressurize the RPV with rates 80 °F/hr or higher.	Maximum Allowable Service Water Temperature (Reference 2) only for depressurization rates > 80 °F/hr For lower depressurization rates the SW has to be below 75 °F. This requirement is derived from the torus temperature calculation (Reference 1). The rate of depressurization was shown in this calculation to have minimal impact on the strategies to control the drywell temperature for SBO.




**Table 3- Primary Containment Initial Conditions and Parameters**

Parameter	Nominal Value	Analysis Value	Basis	Comments
Drywell Temperature	110-170 °F	170 °F	Reference 5	The highest drywell temperature is used.
Drywell Pressure	16.4 psia	16.4 psia	VY Tech Spec (Reference 2)	
Wetwell Temperature	88 °F	90 °F	Maximum Tech Spec Value (Reference 2)	A 2 °F uncertainty is applied via procedure to account for instrument uncertainty (Reference 26)
Wetwell Pressure	14.7 psia	14.7 psia	Normal Torus operating pressure (vented to atmosphere via Standby Gas Treatment System )	
Drywell Humidity	20 -100 %	100% (base case)  Sensitivity performed at 20% humidity	Nominal Values: VY UFSAR (Reference 27)	Use maximum drywell humidity consistent with Reference 1 for the base case. Sensitivities performed at 20% drywell humidity.
Wetwell Humidity	100%	100%	Nominal Values: VY UFSAR (Reference 27)	Minimal to no impact on the SBO drywell temperature.
Wetwell Water Volume	68000 ft <sup>3</sup>	68000 ft <sup>3</sup>	Minimum Tech. Spec. Value (Reference 2)	
Drywell free volume	128,370 -131,470 ft <sup>3</sup>	131,470 ft <sup>3</sup> (includes vents)  The values proposed are consistent with OPL-4A	Reference 5  Consistent with Reference 6, the volume of the drywell side of the torus-drywell vacuum breakers of 372.3 ft <sup>3</sup> will be added to the proposed value.	The maximum value in OPL-4A is used for SBLOCA, IBLOCA and Small Steam Breaks. Vents: 16703 ft <sup>3</sup> (VYC-2306 --Reference 32)  Total Drywell Volume = 131470 – Vents Volume + Drywell side of Vacuum Breakers = 131470 -16703 + 372.3 = 115139.3 ft <sup>3</sup>
Wetwell free volume	For the minimum water level of	Nominal Values used.	Reference 5	The value at Dp>0 of 105,932.0 ft <sup>3</sup> is used for a



Parameter	Nominal Value	Analysis Value	Basis	Comments
	68000 ft <sup>3</sup> , the wetwell free volume is 107,104.8 ft <sup>3</sup> for Dp =0.0 and 105,932.0 for Dp>0.0 where Dp is the pressure difference between drywell and torus.	The values proposed are consistent with OPL-4A	Consistent with Reference 6, the volumes of the drywell side of the torus-drywell vacuum breakers of 99.4 ft <sup>3</sup> will be added the proposed value.	total volume of 105,932 + 68,000 = 173932 ft <sup>3</sup>  Used in calculation: 173932 + 99.4 = 174031.4 ft <sup>3</sup>
Vacuum Breakers-pressure difference between wetwell and drywell for vacuum breakers to be fully open	0.5 psi	0.5 psi	0.5 psi	Reference 2
Drywell-to Wetwell Bypass Leakage	Max allowable area =0.12 ft <sup>2</sup>  Tech Spec Allowable =0.0033 ft <sup>2</sup>	Base case =0.12 ft <sup>2</sup>  Sensitivity =0.0033 ft <sup>2</sup>		Reference 5 for the max leakage, Reference 33 for Tech Spec Allowable

#### **4.1- Assumptions that need Verification or Implementation**

- 1) Two (2) hour restoration of outside power (coping time).
- 2) Ten (10) minutes to start RHR flow through the RHRHX, and the use of 2 RHRSW pumps and CS.
- 3) Acceptability of using 75000 gal from CST (change of level setpoint).
- 4) Maximum CST temperature of 135°F.
- 5) The depressurization rate function of Service Water temperature needs to be verified and proceduralized as follows:
  - For  $SW > 75^{\circ}F$ ; depressurize the vessel at  $80^{\circ}F/hr$  or higher.
  - For lower SW temperature ( $SW \leq 75^{\circ}F$ ) no restrictions on cooldown rates.

#### **4.2 Affected Documents**

- 1) DBD – for Residual Heat Removal – change the maximum tube side fouling resistance from  $0.002 \text{ hr-ft}^2\text{-}^{\circ}F/Btu$  to  $0.0018 \text{ hr-ft}^2\text{-}^{\circ}F/Btu$  as well as the total fouling.
- 2) Change the description of the SBO event in the DBD for Safety Analysis.
- 3) Change all DBDs and documents that address the SBO coping time (identify and modify).
- 4) Change DBD Containment Pressure Suppression System to incorporate results of this calculation.
- 5) Review following documents for need of modification: VY UFSAR, and PUSAR.
- 6) Modify SBO procedure (OT-3122-Reference 36) to incorporate cooldown at one hour and provide guidance to the operators such that RPVED is precluded based on the results of this calculation.

**Note: Section 4.1 & 4.2 items are being tracked via LO-VTYLO-2005-00135.**

## 5.0 Input and Design Criteria

The GOTHIC input from Reference 1 is modified to implement the features described in this section. The modified input is called *SBO-drywell2*.

The main features added to the SBO model are the drywell heat load and drywell heat structures. A schematic of the system modeled is presented in Figure 1

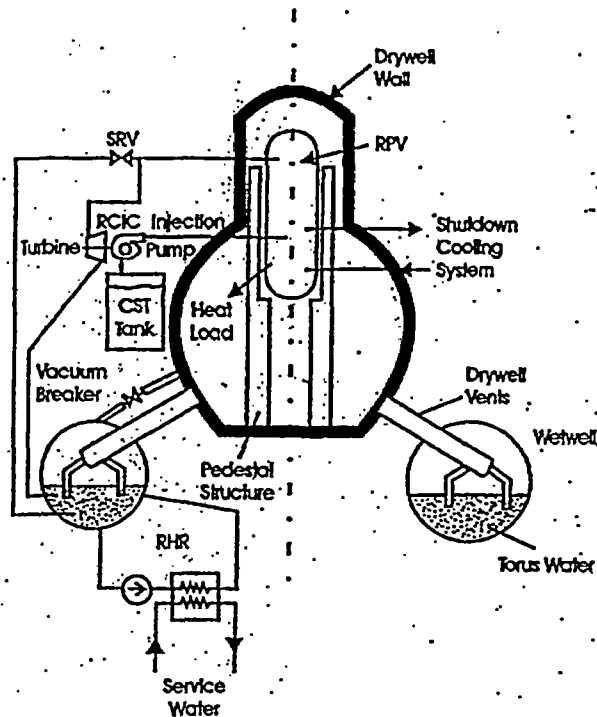


Figure 1 – VY Containment and the Associated Systems

Note: only RCIC pump is shown in this simplified model. Actually, HPCI is assumed to inject.



### 5.1 Drywell Heat Load Calculation

The Drywell Heat Load Summary at Current Licensed Thermal Power (CLTP) is summarized in Reference 10. The total amount of heat given to the drywell at CLTP is 1,691,300 Btu/hr. The drywell heat load was recalculated in Reference 18 for the Extended Power Uprate (EPU) as 1,700,675 Btu/hr. Since the Extended Power Uprate is performed at constant pressure, only the feedwater pipe and valves will be at higher temperatures (Reference 18), hence a higher Q for this component; (124,000 Btu/hr –Reference 10 versus 133,375 Btu/hr at EPU –Reference 18) is calculated.

The total power to the drywell for EPU is presented in Table 4.

**Table 4 Drywell Heat Load (Reference 18)**

Item No.	Component	Cooling Load (Btu/hr)
1	Reactor Vessel	459,000
2	Recirc. Pumps, Valves and Pipe	278,000
3	Feedwater Pipe & Valves	133,375 (EPU Modified-Reference 18)
4	Steam Pipe & Valves	212,000
5	Condensate & Instrument Lead Lines	82,000
6	Control Rod Drive Pipe	50,400
7	Clean-up Pipe & Valves	17,800
8	Shutdown Supply Pipe	8,100
9	Steam Safety/Relief Valves	206,600
10	Biological Shield (Gamma Heating)	16,400
11	Safeguards System Piping	82,000
12	Steam Leak	155,000
<b>Total</b>		<b>1,700,675 Btu/hr</b>



### 5.1.1 Drywell Load Modeling

The drywell heat is modeled as two heater #5H and #6H. The heater 5 represents the heat source which varies function of the liquid temperature in the vessel, while heater 6 represents the heat source which varies as a function of the vapor temperature in the vessel. See explanation of these two heaters in Section 5.1.2.

The heat loads which are exposed to the steam atmosphere (for Heater #6H) are:

**Table 5 Heat Loads Exposed to Steam**

Item No.	Component	Cooling Load (Btu/hr)
1	30% of Reactor Vessel Heat Load	$459,000 * 0.3 = 137,700$
4	Steam Pipe & Valves	212,000
9	Steam Safety/Relief Valves	206,600
12	Steam Leak	155,000
<b>Total</b>		<b>711,300</b>

The normal level is at about 0.3 of the total vessel height. From Reference 34 the distance from the 152 inches above TAF to the top of the vessel is 21.432 ft in the GOTHIC vessel model and to the vessel bottom is 41.193 ft.

The middle range of 152 inches is calculated as  $(177 \text{ inches} + 127 \text{ inches})/2 = 152 \text{ inches}$ . The model assumes a normal level of 172 inches (Table 1) which is 20 inches above the 152 inches, hence from 172 inches above TAF to the top of the vessel there are  $21.432 - 1.667 = 19.765 \text{ ft}$

The liquid height =  $41.193 + 1.667 = 42.86 \text{ ft}$

Total GOTHIC vessel height =  $62.625 \text{ ft}$  (from Reference 34 =  $330.542 - 267.917 = 62.625 \text{ ft}$ )

Steam region =  $19.765 / 62.625 = 0.31$  (used 0.3)

Heater 6 load =  $711,300 / 3600 = 197.58 \text{ Btu/sec}$

Total Heat load =  $1,700,675 / 3600 = 472.41 \text{ Btu/sec}$

Thus, Heater 5 load =  $472.41 - 197.58 = 274.83 \text{ Btu/sec}$



### 5.1.2 Transient Heat Load Behavior

It is assumed that the heat load decreases linearly when the temperature difference between RPV and drywell becomes smaller. In order to calculate the transient heat load, the following transient heat load procedure is used

1. When the difference between the vessel temperature and the drywell temperature is less than or equal to zero, the power of the heat source is zero.
2. When the temperature difference is greater or equal with to  $T_{set}$ , the heater power will increase above the nominal value.
3. When a temperature difference exists between  $T_{set}$  and zero, the power is linearly interpolated between the nominal value and 0.0.

$T_{set}$  is defined in the way that the calculated power of the heat source is equal to the nominal value at the beginning of the transient. Two GOTHIC control variable CV 41 and CV 42 are defined as the temperature difference between the vessel internal water temperature and the temperature inside the drywell (CV41) and between the vessel steam temperature and the temperature inside the drywell (CV42), respectively. The model shows higher steam temperature than saturation because of the heat slab exposed to steam which represents the heat structures in the Reactor Pressure Vessel (RPV) exposed to a steam environment. Sensitivity studies which placed this heat structure in liquid eliminated the steam superheat, as expected. This is a conservatism of the model. In reality all structures will be exposed to  $T_{sat} = T_{liq} = T_{vap}$

The control variables are used as the independent variable of the functions, which gives the transient heat loads to the drywell, as described above.

### 5.2 Drywell Thermal Conductor Model Development

The following thermal conductors are being added to the model.

There are several types of heat sinks and thermal conductors inside the drywell. The components included as heat sinks are the metal mass of 4 RRUs, vent pipes and the drywell liner. Miscellaneous steel exists in the drywell, but has not been previously quantified in detail. Minimum heat sink components are considered conservative; therefore, miscellaneous steel is not included as heat sinks.

Drywell liner divided in (Reference 21):

- 1) Lower Drywell spherical portion,
- 2) Upper Drywell cylindrical portion, and
- 3) Drywell head.

The drywell wall consists of the concrete, the inner surface steel plate and the air gap. Zero heat flux boundary condition on the outside surface of the drywell wall is used.



The data on OPL-4A (Reference 5) is used to model the steel liner. The surface area calculation for the liner was performed in Reference 9.

**Table 6 – Drywell Steel Liner**

Item #—from Ref. 9	Elevation	Steel Thickness (in)	Surface Area (ft <sup>2</sup> )	GOTHIC thermal conductor No.
2, page 47 of Ref. 9	El. 237.74'-El. 257.75'	1.0 page 47 of Ref 9	1856.24	5
3, page 47 of Ref. 9	El. 247.24'-El. 257.75'	0.8125 page 51 of Ref 9	2041.28	6
4.1, page 47,48 of Ref. 9	El. 257.75'-El. 259.92'	0.6875 page 51 of Ref 9	1250.47	9
4.2, page 48 of Ref. 9	El. 259.92'-El. 283.69'	0.6875 page 51 of Ref 9	3802.73	7
5, page 48 of Ref. 9	El. 283.69'-El. 289.61'	2.5 page 51 of Ref 9	780.68	8
6, page 48 of Ref. 9	El. 289.61'-El. 308.00'	0.635 page 51 of Ref 9	1898.24	10
7, page 48,49 of Ref. 9	El. 308.00'- El. 318.50'	1.25 page 51 of Ref 9	1114.72	11
8, page 49 of Ref. 9	El. 318.50'- El. 327.75'	1.25 page 51 of Ref 9	783.4	12
9, page 49 of Ref. 9	El. 327.75'-top of drywell	1.3125 page 51 of Ref 9	1718.3	13
<b>Total</b>			<b>15246.06 ft<sup>2</sup></b>	

The items 2 through 7 have 0.0025 inches of paint per Reference 13 and Reference 9, Appendix VI (for properties) and a 2 inches thick air gap (Reference 14) and a conservative low thickness of concrete of 24 inches is used from Reference 21.

Item 8 (side of drywell head –small cylinder) is modeled, with a 2.5 ft air gap outside the steel wall and conservatively low thickness of 1.5 ft of concrete (scaled from Reference 21). The thermal conductor has an adiabatic heat transfer boundary condition. Only heat conduction is assumed in the air and concrete layers. This is conservative.

Item 9 (top of drywell head) is modeled with a 6.7ft air gap outside the steel wall and a conservative low thickness of 24 inches of concrete (part of the concrete plugs) – (scaled from Reference 21).

RRUs (References 11 and 12)

$A_{RRU} = 1272.8 \text{ ft}^2$ , thickness = 0.125 inches (used in OPL-4A-Reference 12).





### Vent Pipes

Vent pipes surface area

A vent pipe = 2885.7 ft<sup>2</sup>, thickness = 0.125 inches (used in OPL-4A-Reference 12)

NOTE: The total Surface Area of the steel components adds up to the value obtained from OPL-4a (i.e., Table 6 Total = 15246.06 ft<sup>2</sup>, RRUs = 1272.8 ft<sup>2</sup>, Vent Pipes = 2885.7 ft<sup>2</sup>, thus Total = 19405 ft<sup>2</sup>)

### Total Surface area of Concrete Exposed to Drywell Air Space

The surface area of the pedestal is the only concrete component quantified in OPL-4A. The drywell floor is ignored because it may be covered with liquid and not directly exposed to the drywell airspace. Only the outer surface area of the pedestal was considered in OPL-4A as well as Reference 9 because the inner surface has limited communication with the drywell atmosphere. The biological shield wall (BSW) is a concrete structure surrounding the reactor pressure vessel and located above the reactor pedestal. Because of the proximity to the reactor pressure vessel the BSW is at a temperature greater than the drywell (DW) ambient and thus a heat source (already incorporated into the drywell heater) and a heat sink only when its temperature drops below the DW temperature. Because of the uncertainty of the BSW temperature and its limited value as a heat sink, the BSW is not considered here.

The OPL-4A value for the area is used and = 2068 ft<sup>2</sup> (A value of 2108 ft<sup>2</sup> was used in the model, addressed in Case 5).

### Thickness of Concrete Exposed to Drywell Air Space

From Reference 5 = 4ft.

### Properties of Materials

**Table 7 - Thermo physical properties of Passive Heat Sink Materials (Reference 5)**

Material	Density (lbm/ft <sup>3</sup> )	Specific Heat (Btu/lbm-°F)	Thermal Conductivity (Btu/hr-ft °F)	References
Carbon Steel	489.0	0.11	32 °F 31.8 68 °F 31.2 212 °F 30.0 392 °F 27.8 572 °F 26.0	15
Concrete	145	0.156	0.92	16
Paint	288	0.2	0.125	9

### Air Thermal Properties

From Reference 15.

T (°F)	$K_x$ (Btu/hr-ft-°F)	$C_p$ (Btu/lbm-°F)	$\rho$ (lbm/ft <sup>3</sup> )
100	0.0157	0.24	0.07092
150	0.0167	0.241	0.06511
200	0.0181	0.241	0.06017
250	0.0192	0.242	0.05593
300	0.0203	0.243	0.05225
400	0.0225	0.245	0.04617

### Heat Transfer Boundary Conditions

On the inner surface of all the thermal conductors, the heat transfer coefficient is calculated by the GOTHIC code. The following options are used:

- Direct Heat transfer Option.
- Summation of the condensation and convection heat transfer.
- Max of Uchida and Guido-Koestel condensation heat transfer option (sensitivity with Uchida for the limiting cases).
- Radiation heat transfer option is OFF for all heat structures with exception of the drywell dome.(sensitivity with option OFF for the limiting case).
- The surface orientation is "FACE DOWN for the drywell dome", thermal conductor #13,and "VERT SURF" for heat conductors 5 through 12.
- All thermal conductors use "VAP" option.

The outer surface boundary condition is conservatively assumed to be adiabatic. The heat transfer coefficient is set to zero.

### 5.3 GOTHIC Drywell SBO Model Development

The following changes to the input *SBO-NoLeak-80* (Reference 1) to produce *SBO-drywell2* are being added:

- drywell heat load
- drywell heat slabs
- leakage from drywell to wetwell
- modifications to the vacuum breaker modeling

The GOTHIC input is presented in Attachment A.

The GOTHIC model used for all cases is presented in Figure 2.



SBO - 80F-Noleak-drywell1  
 Mar/15/2005 14:09:56  
 GOthic Version 7.0p2(QA) - April 2002  
 File: /home/schor/vyc-2120ccn/SENSITIVITY/SBO/drywell-SBO/SBO-drywell12

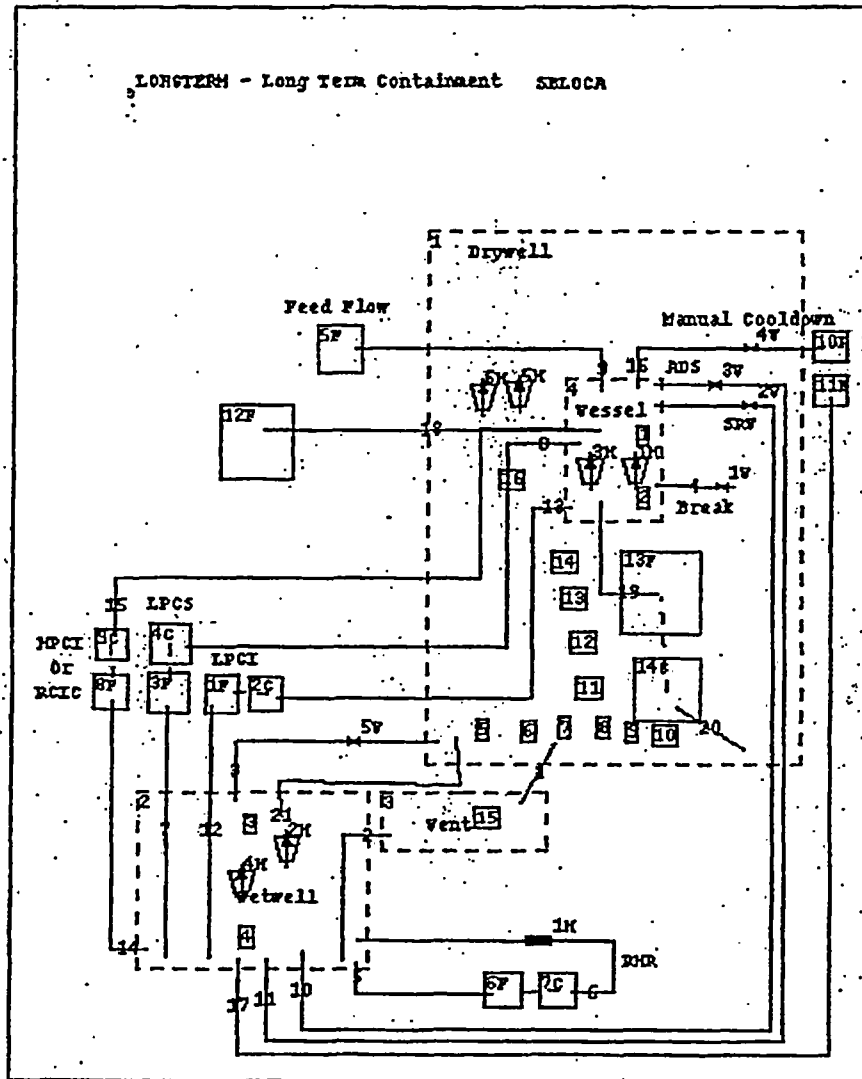


Figure 2 - GOthic SBO Model

### Flow Paths

Flow path 21 is added to model the vacuum breakers leakage path from the drywell air space to the wetwell air space. Per Reference 5, the maximum leakage area is 0.12 ft<sup>2</sup>. The elevations and the height of this junction were elected to be the same as the vacuum breaker junction since the leakage is around the vacuum breakers.

The  $K_{\text{reverse}} = K_{\text{forward}} = 1.5$  (expansion & contraction) (Reference 29)

### Thermal Conductors

Twelve new thermal conductors were added. The description of the thermal conductors was given in Section 5.2.

The temperatures of 11 of the thermal conductors were set at 160 °F, the pedestal thermal conductor is set at 152 °F. On page 73 of Reference 9 the average temperature for the middle and the top drywell node is calculated as 151.94 °F. Hence, the thermal conductors are set, conservatively at 160 °F. The pedestal is in the lower drywell and middle drywell hence 152 °F is used (average for middle and top drywell is conservative). In Case 5, the temperatures of the heat slabs which represent the drywell wall were set at 170 °F (very conservative assumption).

### Functions

Two new functions are added

Function 17 (FF17) represents the power to the drywell from the structures exposed to steam.

The function multiplies  $Q_{\text{initial}}$  and represents  $(T_{\text{liquid}} - T_{\text{drywell}})$ .

The FF17 is:

$\Delta T$ (CV41)	
-500	0
0	0
380	1
380000	1000

The independent variable is the temperature difference between  $(T_{\text{liquid}} - T_{\text{drywell}})$ , CV41.

Function 18 is identical to the Function 17, but the independent variable is CV42  $(T_{\text{vapor}} - T_{\text{drywell}})$

$T_{\text{ref}} = \text{Initial Vessel temperature} - \text{Initial Drywell temperature} = 550^{\circ}\text{F} - 170^{\circ}\text{F} = 380^{\circ}\text{F}$  where 550 °F is the initial vessel temperature, and 170 °F is the initial drywell temperature. (550 is determined from the GOTHIC model at time zero and 170 °F is the maximum drywell temperature, OPL4A-Reference 5).



### Valves

A new valve (V5) was added to represent the vacuum breaker. It opens on trip 33 (0.5 psi difference between wetwell and drywell (Reference 2) and it closes on trip 34 (0.3 psi-arbitrary, since the vacuum breaker valves reseal when the pressure difference becomes less than 0.5 psi. A quick close valve is used for this component since the valve will close as soon as the 0.5 psi difference between wetwell and drywell disappears.

The vacuum breaker valve is modeled as Valve Type 3, with an area of 17.6737 ft<sup>2</sup> (Reference 9). Note: the area of the valve from Reference 9 is slightly larger than the area of the flow path in which it is located. The valve area will have minimal impact on this analysis because the flow is limited by the area of the flow path. The area of the valve was changed to the area of the flow path in the final case analyzed, Case 5.

### Materials

Four new materials are added. The properties for the new materials are described in Section 5.2.

### Trips and Controls

Trip 18 is modified to ADS when the vessel pressure difference between RPV and drywell is lower than 100 psi instead of 50 psi in the original model. This trip is not used, however, the SRV valves will open at a  $\Delta P$  of 100 psi, not 50 psi.

Trip 21 is modified to start depressurization (cooldown) at one hour (3600 seconds) in order to limit the drywell temperatures.

Trips 33 and 34 are added to open the vacuum breakers valves at 0.5 psi pressure difference between wetwell and drywell (trip 33) and close it on a  $\Delta P$  of 0.3 psi.

### Coolers & Heaters

Two new heaters are added, 5H and 6H to model the vessel heat to the drywell. These heaters are described in Section 5.1.

For heater 5H the heat rate of 274.83 is multiplied by the FF 17, while for heater 6H the heat rate of 1997.58 is multiplied by FF 18.



### Heat Transfer Coefficients Types

Two heat transfer coefficients are added.

The following options are used:

- Direct Heat transfer Option.
- Summation of the condensation and convection heat transfer.
- Max of Uchida and Guido-Koestel condensation heat transfer option (sensitivity with Uchida for the limiting cases).
- Radiation heat transfer option is OFF for heat transfer coefficient type 6.
- Radiation heat transfer option is ON for heat transfer coefficient type 7.

The use of the radiation option has no effect on the results at these low temperatures

- The surface orientation is "VERT SURF" for heat transfer coefficient type 6.
- The surface orientation is "FACE DOWN for the drywell dome", heat transfer coefficient type 7.

The use of the surface orientation is appropriate since this is the thermal conductor physical arrangement.

- The heat transfer coefficient types 6 and 7 use "VAP" option since this is the drywell medium.
- Convection bulk T model:  $T_g - T_f$ . The bulk temperature is the calculated vapor temperature.  $T_f$  is the maximum between the calculated wall temperature and the calculated saturation temperature.
- Condensation heat transfer Bulk T Model :  $T_b - T_w$  used.  $T_b$  is the minimum between the calculated vapor temperature and the calculated saturation temperature.

### Control Variables

Two control variables are added, 41 and 42 they represent the  $\Delta T$  between  $T_{liq}$  in RPV and  $T_v$  drywell and between  $T_{vap}$  in RPV and  $T_v$  drywell, respectively. See Section 5.1.2 for additional information on the operation of these Control Variables.

## 6.0 Calculation / Analyses

Five (5) cases are analyzed:

Case 1 is called *SBO-drywell2*. It is the base deck, developed from Reference 1 and described in Section 5.3. Case 1 assumes no RPV leakage, depressurization (cooldown) with a rate of 80 °F/hour a 100% humidity and base deck inputs as described in Section 5.0.

Case 2 is called *Case SBO-drywell2-80-sensy2-NoLeak*. Case 2 is identical to Case 1 with the change in humidity, changes in the leakage area and minor changes in the heat transfer type 6 and 7. Case 2 assumes 20% humidity and minor changes in the heat transfer type 6 and 7. These changes are described in Section 6.2.1.

Case 3 is identical to case *SBO-drywell2-80-sensy2-NoLeak* but with leak. It is called *SBO-drywell2-Leak-80-sensy*. These changes are described in Section 6.3.1.

Case 4 is called *SBO-drywell2-Leak-45-sensy* and is identical to Case 3 but with a slower depressurization (cooldown) rate. It assumes a depressurization of 45 °F/hour with leak in order to show that with an early depressurization and slower cooldown rate the results are not changed and the drywell temperature is not impacted negatively by a slower cooldown. Consistent with Reference 1, the RHRSW temperature is changed to 75 °F. Case 5 addresses changes found during documentation and as part of review. These changes are described in Section 6.4.1.

Case 5 is called *SBO-drywell2-comments*. The following changes are made in Case 5 to address changes found during documentation and review:

- change the temperatures of the steel structures from 160 °F to 170 °F (very conservative assumption),
- change the K reverse for the Junction 3 from to 3.93 from 3.964,
- set the V3 Valve with the same area as the junction, and
- change the area for the pedestal from 2108 ft<sup>2</sup> to 2068 ft<sup>2</sup>, consistent with OPL-4A.

Case 5 changes are described in Section 6.5.1.



### 6.1.1 SBO-drywell2 Model Development

*SBO-drywell2* represents the base model for this calculation. The modification to the input are presented in Section 5.0 and the GOTHIC input deck is presented in Attachment A.

### 6.1.2 Case *SBO drywell2* Results

Figure 3 through Figure 11 present the main parameters for the base case SBO-drywell2. Figure 3 presents the drywell temperature. The drywell temperature increases to about 285 °F after one hour. The heatup is arrested due to depressurization. At about 4 hours into the transient the temperature in the drywell starts increasing due to lower heat removal into the passive heat sinks (walls). The maximum drywell temperature is 290 °F. The air gap acts as an insulation and the steel liner is almost at 245 °F. However, after 2 hours and 10 minutes the low pressure pumps are available so the operators can spray the drywell with the RHR pump, if needed. The results indicate that the temperatures in the drywell stay below the EQ limit and the drywell liner is well below the 281 °F for the SBO coping duration.

Figure 4 presents the containment pressure. Due to the higher leak area the drywell and the wetwell are at the same pressure. At about 2 hours the pressure in the drywell is too low to spray the drywell, (unsafe area of DWSIL(EOP-3 –Primary Containment Control –Reference 30)) however the pressure increases to about 6 psig at about 12000 seconds at which point the operators would be able to spray the drywell with the RHR pump, if needed.

Figure 5 presents the RPV pressure. At one hour into the event it is assumed that the operators start depressurization (cooldown). The pressure drops to the HPCI shutoff pressure of 165 psia at about 12000 seconds. At that point only about 450000 lb were injected from CST (Figure 12). At this point the RPV is depressurized and the CS is available to inject.

Figure 7 presents the RPV level. The core stays covered. There is a dip in the normal level at about 12000 seconds when HPCI stops injecting and CS pump has not yet injected. This is due to the fact that the CS pump was set to inject at 14000 seconds; however CS is ready to inject at 7800 seconds.

Figure 8, Figure 9, and Figure 10 presents the drywell liner temperature. The drywell liner stays below 260 °F for the 7 hours analyzed. After 2 hours and 10 minutes the low pressure pumps are available for suppression pool cooling, drywell spray and maintaining vessel inventory.

Figure 11 presents the suppression pool temperature. Since the vessel is depressurized early, the suppression pool temperature is below the maximum of 182.2 °F calculated in Reference 1, hence no containment overpressure is required.





SBO - 80F-Noleak-drywell1  
 Mar/03/2005 13:28:01  
 GOHIC Version 7.0p2(QA) - April 2002  
 File: /home/schor/vyc-2120ccn/SENSITIVITY/SBO/drywell-SBO/SBO-drywell2

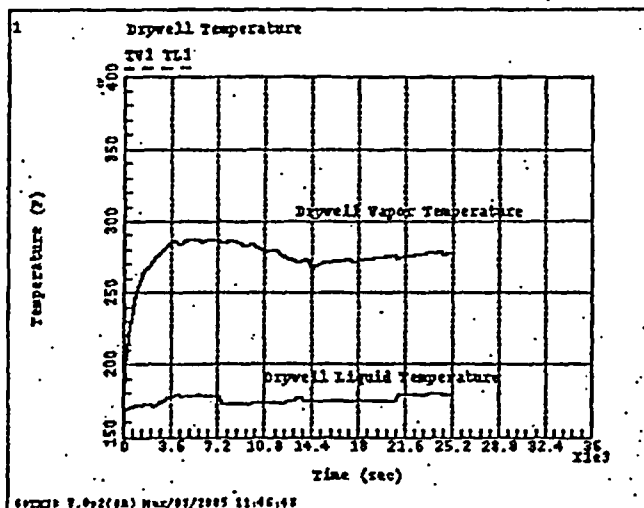


Figure 3 Drywell Temperature Case SBO-drywell2

SBO - 80F-Noleak-drywell1  
 Mar/03/2005 13:33:59  
 GOHIC Version 7.0p2(QA) - April 2002  
 File: /home/schor/vyc-2120ccn/SENSITIVITY/SBO/drywell-SBO/SBO-drywell2

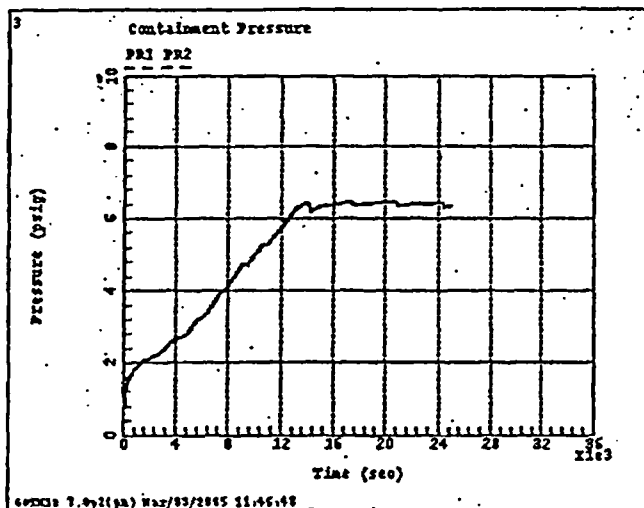


Figure 4 Containment Pressure - case SBO-drywell2



SBO - 80F-Noleak-drywell1  
 Mar/03/2005 13:29:48  
 GOthic Version 7.0p2(QA) - April 2002  
 File: /home/schor/vyc-2120ccn/SENSITIVITY/SBO/drywell-SBO/SBQ-drywell2

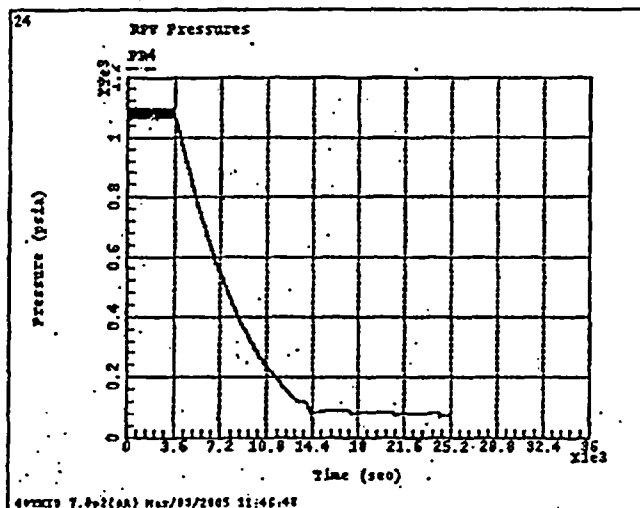


Figure 5 – RPV Pressure - Case SBO –drywell2

SBO - 80F-Noleak-drywell1  
 Mar/03/2005 13:30:33  
 GOthic Version 7.0p2(QA) - April 2002  
 File: /home/schor/vyc-2120ccn/SENSITIVITY/SBO/drywell-SBO/SBO-drywell2

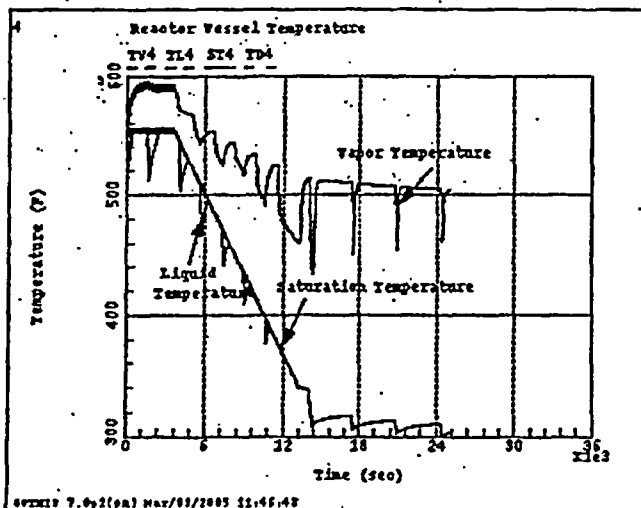


Figure 6- RPV Temperature – Case SBO-drywell2



SBO - 80F-Noleak-drywell1  
 Mar/03/2005 13:01:07  
 GOthic Version 7.0p2(QA) - April 2002  
 File: /home/schor/vyc-2120ccm/SENSITIVITY/SBO/drywell-SBO/SBO-drywell2

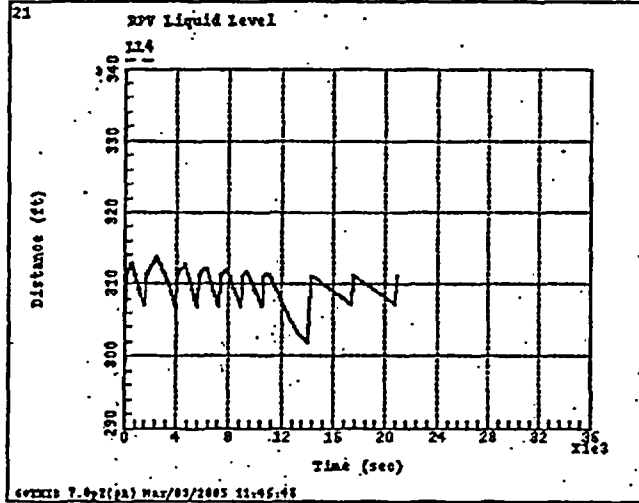


Figure 7 - RPV Level - Case SBO-drywell2

SBO - 80F-Noleak-drywell1  
 Mar/03/2005 13:29:11  
 GOthic Version 7.0p2(QA) - April 2002  
 File: /home/schor/vyc-2120ccm/SENSITIVITY/SBO/drywell-SBO/SBO-drywell2

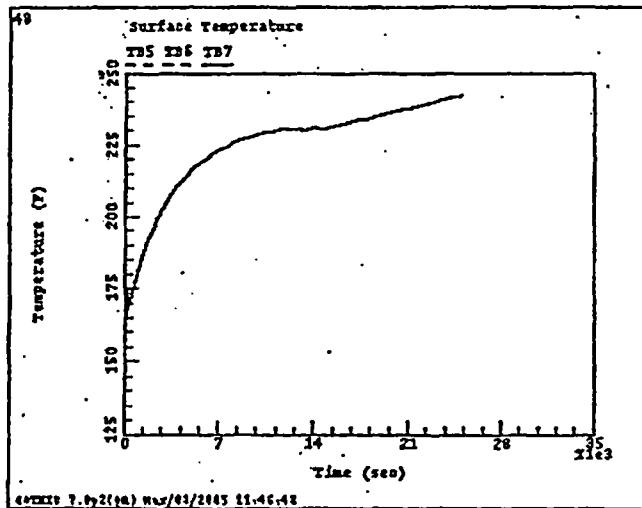


Figure 8 - Surface Temperature for Heat Slabs 5,6 & 7 - Case SBO-drywell2

SBO - 80F-Noleak-drywell1  
Mar/03/2005 13:28:24  
GOTHIC Version 7.0p2(QA) - April 2002  
File: /home/schor/vyc-2120ccn/SENSITIVITY/SBO/drywell-SBO/SBO-drywell2

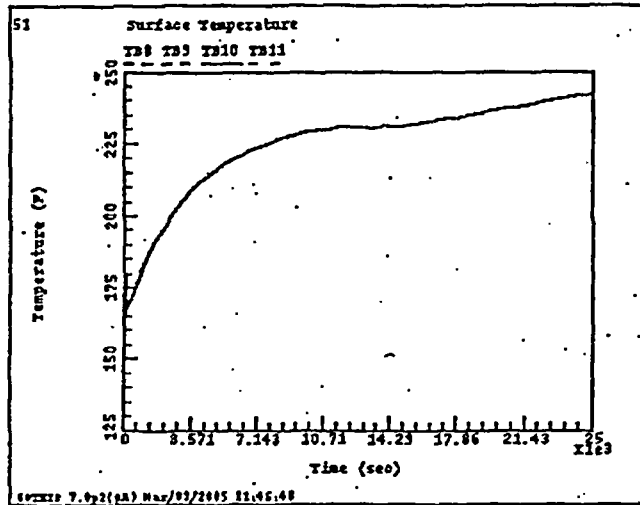


Figure 9 Surface Temperature for Heat Slabs 8,9,10,11 - Case SBO-drywell2

SBO - 80F-Noleak-drywell1  
Mar/14/2005 14:45:07  
GOTHIC Version 7.0p2(QA) - April 2002  
File: /home/schor/vyc-2120ccn/SENSITIVITY/SBO/drywell-SBO/SBO-drywell2

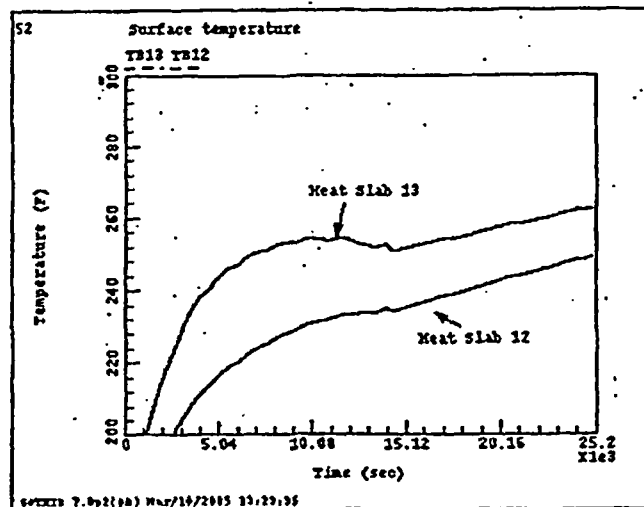


Figure 10 - Surface Temperature for Heat Slabs 12 and 13 - Case SBO-drywell2



SBO - 80F-Noleak-drywell1  
 Mar/03/2005 13:31:38  
 GOHIC Version 7.0p2(QA) - April 2002  
 File: /home/schor/vyc-2120ccn/SENSITIVITY/SBO/drywell-SBO/SBO-drywell2

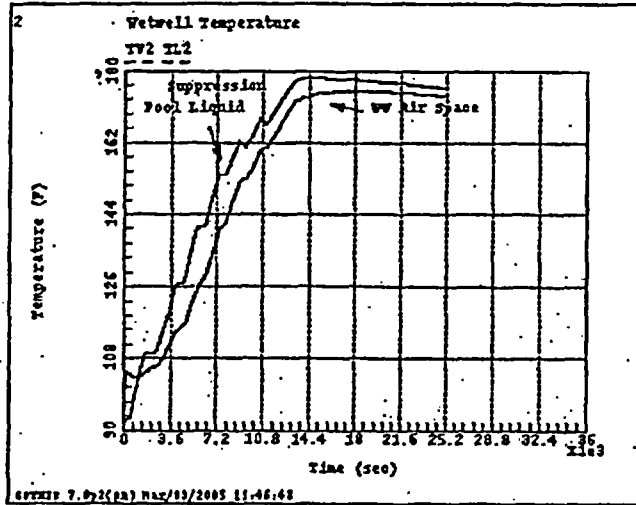


Figure 11 Suppression Pool Temperature case SBO-drywell2

SBO - 80F-Noleak-drywell1  
 Mar/14/2005 14:02:38  
 GOHIC Version 7.0p2(QA) - April 2002  
 File: /home/schor/vyc-2120ccn/SENSITIVITY/SBO/drywell-SBO/SBO-drywell2

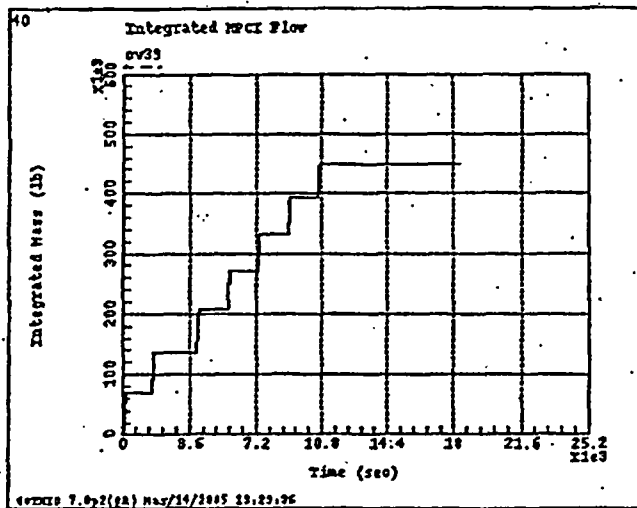


Figure 12- Integrated HPCI Flow – SBO-drywell2



## 6.2 Case *SBO-drywell2-80-sensy2-NoLeak*

### 6.2.1 Model modification

Table 8 presents the modifications to the base deck *SBO-drywell2* to produce *SBO-drywell2-80-sensy2-NoLeak*.

The following modifications were made:

The Heat Transfer Coefficient Types 6 and 7 were modified to use Uchida correlation for condensation heat transfer instead of MAX (maximum of Uchida or Guido-Koestel). For this case since there is no RPV leakage, the choice of condensation correlation should have a minimal impact on results.

For the Heat Transfer Coefficient Type 7 the radiation option was turned off. Again, at these small temperatures, the radiation has a minimal impact on results.

The humidity in Volume 1 (Drywell) was modified from 100% humidity to 20% humidity to encompass all the humidity range in the drywell (Reference 5).

The reverse loss coefficient for the vacuum breakers was changed from 1e18 to 3.964 (equal to the forward loss coefficient).

A coefficient of 3.93 should have been used. This is corrected in Case 5.

The vacuum breaker reverse coefficient is the weighted sum of the flow paths 7, 8 & 9 of Reference 9. (Same as the forward loss coefficient)

$$K \text{ reverse} = 1.168 (15.63/16.23)^2 + 2.528 (15.63/16.23)^2 + 0.5 (1.53/1.53)^2 = 3.93$$

(A K of 3.96 was used, less than a 1% difference)

The area of junction 21 is changed from 0.12 ft<sup>2</sup>, maximum leakage to 0.0033 ft<sup>2</sup> (allowable Tech Spec leakage) –Reference 33.

**Table 8; Input Modifications –*SBO-drywell2-80-sensy2-NoLeak* vs. *SBO-drywell2***



Modifications in /home/schor/vyc-2120ccn/SENSITIVITY/SBO/drywe11-SBO/SBO-drywe112-80-sen  
 Mar/10/2005 10:42:03  
 GOTHIC Version 7.0p2(OA) - April 2002  
 File: /home/schor/vyc-2120ccn/SENSITIVITY/SBO/drywe11-SBO/SBO-drywe112-80-sensy2-NoLeak

Graphs (continued)

Graph #	Title	Mon	1	2	3	4	5
42	Heat to the sup		CQ4H	CQ2H			
43	Leak Flow		FL4	FL19	FL20		
44	Integrated Leak		CV40				
45	Title		CV39				
46			FV18	FL18	FD18		
47			CV38				
48	Surface Tempera		TB5	TB6	TB7		
49	Surface Tempera		TA8	TA9	TA10		
50	Surface Tempera		TA11	TA12	TA13		
51	Surface Tempera		TB8	TB9	TB10	TB11	
52	Surface tempera		TB13	TB12			
53			TP8t600	TP9t600	TP10t60	TP11t60	
54			TP13t50	TP12t50			
55	Drywe11 Tempera		TV1	TL1			

Heat Transfer Coefficient Types - Table 1

Type #	Heat Transfer Option	Nominal Value	Cnd FF	Cnd Cnv Opt	Sp Cnv Opt	HTC	Nat Cnv Opt	For Cnv Opt	Rad Opt
1	Correlat		0				VERT SURF	PIPE FLOW	OFF
2	Correlat		0				VERT SURF	PIPE FLOW	OFF
3	Correlat						FACE DOWN	PIPE FLOW	OFF
4	Correlat						FACE UP	PIPE FLOW	OFF
5	Sp Heat	0.							
6	Direct			ADD UCHI			VERT SURF	PIPE FLOW	OFF
7	Direct			ADD UCHI			FACE DOWN	PIPE FLOW	OFF

Run Control Parameters (Seconds)

Time Int	DT Min	DT Max	DT Ratio	End Time	Print Int	Graph Int	Max CPU	Dump Int	Phs Chng Time Scale
1	1e-06	1.	1.	100.	5.	0.1	1e+06	0.	DEFAULT
2	1e-06	1.	1.	1200.	50.	1.	1e+06	0.	DEFAULT
3	1e-06	1.	1.	1300.	500.	10.	1e+06	0.	DEFAULT
4	1e-06	1.	1.	25000.	600.	10.	1e+06	0.	DEFAULT



Modifications in /home/schor/vyc-2120ccn/SENSITIVITY/SBO/drywell-SBO/SBO-drywell12-80-sen  
 Mar/10/2005 10:42:03  
 GOTHIC Version 7.0p2(OA) - April 2002  
 File: /home/schor/vyc-2120ccn/SENSITIVITY/SBO/drywell-SBO/SBO-drywell12-80-sensy2-NoLeak

Volume Initial Conditions

Vol #	Pressure (psia)	Vapor Temp. (F)	Liquid Temp. F	Relative Humidity (%)	Liquid Volume Fractio	Ice Volume Fract.	Ice Surf.A. (ft2)
def	14.7	80.	80.	60.	0.	0.	0.
1	16.4	170.	170.	20.	0.	0.	0.
2	14.7	90.	90.	100.	0.39497	0.	0.
3	16.4	90.	90.	100.	0.00595	0.	0.
4	1045.2	549.97	533.12	100.	0.60794	0.	0.

Graphs

Graph #	Title	Mon	1	Curve Number	2	3	4	5
1	Drywell Tempera		TV1	TL1				
2	Wetwell Tempera		TV2	TL2				
3	Containment Pre		PR1	PR2				
4	Reactor Vessel		TV4	TL4	ST4		TD4	
5	RHR Heat Exchan		xq1H					
6	Reactor Vessel		AL4					
7	Torus Water Vol		AL2					
8	Heat Exchanger		t11H	t21H				
9	Wetwell. Vessel		TL2	TL4	TL1			
10	Conductor Tempe		TA1	TA2	TA3		TA4	
11	Integral Vessel		QL4	QV4				
12	Vapor & Conduct		TV4	TA1				
13	Liquid & Conduc		TL4	TA2				
14	Vapor & Conduct		TV2	TA3				
15	Liquid & Conduc		TL2	TA4				
16	Vapor Heat Tran		HA1					
17	Liquid Heat Tra		HA2					
18	Vapor Heat Tran		HA3					
19	Liquid Heat Tra		HA4					
20	Feedwater & Bre		FL9	FL4				
21	RPV Liquid Leve		LL4					
22	SRV and ADS Flo		FV10	FV11				
23	Feedwater Entha		cv29					
24	RPV Pressures		PR4					
25	Feedwater Contr		cv27	cv28				
26	Integrated Feed		cv4					
27	RHR Flow		FL5					
28	Vessel Droplet		AD4					
29	ECCS Injection		FL7	FL12	FL14			
30	RPV Pressure		PR4	VC2V	FL7			
31	ADS Valve Posit		VC3V					
32	SRV Position		VC2V					
33	Cooldown Flow		FV16					
34	Vessel Drop Dia		DI4					
35	Reactor Vessel		PR4					
36	Suppression poo		TL2					
37	Reactor Vessel		PR4					
38	Suppression Poo		LL2					
39	HPCI Flow Rate		FL18					
40	Integrated HPCI		cv39					
41	Core Spray Flow		FL8					





Modifications in /home/schor/vyc-2120ccn/SENSITIVITY/SB0/drywe11-SB0/SB0-drywe112-80-sen  
 Mar/10/2005 10:42:03  
 GOTHIC Version 7.0p2(QA) - April 2002  
 File: /home/schor/vyc-2120ccn/SENSITIVITY/SB0/drywe11-SB0/SB0-drywe112-80-sensy2-NoLeak

Flow Paths - Table 2

Flow Path #	Flow Area (ft <sup>2</sup> )	Hyd. Diam. (ft)	Inertia Length (ft)	Friction Length (ft)	Relative Roughness	Dep Bend (deg)	Mom Trn Opt	Strat Flow Opt
1	283.529	6.75	89.13	0.		0.	-	NONE
2	286.114	1.948	4.16	0.		-1.	-	NONE
3	15.63	1.5625	44.925	28.72		0.	-	NONE
4	0.001005	0.03568	0.1			0.	-	NONE
5	3.14	2.	0.01			0.	-	NONE
6	3.14	2.	0.01			0.	-	NONE
7	3.14	2.	0.01			0.	-	NONE
8	3.14	2.	0.01			0.	-	NONE
9	3.14	2.	0.01			0.	-	NONE
10	0.09945	0.35584	0.01			0.	-	NONE
11	0.3978	0.35584	0.01			0.	-	NONE
12	3.14	2.	0.01			0.	-	NONE
13	3.14	2.	0.01			0.	-	NONE
14	3.14	2.	0.01			0.	-	NONE
15	3.14	2.	0.01			0.	-	NONE
16	3.14	2.	0.01			0.	-	NONE
17	3.14	2.	0.01			0.	-	NONE
18	3.14	2.	0.01			0.	-	NONE
19	0.5454	0.8333	0.1	0.1			-	NONE
20	0.5454	0.5454	0.1	0.1			-	NONE
21	0.0033	1.	1.	0.			-	NONE

Flow Paths - Table 3

Flow Path #	Fwd. Loss Coeff.	Rev. Loss Coeff.	Comp. Opt.	Critical Flow Model	Exit. Loss Coeff.	Drop Breakup Model
1	4.2243	4.2243	ON	TABLES	1.	OFF
2	1.	0.78	ON	TABLES	1.	OFF
3	3.964	3.964	ON	OFF	0.	OFF
4	0.		OFF	TABLES	1.	OFF
5			OFF	OFF	0.	OFF
6			OFF	OFF	0.	OFF
7			OFF	OFF	0.	OFF
8			OFF	OFF	0.	OFF
9			OFF	OFF	0.	OFF
10			OFF	TABLES	0.	OFF
11			OFF	TABLES	0.	OFF
12			OFF	OFF	0.	OFF
13			OFF	OFF	0.	OFF
14			OFF	OFF	0.	OFF
15			OFF	OFF	0.	OFF
16		1e+18	OFF	OFF	0.	OFF
17			OFF	OFF	0.	OFF
18			OFF	OFF	0.	OFF
19			OFF	OFF	0.	OFF
20			OFF	OFF	0.	OFF
21	1.5	1.5	OFF	OFF	0.	OFF



### 6.2.2 Case SBO drywell2-80-sensy2-NoLeak Results

Figure 13 through Figure 20 present the main parameters for the case *SBO-drywell2-80-sensy2-NoLeak*. Figure 13 presents the drywell temperature. The maximum drywell temperature is about 289.4 °F and is reached after one hour and 30 minutes. The heatup is arrested due to depressurization. At about 4 hours into the transient the temperature in the drywell starts increasing due to lower heat removal into the passive heat sinks (walls). The air gap acts as an insulation and the steel liner is almost at 255 °F. However, after 2 hours and 10 minutes the low pressure pumps are available so the operators can spray the drywell with the RHR pump, if needed. The results indicate that the temperatures in the drywell stay below the EQ limit and the drywell liner is well below the 281 °F for the SBO coping duration.

Figure 14 presents the containment pressure. Due to a lower leak area the drywell and the wetwell are not at the same pressure, the vacuum breaker opens to relieve the pressure difference at about 14000 seconds. At about 2 hours the pressure in the drywell is too low to spray the drywell, (unsafe area of DWSIL (EOP-3 -Primary Containment Control -Reference 30)) however the pressure increase to about 6 psig at about 10800 seconds at which point the operators would be able to spray the drywell with the RHR pump, if needed.

Figure 15 presents the RPV pressure. At one hour into the event it is assumed that the operators start depressurization. The pressure drops to the HPCI shutoff pressure of 165 psia at about 12000 seconds. At this point only about 450000 lb were injected from CST (Figure 17). The RPV is depressurized, and the CS pump is available to inject.

Figure 16 pump presents the RPV level. The core stays covered. There is a dip in the normal level at about 12000 seconds when HPCI stops injecting and CS does not inject yet. This is due to the fact that the CS pump was set to inject at 14000 seconds; however CS is ready to inject at 7800 seconds, provided the pressure permissive is reached.

Figure 18, Figure 19, and Figure 20 presents the drywell liner temperature. The drywell liner stays below 260 °F for the 7 hours analyzed. After 2 hours and 10 minutes the low pressure pumps are available for suppression pool cooling, drywell spray and maintaining vessel inventory.

The suppression pool temperature for this case is very similar to the case *SBO-drywell2* since the input changes results in minor changes to the drywell temperature and pressure but not in the suppression pool temperature since the heat transferred to the drywell is not subtracted from the vessel energy.



SBO - 80F-NoLeak-drywell2-sensitivities-set2  
 Max/10/2005 10:36:15  
 GOthic Version 7.0p2(QA) - April 2002  
 File: /home/schor/vyc-2120ccn/SENSITIVITY/SBO/drywell-SBO/SBO-drywell12-80

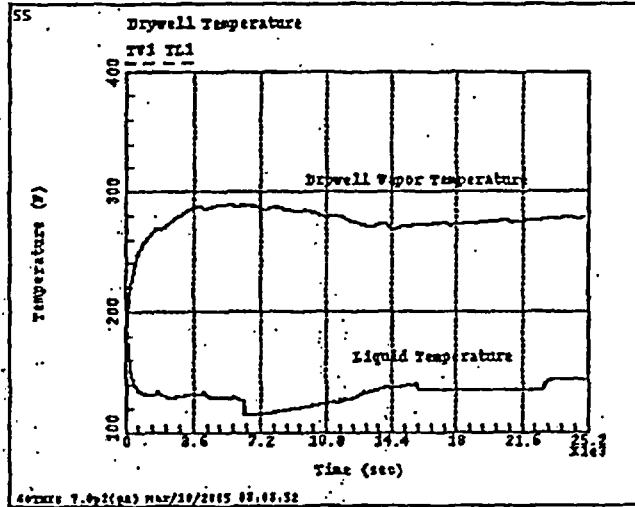


Figure 13 – Drywell Temperature –Case SBO-drywell2-80-sensy2-NoLeak

SBO - 80F-NoLeak-drywell2-sensitivities-set2  
 Max/10/2005 10:56:11  
 GOthic Version 7.0p2(QA) - April 2002  
 File: /home/schor/vyc-2120ccn/SENSITIVITY/SBO/drywell-SBO/SBO-drywell12-80

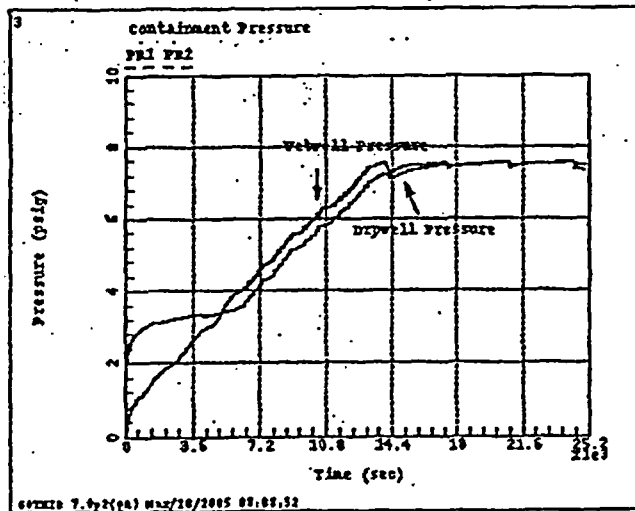


Figure 14 –Containment Pressure - Case SBO-drywell2-80-sensy2-NoLeak



SBO - 80F-NoLeak-drywell2-sensitivities-set2  
 Mar/10/2005 11:11:35  
 GOthic Version 7.0p2(QA) - April 2002  
 File: /home/schor/vyc-2120ccn/SENSITIVITY/SBO/drywell-SBO/SBO-drywell2-80

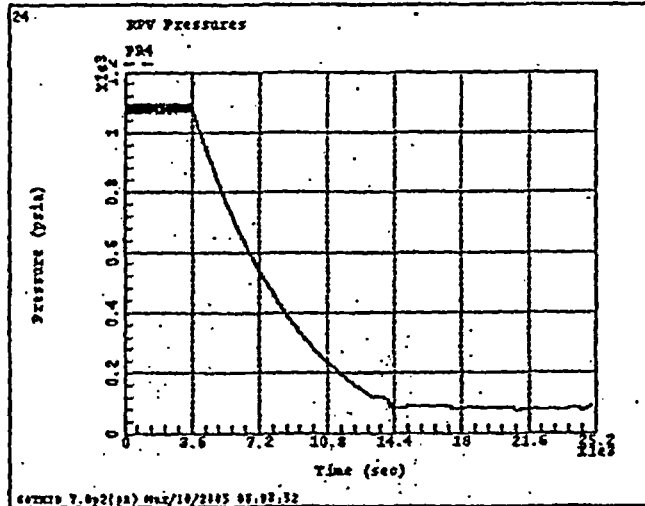


Figure 15 – RPV Pressure - Case SBO-drywell2-80-sensy2-NoLeak

SBO - 80F-NoLeak-drywell2-sensitivities-set2  
 Mar/10/2005 11:15:46  
 GOthic Version 7.0p2(QA) - April 2002  
 File: /home/schor/vyc-2120ccn/SENSITIVITY/SBO/drywell-SBO/SBO-drywell2-80

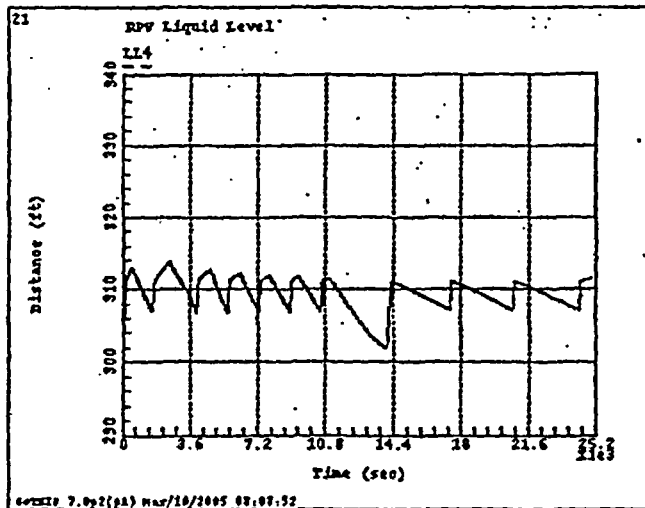


Figure 16 – RPV Level - Case SBO-drywell2-80-sensy2-NoLeak



SBO - 80F-NoLeak-drywell2-sensitivities-set2  
Mar/10/2005 11:10:47  
GOTHIC Version 7.0p2(QA) - April 2002  
File: /home/schor/vyc-2120ccn/SENSITIVITY/SBO/drywell-SBO/SBO-drywell2-80

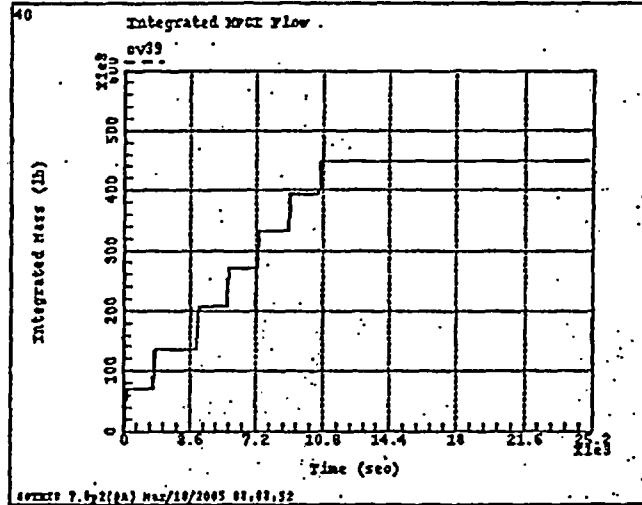


Figure 17 Integrated HPCI Flow - Case SBO-drywell2-80-sensy2-NoLeak

SBO - 80F-NoLeak-drywell2-sensitivities-set2  
Mar/10/2005 10:33:12  
GOTHIC Version 7.0p2(QA) - April 2002  
File: /home/schor/vyc-2120ccn/SENSITIVITY/SBO/drywell-SBO/SBO-drywell2-80

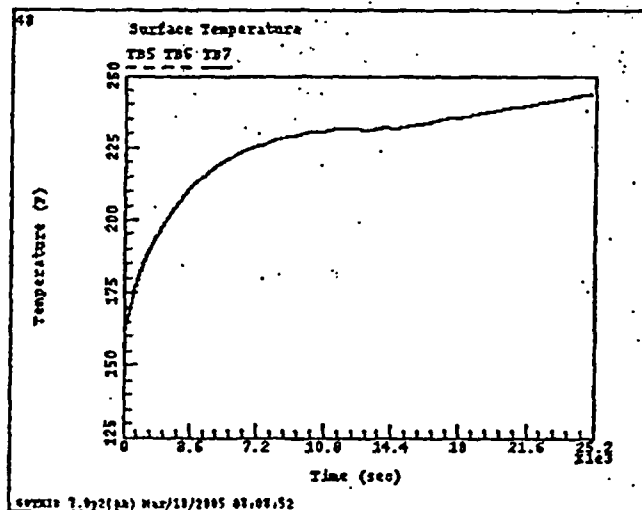


Figure 18- Surface Temperature for Heat Slabs 5,6 & 7 - Case SBO-drywell2-80-sensy2-NoLeak



SBO - 80F-NoLeak-drywell2-sensitivities-set2  
 Mar/10/2005 10:34:30  
 GOthic Version 7.0p2(QA) - April 2002  
 File: /home/schor/vyc-2120ccn/SENSITIVITY/SBO/drywell-SBO/SBO-drywell2-80

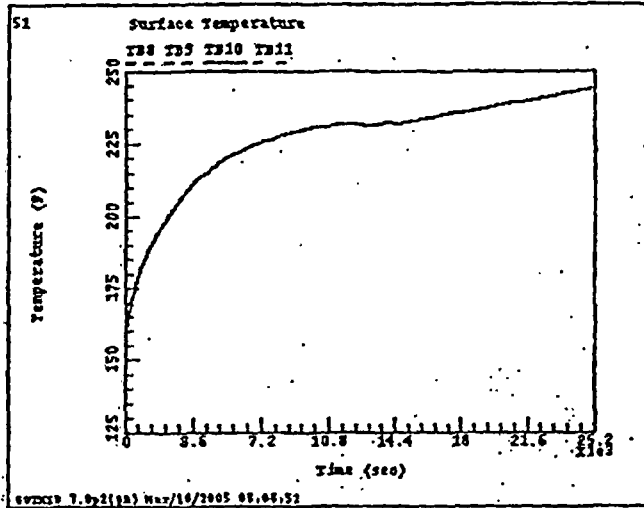


Figure 19 – Surface Temperature for Heat Slabs 8, 9, 10 & 11 - Case SBO-drywell2-80-sensy2-NoLeak

SBO - 80F-NoLeak-drywell2-sensitivities-set2  
 Mar/10/2005 10:32:24  
 GOthic Version 7.0p2(QA) - April 2002  
 File: /home/schor/vyc-2120ccn/SENSITIVITY/SBO/drywell-SBO/SBO-drywell2-80

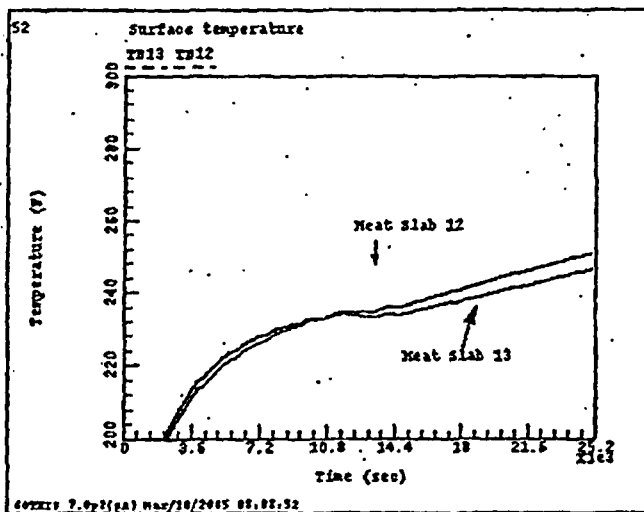


Figure 20 Surface Temperature for Heat Slabs 12 & 13 - Case SBO-drywell2-80-sensy2-NoLeak

### 6.3 Case *SBO-drywell2-Leak-80-sensy*

#### 6.3.1 Model modification

Table 9 presents the modifications to the deck *SBO-drywell2-80-sensy2-NoLeak* to produce *SBO-drywell2-Leak-80-sensy*

The following modifications were made:

On BC 13, the ON trip is set to zero (0). This allows for a constant leak of 8.4585 lb/sec to leave the vessel.

The end time was changes to 14400 seconds (4 hours) since the purpose of this calculation was to show that the drywell temperature stays below the EQ drywell temperature and the drywell shell stays below 281 °F for the duration of 2 hour and 10 minutes.

Table 9 *SBO-drywell2-Leak-80-sensy* vs *SBO-drywell2-80-sensy2-NoLeak*



Modifications in /home/schor/vyc-2120ccn/SENSITIVITY/SBO/drywell-SBO/SBO-drywell2-Leak-8  
 Mar/14/2005 15:38:40  
 GOTHIC Version 7.0p2(QA) - April 2002  
 File: /home/schor/vyc-2120ccn/SENSITIVITY/SBO/drywell-SBO/SBO-drywell2-Leak-80-sensy

Fluid Boundary Conditions - Table 1

BC#	Description	Press. (psia)	Temp. (F)	Flow (lbm/s)	ON Trip	OFF Trip
1F	RHR/LPCI Suctio	20.	160	v-0.002	8	1 13
2C	RHR/LPCI Discha	20.	160			
3F	LPCS Suction	20.	160	v-0.002	7	30 31
4C	LPCS Discharge	20.	160			
5F	Feedwater	1000.	e1	5 1000	9	1 5
6F	RHR/Torus Sucti	20.	160	v-0.002	6	21 1
7C	RHR/Torus Disch	20.	160			0
8F	HPCI/RCIC Sucti	20.	160	-326.1	9	1 0
9C	HPCI/RCIC Disch	20.	160			
10P	Cooldown Inlet	1. 10	1	11		21 0
11F	Cooldown Outlet	1. 10	1	11		1 12
12F	CST Tank	14.7	135	587	13	28 27
13F	Vessel Leak	1050.	554.	-8.4585	13	0
14C	Vessel leak to	1050. 0	554			

Run Control Parameters (Seconds)

Time Int	DT Min	DT Max	DT Ratio	End Time	Print Int	Graph Int	Max CPU	Dump Int	Phs Chng Time Scale
1	1e-06	1.	1.	100.	5.	0.1	1e+06	0.	DEFAULT
2	1e-06	1.	1.	1200.	50.	1.	1e+06	0.	DEFAULT
3	1e-06	1.	1.	1300.	500.	10.	1e+06	0.	DEFAULT
4	1e-06	1.	1.	14400.	600.	10.	1e+06	0.	DEFAULT

Graphs

Graph #	Title	Mon	1	2	3	4	5
1	Drywell Tempera		TV1	TL1			
2	Wetwell Tempera		TV2	TL2			
3	Containment Pre		PR1	PR2			
4	Reactor Vessel		TV4	TL4	ST4	TD4	
5	RHR Heat Exchan		xq1H				
6	Reactor Vessel		AL4				
7	Torus Water Vol		AL2				
8	Heat Exchanger		t11H	t21H			
9	Wetwell Vessel		TL2	TL4	TL1		
10	Conductor Tempe		TA1	TA2	TA3	TA4	
11	Integral Vessel		QL4	QV4			
12	Vapor & Conduct		TV4	TA1			
13	Liquid & Conduc		TL4	TA2			
14	Vapor & Conduct		TV2	TA3			
15	Liquid & Conduc		TL2	TA4			
16	Vapor Heat Tran		HA1				
17	Liquid Heat Tra		hA2				
18	Vapor Heat Tran		HA3				
19	Liquid Heat Tra		hA4				
20	Feedwater & Bre		FL9	FL4			





Modifications in /home/schor/vyc-2120ccn/SENSITIVITY/SBO/drywe11-SBO/SBO-drywe112-Leak-8  
 Mar/14/2005 15:38:40  
 GOthic Version 7.0p2(QA) - April 2002  
 File: /home/schor/vyc-2120ccn/SENSITIVITY/SBO/drywe11-SBO/SBO-drywe112-Leak-80-sensy

Graphs (continued)

Graph #	Title	Mon	Curve Number					
			1	2	3	4	5	
21	RPV Liquid Level		LL4					
22	SRV and ADS Flo		FV10	FV11				
23	Feedwater Entha		cv29					
24	RPV Pressures		PR4					
25	Feedwater Contr		cv27	cv28				
26	Integrated Feed		cv4					
27	RHR Flow		FL5					
28	Vessel Droplet		AD4					
29	ECCS Injection		FL7	FL12	FL14			
30	RPV Pressure		PR4	VC2V	FL7			
31	ADS Valve Posit		VC3V					
32	SRV Position		VC2V					
33	Cooldown Flow		FV16					
34	Vessel Drop Dia		DI4					
35	Reactor Vessel		PR4					
36	Suppression poo		TL2					
37	Reactor Vessel		PR4					
38	Suppression Poo		LL2					
39	HPCI Flow Rate		FL18					
40	Integrated HPCI		cv39					
41	Core Spray Flow		FL8					
42	Heat to the sup		CO2H	CO2H				
43	Leak Flow		FL4	FL19	FL20			
44	Integrated Leak		cv40					
45	Title		cv39					
46			FV18	FL18	FD18			
47			cv38					
48	Surface Tempera		TB5	TB6	TB7			
49	Surface Tempera		TA8	TA9	TA10			
50	Surface Tempera		TA11	TA12	TA13			
51	Surface Tempera		TB9	TB9	TB10	TB11		
52	Surface Tempera		TB13	TB12				
53			TP8t600	TP9t600	TP10t60	TP11t60		
54			TP13t50	TP12t50				
xxxxx	xxxxxxxx		xxx	xxxxxxxx	xxxxxxxx	xxxxxxxx	xxxxxxxx	xxxxxxxx



### 6.3.2 Results Case SBO-drywell2-Leak-80-sensy

Figure 21 through Figure 29 present the main parameters for the case *SBO-drywell2-Leak-80-sensy*. Figure 21 presents the drywell temperature. The maximum drywell temperature is about 290 °F and is reached at about 12240 seconds (3.4 hours). The drywell heatup rate is arrested due to depressurization, however the leak brings enough energy from the vessel to continue the heatup. At 7800 seconds the drywell temperature is 285.8 °F, well below the EQ limit of 325 °F.

Figure 22 presents the containment pressure. The available water to spray the drywell (Reference 30) is the Diesel fire pump per Appendix M of OE 3107 (Reference 35) and it takes about one hour for aligning the fire pump for drywell spray. The drywell pressure is high enough to allow for drywell spray, if needed. The drywell temperature does not exceed the EQ drywell temperature limit and the drywell shell temperature stays below the limit of 281 °F hence the analysis shows that drywell spray is not needed for the coping duration. At about 3 hours and 30 minutes the wetwell pressure reaches equilibrium with drywell and slightly exceeds the drywell pressure. The vacuum breakers do not open during the time of interest.

At about 4 hours the wetwell pressure is about 26 psig, close to the PSP limit of 27 psig. However at this time the RHR pump is available for containment spray.

Figure 23 presents the RPV pressure. At one hour into the event it is assumed that the operators start depressurization. The pressure drops to the HPCI shutoff pressure of 165 psia at about 12000 seconds. At that point only about 540000 lb were injected from CST (Figure 25). At this time the RPV is depressurized, and the CS pump is available to inject.

Figure 24 pump presents the RPV level. The core stays covered. There is a dip in the normal level at about 12000 seconds when HPCI stops injecting and CS does not inject yet. This is due to the fact that the CS pump was set to inject at 14000 seconds; however, CS is ready to inject at 7800 seconds, provided the pressure permissive is reached.

Figure 27, Figure 28, and Figure 29 presents the drywell liner temperature. The drywell liner stays below 280 °F for the 4 hours analyzed. After 2 hours and 10 minutes the low pressure pumps are available for suppression pool cooling, drywell spray and maintaining vessel inventory.

The suppression pool temperature is not a parameter of importance for this calculation. In Reference 1 it was shown that the suppression pool temperature is lower for the cases RPV with leakage and lower for earlier depressurization hence the maximum suppression pool temperature will be lower than 182.2 °F, calculated in Reference 1.

SBO - 80F-Noleak-drywell2-Leak-80-sensitivities  
Mar/14/2005 11:02:51  
GOTHIC Version 7.0p2(OA) - April 2002  
File: /home/schor/vyc-2120ccn/SENSITIVITY/SBO/drywell-SBO/SBO-drywell2-Le

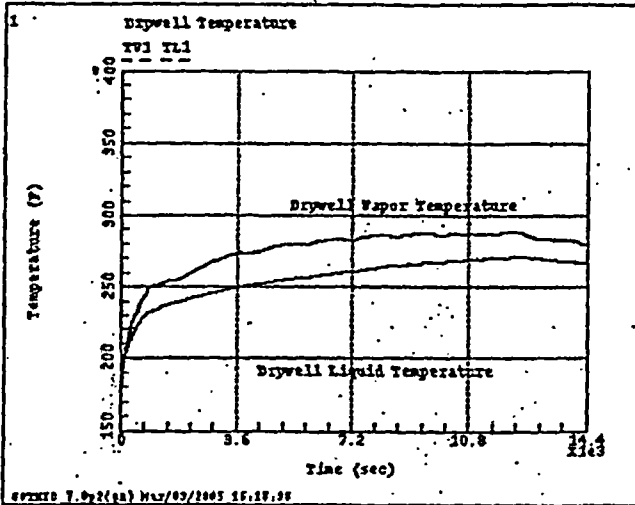


Figure 21 - Drywell Temperatures - SBO-drywell2-Leak-80-sensy

SBO - 80F-Noleak-drywell2-Leak-80-sensitivities  
Mar/14/2005 11:03:43  
GOTHIC Version 7.0p2(OA) - April 2002  
File: /home/schor/vyc-2120ccn/SENSITIVITY/SBO/drywell-SBO/SBO-drywell2-Le

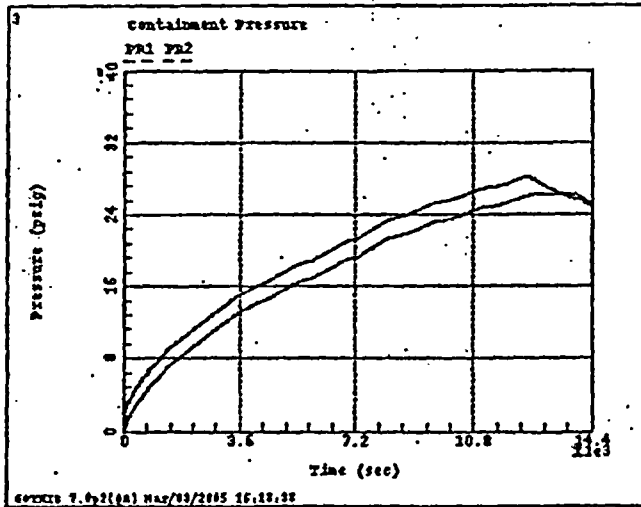


Figure 22 - Containment Pressure - SBO-drywell2-Leak-80-sensy

SBO - 80F-Moleak-drywell2-Leak-80-sensitivities  
 Mar/14/2005 11:05:31  
 GOthic Version 7.0p2(QA) - April 2002  
 File: /home/schor/vyc-2120ccn/SENSITIVITY/SBO/drywell-SBO/SBO-drywell2-Le

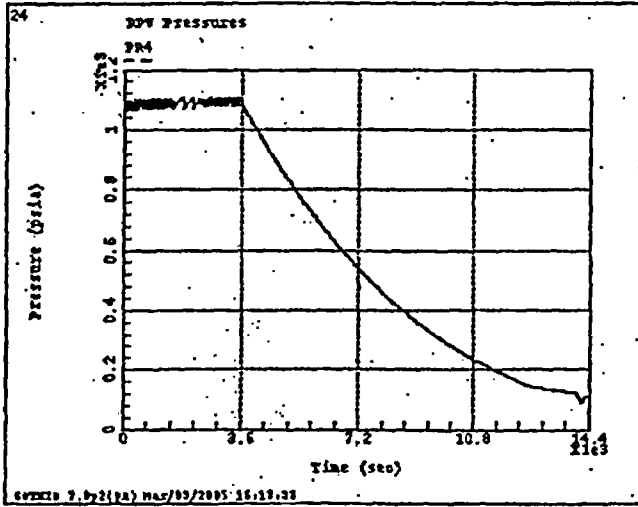


Figure 23 – RPV Pressure - SBO-drywell2-Leak-80-sensy

SBO - 80F-Moleak-drywell2-Leak-80-sensitivities  
 Mar/14/2005 11:04:51  
 GOthic Version 7.0p2(QA) - April 2002  
 File: /home/schor/vyc-2120ccn/SENSITIVITY/SBO/drywell-SBO/SBO-drywell2-Le

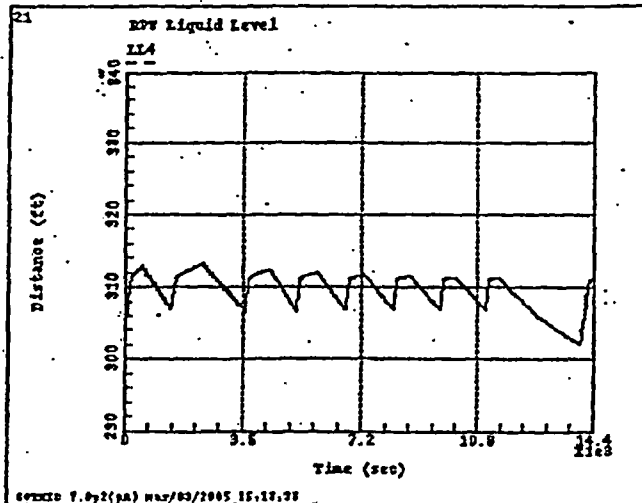


Figure 24 RPV Level - SBO-drywell2-Leak-80-sensy



SBO - 80F-Noleak-drywell2-Leak-80-sensitivities  
Mar/14/2005 11:09:57  
GOTHIC Version 7.0p2(QA) - April 2002  
File: /home/schor/vyc-2120ccm/SENSITIVITY/SBO/drywell-SBO/SBO-drywell2-Le

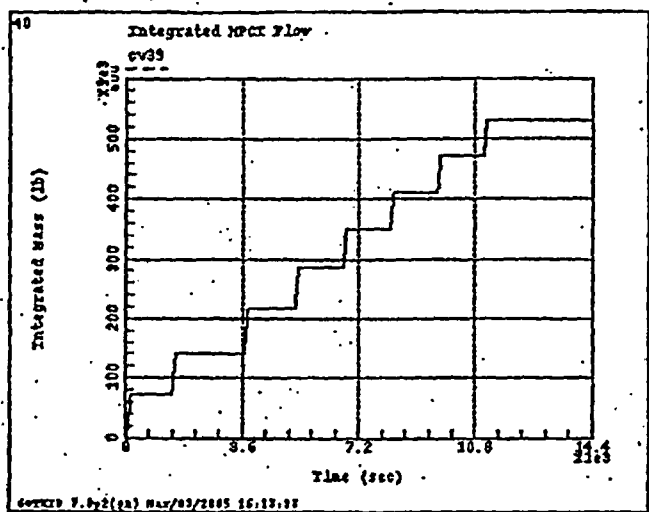


Figure 25 - Integrated HPCI Flow - SBO-drywell2-Leak-80-sensy

SBO - 80F-Noleak-drywell2-Leak-80-sensitivities  
Mar/14/2005 11:10:57  
GOTHIC Version 7.0p2(QA) - April 2002  
File: /home/schor/vyc-2120ccm/SENSITIVITY/SBO/drywell-SBO/SBO-drywell2-Le

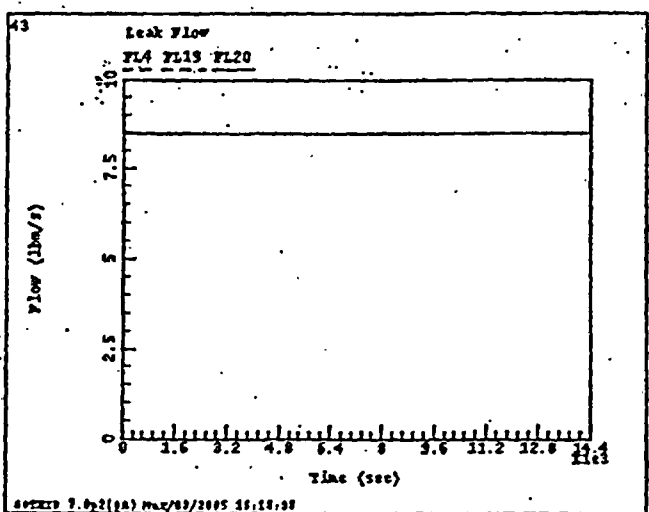


Figure 26 - Leak Flow - SBO-drywell2-Leak-80-sensy



SBO - 80F-NoLeak-drywell2-Leak-80-sensitivities  
 Mar/14/2005 11:07:22  
 GOthic Version 7.0p2(QA) - April 2002  
 File: /home/schor/vyc-2120ccn/SENSITIVITY/SBO/drywell-SBO/SBO-drywell2-Le

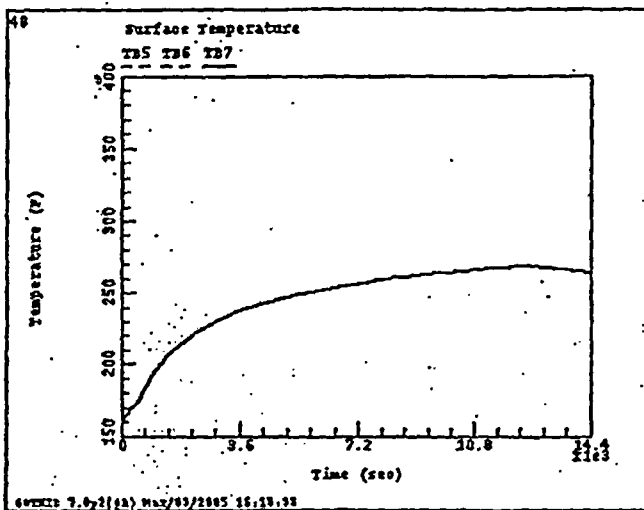


Figure 27 - Surface Temperature, Heat Structures 5,6,7 - SBO-drywell2-Leak-80-sensy

SBO - 80F-NoLeak-drywell2-Leak-80-sensitivities  
 Mar/14/2005 11:06:34  
 GOthic Version 7.0p2(QA) - April 2002  
 File: /home/schor/vyc-2120ccn/SENSITIVITY/SBO/drywell-SBO/SBO-drywell2-Le

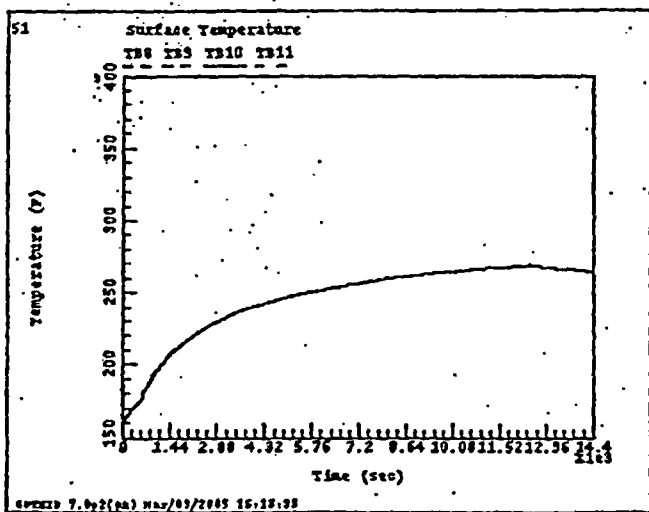


Figure 28 - Surface Temperature, Heat Structures 8, 9, 10, 11 - SBO-drywell2-Leak-80-sensy



SBO - 80F-Noleak-drywell2-Leak-80-sensitivities  
Mar/14/2005 11:09:22  
GOTHIC Version 7.0p2(QA) - April 2002  
File: /home/schor/vyc-2120ccn/SENSITIVITY/SBO/drywell-SBO/SBO-drywell2-Le

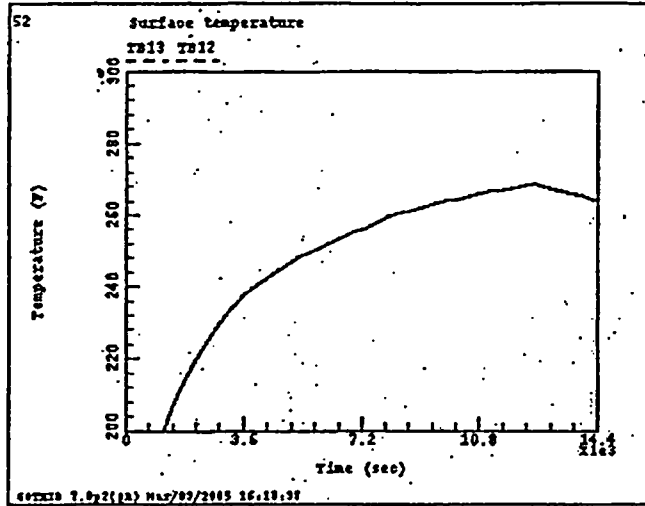


Figure 29 - Surface Temperature, Heat Structures 12,13 - SBO-drywell2-Leak-80-sensy



## **6.4 Case SBO-drywell2-Leak-45-sensy**

### **6.4.1 Model modification**

Table 10 presents the modifications to the deck *SBO-drywell2-Leak-80-sensy* to produce *SBO-drywell2-Leak-45-sensy*.

Two modifications are made, the depressurization (cooldown) table, is changed from 80 °F/hour to 45 °F/hr (same cooldown curve as in Reference 1- Function 10).

The RHRSW temperature is changed from 85 °F to 75 °F consistent with Assumption 13 and Reference 1.

Table 10 *SBO-drywell2-Leak-45-sensy* vs *SBO-drywell2-Leak-80-sensy*





Modifications in /home/schor/vyc-2120ccn/SENSITIVITY/SBO/drywell-SBO/SBO-drywell12-Leak-4  
 Mar/14/2005 17:49:07  
 GOTHIC Version 7.0p2(QA) - April 2002  
 File: /home/schor/vyc-2120ccn/SENSITIVITY/SBO/drywell-SBO/SBO-drywell12-Leak-45-sensy

Functions

FF#	Description	Ind. Var.	Dep. Var.	Points
0	Constant	-	-	0
1	RHR Hx Tube	Reynolds N	Nusselt Nu	34
2	RHR Hx Shell	Reynolds N	Nusselt Nu	34
3	Decay Heat	Time (sec)	Decay Heat	50
4	Pump Heat	Time (sec)	Heat Rate	6
5	Feed Enthalpy	cv4	Dep. Var.	34
6	RHR/Torus	Time (sec)	Flow (gpm)	3
7	LPCS Flow Curve	cv26	Flow (gpm)	13
8	LPCI Flow Curve	cv26	Flow (gpm)	12
9	Feed Flow	cv28	Dep. Var.	3
10	Cooldown Pressu	Time (sec)	Pressure (	39
11	Cooldown Temper	cv33	Dep. Var.	3
12	Cooldown Flow	cv32	Dep. Var.	3
13	Constant	Ind. Var.	Dep. Var.	6
14	ECCS Pump Heat	Time (sec)	Heat Rate	6
15	Check Valve	Ind. Var.	Dep. Var.	6
16	SW	Time (sec)	Service Wa	6
17	Drywell Power C	cv41	Dep. Var.	4
18	Drywell Power C	cv42	Dep. Var.	4

Heat Exchangers - Table 2

Heat Ex. #	Scndy Flow (lbm/s)	Scnd Flow FF	Scndy Temp (F)	Scnd Temp FF	Ext. Flow (lbm/s)	Ext. Flow FF	Ext. Heat (Btu/s)	Ext. Heat FF
1H	1.	16	75.					

Graphs

Graph #	Title	Mon	1	Curve Number 2	3	4	5
1	Drywell Tempera		TV1	TL1			
2	Wetwell Tempera		TV2	TL2			
3	Containment Pre		PR1	PR2			
4	Reactor Vessel		TV4	TL4	ST4	TD4	
5	RHR Heat Exchan		xq1H				
6	Reactor Vessel		AL4				
7	Torus Water Vol		AL2				
8	Heat Exchanger		t11H	t21H			
9	Wetwell. Vessel		TL2	TL4	TL1		
10	Conductor Tempe		TA1	TA2	TA3	TA4	
11	Integral Vessel		QL4	QV4			
12	Vapor & Conduct		TV4	TA1			
13	Liquid & Conduc		TL4	TA2			
14	Vapor & Conduct		TV2	TA3			
15	Liquid & Conduc		TL2	TA4			
16	Vapor Heat Tran		HA1				
17	Liquid Heat Tra		HA2				
18	Vapor Heat Tran		HA3				





Modifications in /home/schor/vyc-2120ccn/SENSITIVITY/SBO/drywe11-SBO/SBO-drywe112-Leak-4  
 Mar/14/2005 17:49:07  
 GOTHIC Version 7.0p2(OA) - April 2002  
 File: /home/schor/vyc-2120ccn/SENSITIVITY/SBO/drywe11-SBO/SBO-drywe112-Leak-45-sensy

Function			
10			
Cooldown Pressure			
Ind. Var.: Time (sec)			
Dep. Var.: Pressure (psia)			
Ind. Var.	Dep. Var.	Ind. Var.	Dep. Var.
0.	1078.5	600.	1014.5
1200.	953.5	1800.	895.3
2400.	839.8	3000.	787.
3600.	736.8	4200.	689.1
4800.	643.7	5400.	600.7
6000.	559.9	6600.	521.3
7200.	484.8	7800.	450.2
8400.	417.6	9000.	386.8
9600.	357.8	10200.	330.5
10800.	304.9	11400.	280.8
12000.	258.2	12600.	237.1
13200.	217.3	13800.	198.9
14400.	181.7	15000.	165.6
15600.	150.8	16200.	136.9
16800.	124.2	17400.	112.3
18000.	101.4	18600.	91.3
19200.	82.1	19800.	73.6
20400.	65.8	21000.	58.7
21600.	52.3	22200.	46.4
1000000.	46.4		



#### 6.4.2 Results Case SBO-drywell2-Leak-45-sensy

Figure 30 through Figure 38 present the main parameters for the case *SBO-drywell2-Leak-45-sensy*. Figure 30 presents the drywell temperature. The maximum drywell temperature is about 293 °F and is reached at the end of the run (4 hours). The run was not extended beyond the 4 hours even though the drywell temperature continues to increase because at 4 hours the RHR pump is available for drywell spray, if needed. The mission time of 2 hour and 10 minutes is achieved. The drywell heatup rate is arrested due to depressurization; however the leak brings enough energy from the vessel to continue the heatup. At 7800 seconds the drywell temperature is about 290 °F, well below the EQ limit of 325 °F.

Figure 31 presents the containment pressure. The drywell pressure is high enough to allow for drywell spray after one hour into the transient, if needed. The available water to spray is the Diesel fire pump (Reference 30) per Appendix M of OE 3107 (Reference 35) and it takes about one hour for aligning the fire pump for drywell spray. The drywell temperature does not exceed the EQ drywell temperature limit and the drywell shell temperature stays below the limit of 281 °F for the mission time of 2 hour and 10 minutes hence spray from Diesel fire pump is not needed.

The vacuum breakers do not open during the time of interest.

At 4 hours the torus pressure is about 25 psig and increasing, close to the PSP limit of 27 psig. However at this time the RHR pump is available for containment spray.

Figure 32 presents the RPV pressure. At one hour into the event it is assumed that the operators start depressurization. The vessel pressure during the 4 hours of the run time does not reach the shutoff pressure for the HPCI pumps, so at 4 hours the HPCI pumps still inject to maintain inventory. At 4 hour into the event only about 540000 lb were injected from CST (Figure 34). At this time the RPV is not depressurized, and the HPCI pump continues to inject.

Figure 33 presents the RPV level. The core stays covered and HPCI maintains inventory for the duration of the analyses. There is no need to continue the calculation beyond 4 hours because the coping time of 2 hours was demonstrated.

Figure 35 shows that the leak is maintain constant for the duration of the transient.

Figure 36, Figure 37, and Figure 38 presents the drywell liner temperature. The drywell liner stays below 280 °F for the 4 hours analyzed. After 2 hours and 10 minutes the low pressure pumps are available for suppression pool cooling, drywell spray and maintaining vessel inventory.

The suppression pool temperature is not a parameter of importance for this calculation. In Reference 1 it was shown that the suppression pool temperature is lower for the cases with leak and lower for earlier depressurization hence the maximum suppression pool temperature will be lower than 182.2 °F, calculated in Reference 1.



SBO - drywell2-Leak-45-sensitivities  
 Mar/09/2005 18:54:07  
 GOthic Version 7.0p2(QA) - April 2002  
 File: /home/schor/vyc-2120ccn/SENSITIVITY/SBO/drywell-SBO/SBO-drywell2-Le

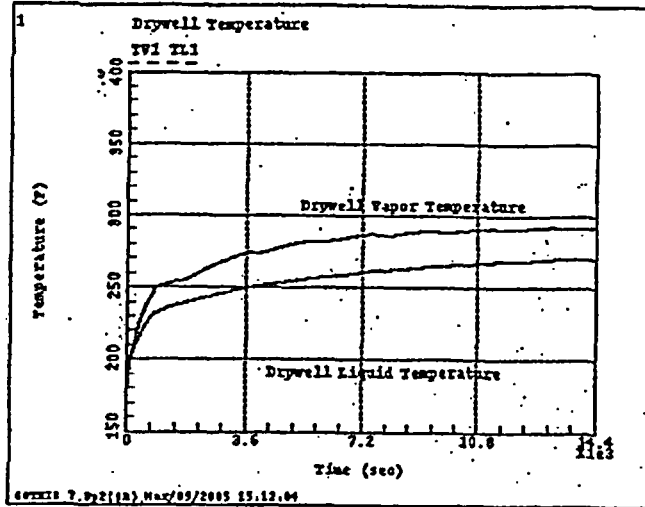


Figure 30 - Drywell Temperature - Case SBO-drywell2-Leak-45-sensy

SBO - drywell2-Leak-45-sensitivities  
 Mar/14/2005 17:59:16  
 GOthic Version 7.0p2(QA) - April 2002  
 File: /home/schor/vyc-2120ccn/SENSITIVITY/SBO/drywell-SBO/SBO-drywell2-Le

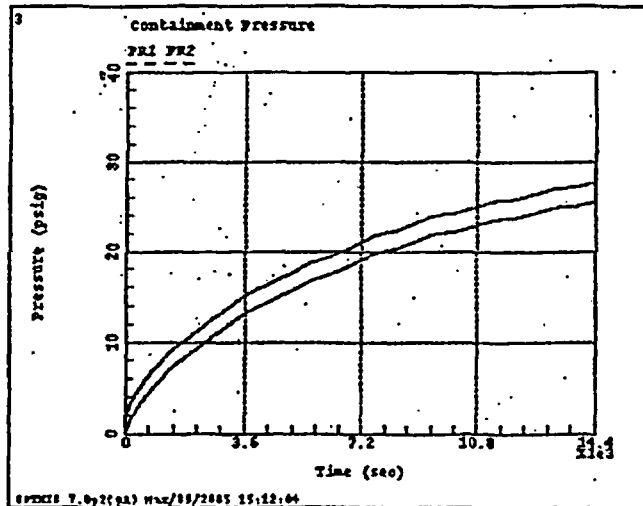


Figure 31-Containment Pressure - Case SBO-drywell2-Leak-45-sensy



SBO - drywell2-Leak-45-sensitivities  
 Mar/09/2005 18:59:19  
 GOthic Version 7.0p2(QA) - April 2002  
 File: /home/schor/vyc-2120ccm/SENSITIVITY/SBO/drywell-SBO/SBO-drywell2-Le

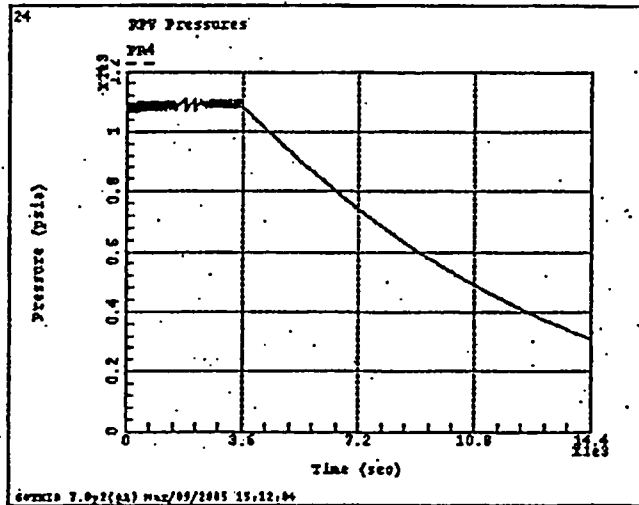


Figure 32 – RPV Pressure –Case SBO-drywell2-Leak-45-sensy

SBO - drywell2-Leak-45-sensitivities  
 Mar/09/2005 19:05:53  
 GOthic Version 7.0p2(QA) - April 2002  
 File: /home/schor/vyc-2120ccm/SENSITIVITY/SBO/drywell-SBO/SBO-drywell2-Le

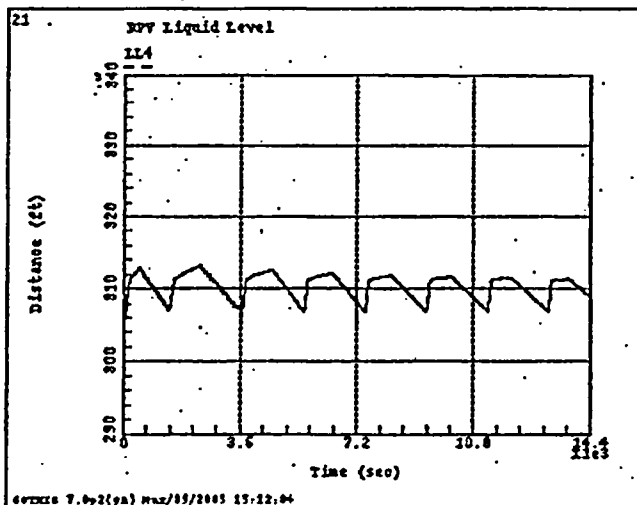


Figure 33 – RPV Level - Case SBO-drywell2-Leak-45-sensy



SBO - drywell2-Leak-45-sensitivities  
 Mar/09/2005 19:14:51  
 GOHIC Version 7.0p2(QA) - April 2002  
 File: /home/schor/vyc-2120ccn/SENSITIVITY/SBO/drywell-SBO/SBO-drywell2-Le

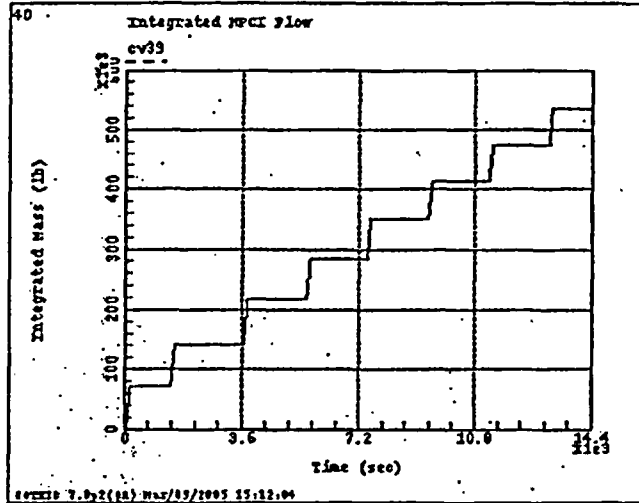


Figure 34 – Integrated HPCI Flow - Case SBO-drywell2-Leak-45-sensy

SBO - drywell2-Leak-45-sensitivities  
 Mar/09/2005 19:16:54  
 GOHIC Version 7.0p2(QA) - April 2002  
 File: /home/schor/vyc-2120ccn/SENSITIVITY/SBO/drywell-SBO/SBO-drywell2-Le

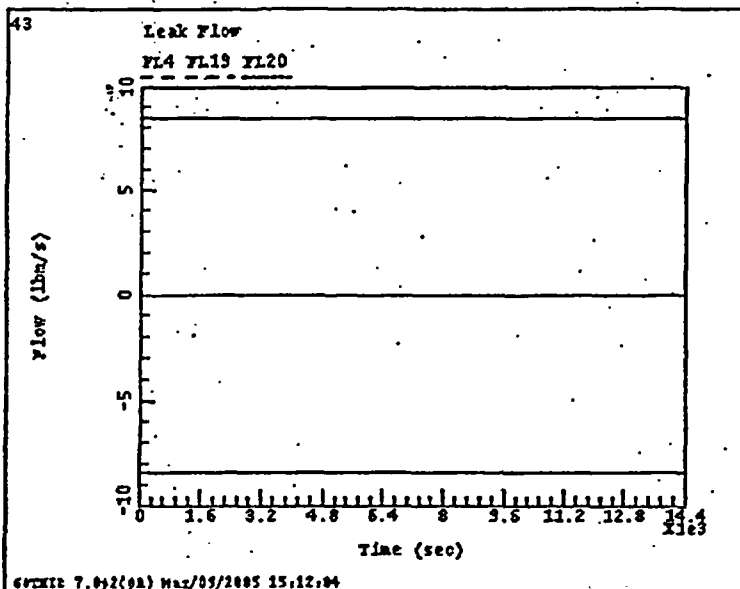


Figure 35 – Leak Flow –Case SBO-drywell2-Leak-45-sensy



SBO - drywell2-Leak-45-sensitivities  
 Mar/09/2005 19:06:59  
 GOthic Version 7.0p2(QA) - April 2002  
 File: /home/schor/vyc-2120ccn/SENSITIVITY/SBO/drywell-SBO/SBO-drywell2-Le

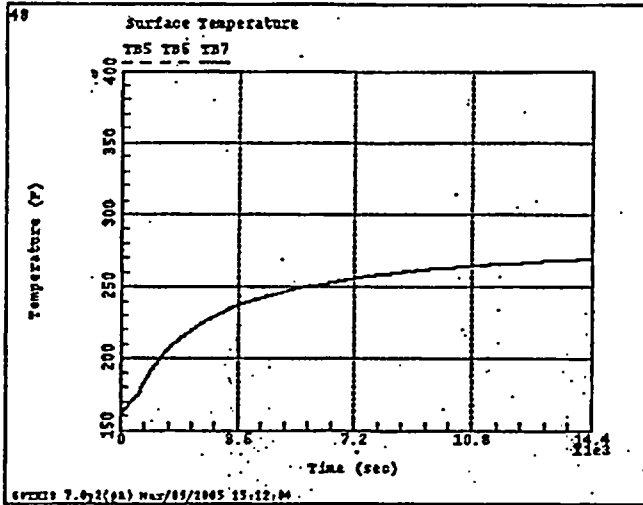


Figure 36 - Surface Temperature, Heat Structures 5,6,7 - SBO-drywell2-Leak-45-sensy

SBO - drywell2-Leak-45-sensitivities  
 Mar/09/2005 19:08:37  
 GOthic Version 7.0p2(QA) - April 2002  
 File: /home/schor/vyc-2120ccn/SENSITIVITY/SBO/drywell-SBO/SBO-drywell2-Le

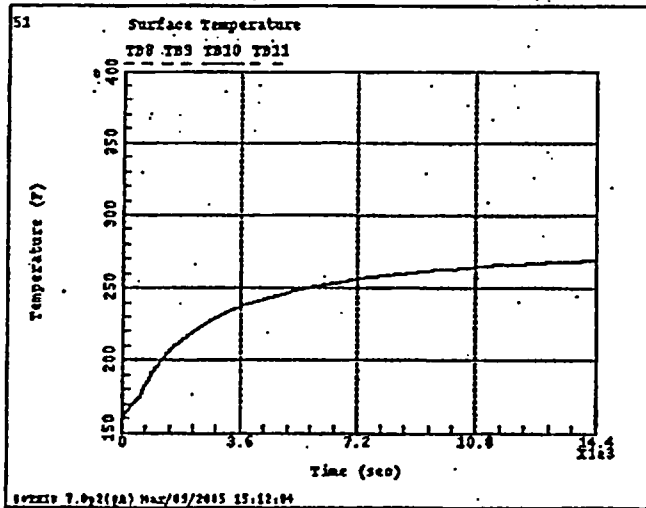


Figure 37 Surface Temperature, Heat Structures 8,9,10,11 - SBO-drywell2-Leak-45-sensy





SBO - drywell2-Leak-45-sensitivities  
Mar/09/2005 19:11:15  
GOTHIC Version 7.0p2(QA) - April 2002  
File: /home/schor/vyc-2120ccn/SENSITIVITY/SBO/drywell-SBO/SBO-drywell2-Le

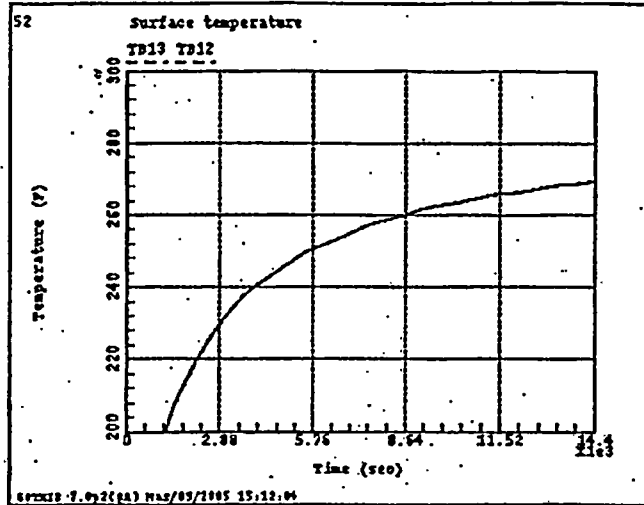


Figure 38 - Surface Temperature, Heat Structures 12,13 - SBO-drywell2-Leak-45-sensy

## **6.5 Case SBO-drywell-comments**

### **6.5.1 Model Modifications**

This case addresses the reviewer comments and also some discrepancies found during the documentation. The following changes are being made:

- change the initial temperature for Heat Structures 14 from 160 °F to 170 °F.
- change the  $K_{\text{reverse}}$  in junction 3 to 3.93 from 3.964.
- change the flow area of the valve V3 to 15.63 ft<sup>2</sup>, same as the flow path flow area
- change the surface area of the concrete pedestal to 2068 ft<sup>2</sup>

The changes are made to case 2 but it could be done to any of the other cases.

Table 11 presents the modifications made to file *SBO-drywell2-80-sensy2-NoLeak* to create *SBO-drywell2-comments*.

Table 11 Comparison between *SBO-drywell-comments* vs *SBO-drywell2-80-sensy2-NoLeak*.



Modifications in /home/schor/vyc-2120ccn/SENSITIVITY/SBO/drywell-SBO/SBO-drywell-comment  
 Mar/15/2005 14:07:44  
 GOTHIC Version 7.0p2(QA) - April 2002  
 File: /home/schor/vyc-2120ccn/SENSITIVITY/SBO/drywell-SBO/SBO-drywell-comments

Flow Paths - Table 3

Flow Path #	Fwd. Loss Coeff.	Rev. Loss Coeff.	Comp. Opt.	Critical Flow Model	Exit Loss Coeff.	Drop Breakup Model
1	4.2243	4.2243	ON	TABLES	1.	OFF
2	1.	0.78	ON	TABLES	1.	OFF
3	3.964	3.93	ON	OFF	0.	OFF
4	0.		OFF	TABLES	1.	OFF
5			OFF	OFF	0.	OFF
6			OFF	OFF	0.	OFF
7			OFF	OFF	0.	OFF
8			OFF	OFF	0.	OFF
9			OFF	OFF	0.	OFF
10			OFF	TABLES	0.	OFF
11			OFF	TABLES	0.	OFF
12			OFF	OFF	0.	OFF
13			OFF	OFF	0.	OFF
14			OFF	OFF	0.	OFF
15			OFF	OFF	0.	OFF
16		1e+18	OFF	OFF	0.	OFF
17			OFF	OFF	0.	OFF
18			OFF	OFF	0.	OFF
19			OFF	OFF	0.	OFF
20			OFF	OFF	0.	OFF
21	1.5	1.5	OFF	OFF	0.	OFF

Thermal Conductors - Table 1

Cond #	Description	Vol A	HT Co	Vol B	HT Co	Cond Type	S. A. (ft2)	Init. T.(F)	Or
1	Steam Exposure	4	1	4	1	1	2965.72	609.23	I
2	Liquid Exposure	4	2	4	2	1	11521.8	647.4	I
3	Torus, Vapor	2	3	2	5	2	13553.7	90.	I
4	Torus, Liquid	2	4	2	5	2	13553.7	90.	I
5	Lower Drywell	1	5	1	6	3	1856.24	170.	I
6	Lower Drywell	1	5	1	6	4	2041.28	170.	I
7	Middle Drywell	1	5	1	6	5	3802.73	170.	I
8	Middle Drywell	1	5	1	6	6	780.68	170.	I
9	Middle Drywell	1	5	1	6	5	1250.47	170.	I
10	Middle drywell	1	5	1	6	7	1898.24	170.	I
11	Middle Drywell	1	5	1	6	8	1114.72	170.	I
12	Top Drywell	1	5	1	6	13	783.45	170.	I
13	Top Drywell	1	5	1	6	14	1718.3	170.	I
14	RRUs	1	5	1	6	11	1272.8	170.	I
15	Vent Pipes	3	5	3	6	11	2885.7	160.	I
16	Concrete Shield	1	5	1	6	12	2068.	152.	I

Modifications in /home/schor/vyc-2120ccn/SENSITIVITY/SBO/drywell-SBO/SBO-drywell-comment  
 Mar/15/2005 14:07:44  
 GOTHIC Version 7.0p2(QA) - April 2002  
 File: /home/schor/vyc-2120ccn/SENSITIVITY/SBO/drywell-SBO/SBO-drywell-comments

Valve/Door Types

Valve Type #	Valve Option	Stem Travel Curve	Loss Coeff. Curve	Flow Area (ft2)
1	QUICK OPEN	0	0	1.
2	CHECK VALVE	0	15	3.141
3	QUICK CLOSE	0	0	15.63



**6.5.2 Case SBO-drywell-comments Results**

The results of this case are presented in Figure 39 through Figure 40. Figure 39 presents the drywell temperature. Due to the fact that the initial temperature for the drywell thermal conductors increase by 10 °F, the drywell temperature is increased from 289.4 °F to 295.2 °F.

The containment pressure (Figure 40) is identical to the Case 2, hence the changes in the vacuum breaker inputs have no effect on results, as described in section 6.2.1.

Figure 41, Figure 42, Figure 44 presents the drywell liner temperature. The drywell liner stays below 260 °F for the 7 hours analyzed. After 2 hours and 10 minutes the low pressure pumps are available for suppression pool cooling, drywell spray and maintaining vessel inventory.

SBO - 80F-NoLeak-drywell2-sensitivities-comments  
 Mar/15/2005 14:03:50  
 GOthic Version 7.0p2(QA) -- April 2002  
 File: /home/schor/vyc-2120ccn/SENSITIVITY/SBO/drywell-SBO/SBO-drywell-com

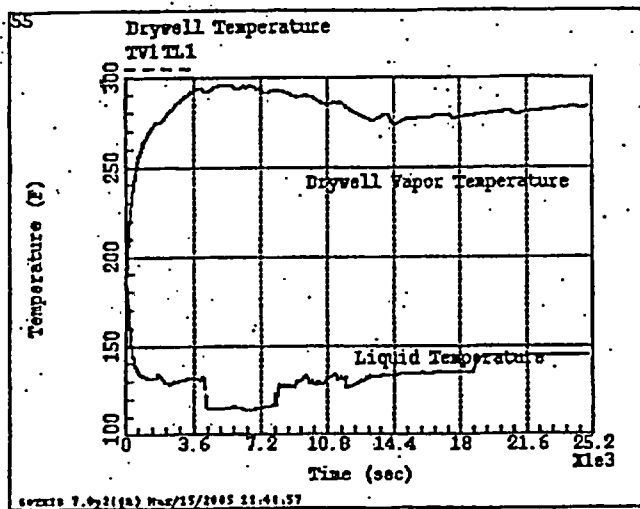


**Figure 39 – Drywell Temperature - Case SBO-drywell-comments**



SBO - 80F-Noleak-drywell2-sensitivities-comments  
 Mar/15/2005 14:05:35  
 GOthic Version 7.0p2(OA) - April 2002  
 File: /home/schor/vyc-2120ccn/SENSITIVITY/SBO/drywell-SBO/SBO-drywell-com

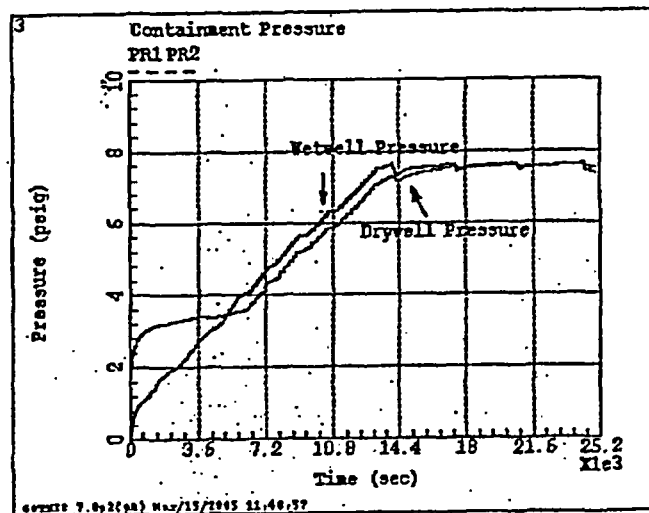


Figure 40 – Containment Pressure – Case SBO-drywell-comments

SBO - 80F-Noleak-drywell2-sensitivities-comments  
 Mar/15/2005 14:04:06  
 GOthic Version 7.0p2(OA) - April 2002  
 File: /home/schor/vyc-2120ccn/SENSITIVITY/SBO/drywell-SBO/SBO-drywell-com

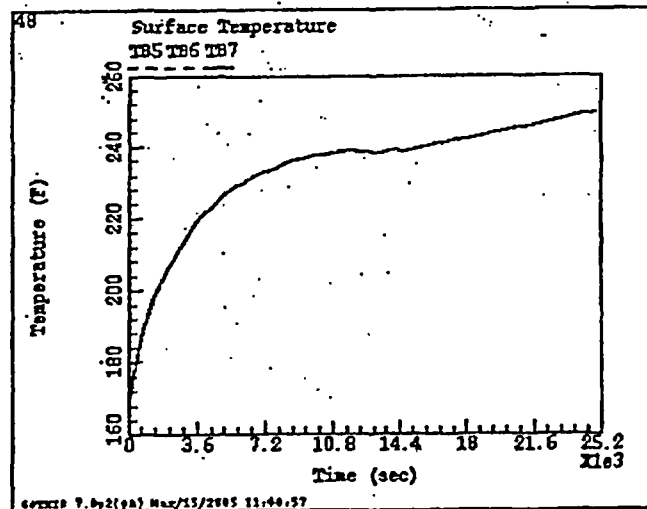


Figure 41 - Surface Temperature, Heat Structures 5,6,7 - SBO-drywell-comments



SBO - 80F-Noleak-drywell2-sensitivities-comments  
 Mar/15/2005 14:04:52  
 COTHIC Version 7.0p2(QA) - April 2002  
 File: /home/schor/vyc-2120ccn/SENSITIVITY/SBO/drywell-SBO/SBO-drywell-com

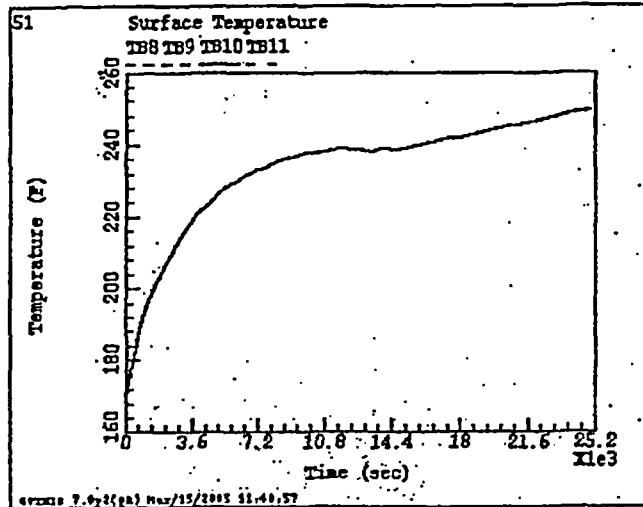


Figure 42 - Surface Temperature, Heat Structures 8,9,10,11 - SBO-drywell-comments

SBO - 80F-Noleak-drywell2-sensitivities-comments  
 Mar/15/2005 14:05:12  
 COTHIC Version 7.0p2(QA) - April 2002  
 File: /home/schor/vyc-2120ccn/SENSITIVITY/SBO/drywell-SBO/SBO-drywell-com

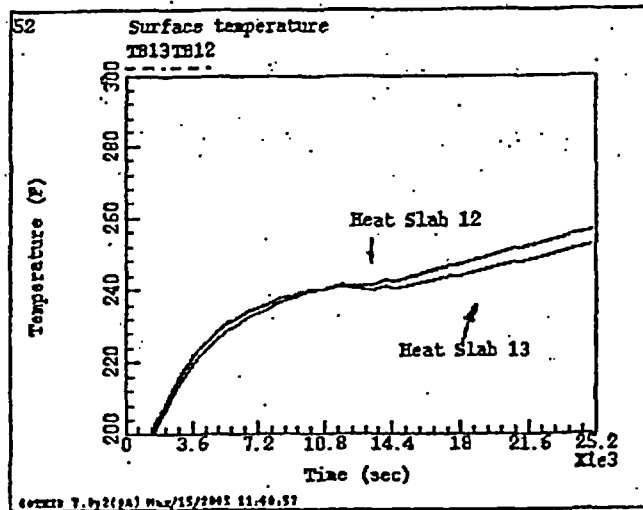


Figure 43 - Surface Temperature, Heat Structures 8,9,10,11 - SBO-drywell-comments



SBO - 80F-Moleak-drywell2-sensitivities-comments  
 Mar/15/2005 14:05:12  
 GOTHIC Version 7.0p2(QA) - April 2002  
 File: /home/schor/vyc-2120ccn/SENSITIVITY/SBO/drywell-SBO/SBO-drywell-com

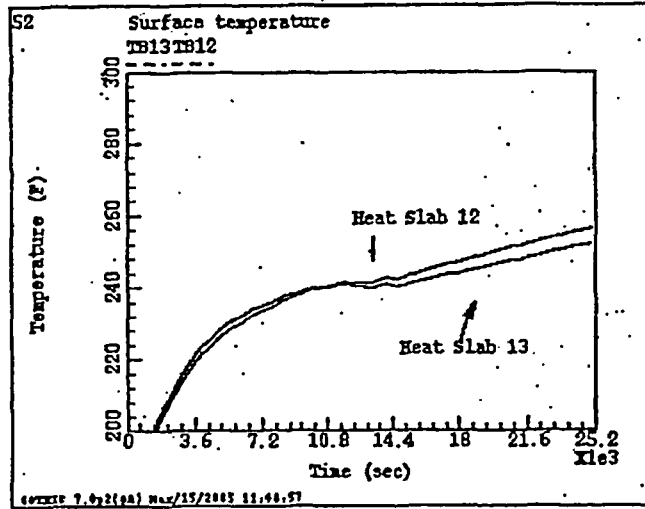


Figure 44 – Surface Temperature Heat Structures 12, 13 – Case SBO-drywell-comments

## 7.0 Results and Conclusions

Assuming a Station Blackout with RPV depressurization (cooldown) at 1 hour after the event the following results and conclusions are found:

- 1) The drywell temperature for all cases analyzed stays below the EQ drywell temperature profile for the entire SBO coping period of 2 hours and the additional 10 minutes to power the low pressure pumps (i.e., the drywell temperature for all cases analyzed stays below 300 °F for more than 4 hours of transient).
- 2) The drywell liner temperature stays below the design temperature of 281 °F for more than 4 hours after the SBO event.
- 3) The drywell pressure stays below the design pressure of 56 psig.
- 4) For 2 hour and 10 minutes the wetwell pressure stays below the PSP curve for all cases analyzed.
- 5) The analysis shows that there is no need to spray the drywell when in the unsafe region of DWSIL.
- 6) There is enough inventory in the CST to insure that the CST is not depleted before the time of low pressure pumps availability such that the core stays covered. A CST inventory of 75000 gallons was assumed.
- 7) The maximum suppression pool temperature for all cases stays below 182.2 °F.
- 8) The analysis predicts a conservatively high drywell temperature. Several factors contribute to this conservatism:
  - The heat transfer from the vessel to the drywell is based on a constant heat transfer coefficient at normal operating differential temperatures. However, this heat transfer coefficient will vary with the temperature difference to the  $\frac{1}{4}$  power based on the dependence on the Grashoff number.
  - The heat transfer to the drywell from the drywell heaters is not subtracted from the vessel.
  - The reactor building side of the thermal conductors are considered adiabatic.
  - A constant leakage is assumed; the leakage will decrease as the vessel is depressurized.
- 9) No restriction on the rate of cooldown is applied to protect the drywell temperature beyond the restriction of depressurization (cooldown) function of RHRSW temperature (Reference 1).

Note: "Unverified Assumptions" and "Affected Documents" items are being tracked via LO-VTYLO-2005-00135 (also see Section 4.1 and 4.2).



## 8.0 References

The References are divided into Section 8.1 and General References (Section 8.2). Section 8.1 includes all references.

### 8.1 Design Input References and General References:

- 1 VYC-2398 Rev 0 Torus Temperature Calculation for a Station Blackout Event at Extended Power Uprate, dated March 2005.
- 2 VY Tech Spec.
- 3 NUMARC 87-00, dated 11/20/87, including NRC accepted errata and Q&A from NUMARC seminars and Topical Report F.
- 4 VYC-2397, Maximum RHRSW Flow to RHRHX for SBO & Appendix R, dated 1/24/2005.
- 5 DRF 0000-0011-5646, OPL-4A (Containment Analysis Input Values) for Vermont Yankee Nuclear Power Station EPU/MELLLA+, dated 2/6/03.
- 6 Calculation VYC-1628 Rev 0, Torus Temperature and Pressure Response to Large Break LOCA and MSLB Accident Scenarios, dated 4/27/98.
- 7 George, T. L., et. al, GOTHIC Containment Analysis Package, Version 7.0, July 2001.
- 8 VYC-2208 "GOTHIC 7.0 Code Installation Validation and Verification at VY", dated July 18, 2002.
- 9 VYC-1457, VY Containment Heatup Analysis – Appendix R Application, dated 8/19/96.
- 10 GE Design Specification, No. 22A1184, "Drywell Atmosphere Cooling System", Table I, Drywell Cooling Load Summary, #8 on Sheet 9.
- 11 VYC-1254 Rev 3, Containment and RPV Volume Calculations, dated 5/21/98.
- 12 VYC-1850 Rev 1, OPL-4A Input Preparation, dated 6/22/99.
- 13 GE Design Specification # 22A1182 Rev1 "Protective Coatings-Special"
- 14 Drawing G191526 Rev 2.
- 15 J. P. Holman, "Heat Transfer", McGraw Hill Book Company, 1981.
- 16 Standard Review Plan Branch Technical Position CSB 6-1.
- 17 VYC-1628D Rev 0 CCN02, Torus Temperature and Pressure Response for to Appendix R and Station Blackout Scenarios, dated 06/23/2003.

- 18 VYC-2279, Evaluation of EPU Impact on Ambient Space Temperatures During Normal Operation, dated 8/26/2003.
- 19 EQ Manual Vol 1.
- 20 22A1265, Rev 1, Reactor Containment Design Specification, September 1969.
- 21 VY Drawing G191489 Rev 2.
- 22 VYC-1290 Rev 0, Vermont Yankee Post-LOCA Torus Temperature and RHR Heat Exchanger Evaluation, approved August 1, 1994.
- 23 VYC-2045 Rev 0 Residual Heat Removal Heat Exchangers Fouling Factors and Projected Heat Rates for Cycle 21, dated 12/1/99.
- 24 GE-VYNPS-AEP-146, Letter Michael Dick (GE) to Craig Nichols (ENOI), VYNPS EPU Task T0400: Decay Heat for Containment Analysis dated March 10, 2003.
- 25 TE-2003-020, Feedwater Parameters for Power Uprate, April 14, 2003.
- 26 VY Memo VYS 2000/39, P A Rainey/T. P. Bowman to J. R. Lynch, "Torus Temperature/SW Design Temperature Recommendations", April 16, 2000.
- 27 VY UFSAR Rev. 19.
- 28 OP 0105 Rev 11, Reactor Operation.
- 29 Crane Technical Paper No. 410, Flow of Fluids through Valves, Fittings, and Pipe, 1976 Crane Co.
- 30 EOP-3 Primary Containment Control, Rev3, dated 10/19/02.
- 31 ASME Steam Tables -Third Edition, 1977.
- 32 VYC-2306, Torus Temperature for Appendix R events at EPU Conditions, dated 08/29/2003.
- 33 VYC-1850A Rev 0, "OPL 4A Input Preparation", dated 7/28/99.
- 34 VYC-1628B Rev 0, "Torus Temperature and Pressure Response to Small Break LOCA Scenarios, Model Development", dated 11/3/98.
- 35 OE-3107 Rev 17, EOP/SAG Appendices dated 04/29/2004.
- 36 OT 3122 Rev 19, Loss of Normal Power, dated 04/18/2000.
- 37 EOP-1 Rev2 RPV Control, dated 10/19/02

### 8.1 General References

George, T. L., et. al, GOTHIC Containment Analysis Package, Version 7.0, July 2001

GOTHIC 7.0 Code Installation Validation and Verification at VY, dated July 18, 2002.

ASME Steam Tables –Third Edition, 1977



J. P. Holman, “Heat Transfer”, McGraw Hill Book Company, 1981

Crane Technical Paper No. 410, Flow of Fluids through Valves, Fittings, and Pipe, 1976  
Crane Co.



ATTACHMENT 9.10

COMPUTER RUN SUMMARY SHEET

COMPUTER RUN SUMMARY SHEET			
			Page 1 of 1
Calculation No. <u>VYC-2405</u>	Revision <u>0</u>	Date <u>16 March 2005</u>	
Sheet <u>1</u> of <u>1</u>			
Subject: <b>Drywell Temperature Calculation for a Station Blackout Event at Extended Power Uprate</b>			
Code <u>GOTHIC V7.0p2</u>	Catalog No. <u>02543</u>	Version <u>7.0</u>	
SQA Classification Level <u>A</u>			
Run Title (variable, described in Section 6.0 and Att. A)			
Run No. No. _____	Run Date _____	By _____	
Output Use:	<input type="checkbox"/> Variable Values As Noted	<input checked="" type="checkbox"/> Plot Attached	
	<input checked="" type="checkbox"/> Disk _____	<input type="checkbox"/> File No. _____	
Description Of Output:			
<ul style="list-style-type: none"> <li>• Figures in text.</li> <li>• Input file on Disk.</li> <li>• Multiple cases were run, all are described in Section 6.0.</li> <li>• One case (base case) is attached in attachment A).</li> <li>• The Figures in text, for each case, have the date of the run &amp; the run name.</li> </ul>			
Comments: None			
(Attached additional pages if necessary)			
Review:	<input checked="" type="checkbox"/> Information Entered Above is Accurate		
	<input checked="" type="checkbox"/> Input Entry Accurate		
	<input checked="" type="checkbox"/> Code Properly Executed (Based on User Manual)		
	<input checked="" type="checkbox"/> Output Accurately Extracted or Location Specified		
Reviewer Comments <u>None.</u>			
Preparer (Print/Sign) Liliane Schor	Date	Reviewer (Print/Sign) Alan L. Robertshaw	Date
	<u>3/17/05</u>		<u>3/17/05</u>



**Calculation Impact Review Pages (ENN-DC-126 Attachment 9.7)**

From System Engineering

	<b>NUCLEAR MANAGEMENT MANUAL</b>	QUALITY RELATED	ENN-DC-126	REV. 4
		INFORMATIONAL USE	PAGE 35 OF 57	

ATTACHMENT 9.7

CALCULATION IMPACT REVIEW PAGE

Date: 14 February 2005
CALCULATION IMPACT REVIEW PAGE
 QR
 NQR

CALCULATION IMPACT REVIEW PAGE

(Note: X indicates required distribution)

- To:
- |  |  |  |
|--|--|--|
| <input type="checkbox"/> Mechanical Engineering                    | <input checked="" type="checkbox"/> Licensing  | <input checked="" type="checkbox"/> Operations |
| <input type="checkbox"/> I&C Engineering                           | <input type="checkbox"/> Elect Maintenance     | <input type="checkbox"/> Chemistry             |
| <input type="checkbox"/> Electrical Engineering                    | <input type="checkbox"/> I&C Maintenance       | <input type="checkbox"/> HP/Radiological       |
| <input type="checkbox"/> Civil Engineering                         | <input type="checkbox"/> Mech Maintenance      | <input type="checkbox"/> Computer Applications |
| <input checked="" type="checkbox"/> System Engineering             | <input type="checkbox"/> Component Engineering | <input type="checkbox"/> Rad Engineering       |
| <input type="checkbox"/> Reactor Engineering                       | <input type="checkbox"/> Program Engineering   | <input type="checkbox"/> ISI Engineering       |
| <input checked="" type="checkbox"/> DBD Owner <u>RHR, P. Perez</u> | <input type="checkbox"/> Nuclear Engineering   | <input type="checkbox"/> IST Engineering       |
| <input checked="" type="checkbox"/> DBD Owner <u>SA, P. Perez</u>  | <input type="checkbox"/> EQ                    | <input type="checkbox"/> PSA                   |
- (Name) (Other)

From: Liliane Schor 802-451-3013  
 (Originator Print Name and Phone extension)

Calculation No.: VYC-2405 Revision No. 0

Title: Drywell Temperature Calculation for a Station Blackout Event at Extended Power Uprate

Reference: NA

Date Response Required: 16 February 2005

**MESSAGE:** Work organizations are requested to review the subject calculation (parts attached) to identify impacted calculations, procedures, Technical Specifications, FSAR sections, other design documents (e.g., EQ files, DBD, Appendix R, ISI/IST, PSA, MOVs/AOVs, etc.) and other documents, which must be updated because of the calculation results. Also provide the name of the individual responsible for the action and the tracking number. The tracking item should include a requirement to ensure that any ER implementation associated with the item is completed prior to revising the impacted document. Sign and return the form to the originator.

IMPACT REVIEW RESULTS:

Affected Documents	Responsible Individual	Tracking Number	Remarks
<u>EOP-3</u>			
<u>EOP Study Guide</u>			
<u>DBD-SADBD</u>			

Responding Supervisor/Manager (or designee): Brian Naeck 3/16/05  
Name/Signature Date

**Calculation Impact Review Pages (ENN-DC-126 Attachment 9.7), Continued**

From System Engineering

	<b>NUCLEAR MANAGEMENT MANUAL</b>	QUALITY RELATED	ENN-DC-126	REV. 4
		INFORMATIONAL USE	PAGE 35 OF 57	

ATTACHMENT 9.7 CALCULATION IMPACT REVIEW PAGE

**CALCULATION IMPACT REVIEW PAGE**

Date: 14 February 2005  QR  NQR

(Note: X indicates required distribution)

- |   |  |  |
|---|--|--|
| To: <input type="checkbox"/> Mechanical Engineering               | <input checked="" type="checkbox"/> Licensing  | <input checked="" type="checkbox"/> Operations |
| <input type="checkbox"/> I&C Engineering                          | <input type="checkbox"/> Elect Maintenance     | <input type="checkbox"/> Chemistry             |
| <input type="checkbox"/> Electrical Engineering                   | <input type="checkbox"/> I&C Maintenance       | <input type="checkbox"/> HP/Radiological       |
| <input type="checkbox"/> Civil Engineering                        | <input type="checkbox"/> Mech Maintenance      | <input type="checkbox"/> Computer Applications |
| <input checked="" type="checkbox"/> System Engineering            | <input type="checkbox"/> Component Engineering | <input type="checkbox"/> Rad Engineering       |
| <input type="checkbox"/> Reactor Engineering                      | <input type="checkbox"/> Program Engineering   | <input type="checkbox"/> ISI Engineering       |
| <input checked="" type="checkbox"/> DBD Owner <u>R.H.P. Perez</u> | <input type="checkbox"/> Nuclear Engineering   | <input type="checkbox"/> IST Engineering       |
| <input checked="" type="checkbox"/> DBD Owner <u>S.A.P. Perez</u> | <input type="checkbox"/> EQ                    | <input type="checkbox"/> PSA                   |
| (Name)  | (Other)  |  |

From: Liliane Schor 802-451-3013  
(Originator Print Name and Phone extension)

Calculation No.: VYC-2405 Revision No. 0

Title: Drywell Temperature Calculation for a Station Blackout Event at Extended Power Uprate.

Reference: N/A

Date Response Required: 16 February 2005

MESSAGE: Work organizations are requested to review the subject calculation (parts attached) to identify impacted calculations, procedures, Technical Specifications, FSAR sections, other design documents (e.g., EQ files, DBD, Appendix R, ISI/IST, PSA, MOVs/AOVs, etc.) and other documents, which must be updated because of the calculation results. Also provide the name of the individual responsible for the action and the tracking number. The tracking item should include a requirement to ensure that any ER implementation associated with the item is completed prior to revising the impacted document. Sign and return the form to the originator.

**IMPACT REVIEW RESULTS:**

Affected Documents	Responsible Individual	Tracking Number	Remarks
OP 4032	S. Jonasch		See attached comments

Responding Supervisor/Manager (or designee): Stephen Jonasch 3/16/05  
Name/Signature Date

## Calculation Impact Review Pages (ENN-DC-126 Attachment 9.7), Continued

From RHR and SA DBD Owner

	NUCLEAR MANAGEMENT MANUAL	QUALITY RELATED	ENN-DC-126	REV. 4
		INFORMATIONAL USE	PAGE 35 OF 57	

ATTACHMENT 9.7

CALCULATION IMPACT REVIEW PAGE

CALCULATION IMPACT REVIEW PAGE

Date: 14 February 2005  QR  NQR

(Note: X indicates required distribution)

To:  Mechanical Engineering  Licensing  Operations  
 I&C Engineering  Elect Maintenance  Chemistry  
 Electrical Engineering  I&C Maintenance  HP/Radiological  
 Civil Engineering  Mech Maintenance  Computer Applications  
 System Engineering  Component Engineering  Rad Engineering  
 Reactor Engineering  Program Engineering  ISI Engineering  
 DBD Owner RHR, P. Perez  Nuclear Engineering  IST Engineering  
 DBD Owner SA, P. Perez  EQ  PSA  
 (Name) (Other)

From: Lillane Schor 802-451-3013  
 (Originator Print Name and Phone extension)

Calculation No.: VYC-2405 Revision No. 0

Title: Drywell Temperature Calculation for a Station Blackout Event at Extended Power Update.

Reference: N/A

Date Response Required: 16 February 2005

**MESSAGE:** Work organizations are requested to review the subject calculation (parts attached) to identify impacted calculations, procedures, Technical Specifications, FSAR sections, other design documents (e.g., EQ files, DBD, Appendix R, ISI/IST, PSA, MOVs/AOVs, etc.) and other documents, which must be updated because of the calculation results. Also provide the name of the individual responsible for the action and the tracking number. The tracking item should include a requirement to ensure that any ER implementation associated with the item is completed prior to revising the impacted document. Sign and return the form to the originator.

**IMPACT REVIEW RESULTS:**

Affected Documents	Responsible Individual	Tracking Number	Remarks
SA DBD	P. Perez	LO-VTYLO-2005-00135	May need update for Drywell - SBO assumptions / Methodology of VYC-2405.

Responding Supervisor/Manager (or designee):

JG Roger  
Name/Signature

3-16-05  
Date

## Calculation Impact Review Pages (ENN-DC-126 Attachment 9.7), Continued

From Operations – EPU Engineering

	NUCLEAR MANAGEMENT MANUAL	QUALITY RELATED	ENN-DC-126	REV. 4
		INFORMATIONAL USE	PAGE 35 OF 57	

ATTACHMENT 9.7

CALCULATION IMPACT REVIEW PAGE

### CALCULATION IMPACT REVIEW PAGE

 Date: 14 February 2005
 QR

 NQR

(Note: X indicates required distribution)

To: <input type="checkbox"/> Mechanical Engineering <input type="checkbox"/> I&C Engineering <input type="checkbox"/> Electrical Engineering <input type="checkbox"/> Civil Engineering <input checked="" type="checkbox"/> System Engineering <input type="checkbox"/> Reactor Engineering <input checked="" type="checkbox"/> DBD Owner <u>RHR, P. Perez</u> <input checked="" type="checkbox"/> DBD Owner <u>SA, P. Perez</u> (Name)	<input checked="" type="checkbox"/> Licensing <input type="checkbox"/> Elect Maintenance <input type="checkbox"/> I&C Maintenance <input type="checkbox"/> Mech Maintenance <input type="checkbox"/> Component Engineering <input type="checkbox"/> Program Engineering <input type="checkbox"/> Nuclear Engineering <input type="checkbox"/> EQ (Other)	<input checked="" type="checkbox"/> Operations <input type="checkbox"/> Chemistry <input type="checkbox"/> HP/Radiological <input type="checkbox"/> Computer Applications <input type="checkbox"/> Rad Engineering <input type="checkbox"/> ISI Engineering <input type="checkbox"/> IST Engineering <input type="checkbox"/> PSA
---	--	--

 From: Liliane Schor 802-451-3013

(Originator Print Name and Phone extension)

 Calculation No.: VYC-2405

 Revision No. 0

 Title: Drywell Temperature Calculation for a Station Blackout Event at Extended Power Uprate.

 Reference: N/A

 Date Response Required: 16 February 2005

**MESSAGE:** Work organizations are requested to review the subject calculation (parts attached) to identify impacted calculations, procedures, Technical Specifications, FSAR sections, other design documents (e.g., EQ files, DBD, Appendix R, ISI/IST, PSA, MOVs/AOVs, etc.) and other documents, which must be updated because of the calculation results. Also provide the name of the individual responsible for the action and the tracking number. The tracking item should include a requirement to ensure that any ER implementation associated with the item is completed prior to revising the impacted document. Sign and return the form to the originator.

**IMPACT REVIEW RESULTS:**

Affected Documents	Responsible Individual	Tracking Number	Remarks
<u>EOP-3 Study Guide</u>			
<u>OT-3122</u>			
<u>Lesson Plan for EOP-3</u>			
<u>ON-3147</u>			
<u>ON 3148</u>			

 Responding Supervisor/Manager (or designee): Bryan Croke 3/16/2005

Name/Signature

Date





## Calculation Impact Review Pages (ENN-DC-126 Attachment 9.7), Continued

From Licensing

	NUCLEAR MANAGEMENT MANUAL	QUALITY RELATED	ENN-DC-126	REV. 4
		INFORMATIONAL USE	PAGE 35 OF 57	

ATTACHMENT 9.7

CALCULATION IMPACT REVIEW PAGE

Date: 14 February 2005  QR  NQR

CALCULATION IMPACT REVIEW PAGE

(Note: X Indicates required distribution)

To: <input type="checkbox"/> Mechanical Engineering <input type="checkbox"/> I&C Engineering <input type="checkbox"/> Electrical Engineering <input type="checkbox"/> Civil Engineering <input checked="" type="checkbox"/> System Engineering <input type="checkbox"/> Reactor Engineering <input checked="" type="checkbox"/> DBD Owner RHR, P. Perez <input checked="" type="checkbox"/> DBD Owner SA, P. Perez (Name)	<input checked="" type="checkbox"/> Licensing <input type="checkbox"/> Elect Maintenance <input type="checkbox"/> I&C Maintenance <input type="checkbox"/> Mech Maintenance <input type="checkbox"/> Component Engineering <input type="checkbox"/> Program Engineering <input type="checkbox"/> Nuclear Engineering <input type="checkbox"/> EQ (Other)	<input checked="" type="checkbox"/> Operations <input type="checkbox"/> Chemistry <input type="checkbox"/> HP/Radiological <input type="checkbox"/> Computer Applications <input type="checkbox"/> Rad Engineering <input type="checkbox"/> ISI Engineering <input type="checkbox"/> IST Engineering <input type="checkbox"/> PSA
---	--	--

From: Liliane Schor 802-451-3013  
 (Originator Print Name and Phone extension)

Calculation No.: VYC-2405 Revision No. 0

Title: Drywell Temperature Calculation for a Station Blackout Event at Extended Power Uprate.

Reference: N/A

Date Response Required: 16 February 2005

**MESSAGE:** Work organizations are requested to review the subject calculation (parts attached) to identify impacted calculations, procedures, Technical Specifications, FSAR sections, other design documents (e.g., EQ files, DBD, Appendix R, ISI/IST, PSA, MOVs/AOVs, etc.) and other documents, which must be updated because of the calculation results. Also provide the name of the individual responsible for the action and the tracking number. The tracking item should include a requirement to ensure that any ER implementation associated with the item is completed prior to revising the impacted document. Sign and return the form to the originator.

**IMPACT REVIEW RESULTS:**

Affected Documents	Responsible Individual	Tracking Number	Remarks
<i>see notes FSAR</i>	<i>DBD Owner</i>	<i>see note (2)</i>	<i>None</i>

Responding Supervisor/Manager (or designee): Jim Delvaux 3/17/05  
 Name/Signature Date

- ① This may consist of "New or Revised safety analysis" per AP4036. As part of the ER on EPU consideration to include a summary in the FSAR.
- ② To be generated by during the development / close out.



## Calculation Design Verification and Review (ENN-DC-134)

ENN-DC-134 REVISION 1      ATTACHMENT 9.1      DESIGN VERIFICATION COVER PAGE

### DESIGN VERIFICATION COVER PAGE

<input type="checkbox"/> IP-2 <input type="checkbox"/> IP-3 <input type="checkbox"/> JAF <input type="checkbox"/> PNPS <input checked="" type="checkbox"/> VY		
Document No. VYC-2405	Revision 0	Page 1 of 8
Title: Drywell Temperature Calculation for a Station Blackout Event at Extended Power Uprate		
<input checked="" type="checkbox"/> Quality Related <input type="checkbox"/> Non Quality Related		
DV Method: <input checked="" type="checkbox"/> Design Review <input type="checkbox"/> Alternate Calculation <input type="checkbox"/> Qualification Testing		
VERIFICATION REQUIRED	DISCIPLINE	VERIFICATION COMPLETE AND COMMENTS RESOLVED (DV print, sign, and date)
<input type="checkbox"/>	Electrical	
<input type="checkbox"/>	Mechanical	
<input type="checkbox"/>	Instrument and Control	
<input type="checkbox"/>	Civil/Structural	
<input checked="" type="checkbox"/>	<u>Design Engineering</u> <u>Fluid Systems</u>	Alan L. Robertshaw <i>Alan L. Robertshaw</i> 3/17/05
<input type="checkbox"/>		
Print/Sign After Comments Have Been Resolved		
Originator: Liliane Schor		Date: 3/17/05



PENN-DC-134 REVISION 1      ATTACHMENT 9.7      CALCULATION DESIGN VERIFICATION CHECKLIST

<b>IDENTIFICATION:</b>		<b>DISCIPLINE:</b>	
Document Title: <b>Drywell Temperature Calculation for a Station Blackout Event at Extended Power Uprate</b>		<input type="checkbox"/> Civil/Structural	
Doc. No.: <b>VYC-2405</b> Rev. <b>0</b> QA Cat.		<input type="checkbox"/> Electrical	
Verifier: <u>Alan L. Robertshaw</u>		<input type="checkbox"/> I & C	
Print	Sign	<input type="checkbox"/> Mechanical	
Date		<input type="checkbox"/> Nuclear	
Manager authorization for supervisor performing verification.		<input checked="" type="checkbox"/> Other:	
<input type="checkbox"/> N/A		<u>Design Engineering,</u>	
Print		<u>Fluid Systems</u>	
Sign			
Date			
<b>METHOD OF VERIFICATION:</b>			
Design Review <input checked="" type="checkbox"/> Alternate Calculations <input type="checkbox"/> Qualification Test <input type="checkbox"/>			
1. <b>Design Inputs – Were the inputs correctly selected and incorporated into the design?</b>		<b>Reference</b>	
Design inputs include design bases, plant operational conditions, performance requirements, regulatory requirements and commitments, codes, standards, field data, etc. All information used as design inputs should have been reviewed and approved by the responsible design organization, as applicable.		Page No. <u>Section 5 of VYC-2405</u>	
All inputs need to be retrievable or excerpts of documents used should be attached.		OR	
See site specific design input procedures for guidance in identifying inputs.		Paragraph No. _____	
Yes <input checked="" type="checkbox"/> No <input type="checkbox"/> N/A <input type="checkbox"/>		Completion of the Reference Boxes is optional for all questions.	
<b>Verifier Comments:</b>			
Section 5.0, Input and Design Criteria, of VYC-2405, has been satisfactorily reviewed. Any identified Design Input needing verification is listed in Section 4.1 of VYC-2405 and tracked via LO-VTYLO-2005-00135 (see Item #2 of this Calculation Design Verification Checklist). All other Design Input has been verified in VYC-2405.			
Resolution: None needed.			



<p><b>2. Assumptions – Have the assumptions been verified?</b></p> <p>Yes <input type="checkbox"/>    No <input checked="" type="checkbox"/>    N/A <input type="checkbox"/></p> <p><b>Verifier Comments:</b></p> <p>Section 4.1, Assumptions that need Verification or Implementation, and LO-VTYLO-2005-00135 CA02, document identified "Unverified Assumptions" from VYC-2405 Drywell Temperature Calculation for a Station Blackout Event at Extended Power Uprate. The following lists the various "Unverified Assumptions" from VYC-2405:</p> <ol style="list-style-type: none"> <li>1) 2 hour restoration of outside power (coping time).</li> <li>2) 10 minutes to start RHR through the RHRHX, 2 RHRSW pumps and CS.</li> <li>3) Acceptability of using 75000 gal from CST (change of level setpoint).</li> <li>4) Maximum CST temperature of 135°F.</li> <li>5) The depressurization rate function of Service Water temperature needs to be verified and proceduralized as follows:             <ul style="list-style-type: none"> <li>- For SW &gt; 75°F; depressurize the vessel at 80°F/hr or higher.</li> <li>- For lower SW temperature (SW ≤ 75°F) no restrictions on depressurization rates.</li> </ul> </li> </ol> <p>Upon verification of these assumptions, the calculation should be revised to convert the assumptions to Design Input and the calculation Status should be changed.</p> <p><b>Resolution:</b></p> <p>LO-VTYLO-2005-00135 CA02 has been issued to track these Unverified Assumptions.</p> <p>Upon verification of these assumptions, the calculation should be revised to convert the assumptions to Design Input and the calculation Status should be changed.</p>	<p style="text-align: center;"><b>Reference</b></p> <p>Page No. <u>Calculation Summary Page and Sect 4.1 of VYC-2405</u></p> <p>OR</p> <p>Paragraph No. _____</p>
<p><b>3. Quality Assurance – Is the Quality level correct?</b></p> <p>Yes <input checked="" type="checkbox"/>    No <input type="checkbox"/>    N/A <input type="checkbox"/></p> <p><b>Verifier Comments:</b> VYC-2405 is correctly designated "Quality Related."</p> <p><b>Resolution:</b> None needed.</p>	<p style="text-align: center;"><b>Reference</b></p> <p>Page No. <u>Cover Sheet of VYC-2405</u></p> <p>OR</p> <p>Paragraph No. _____</p>



<p><b>4. Codes, Standards and Regulatory Requirements –</b> Are the applicable codes, standards and regulatory requirements, including issue and addenda properly identified and are their requirements for design met?</p> <p>Yes <input checked="" type="checkbox"/>    No <input type="checkbox"/>    N/A <input type="checkbox"/></p> <p><b>Verifier Comments:</b> Appropriate use of requirements (inputs, assumptions, methodology) set forth in the VY Technical Specifications and UFSAR have been followed in VYC-2405 as needed.</p> <p><b>Resolution:</b> None needed.</p>	<p style="text-align: center;"><b>Reference</b></p> <p>Page No. _____</p> <p>OR</p> <p>Paragraph No. _____</p>
<p><b>5. Operating Experience –</b> Have applicable construction and operating experience been considered?</p> <p>Yes <input checked="" type="checkbox"/>    No <input type="checkbox"/>    N/A <input type="checkbox"/></p> <p><b>Verifier Comments:</b></p> <p>Consideration (discussions and reviews) has been given to various timelines for operator actions, equipment start times, cooldown rates, etc. Some Unverified Assumptions exists which will rely on, in part, to VY operating experience (e.g., two hour restoration of outside power (coping time of 2 hours and 10 minutes), ten minutes to start RHR flow through the RHRHX, the use of 2 RHRSW pumps and CS, and the acceptability of using 75000 gal from CST (change of level setpoint). See Item #2, Assumptions, of this Calculation Design Verification Checklist.</p> <p><b>Resolution:</b> Consideration has been given to VY operating experience. Some Unverified Assumptions exist (for which commitments have been issued). See Resolution of Item #2, Assumptions, of this Calculation Design Verification Checklist.</p>	<p style="text-align: center;"><b>Reference</b></p> <p>Page No. _____</p> <p>OR</p> <p>Paragraph No. _____</p>
<p><b>6. Interfaces –</b> Have the design interface requirements been satisfied and documented?</p> <p>Yes <input checked="" type="checkbox"/>    No <input type="checkbox"/>    N/A <input type="checkbox"/></p> <p><b>Verifier Comments:</b></p> <p>The relationship between the Fluid Systems (“design group”) and other organizations within VY have been satisfactorily met using the Calculation Impact Review Page. The Calculation Impact Review Page was completed by persons in the Operations Department, System Engineering, Licensing, and various DBD owners.</p> <p><b>Resolution:</b></p> <p>None Needed.</p>	<p style="text-align: center;"><b>Reference</b></p> <p>Page No. _____</p> <p>OR</p> <p>Paragraph No. _____</p>



<p>7. <b>Methods – Was an appropriate analytical method used?</b></p> <p>Yes <input checked="" type="checkbox"/>      No <input type="checkbox"/>      N/A <input type="checkbox"/></p> <p><b>Verifier Comments:</b></p> <p>The GOTHIC code (Reference 7 &amp; 8 of VYC-2405), Version 7.0p2 was selected for use in VYC-2405.</p> <p><b>Resolution:</b> None Needed.</p>	<p style="text-align: center;"><b>Reference</b></p> <p>Page No. <u>Section 3 of VYC-2405</u></p> <p>OR</p> <p>Paragraph No. _____</p>
<p>8. <b>Design Outputs – Is the output reasonable compared to the inputs?</b></p> <p>Yes <input checked="" type="checkbox"/>      No <input type="checkbox"/>      N/A <input type="checkbox"/></p> <p><b>Verifier Comments:</b> The output is reasonable compared to the inputs. Previous, similar Drywell SBO analyses are familiar with the preparer and reviewer of this SBO calculation and thus the output given in VYC-2405 was reasonable for the various changes and modifications made to the previous input.</p> <p><b>Resolution:</b> None Needed.</p>	<p style="text-align: center;"><b>Reference</b></p> <p>Page No. _____</p> <p>OR</p> <p>Paragraph No. _____</p>
<p>9. <b>Acceptance Criteria – Are the acceptance criteria incorporated in the calculation sufficient to allow verification that design requirements have been satisfactorily accomplished?</b></p> <p>Yes <input checked="" type="checkbox"/>      No <input type="checkbox"/>      N/A <input type="checkbox"/></p> <p><b>Verifier Comments:</b></p> <p>Section 2.1 was added to include the Acceptance Criteria.</p> <p><b>Resolution:</b></p> <p>None Needed.</p>	<p style="text-align: center;"><b>Reference</b></p> <p>Page No. <u>Section 2.1 of VYC-2405</u></p> <p>OR</p> <p>Paragraph No. _____</p>



<p><b>10. Records and Documentation – Are requirements for record preparation, review, approval, retention, etc., adequately specified?</b></p> <p>Are all documents prepared in a clear legible manner suitable for microfilming and/or other documentation storage method? Have all impacted documents been identified for update?</p> <p>Yes <input checked="" type="checkbox"/>      No <input type="checkbox"/>      N/A <input type="checkbox"/></p> <p><b>Verifier Comments:</b> VYC-2405 was prepared in a clear legible manner suitable for microfilming and/or other documentation storage method. All impacted documents (Design Output) have been identified for update in Section 4.2 of VYC-2405 and in LO-VTYLO-2005-00135 CA01.</p> <p><b>Resolution:</b> LO-VTYLO-2005-00135 CA01 has been issued to track these affected documents. If any other documents are identified during the Calculation Impact Review process, other commitments will be generated.</p>	<table border="1" style="width: 100%; border-collapse: collapse;"> <tr> <td style="text-align: center; padding: 2px;"><b>Reference</b></td> </tr> <tr> <td style="padding: 2px;">Page No. <u>Section 4.2 of VYC-2405</u></td> </tr> <tr> <td style="text-align: center; padding: 2px;">OR</td> </tr> <tr> <td style="padding: 2px;">Paragraph No. _____</td> </tr> </table>	<b>Reference</b>	Page No. <u>Section 4.2 of VYC-2405</u>	OR	Paragraph No. _____
<b>Reference</b>					
Page No. <u>Section 4.2 of VYC-2405</u>					
OR					
Paragraph No. _____					
<p><b>11. Software Quality Assurance- For a calculation that utilized software applications (e.g., GOTHIC, SYMCORD), was it properly verified and validated in accordance with ENN IT-104 or previous site SQA Program?</b></p> <p>Yes <input checked="" type="checkbox"/>      No <input type="checkbox"/>      N/A <input type="checkbox"/></p> <p><b>Verifier Comments:</b> The GOTHIC code (Reference 7 &amp; 8 of VYC-2405), Version 7.0p2 was selected for use in VYC-2405. This code was used in similar SBO analysis (References 1 of VYC-2405). This specific version of the code has been installed and complies with the ENVY SQA procedures ENN-IT-104 (replaced VY procedure AP-6030) as documented in calculation VYC-2208 (Reference 8 of VYC-2405).</p> <p><b>Resolution:</b> None Needed.</p>	<table border="1" style="width: 100%; border-collapse: collapse;"> <tr> <td style="text-align: center; padding: 2px;"><b>Reference</b></td> </tr> <tr> <td style="padding: 2px;">Page No. <u>Section 3 of VYC-2405</u></td> </tr> <tr> <td style="text-align: center; padding: 2px;">OR</td> </tr> <tr> <td style="padding: 2px;">Paragraph No. _____</td> </tr> </table>	<b>Reference</b>	Page No. <u>Section 3 of VYC-2405</u>	OR	Paragraph No. _____
<b>Reference</b>					
Page No. <u>Section 3 of VYC-2405</u>					
OR					
Paragraph No. _____					
<p><b><u>OTHER COMMENTS</u></b></p> <p>See Attached list of General comments from review of VYC-2405</p> <p><b><u>RESOLUTIONS</u></b></p> <p>Attached General comments have been made to reviewer's satisfaction.</p> <p>All comments for "NO" answers have been resolved satisfactorily.</p>					

General Comments from Alan L. Robertshaw from Review of VYC-2405  
(Attached to Calculation Design Verification Checklist)

- In Section 2.0, Add addition Section (2.1) entitled "Acceptance Criteria" and add appropriate acceptance criteria.

*Done*

- In Section 3.0, discussion of GOTHIC code and V&V calculation need appropriate references.

*Done*

- In Section 4.0:

1. For Assumption #4, please correct the units for density (value is correct).
2. For Assumption #9, add that 61 gpm is from Reference 3.
3. Add VYC-2306 to Reference (from Drywell Free Volume of Table 3).

*Added*

- In Section 5.0:

1. In Section 5.3.1, show in more detail how total Heater #5 loads are calculated.

*Done*

2. In Section 5.4, recommend addition of "simple" drawing of Drywell

*Done*

3. In Section 5.4 show that the total Surface Area adds up to the Value obtained from OPL-4a (i.e., Table A Total = 15246.06 ft<sup>2</sup>, RRUs = 1272.8 ft<sup>2</sup>, Vent Pipes = 2885.7 ft<sup>2</sup>, thus Total = 19405 ft<sup>2</sup>).

*Added*

4. Add to description of Item 8 "Side of Drywell Head."
5. Add to description of Item 9 "Top of Drywell Head."

*Done, both items*

6. Is RRU area Reference 11 or 12 or other? Please correct if needed.

*Both, added*

7. Flow Path 21 Forward and Reverse loss coefficients should reference CRANE (or similar), data not found in steam table. Need to add CRANE to references

*Done*

8. Please add additional information on new valve added (vacuum breaker, Valve #5. e.g., size, type, etc.).

*Done*





9. Also for Valve discussion, note that the valve area is different from the line area used in Flow Path 21

*Added*

10. Initial Temperatures of the Thermal Conductors are not given (and reference).

*Added*

11. Please further explain why a loss coefficient of 3.964 was used instead of the calculated value of 3.93 for the vacuum breaker flow path. Any impact on analysis?

*I added this discussion in the document, I also said that the difference is less than 1% and will make no difference on the analysis. Anyway, was corrected in Case 5.*

- In Section 6.0:

1. List Five case individually to add clarity.

*Done*

2. See minor grammatical / spelling concerns noted in marked-up calc draft

*Done*

3. Section 6.2.1 please add info on Flow Path 21 (Leakage) area change.

*Done*

- In Section 8.0, Reference Section:

1. Need to add Reference for ASME Steam Tables and one for CRANE Technical Paper (if needed)

*Added*

2. Are References 11 and 13 used?

*Yes, Reference 11 and 12 are RRU references and 13 is for the paint (added some more discussion about the paint)*

- In the GOTHIC Input Deck, Thermal Conductor #16, Concrete Shield, a surface area value of 2108 ft<sup>2</sup> was used. A value of 2068 ft<sup>2</sup> was given in the text of VYC-2405 (Section 5.4). Both of these numbers are found on page 35 of VYC-1850; Rev. 1 for OPL-4A preparation. The larger value (2108 ft<sup>2</sup>) is for total surface area, the smaller value (2068 ft<sup>2</sup>) subtracts the "Slots." The value used in VYC-1850, Rev. 1 CCN-01 (OPL-4A, Resolved for Analysis) uses the 2068 ft<sup>2</sup> value. Please discuss this in the analysis and determine which value to use, any sensitivities, etc.

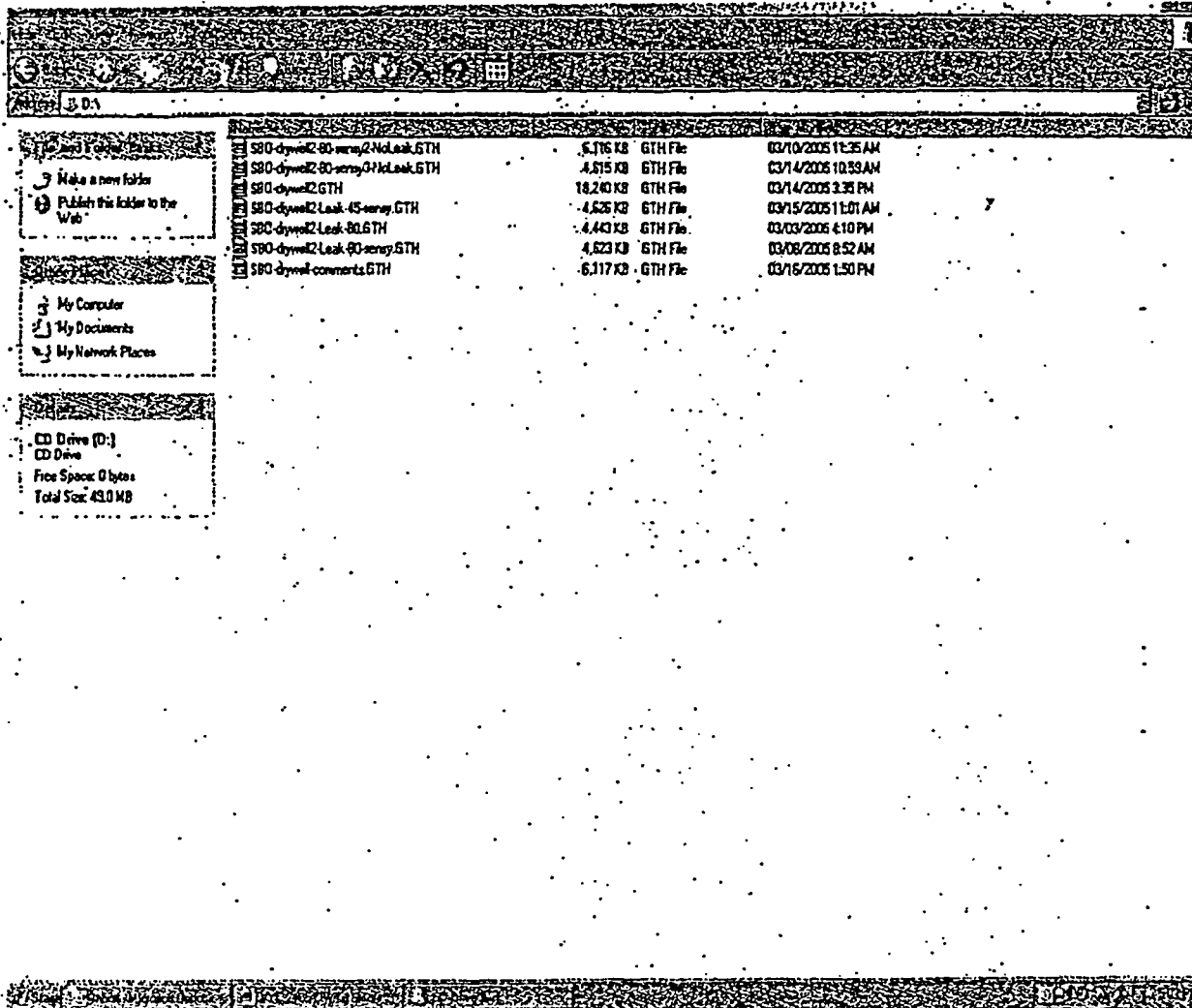
*Case 5 addresses this.*

- In Attachment A, it appears that Figure on page A14 is a duplicate figure and should be removed.

*Removed*



## Files on CD



File Name	Size	Type	Date
SBO-drywell2-80-senry2-NoLeak.GTH	5,176 KB	GTH File	03/10/2005 11:35 AM
SBO-drywell2-80-senry2-NoLeak.GTH	4,815 KB	GTH File	03/14/2005 10:33 AM
SBO-drywell2.GTH	18,240 KB	GTH File	03/14/2005 3:35 PM
SBO-drywell2-Leak-45-senry.GTH	4,626 KB	GTH File	03/15/2005 11:01 AM
SBO-drywell2-Leak-80.GTH	4,443 KB	GTH File	03/03/2005 4:10 PM
SBO-drywell2-Leak-80-senry.GTH	4,623 KB	GTH File	03/08/2005 8:52 AM
SBO-drywell-comments.GTH	6,117 KB	GTH File	03/16/2005 1:50 PM

**Exhibit SPSB-C-52-5**

Vermont Yankee Nuclear Power Station

Proposed Technical Specification Change No. 263 – Supplement No. 30

Extended Power Uprate

Response to Request for Additional Information

Calculation VYC-2279, Rev.0

Total number of pages in this Exhibit  
(excluding this cover sheet) is 14.

This document contains Vermont Yankee proprietary information. This information may not be transmitted in whole or in part, to any other organization without permission of Vermont Yankee.

VY CALCULATION TITLE PAGE

VYC-2279 0 N/A N/A
VY Calculation Number Revision Number Vendor Calculation Number Revision Number

Title: Evaluation of EPU impact on Ambient Space Temperatures During Normal Operation

QA Status: [X] SC [ ] NNS [ ] OQA Operating Cycle Number\* N/A

\* The Operating Cycle Number should only be entered here if the results of the calculation only apply during a specific operating cycle otherwise enter "N/A".

Calculation Supports A Design Change/Specification? [X] Yes [ ] No VYDC 2003-008
VYDC/MM/TM/Spec No.

Implementation Required? [X] Yes [ ] No Calculation Done as a Study Only? [ ] Yes [X] No

Safety Evaluation Number: N/A

Superseded Calculation Number, Title and Revision: N/A

For Revisions: List CCNs, IJJs, or SAs incorporated/superseded by this revision: N/A

Computer Code(s): None used

Are there open items in this calculation/revision? [X] Yes [ ] No

Review and Approval: (Print and Sign Name)

Preparer: Gene O'Brien Date: 8/26/03
Interdiscipline (Heat Balance, Att. B only) Preparer(s): N. Zervos Date: 8/26/03
Interdiscipline (Heat Balance, Att. B only) Reviewer(s): R. Srinivasan Date: 8/26/03
Independent Reviewers(s): Mansour Mojibian Date: 8/26/03
Approved: Ed Duda DAN YASI Date: 8/26/03
Accepted (only for AP 0017 calculations performed by vendors) [ ] N/A
Ed Duda Ed Duda Date: 8/27/2003

Final Turnover to DCC (Section 2):

- 1) All open items, if any, have been closed.
2) Implementation Confirmation (Section 2.3.4)

Total No. Pages in Package 64
(including all attachments)

[ ] Calculation accurately reflects existing plant configuration,
(confirmation method indicated below)

[ ] Walkdown [ ] As-Built input review [ ] Discussion with
(Print Name)

OR

[ ] N/A, calculation does not reflect existing plant configuration

- 3) Resolution of documents identified in the Design Output Documents Section of VYAPF 0017.07 has been initiated as required (Section 2.3.6, 2.3.7)

Printed Name Signature Date

\* For calculations performed using AP 0017 this is the number of pages in the body of the calculation. For vendor calculations, this is the number of pages of AP 0017 forms added. (Title page, review forms, data sheets, 50.59, etc.)

# TABLE OF CONTENTS

<u>SECTION</u>	<u>PAGE NO.</u>
VY CALCULATION TITLE PAGE .....	1
VY CALCULATION DATABASE INPUT FORM .....	2
TABLE OF CONTENTS .....	6
I Calculation .....	7
1.1 Objective .....	7
1.2 Summary of Results .....	7
1.3. Method of Solution .....	8
1.4 Inputs and Assumptions .....	10
1.4.1 Inputs .....	10
1.4.2 Assumptions .....	14
1.5 Calculation .....	14
1.6 Results .....	26
1.7 Conclusion .....	27
Attachments .....	28
Attachment A .....	A1
Attachment B .....	B1
Attachment C .....	C1
Attachment D .....	D1
Attachment E .....	E1

# 1 Calculation

## 1.1 Objective

The purpose of this calculation is to evaluate ambient temperature increases in several plant spaces following the increase in reactor power level to 102% of 120%, hereafter referred to as Extended Power Uprate (EPU). The EPU will increase core thermal power from the current licensed level of 1593 MWt to 1912 MWt. For bounding purposes, the 122% (1950.9 MWt) heat balances are used for EPU HVAC evaluations.

This calculation evaluates the EPU impact on ambient air temperature in the following buildings or areas during normal plant operation:

### Reactor Building

- Drywell
- Steam Tunnel
- Other Reactor Building Areas

### Turbine Building

- Reactor Feed Pump Room
- Condensate Pump Room
- HP Heater Area (including steam line shelf containing main steam lines)
- LP Heater Area

**Note:** Comments to this calculation provided by letters PUPVY-03-208 dated 7/16/03 and PUPVY-03-212 dated 7/18/03 have been reviewed and incorporated (see Attachment D).

Increases in area heat gain and ambient air temperatures, as a result of EPU, are predominately caused by increases in operating temperature of piping systems, and equipment, and air-cooled motors operating under increased loads. The preuprate piping system temperatures are selected or extrapolated from a PEPSE Heat Balance that is tuned to match preuprate (current) plant data. The EPU piping system temperatures are selected or extrapolated from a PEPSE Heat Balance that provides the most conservative results.

Affected areas are evaluated to determine the temperature gain due to increases in heat loss from piping and mechanical equipment.

## 1.2 Summary of Results

The results of this calculation show the effects of the EPU in terms of increased ambient temperature and heat load are due to increased feedwater temperature, as well as increased horsepower from the condensate and feedwater pumps. The ambient temperature increases are specified in Section 1.6 (Results).

### 1.3. Method of Solution

This calculation evaluates the temperature increase in a specified area using current fluid and ambient air temperatures and EPU fluid temperatures to predict the EPU ambient air temperature and corresponding temperature rise. PEPSE Heat Balances at 100% CTP and EPU at 122% CTP (References 7 and 8) are used to obtain preuprate and EPU piping temperatures. The increase in heat loss from piping is determined by comparing the ratio of "temperature differential between EPU pipe and area air temperatures" to "differential temperature between pre-uprate pipe and pre-uprate area ambient air".

The basis for using this scaling approach to determine increased heat loss from piping and equipment can be obtained by referencing the ASHRAE Fundamental Handbook (Reference 12) Section 20.

Formula (9) - ASHRAE 20.9 is used for flat surfaces

$$q_s = (t_{is} - t_{os}) / R$$

Formula (10) -ASHRAE 20.9 is used for cylindrical flat surfaces

$$q_s = (t_{is} - t_{os}) / [r_s \ln (r_i/r_i)]/k_1 + [r_s \ln (r_s/r_1)]/k_2$$

Formula (11) -ASHRAE 20.9 for determining heat flow per area of pipe surface

$$q_o = q_s (r_s / t_i)$$

Where

$q_s$  = rate of heat transfer per unit area of outer surface of insulation

$q_o$  = rate of heat flow per unit area of pipe surface, Btu/(hr)(ft<sup>2</sup>)

R = surface to surface thermal resistance

k = thermal conductivity of insulation at calculated mean temperature.

$t_{is}$  = Temperature of inner surface

$t_{os}$  = Temperature of outer surface

$r_i$  = inner radius of insulation

$r_1, r_2$  = outer radius of intermediate insulation

$r_s$  = outer radius of insulation

ln = natural or Napernian logarithm

For the purposes of this calculation it can be assumed that there is one layer of insulation, therefore Formula 10 can be simplified as follows:

$$q_s = (t_{is} - t_{os}) / [r_s \ln (r_i/r_i)]/k_1$$

The increase or delta in heat transfer per unit area of insulation can be stated as follows:

$$\Delta q = \text{EPU} [(t_{is} - t_{os}) / [r_s \ln (r_i/r_i)]/k_1] / \text{pre-EPU} [(t_{is} - t_{os}) / [r_s \ln (r_i/r_i)]/k_1]$$

There is no change in either:  $r_i, r_s,$  or  $r_1,$

Based on the predicted temperature increases in the various process streams it can be assumed that there is no appreciable change between the preuprate and EPU values for k.

Therefore

$$\Delta q = \text{EPU} [(t_{is} - t_{os}) / \text{pre-EPU} [(t_{is} - t_{os})]$$

Present station operating ambient air temperatures are used in the evaluation. If operating data is not available, plant design area temperatures are used. An iterative process using an Excel spreadsheet is utilized. First, an EPU ambient air temperature is estimated. Next, the EPU area heat gain multiplier is obtained using the ratio of the EPU pipe / ambient air temperature difference to the preuprate (current) pipe / ambient air temperature difference as shown below:

$$\frac{(\text{EPU pipe temperature} - \text{EPU ambient air temperature})}{(\text{preuprate pipe temperature} - \text{preuprate ambient air temperature})} = \text{EPU Area Heat Gain Multiplier}$$

The EPU factor is obtained by subtracting 1 from the EPU heat gain multiplier.

The EPU factor is then multiplied by the preuprate temperature difference between the air in and out of a particular air handling unit to calculate the estimated EPU temperature rise. The temperature rise is then compared to the difference of estimated EPU and preuprate ambient air temperatures. If required, a new EPU ambient air temperature is estimated and the process repeated until the temperature rise is equal to the difference of estimated EPU and preuprate ambient air temperatures.

~~For Feedwater and Condensate pumps, flows from preuprate and EPU PEPSE Heat Balances along with appropriate pump curves will be used to determine horsepower changes in the respective pump motors to determine the heat gain increase to the room. The percentage increase in heat gain to the room will be utilized with the temperature rise of ventilating/cooling air currently being supplied to the room or area being evaluated.~~

~~The heat load from the condensate and feedwater pumps is evaluated by calculating brake horsepower (BHP) at preuprate and EPU flows. BHP is calculated using the following equation from page B-9 of Reference 14:~~

$$\text{Bhp (hp)} = Q(\text{gpm}) * H(\text{ft}) * \rho(\text{lb}_m/\text{ft}^3) / [247,000 * \text{pump efficiency}]$$

~~The flow, Q, is calculated from the mass flow rate specified on the heat balance using the fluid density,  $\rho$ , calculated at the average of pump inlet and outlet temperatures. The pump head, H, and efficiency are obtained from the pump curve.~~

~~The heat generated is due to pump motor inefficiency and is calculated using Chapter 26, Equation 21 from Reference 12:~~

$$q \text{ (BTU/hr)} = \text{BHP (hp)} * 2545 \text{ (BTU/hr hp)} * [100 - \% \text{ efficiency}] / \% \text{ efficiency}$$

~~The heat load due to the pump motor inefficiency is calculated for preuprate and EPU conditions. The overall heat removal capability of the coolers at preuprate conditions is determined and the sensible heat load due to piping is obtained by subtracting pump heat load from cooler heat removal capacity. The piping heat load at EPU is scaled due to the increase in fluid temperature and added to the EPU pump heat load to obtain total heat load for the room. The temperature increase across the coolers is calculated using Equation 39.6(b) from Reference 13:~~



6

$$[T_{in} - T_{out}]^{\circ}F = q \text{ (Btu/hr)} / [cfm * 1.08 \text{ (Btu min/(ft}^3 \text{ hr }^{\circ}F))]$$

Both the feedwater and condensate pump rooms are evaluated in this manner.

### 1.4 Inputs and Assumptions

#### 1.4.1 Inputs

The inputs for this evaluation are the fluid temperature in system piping and ambient room temperature of the areas considered. The pre EPU fluid temperatures are obtained from a PEPSE heat balance based upon current plant operating data adjusted to 5.00" Hg. condenser backpressure to obtain maximum fluid temperatures (Reference 7). For those cases where the fluid temperature is not explicitly listed, the temperature is obtained based upon the pressure and enthalpy listed using ASME steam tables (Reference 9). The EPU fluid temperatures are obtained from the 122% heat balance with a condenser pressure of 5.00" Hg (Reference 8) which provided the highest, and therefore conservative, temperatures.

The current ambient steam tunnel and pump room temperatures are obtained from HVAC system design criteria (Reference 5). The main steam tunnel design temperature is 130°F, the reactor feedwater pump room and condensate pump room design temperatures are 105°F. The current HP and LP heater area temperatures are 125°F as taken from the Environmental Qualification Program Manual (Reference 6, page 11). The 20°F Pre-EPU Vent/Cooling Air ΔT contained in the Table below for the HP and LP heater area spaces is based upon transfer air at 105°F.

The design conditions for the air handling units are obtained from Reference 4, except for TRU-5 and TSF1A/1B, which have their design conditions specified in Reference 19.

Table 1.4-1

Area	Equip. ID	Flow, cfm	T <sub>in</sub> (°F)	T <sub>out</sub> (°F)	ΔT
Reactor Feedwater Pump Room	TRU-1,-2,-3,-4	16,750	105	85	20
Condensate Pump Room	TRU-5	21,400	105	85	20
Condensate Pump Room	TSF-1A/1B	5,000	90	105	15
Drywell	RRU-1,-2,-3,-4	16,000	135	97	38
Main Steam Tunnel	RRU-17A, -17B*	5000	130	105	25

\*Per Reference 18, the coils for these coolers are incorrectly piped as parallel flow rather than counter flow

The design inputs for piping are summarized in the table below:

Table 1.4-2

	Pre-EPU pipe Temp °F (Ref. 7)	EPU pipe Temp °F (Ref. 8)	Pre-EPU ambient air Temp °F	Pre-EPU Vent/Clg Air ΔT °F
<del>HP Heater Area</del>				
ESS to FWH1	383.3	403.7	125.0	20.0
FWH1 Shell	383.3	403.7	125.0	20.0
FW to FWH1	330.7	346.4	125.0	20.0
FW lvg FWH1	374.4	392.6	125.0	20.0
Drains lvg FWH1	343.6	356.9	125.0	20.0

	Pre-EPU pipe Temp °F (Ref. 7)	EPU pipe Temp °F (Ref. 8)	Pre-EPU ambient air Temp °F	Pre-EPU Vent/Clg Air ΔT °F
ESS to FWH2	338.0	358.1	125.0	20.0
FWH2 Shell	338.0	358.1	125.0	20.0
FW to FWH2	299.3	312.5	125.0	20.0
FW lvg FWH2	330.7	346.4	125.0	20.0
Drains lvg FWH2	309.7	322.6	125.0	20.0
<b>LP Heater Area</b>				
ESS to FWH3	305.4	321.2	125.0	20.0
FWH3 Shell	305.4	321.2	125.0	20.0
CND to FWH3	227.6	238.4	125.0	20.0
CND lvg FWH3	296.6	309.8	125.0	20.0
Drains lvg FWH3	235.0	247.4	125.0	20.0
ESS to FWH4	239.0	252.1	125.0	20.0
FWH4 Shell	239.0	252.1	125.0	20.0
CND to FWH4	167.9	180.9	125.0	20.0
CND lvg FWH4	227.6	238.4	125.0	20.0
Drains lvg FWH4	175.1	189.1	125.0	20.0
ESS to FWH5	173.9	181.8	125.0	20.0
FWH5 Shell	173.9	181.8	125.0	20.0
CND to FWH5	135.1	134.7	125.0	20.0
CND lvg FWH5	167.9	180.9	125.0	20.0
Drains lvg FWH5	145.1	141.8	125.0	20.0
<b>CND Pump Room</b>				
CND to CNP	133.8	133.8	105.0	20.0



	Pre-EPU pipe Temp °F (Ref. 7)	EPU pipe Temp °F (Ref. 8)	Pre-EPU ambient air Temp °F	Pre-EPU Vent/Clg Air ΔT °F
<del>CND lvg CNP</del>	<del>133.1</del>	<del>133.1</del>	<del>105.0</del>	<del>20.0</del>
<del>RFW Pump Room</del>	<del></del>	<del></del>	<del></del>	<del></del>
<del>CND to RFP</del>	<del>296.6</del>	<del>309.8</del>	<del>105.0</del>	<del>20.0</del>
<del>FW lvg RFP</del>	<del>299.3</del>	<del>312.5</del>	<del>105.0</del>	<del>20.0</del>
<b>Main Steam Tunnel</b>				
<b>FW lvg FWH1</b>	374.4	392.6	130.0	25.0
<b>Main Steam</b>	547.6	547.6	130.0	25.0

Pump information:

**Reactor Feedwater Pumps**

Table 1.4-3

	Preuprate (Reference 7)	EPU (Reference 8)
Flow	6407526 lb/hr	8048044 lb/hr
# of RFPs	2	3
per pump	3203763 lb/hr	2682681 lb/hr
Tin	296.6 °F	309.8 °F
Tout	299.3 °F	312.5 °F

**Condensate Pumps**

Table 1.4-4

	Preuprate (Reference 7)	EPU (Reference 8)
Flow	6437526 lb/hr	8076444 lb/hr
# of CNPs	3	3
per pump	2145842 lb/hr	2692148 lb/hr
Tin	133.8 °F	133.8 °F
Tout	133.1 °F	133.1 °F

Drywell information (Reference 17):

**Drywell Cooling Load Summary\***

Table 1.4-5

Component	Btu/hr
Reactor Pressure Vessel	459,000
Recirc. Pumps, Valves, and Pipe	278,000
Feedwater Pipe & Valves	124,000
Steam Pipe & Valves	212,000
Condensate & Instrument Lead Lines	82,000

9

Component		Btu/hr
Control Rod Drive Pipe		50,400
Control Rod Drive Pipe	569,000**	
Clean-up Demineralizer Pipe & Valves		17,800
Shutdown Supply Pipe		8,100
Steam Safety/Relief Valves		206,600
Biological Shield (Gamma Heating)		16,400
Safeguards system Piping (RCIC, LPCI, HPCI, and core spray)		82,000
	Sensible Heat Gain Total, Normal Operation	1,536,300
Steam Leak, Valves	155,000	
	Latent Heat Gain Total, Normal Operation	155,000
	Total Cooling Load, Normal Operation	1,691,300

\* Excluding allowance for drywell cooler motors

\*\* Temporary initial load immediately following scram

## 1.4.2 Assumptions

For the piping in the main steam tunnel, it is assumed the feedwater piping contributes 1/3 to the total heat gain and the main steam piping contributes 2/3 due to their respective surface areas. This is based upon the fact there are four 18" main steam lines and two 16" feedwater lines. From Reference 14, the external surface area of four 18" pipes is  $4 * 4.712 \text{ ft}^2$  per foot of pipe =  $18.848 \text{ ft}^2$  per foot of pipe and the external surface area of two 16" pipes is  $2 * 4.189 \text{ ft}^2$  per foot of pipe =  $8.378 \text{ ft}^2$  per foot of pipe. No confirmation is required.

It is assumed there is no appreciable change between the preuprate and EPU values for the thermal conductivity, k, of the pipe insulation based on the predicted temperature increases in the various process streams.

## 1.5 Calculation

### Piping:

A sample calculation for the estimated temperature rise from the feedwater piping in the steam tunnel is shown below.

Preuprate pipe temp. (°F)	374.4	Reference 7
EPU pipe temp. (°F)	392.6	Reference 8
Preuprate ambient air temp. (°F)	130	Reference 5
Preuprate Air Handling Unit (AHU) $\Delta T$ (°F)	25	Reference 4 (RRU-17A, $130 - 105 = 25$ )

The EPU ambient air temperature is initially estimated at 131 °F. [used for initial iteration and checked later]

The EPU Area Heat Gain Multiplier is obtained using the equation in Section 1.3.

$$\text{EPU Area Heat Gain Multiplier} = \frac{(\text{EPU pipe temperature} - \text{EPU ambient air temperature})}{(\text{preuprate pipe temperature} - \text{preuprate ambient air temperature})}$$

$$\text{EPU Area Heat Gain Multiplier} = \frac{(392.6 - 131)^\circ\text{F}}{(374.4 - 130)^\circ\text{F}}$$

$$\text{EPU Area Heat Gain Multiplier} = 1.070$$

The EPU factor is obtained by subtracting 1 from the EPU Area Heat Gain Multiplier:

$$\text{EPU factor} = 1.070 - 1 = 0.070$$

From Assumptions section, the feedwater piping contributes 1/3 to the total heat gain in the main steam tunnel, so the EPU factor becomes:

$$\text{EPU factor} = 0.070 * 1/3$$

$$\text{EPU factor} = 0.023$$

(11)

The temperature rise is then calculated by multiplying the EPU factor by the AHU temperature differential.

$$\text{Temp. rise} = 0.023 * 25.0^{\circ}\text{F} = 0.586$$

The difference between estimated EPU and preuprate ambient air temperatures is:

$$131 - 130 = 1 \text{ (this is not close enough to the calculated temperature rise of } 0.586^{\circ}\text{F)}$$

Try a different EPU ambient air temperature of 130.6 and repeat the process.

Preuprate pipe temp. ( $^{\circ}\text{F}$ )	374.4	Reference 7
EPU pipe temp. ( $^{\circ}\text{F}$ )	392.6	Reference 8
Preuprate ambient air temp. ( $^{\circ}\text{F}$ )	130	Reference 5
Preuprate AHU $\Delta\text{T}$ ( $^{\circ}\text{F}$ )	25	Reference 4 (RRU-17A, $130 - 105 = 25$ )

The EPU ambient air temperature is estimated at  $130.6^{\circ}\text{F}$ .

The EPU Area Heat Gain Multiplier is obtained using the equation in Section 1.3.

$$\text{EPU Area Heat Gain Multiplier} = \frac{(\text{EPU pipe temperature} - \text{EPU ambient air temperature})}{(\text{preuprate pipe temperature} - \text{preuprate ambient air temperature})}$$

$$\text{EPU Area Heat Gain Multiplier} = \frac{(392.6 - 130.6)}{(374.4 - 130)}$$

$$\text{EPU Area Heat Gain Multiplier} = 1.072$$

The EPU factor is obtained by subtracting 1 from the EPU Area Heat Gain Multiplier:

$$\text{EPU factor} = 1.072 - 1 = 0.072$$

From Assumptions section, the feedwater piping contributes 1/3 to the total heat gain in the main steam tunnel, so the EPU factor becomes:

$$\text{EPU factor} = 0.072 * 1/3$$

$$\text{EPU factor} = 0.024$$

The temperature rise is then calculated by multiplying the EPU factor by the AHU temperature differential.

$$\text{Temp. rise} = 0.024 * 25.0^{\circ}\text{F} = 0.6^{\circ}\text{F}$$

The difference between estimated EPU and preuprate ambient air temperatures is:

$$130.6 - 130 = 0.6 \text{ (this equals the calculated temperature rise of } 0.6^{\circ}\text{F)}$$

The temperature rises for the remainder of the pipelines was calculated using the same method using an Excel spreadsheet.

The results are shown in Table 1.5-1.

Table 1.5-1 - Design Temperature Differential

$\text{EPU pipe temperature} - \text{EPU ambient temperature} = \text{EPU Area} \times \text{Heat Gain Multiplier}$   
 $\text{predicted pipe temperature} - \text{predicted ambient temperature}$

	Pre EPU pipe Temp °F (Para 1)	EPU pipe Temp °F (Para 2)	Pre EPU ambient air temp °F (Para 3)	EPU ambient air temp °F (Para 4)	EPU Heat Gain Multiplier	Pipe's percentage of total area heat gain	Weighted Factor	Pre EPU Vmax/G Air ΔT °F (Para 5)	Design EPU Temperature Increase for Specified EPU, °F	Bulk EPU Temperature Increase for Area, °F	Predicted EPU Area Temperature °F	Comments	
<b>RP Heater Area</b>													
ESS to FWH	303.3	403.7	125.0	126.5	1.073	See Comment	0.073	20.0	1.5			Determination of what percentage each pipe section contributes to the area heat gain was not performed. Bulk air temperature increase of 1.7°F conservatively based on predicted discrete temperature increase	
FWH Shell	303.3	403.7	125.0	126.5	1.073	See Comment	0.073	20.0	1.5				
FW to FWH	300.7	346.4	125.0	126.4	1.070	See Comment	0.070	20.0	1.4				
FW by FWH	374.4	392.6	125.0	126.4	1.058	See Comment	0.058	20.0	1.4				
Drains by FWH	343.8	398.9	125.0	126.1	1.058	See Comment	0.058	20.0	1.1	1.7	126.7		
ESS to FWHQ	338.0	398.1	125.0	126.7	1.057	See Comment	0.057	20.0	1.7				
FWH Shell	338.0	398.1	125.0	126.7	1.057	See Comment	0.057	20.0	1.7				
FW to FWHQ	339.3	372.5	125.0	126.4	1.058	See Comment	0.058	20.0	1.4				
FW by FWHQ	330.7	346.4	125.0	126.4	1.070	See Comment	0.070	20.0	1.4				
Drains by FWHQ	300.7	322.8	125.0	126.3	1.063	See Comment	0.063	20.0	1.3				
<b>LP Heater Area</b>													
ESS to FWHQ	308.4	321.2	125.0	126.8	1.079	See Comment	0.079	20.0	1.8				Determination of what percentage each pipe section contributes to the area heat gain was not performed. Bulk air temperature increase of 4.1°F conservatively based on predicted discrete temperature increase
FWHQ Shell	308.4	321.2	125.0	126.8	1.079	See Comment	0.079	20.0	1.8				
CHD to FWHQ	227.8	228.4	125.0	126.8	1.080	See Comment	0.080	20.0	1.8				
CHD by FWHQ	256.8	308.8	125.0	126.4	1.059	See Comment	0.059	20.0	1.4				
Drains by FWHQ	230.0	267.4	125.0	126.9	1.058	See Comment	0.058	20.0	1.9				
ESS to FWH	239.0	252.1	125.0	126.8	1.059	See Comment	0.059	20.0	1.9				
FWH Shell	239.0	252.1	125.0	126.8	1.059	See Comment	0.059	20.0	1.9	4.1	129.1		
CHD to FWH	167.9	180.9	125.0	129.1	1.207	See Comment	0.207	20.0	4.1				
CHD by FWH	227.8	228.4	125.0	126.8	1.080	See Comment	0.080	20.0	1.8				
Drains by FWH	175.1	188.1	125.0	129.0	1.201	See Comment	0.201	20.0	4.0				
ESS to FWHQ	173.9	181.8	125.0	127.2	1.116	See Comment	0.116	20.0	2.9				
FWH Shell	173.9	181.8	125.0	127.2	1.116	See Comment	0.116	20.0	2.9				
CHD to FWH	135.1	134.7	125.0	129.1	1.207	See Comment	0.207	20.0	4.1				
CHD by FWH	167.9	180.9	125.0	129.1	1.207	See Comment	0.207	20.0	4.1				
Drains by FWH	145.3	161.9	125.0	129.0	1.201	See Comment	0.201	20.0	4.0				
<b>RW Pump Room</b>													
CHD to RP	296.8	329.8	105.0	108.2	1.082	See Comment	0.082	20.0	1.2	N/A	N/A	See Section 1.6 for temperature increase due to pump motors and piping	
FW by RP	309.3	372.5	105.0	108.2	1.082	See Comment	0.082	20.0	1.5	N/A	N/A		
<b>CRD Pump Room</b>													
CHD to CRP	133.0	133.0	105.0	105.0	1.000	See Comment	0.000	20.0	0.0	N/A	N/A	See Section 1.6 for temperature increase due to pump motors and piping	
CHD by CRP	133.1	133.1	105.0	105.0	1.000	See Comment	0.000	20.0	0.0	N/A	N/A		
<b>Main Steam Tunnel</b>													
FW by FWH	374.4	392.6	130.0	130.8	1.072	0.333	0.074	25.0	0.8	0.8	130.8	Determination of 0.8°F temperature rise in tunnel obtained surface area of FW lines represents 33% of Heat Gain	
Main Steam	547.8	547.8	130.0	130.8	1.000	0.666	0.000	25.0	0.0				

NOTES:

1. Pre EPU Pipe temperatures based upon VY PEPSE Heat Balance 9829-H(05) V0, Rev. 0 5/1/03 (See Attachment 3)
2. Post EPU Pipe temperatures based upon VY PEPSE Heat Balance 9829-H(05) V03, Rev. 0 3/16/03
3. Pre-ops ambient air temperatures were taken from EBASCO Summary of HVAC Design Criteria and Calculation Data, transmitted by EBASCO letter dated 3/25/78. For areas not specified in this letter, the dry bulb from EQ manual.
4. EPU ambient temperature is obtained by manual iteration by initially using measured ambient air temperature in the remainder of the formula.
5. Pre-ops temperature rise of 1.7°F based on air was obtained by taking the difference between pipe ambient air temperature and based on the HVAC Flow Diagrams one of the following temperatures. Includes air, transfer air or heating air from pipe cooler. Referenced EBASCO Summary of HVAC Design Criteria and Calculation Data, transmitted by EBASCO letter dated 3/25/78

125

13

The Total Cooling Load for Normal EPU Operation is: 1,700,675 Btu/hr

The ratio of cooling loads to differential temperatures is:

$$q_{epu} / q_{pre} = \Delta T_{epu} / \Delta T_{pre}$$

$$\Delta T_{epu} = (q_{epu} * \Delta T_{pre}) / q_{pre} = (1,700,675 \text{ Btu/hr} * (135 - 97)^\circ\text{F}) / 1,691,300 \text{ BTU/hr}$$

$$\Delta T_{epu} = 38.21^\circ\text{F}$$

$$\text{Since } \Delta T_{pre} = 135 - 97 = 38^\circ\text{F}$$

The increase in drywell temperature due to the higher feedwater temperature is:

$$\Delta T = \Delta T_{epu} - \Delta T_{pre} = 38.2^\circ\text{F} - 38^\circ\text{F}$$

$$\Delta T = 0.2^\circ\text{F}$$

The ambient drywell temperature at EPU is  $135^\circ\text{F} + 0.2^\circ\text{F} = 135.2^\circ\text{F}$

#### Main Steam Tunnel (RRU-17A, -17B)

$$q \text{ (Btu/hr)} = \text{cfm} * 1.08 \text{ (Btu min/ft}^3 \text{ hr }^\circ\text{F)} * [T_{in} - T_{out}]^\circ\text{F}$$

$$q = 5000 \text{ cfm} * 1.08 \text{ (Btu min/ft}^3 \text{ hr }^\circ\text{F)} * [130 - 105]^\circ\text{F}$$

$$q = 1.35 \times 10^5 \text{ Btu/hr}$$

The main steam tunnel piping is evaluated using the Excel spreadsheet described above. As stated in the assumption section, the temperature rise from the feedwater piping is "weighted" at 33% based upon its surface area ratio when compared to main steam piping. The increased feedwater temperature will result in an ambient temperature increase of approximately  $0.6^\circ\text{F}$  to  $130.6^\circ\text{F}$ . As previously noted, the service water to RRU-17A&B is piped backwards, such that there is parallel flow rather than counter flow (Reference 18). Because of this, both coils are in continuous operation rather than the initial design of one in operation and the other as a back-up. The minimal increase in ambient temperature due to EPU will not adversely affect current operation due to the fact the current peak allowable temperature in the tunnel is  $150^\circ\text{F}$  (Reference 6, pg. 10). Also, per Reference 6, Section 7.5.2.5, the high space temperature alarm set point is  $160^\circ\text{F}$  and the MSIV close/scram set point is  $200^\circ\text{F}$ .

#### Reactor Feedwater Pump Room (TRU-1,-2,-3,-4)

The heat removal capability of the reactor feedwater pump room is:

$$q \text{ (Btu/hr)} = \text{cfm} * 1.08 \text{ (Btu min/ft}^3 \text{ hr }^\circ\text{F)} * [T_{in} - T_{out}]^\circ\text{F}$$

$$q = 4 * 16750 \text{ cfm} * 1.08 \text{ (Btu min/ft}^3 \text{ hr }^\circ\text{F)} * [105 - 85]^\circ\text{F}$$

$$q = 1.45 \times 10^6 \text{ Btu/hr}$$

From above, the preuprate heat load due to two pumps operating is  $0.97 \times 10^6 \text{ Btu/hr}$  and the EPU heat load due to three pumps operating is  $1.47 \times 10^6 \text{ Btu/hr}$ .

Using the heat removal capability with all four coolers running, the preuprate heat load due to the piping is:

$$1.45 \times 10^6 \text{ Btu/hr} - 0.97 \times 10^6 \text{ Btu/hr} = 0.50 \times 10^6 \text{ Btu/hr}$$

The temperature scaling method using the preuprate and EPU heat balances shows the ambient temperature will increase  $1.2^\circ\text{F}$ .

The EPU increase in piping heat load due to higher feedwater temperature can be approximated using:

$$q_{pre} = mC_p \Delta T_{pre} \text{ and } q_{epu} = mC_p \Delta T_{epu}$$

Since  $mC_p$  is the same preuprate and EPU,

$$q_{epu} / q_{pre} = \Delta T_{epu} / \Delta T_{pre} \text{ or}$$

$$q_{epu} = q_{pre} * (\Delta T_{epu} / \Delta T_{pre})$$



14

The areas that contain condensate and feedwater piping are the only areas that will experience an ambient temperature increase during normal operation due to EPU. The following systems will not experience an ambient temperature increase during normal operation due to EPU: Reactor Recirculation (RRS), Reactor Core Isolation Cooling (RCIC), Residual Heat Removal (RHR), Reactor Water Clean Up (RWCU), High Pressure Coolant Injection (HPCI) and Core Spray (CS) (References 20 through 25).

Reactor Building open areas

Temperatures in the open areas of the reactor building will not increase during normal operation as a result of EPU (Reference 26).

Control Room

As shown in Calculation VYC-1502 (Reference 28), Section 2.1, heat sources in the control room are from electrical equipment, ambient outside air temperature, and personnel. None of these sources will increase at EPU. Therefore, the Control Room HVAC system's ability to provide appropriate temperature and humidity conditions for personnel and equipment during all modes of operation and emergency condition is not impacted by EPU.

**1.6 Results**

The results of this calculation are shown in Table 1.6-1 below.

Table 1.6-1

Area	EPU Ambient Temperature Increase (°F)
Drywell	0.2
Main Steam Tunnel	0.6
LP Heater Area	4.1
HP Heater Area	1.7
Feedwater Pump Room	7.6
Condensate Pump Room	3.5

The increase in drywell ambient temperature due to the higher EPU feedwater temperature is 0.2°F to 135.2°F.

The increase in main steam tunnel ambient temperature due to the higher EPU feedwater temperature is 0.6°F to 130.6°F.

The results of the piping evaluation are shown in Table 1.5-1. At normal operating EPU conditions, the ambient temperature in the LP heater area will increase approximately 4.1°F to 129.1°F and the HP heater area will increase 1.7°F to 126.7°F.

The increase in feedwater pump room ambient temperature due to the higher EPU feedwater temperature is 7.6°F to 112.6°F. This result was achieved using both design and empirical information.

The increase in condensate pump room ambient temperature due to the higher EPU feedwater temperature is 3.5°F. The ambient temperature in the condensate pump room at EPU based upon design information is 113.2°F and 122.5°F based upon empirical data.

It is noted that the temperatures obtained in this calculation are conservative maximum temperatures for the purposes of obtaining bounding temperature increases within the subject areas. Actual EPU maximum temperatures are anticipated to be lower than those calculated.

**Exhibit SPSB-C-52-6**

Vermont Yankee Nuclear Power Station

Proposed Technical Specification Change No. 263 – Supplement No. 30

Extended Power Uprate

Response to Request for Additional Information

Operation Procedure OP- 2192, Rev. 31

Total number of pages in this Exhibit  
(excluding this cover sheet) is 5.

1

VERMONT YANKEE NUCLEAR POWER STATION

**OPERATING PROCEDURE**

OP 2192

REVISION 31

**HEATING, VENTILATING, AND AIR CONDITIONING SYSTEM**

USE CLASSIFICATION: REFERENCE

RESPONSIBLE PROCEDURE OWNER: Manager, Operations

REQUIRED REVIEWS		Yes/No
E-Plan	10CFR50.54(q)	No
Security	10CFR50.54(p)	No
Probable Risk Analysis (PRA)		No
Reactivity Management		No

LPC No.	Effective Date	Affected Pages
1	10/26/04	App A Pg 15 of 24
2	11/16/04	51 & ADDED 51A of 62
3	01/22/05	60 of 62
4	05/26/05	29 of 62

**Implementation Statement: N/A**

Issue Date: 07/06/2004

2

TABLE OF CONTENTS

PURPOSE..... 3

DISCUSSION ..... 3

ATTACHMENTS ..... 6

QA REQUIREMENTS CROSS REFERENCE..... 6

REFERENCES AND COMMITMENTS..... 7

PRECAUTIONS/LIMITATIONS ..... 9

PREREQUISITES ..... 11

PROCEDURE..... 12

    Startup, Shutdown and Transfer of Service Building HVAC ..... 12

    Startup, Shutdown and Transfer of Turbine Building HVAC ..... 15

    Startup, Shutdown and Transfer of Reactor Building HVAC..... 25

    Startup, Shutdown and Transfer of Radwaste Building HVAC ..... 31

    Startup and Shutdown of Intake Structure HVAC ..... 33

    Startup and Shutdown of Discharge Structure HVAC ..... 34

    Startup and Shutdown of Switchyard House HVAC ..... 34

    Startup and Shutdown of Steam Heat HVAC ..... 37

    Startup, Shutdown and Transfer of Advanced Off Gas Building HVAC..... 38

    Operation of Control Room and Cable Vault Battery Room HVAC ..... 42

    Operation of Chiller Units SCH-1 and 2 ..... 44

    Cross-Connecting SAC-1 and 2 Chilled Water Systems ..... 46

    Startup and Shutdown of UPS-2A-AC1 HVAC ..... 48

    John Deere Diesel Generator Ventilation Controls ..... 50

    Startup and Shutdown of Turbine Deck Office HVAC ..... 51

    Startup and Shutdown of Switchgear Room HVAC ..... 52

    Loss of Control Room Ventilation (UND98080)..... 53

    Local Manual Operation of EDG Room A(B) Exhaust Fan TEF-2(3) (Use  
        VYOPF 2192.01) (ER990738\_01)..... 53

    Startup and Shutdown of Steam Heat to the CST ..... 55

    SCH-1-1 and SCH-1-2 Reset After Low Pressure Trip ..... 56

    Temporary Space Heating..... 57

FINAL CONDITIONS ..... 62

The Turbine Lube Oil Room fire dampers are controlled by a local hand switch located outside the Lube Oil Room door.

The air is exhausted to the atmosphere by wall exhaust fans, roof exhaust fans or through the station stack. Several areas, such as the Control Room and office spaces recirculate air on a continuous cycle.

The system serving the Control Room is designed to provide cooling during the summer and heating during the winter. Air is circulated through a chilled water cooling coil, steam preheat coil, a steam reheat coil and ductwork by one of two system fans. Fresh air is normally drawn into the system mixing with the recirculated flow. A humidistat, on the west hallway wall in the first fan room, controls the relative humidity between 20% and 50% with a humidifier located in SRHC-1. It is operated with instrument air and controls humidity by spraying steam into the air flow. Two exhaust fans in the North wall of the Control Room, kitchen and rest room, serve to exhaust these rooms. The "Control Room H and V" switch on CRP 9-25 is provided to allow the operator to isolate the Control Room and Computer Room by closing the fresh air dampers and the Control Room kitchen and bathroom exhaust vents during off normal conditions. This is accomplished by moving the switch from "NORMAL" to "EMER". If a report was received of a toxic gas release which could affect Control Room personnel, the operators would don the self-contained breathing apparatus located in the Control Room. If Control Room cooling is completely lost, emergency cooling can be initiated using portable smoke ejectors. (UND98080)

The Control Room and Service Building chilled water cooling coils are located in the SAC-1 and SAC-2 supply fan housings respectively. The cooling coils are cooled by dual compressor refrigeration units SCH-1 and 2 that cycle as necessary to maintain chilled water temperature. Demineralized water from the chilled water pumps circulates through the chiller heat exchanger and gives off its heat to the chiller units. The cooled water passes from the chiller units to the cooling coils. The amount of chilled water flowing into the cooling coils is controlled by the mixing valves. Each mixing valve is controlled by a thermostat that senses supply air temperature. The Services Building chilled water piping system can be valved into the Control Room HVAC because both the NNS piping system and the current SC3 piping system, respectively, were designed and built to the same specifications (i.e., non-seismic), therefore, failure mechanism(s) are the same for each system. In addition, isolation of the NNS and SC3 systems can be accomplished because the valves are in a mild environment area. Continued operation of the Control Room HVAC by valving in the Service Building HVAC to supply chilled water is consistent with the Safety Class Manual and the HVAC DBD.

Air for air compressor cooling is drawn through a wall louver located in the outside wall. This louver also supplies any required room ventilation air. Discharge dampers which exhaust into the room are located on the air compressor discharge duct to allow for air recirculation.

Two oil-fired steam boilers supply steam for the heating coils and some of the unit heaters. Other unit heaters are run electrically.

All RRUs and TRUs utilize service water as the cooling medium except the drywell RRU-1 through RRU-4 which use RBCCW. (MOOID9502\_14)

7. For minimum ECCS RRU corner room support operation, RRU 7 must be operable for the Northeast corner room and RRU 8 must be operable for the Southeast corner room. RRUs 7 and 8 can be removed from service for maintenance and the associated Core Spray Pump/RHR Pump may remain operable. Refer to OP 2181, Service Water/Alternate Cooling Operating Procedure, Precautions and Limitations, for administrative requirements and actions necessary to maintain operability.
8. SP-1, SCH-1 and SAC-1 supply air conditioning for the Control Room. This is a Safety Class 3 system and requires special consideration for its timely repair.
9. To prevent the possibility of reverse air flow, building ventilation should be secured in the following order:
  - a. Radwaste Building
  - b. Turbine Building
  - c. Reactor Building
  - d. Service Building
10. Minimize the time that TEF-2/3 are operated in manual. The UFSAR specified minimum Turbine Building design temperature, which includes the DG rooms, is 50°F and the AS-2 battery load calculation assumes an electrolyte temperature of 50°F. (ER960055\_01)
11. Securing TRU-5 with the condensate pumps running will result in a condensate pump bearing temperature rise. Planned maintenance on TRU-5 should be coordinated such that the time the unit is out of service is minimized.
12. Control Room temperatures in excess of 78°F are indicative of a need for corrective action. Corrective actions need to be completed prior to exceeding 95°F to ensure the Control Room does not reach 120°F (upper temperature operability limit for Control Room instrumentation). (UND98080)
13. HS-139 and HS-140 in the Reactor Building must remain locked closed during plant operation due to House Heating Steam, High Energy Line Break concerns. These valves may only be opened with the permission of the Design Engineering Department. (ER96-0482, TAG\_REVIEW\_9703\_26)
14. The Main Station Battery Room must be maintained at  $\geq 60^\circ\text{F}$ . The main station battery load calculations are based upon this minimum temperature.
15. One of the two standby gas treatment trains should be placed in service whenever normal Reactor Building ventilation is secured.
16. In order to meet environmental qualification program requirements, the RCIC room fan or alternate ventilation from the Reactor Building must be operable and the RCIC room temperature must be less than 112°F. However, to satisfy station blackout analysis, the RCIC Room temperature must be maintained less than 104°F. (EPC\_9504)

2. Shutdown

- a. Secure the West Switchgear Room exhaust fan SWGR-EF-1A.
- b. If the temperature cannot be maintained in the required range, notify the Operations Manager of the need to initiate actions to provide supplemental heating/cooling.

Q. Loss of Control Room Ventilation (UND98080)

- 1. If a loss of normal Control Room ventilation occurs, refer to Section J and place SAC-1B in service.
- 2. If Control Room cooling is lost, perform applicable action:
  - a. Refer to Section L and cross-connect chilled water from the Service Building to the Control Room.
  - b. Perform the following:
    - 1) In the Control Room back panel area, remove 11 full size ceiling tiles.
    - 2) Open Control Room panel doors.
    - 3) Notify Security and Shift Engineer that Control Room doors will be opened.
    - 4) Open Control Room doors.
    - 5) Using two smoke ejectors or other portable cooling equipment to create temporary air flow paths, ventilate Control Room.
    - 6) Implement the administrative requirements of AP 0077.

R. Local Manual Operation of EDG Room A(B) Exhaust Fan TEF-2(3) (Use VYOPF 2192.01) (ER990738\_01)

- 1. Ensure the selected EDG Room temperature is  $\geq 60^{\circ}\text{F}$  [RATS-1A(B)].
- 2. Obtain Shift Manager permission for local manual operation of TEF-2(3).
- 3. Obtain key #D018.
- 4. Station a dedicated Auxiliary Operator at the selected Diesel Generator Room area.

**Exhibit EMEB-B-138-1**

**Vermont Yankee Nuclear Power Station**

**Proposed Technical Specification Change No. 263 – Supplement No. 30**

**Extended Power Uprate**

**Response to Request for Additional Information**

**Prediction of Unsteady Loading on A Circular Cylinder in High Reynolds Number Flows  
using Eddy Simulation.**

**Total number of pages in this Exhibit  
(excluding this cover sheet) is 9.**



OMAE 2005-67044

## PREDICTION OF UNSTEADY LOADING ON A CIRCULAR CYLINDER IN HIGH REYNOLDS NUMBER FLOWS USING LARGE EDDY SIMULATION

Sung-Eun Kim  
Fluent Incorporated, Lebanon, N.H.  
03766, U.S.A.

L. Srinivasa Mohan  
Fluent India  
Pune, India

### ABSTRACT

Large eddy simulations were carried out for the flow around a hydrodynamically smooth, fixed circular cylinder at two Reynolds numbers, one at a subcritical Reynolds number ( $Re = 1.4 \times 10^5$ ) and the other at a supercritical Reynolds number ( $Re = 1.0 \times 10^6$ ). The computations were made using a parallelized finite-volume Navier-Stokes solver based on a multidimensional linear reconstruction scheme that allows use of unstructured meshes. Central differencing was used for discretization of both convection and diffusion terms. Time-advancement scheme, based on an implicit, non-iterative fractional-step method, was adopted in conjunction with a three-level, backward second-order temporal discretization. Subgrid-scale turbulent viscosity was modeled by a dynamic Smagorinsky model adapted to arbitrary unstructured meshes with the aid of a test-filter applicable to arbitrary unstructured meshes. The present LES results closely reproduced the flow features observed in experiments at both Reynolds numbers. The time-averaged mean drag coefficient, root-mean-square force coefficients and the frequency content of fluctuating forces (vortex-shedding frequency) are predicted with a commendable accuracy.

### INTRODUCTION

Unsteady loading on a circular cylinder caused by the flow is a precursor to its vortex-induced vibration (VIV). The major difficulty of computing flows around circular cylinders originate from the fact that circular cylinder flows of practical interest are high Reynolds number ( $Re$ ) flows, often involving a laminar-to-turbulent transition in various regions of the flows such as boundary layer, separated shear-layer, or near-wake. The location of transition and the extent of laminar or turbulent flow regime, in real flows, depend on such factors as Reynolds number, freestream turbulence, surface roughness, span-diameter ratio ( $L/D$ ), and blockage, among others. The state of the flow in those regions dictates the formation and evolution

of large-scale turbulent structure around a circular cylinder, which in turn affects unsteady loading on the cylinder. Apparently, turbulence modeling is an issue here.

There are largely three approaches being explored by CFD practitioners to modeling high- $Re$  turbulent flows around circular cylinders and bluff bodies in general. One approach employs unsteady Reynolds-averaged Navier-Stokes (URANS) equations supplemented by turbulence models as the governing equations. URANS-based approach, despite its low computational cost mainly due to less demanding mesh resolution requirement, is fundamentally ill equipped to capture large-scale turbulent structure present in the flows. Results obtained using URANS computations typically underpredict the amplitudes of fluctuating forces. Obviously, this shortcoming has a serious negative implication to accurate prediction of VIV.

Fundamentally more viable than URANS-based approach for bluff-body flows is large eddy simulation (LES). LES is designed to directly resolve large eddies, with the effects of unresolved smaller eddies, namely subgrid-scale turbulence, on the resolved large eddies accounted for by turbulence models. However, LES is computationally very expensive, often prohibitively, especially when thin turbulent boundary layer is a predominant feature of the flow in question to be accurately resolved in a LES. Resolving near-wall turbulence with infinitesimal length and time scales requires extremely fine mesh and small time-step size. For that matter, LES is more feasible for free flows such as jets, mixing layer, and wakes, and massively separated flows.

There are very few LES studies published in the literature of flows around circular cylinders at high Reynolds numbers. Breuer [1] was the one of the very few who tackled the case of a high subcritical Reynolds number,  $Re = 1.4 \times 10^5$ , at which the experiment of Cantwell and Coles [2] was conducted. Using a multi-block, structured-mesh-based finite-volume solver with an explicit time-marching scheme, Breuer was able to predict the global parameters of the flow, and the mean flow and turbulence with a commendable accuracy. More recently,

Catalano *et al.* [3] attempted LES for three Reynolds numbers in critical to supercritical Reynolds regime ( $Re = 0.5 \times 10^6, 1.0 \times 10^6, 2.0 \times 10^6$ ). Their predictions of the global flow parameters were in reasonable agreement with the experimental data, although the skin-friction and the Reynolds number-dependency of the mean drag coefficient were poorly predicted.

A more recent trend in turbulence modeling of bluff-body flows is to employ what may be called "hybrid" approaches in which one attempts to adjust turbulence models to local mesh resolution in one way or another. In one such approach referred to, in the literature, as detached eddy simulation (DES), either a RANS-based or a subgrid-scale (SGS) turbulence model is invoked depending on whether or not the filter-length (local mesh size) is larger than the local integral length-scale of turbulence. In DES, turbulence models essentially reduce to RANS models in near-wall region or when the local mesh size is too coarse to explicitly resolve energy-containing eddies. One fundamental criticism about DES comes down to the lingering question of how one can possibly reconcile a RANS turbulence model and a subgrid-scale turbulence model, two very different models in terms of their spectral content, at the common interface. It should also be realized that, as a consequence of falling back to a RANS model in near-wall region, the fidelity of DES would be solely determined by that of the embedded RANS model. Quite a few studies employing DES have appeared recently on circular cylinder flows. Among others, Travin *et al.* [4], Vatsa and Singer [5], and more recently Pandya *et al.* [6] all employed DES based on an eddy-viscosity transport model to study the flow around a smooth circular cylinder at subcritical and supercritical Reynolds numbers. The results of these DES are mixed, insofar as some of the global flow parameters such as the r.m.s. force coefficients and the mean flow in the near-wake were predicted poorly.

The objective of this study is to assess the feasibility of LES for high Reynolds number flows around a fixed, smooth circular cylinder. To that end, two Reynolds numbers, one in subcritical ( $Re = 1.4 \times 10^5$ ) and the other in supercritical ( $Re = 1.0 \times 10^6$ ) regime were deliberately chosen so that they straddle the critical Reynolds number ( $\sim 3 \times 10^5$ ). The main concern is how well LES can reproduce the known characteristics of the flow at the two Reynolds numbers and the changes in the global flow parameters such as drag coefficient, r.m.s. force coefficients, and vortex-shedding frequency as the Reynolds number increases.

The results of the LES will be compared whenever possible, with the experimental data and other LES and DES results reported in the literature.

## NUMERICAL METHOD

The computations were carried out using the *segregated* solver in FLUENT, a general-purpose CFD software. The details of the numerical method are described in the following.

## SPATIAL DISCRETIZATION SCHEMES

FLUENT employs a cell-centered finite-volume method based on a multidimensional linear reconstruction scheme that permits use of computational elements (cells) with arbitrary polyhedral topology, including quadrilateral, hexahedral,

triangular, tetrahedral, pyramidal, prismatic, and hybrid meshes. The solution gradients at cell centers that are needed to compute convective and diffusive fluxes are determined applying the Green-Gauss theorem [7]. Diffusive fluxes are discretized using central differencing. Discretization of convective fluxes requires great caution in LES. Upwind-biased schemes such as second-order upwind scheme have been widely used for RANS computations. Unfortunately, numerical diffusion introduced by upwind schemes, which might be acceptable in RANS computations for high-Re flows where eddy-viscosity is larger than molecular viscosity by orders of magnitude, can overwhelm physical diffusion that is typically much smaller in LES; subgrid-scale turbulent viscosity is smaller than RANS-based eddy viscosity by orders of magnitude. For this reason, a central differencing scheme [13] was employed for the discretization of convection terms in this study.

## TIME-ADVANCEMENT SCHEMES

An implicit fractional-step method (FSM) [8] in combination with a second-order accurate, three-level backward-differencing scheme for time-discretization was employed to advance the solution in time. In this algorithm, the momentum equations are decoupled from the continuity equation using an approximate factorization of the coupled Navier-Stokes equations. For incompressible flows, the FSM preserves the formal second-order temporal accuracy without having to perform, at each time-step, costly outer iterations to couple velocity and pressure. The FSM thus provides a highly efficient algorithm for CPU-intensive transient computations like LES.

Consider a semi-discrete form of the Navier-Stokes equations in "pressure-correction" ( $\delta p^{n+1} = p^{n+1} - p^n$ ) form,

$$\begin{bmatrix} A & G \\ D & 0 \end{bmatrix} \begin{pmatrix} \mathbf{u}^{n+1} \\ \delta p^{n+1} \end{pmatrix} = \begin{pmatrix} \mathbf{r} \\ 0 \end{pmatrix} \quad (1)$$

where  $\mathbf{u}^{n+1}$  and  $\mathbf{r}$  are the velocity vector and the momentum source vector, respectively, and the integer  $n$  the time level, with  $n+1$  refers to the current time level.  $A$  is the coefficient matrix defined in terms of the discrete convective and diffusive operators and the time-advancement scheme chosen, and  $G$  and  $D$  the discrete gradient and divergence operators, respectively.

The coupled system of equations in Equation (1) is extremely difficult to solve as it stands, since the matrix  $A$  has to be inverted for every iteration. In the FSM, the original coupled equations in Equation (1) are approximated by

$$\begin{bmatrix} A & 0 \\ D & \Delta t DG \end{bmatrix} \begin{bmatrix} \mathbf{u} \\ \delta p^{n+1} \end{bmatrix} = \begin{pmatrix} \mathbf{r} \\ 0 \end{pmatrix} + [O(\Delta t^2)] \quad (2)$$

Factorizing equation (2), we have a series of split operations that consist of

$$\begin{aligned} A\hat{\mathbf{u}} &= -Gp^n + \mathbf{r}^n \\ \Delta t DG\delta p^{n+1} &= D\hat{\mathbf{u}} \\ \mathbf{u}^{n+1} &= \hat{\mathbf{u}} - \Delta t G\delta p^{n+1} \end{aligned} \quad (3)$$

On a per-iteration basis, the series of operations in Equation (3) closely resemble the SIMPLEC scheme. The difference is that, in the iterative SIMPLEC scheme, the series of operations in Equation (3) are repeated in a loop until the solutions converge, while the FSM needs only one sweep. To preserve second-order accuracy with the FSM, however, sub-iterations are needed for the set of three momentum equations and individual scalar equations to account for the nonlinearity in and coupling among the individual equations and high-order source terms. Yet, the non-iterative FSM is takes much less CPU time than the iterative SIMPLEC scheme.

The system of discretized governing equations are solved using a point-implicit, Gauss-Seidel relaxation along with an algebraic multigrid (AMG) method to accelerate solution convergence. The solver and the subgrid-scale turbulence model are fully parallelized.

As a validation for the spatial discretization schemes and the transient algorithm, we computed laminar flow around a circular cylinder at the Reynolds number of 100 with both non-iterative FSM and iterative SIMPLEC scheme. At this Reynolds number, the flow exhibits a periodic vortex-shedding. A C-type structured mesh with 48,000 cells was used for the computation. A dimensionless time-step size of  $\Delta t = 0.04$  (non-dimensionalized by  $D/U_0$ ,  $D$  being the cylinder diameter,  $U_0$  the freestream velocity) was used, with which one period of the vortex-shedding was resolved with approximately 150 time-steps. The predicted mean drag coefficient ( $\overline{C_D}$ ), r.m.s. lift coefficient ( $C'_L$ ), and Strouhal number ( $St$ ) are summarized in Table 1. The FSM gives practically the same predictions as the iterative SIMPLEC scheme, and the global parameters predicted by both methods are seen to closely match the other predictions and the experimental data.

**Table 1. Summary of the global flow parameters predicted for laminar flow ( $Re = 100$ ) – Norberg [10] compiled numerical results whose references can be found in ref. [10]**

	$\overline{C_D}$	$C'_L$	$St$
Present - FSM	1.336	0.28	0.165
Present - SIMPLEC	1.345	0.28	0.166
Park <i>et al.</i> [9]	1.33	0.33	0.165
Norberg [10]	-	0.23/0.29	-
Williamson [11]	-	-	0.164

### SUBGRID-SCALE TURBULENCE MODELING

For incompressible flows, the filtered Navier-Stokes equations can be written as

$$\frac{\partial \overline{u}_i}{\partial t} + \frac{\partial \overline{u}_i \overline{u}_j}{\partial x_j} = -\frac{1}{\rho} \frac{\partial p}{\partial x_i} - \frac{\partial \tau_{ij}}{\partial x_j} + \frac{\partial}{\partial x_j} \left\{ \nu \frac{\partial \overline{u}_i}{\partial x_j} \right\} \quad (4)$$

where  $\tau_{ij} = \overline{u_i u_j} - \overline{u}_i \overline{u}_j$  is the subgrid-scale turbulent stress. In this study, the subgrid-scale (SGS) stress is modeled using isotropic eddy-viscosity as

$$\tau_{ij} - \frac{\delta_{ij}}{3} \tau_{kk} = -2C_v \overline{\Delta}^2 |\overline{S}| \overline{S}_{ij} \quad (5)$$

We determine the model constant,  $C_v$ , using the dynamic Smagorinsky model (DSM) originally proposed by Germano *et al.* [12]. To implement the dynamic procedure for the present finite-volume solver requires a special test-filter applicable to arbitrary unstructured meshes. The dynamic procedure employed in the present study is "local" in the sense that it does not require the existence of any statistically homogeneous directions, being applicable to arbitrary complex three-dimensional flows. The details of the implementation of the DSM in the framework of unstructured mesh based finite-volume solver can be found in Kim [13]. The DSM has been validated for a number of wall-bounded flows such as a square cylinder and a sphere.

### SOLUTION DOMAIN AND COMPUTATIONAL MESH

Our choices of the solution domain and the computational mesh were guided by the findings in Breuer's LES study [1]. What one should keep in mind in determining the size of the solution domain is that the spanwise extent of the domain should be larger than the spanwise correlation length of turbulence. Fortunately, the spanwise correlation length is known to decrease as the Reynolds number increases. We took advantage of this fact, having decided to use a spanwise length of  $2.0D$  for both the subcritical and the critical  $Re$  numbers. The top and bottom boundaries of the domain were placed at  $10.5D$  from the cylinder axis. Thus, the blockage ratio of our numerical model ( $H/D$ , where  $H$  is the height of the domain) is approximately 4.8%. The upstream inlet and the downstream exit boundaries are located at  $8.5D$  upstream and  $20.5D$  downstream of the cylinder axis, respectively.

A locally refined, hexahedral mesh with a total of 6.8 million cells was used for the computations for both Reynolds numbers. The overall mesh resolution is comparable to case "B1" in Breuer [1]. The near-wall mesh resolution is such that the distance from the cylinder surface is  $10^{-4}D$  at the wall-adjacent cells, which translates to  $y^+ (=u_\tau y/\nu)$  well under 1.0 for the subcritical flow, and below 6.0 for the supercritical flow. For the subcritical flow, the boundary layer was resolved with 10 – 18 cells in the laminar region.

### BOUNDARY CONDITIONS AND OTHER DETAILS OF COMPUTATION

On the cylinder wall, we employ a law-of-the-wall that invokes proper wall-laws depending on the mesh resolution, namely,  $y^+$  at the wall adjacent cells. The top and bottom wall boundaries were treated as a slip (zero-stress) wall. A periodicity condition was applied on the pair of lateral boundaries in the span-wise direction. At the upstream inlet boundary, the freestream condition was specified. At the downstream exit boundary, we extrapolated the solution variables from the adjacent interior cells in a mass-conserving manner.

The time-step size ( $\Delta t$ ) used for the computations is 0.005 in a dimensionless unit for both Reynolds numbers. The time-step size was determined based on the estimate of the

characteristic length and time scales of the smallest resolved eddies,  $\tau = \ell / u'$ , where  $\ell$  was taken as  $0.05D$ , and  $u'$  as  $0.2U_0$ . From these rough estimates and with the dimensionless time-step size of 0.005, one turnover time of the smallest resolved eddies will be resolved with 50 time steps.

To shorten the initial transient period of the solution and to quickly attain a statistically stationary state, we took, as the initial condition, a partially converged steady RANS solution with pseudo-random fluctuating velocity components superimposed on the mean velocity field.

The computations were carried out on a 16-CPU Inx86 cluster with AMD Opteron processors and Infiniband interconnects. With the non-iterative FSM, the computation took approximately 12 CPU-seconds per a time-step, which translates into being able to complete roughly 7,200 time-steps in 24 hours.

## RESULTS

### Subcritical Reynolds number ( $Re = 1.4 \times 10^5$ )

Figure 1 depicts the flow structure around the cylinder. Although the near-wake flow appears chaotic, the figure clearly shows the existence of a large-scale motion, namely alternate vortex-shedding known to occur in the subcritical  $Re$  number range. The color map of the resolved turbulent kinetic energy in Figure 1 also indicates that the boundary layer remains laminar up to the separation point, and transition occurs in the separated shear layer.



Figure 1. The flow structure behind the circular cylinder at  $Re = 1.4 \times 10^5$  - iso-surface of the second invariant of velocity deformation tensor, colored by the resolved turbulent kinetic energy

The global flow parameters predicted by the present LES are summarized in Table 2 along with the LES prediction of Breuer [1] and the DES predictions of Travin *et al.* [4], and the experimental data. As for Breuer's LES result, among the cases involving different mesh resolution and SGS turbulence models, we picked the result of case "B1" whose mesh and SGS turbulence model (dynamic Smagorinsky mode) closely match ours. In selecting the experimental data for the comparison, we gave more weight to the ones measured on smooth cylinder surface, and with sufficiently large span-wise lengths ( $L/D > 5$ ) and smaller blockage-ratio ( $H/D < 0.1$ ).

Table 2. Summary of the global flow parameters predicted by the present LES for  $Re = 1.4 \times 10^5$ , compared with other numerical results (Breuer [1]; DES-TS - Travin *et al.* [4]; DES-LS - Travin *et al.* [4]; and experimental data (CC - Cantwell & Coles [2], WA - West & Apelt [14], SB: Szepessy & Bearman [15], NO - Norberg [10], ZD: Zdravkovich [16])

	$\bar{C}_D$	$C'_L$	$-\bar{C}_{PB}$	$L_r$	$St$
LES (Present)	1.13	0.59	1.20	0.67	0.205
LES (Breuer)	1.45	-	1.76	0.34	0.204
DES-TS	0.59	0.06	0.67	1.2	0.31
DES-LS	1.08	0.29	1.04	1.1	0.21
Exp.(CC)	1.24	-	1.21	0.5	0.18
Exp.(WA)	1.3	0.58	-	-	-
Exp.(SB)	1.35	0.5	1.05	-	-
Exp.(NO)	-	0.52	-	-	0.18/0.195
Exp. (ZD)	1.15	0.5/0.6	1.05/1.2	-	0.18/0.21

The present LES gave the mean  $C_D$  around 1.13, which falls within the scatter of the experimental data (1.1 - 1.35) for smooth cylinders. Interestingly, our prediction came out substantially lower than Breuer's prediction despite the comparable mesh resolution, the same formal order of spatial accuracy (second-order) and the same dynamic SGS turbulence model used in both computations.

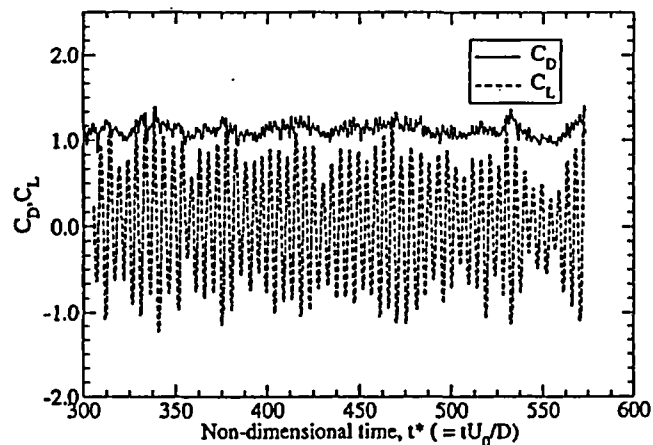


Figure 2. Time histories of the drag and lift coefficients predicted by the present LES for  $Re = 1.4 \times 10^5$

The DES-TS result [4] is shown to severely underpredict the mean  $C_D$ , better matching the data obtained with rough cylinders [17], which is consistent with the DES predictions by others [5, 6]. It has been found that DES, run in a normal mode with finite freestream turbulence, essentially yields a tripped boundary layer, leading to a premature transition to turbulence and an early drag crisis even at a subcritical Reynolds number. The DES-LS result [4] based on the so-called "tripless" approach, in which laminar flow is essentially enforced in the boundary layer, better predicts the mean  $C_D$ .

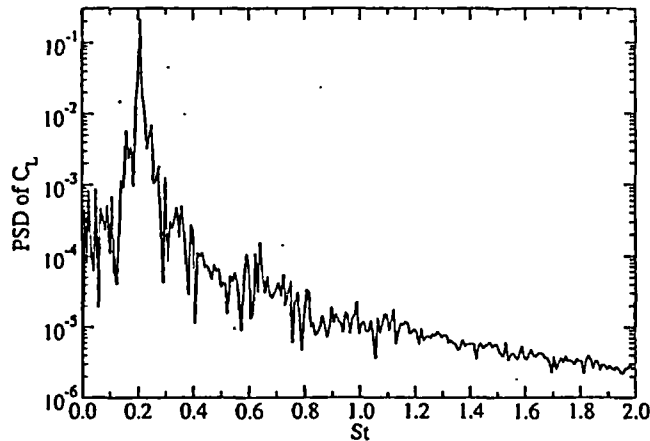


Figure 3. Power spectral density of  $C_L$  time-history for  $Re = 1.4 \times 10^5$

The r.m.s. lift coefficient predicted by the present LES is within the scatter of the experimental data, although it is closer to the upper bound. The  $C_L$  history Figure 2 clearly shows that, despite modulation of the amplitude, there is a distinct frequency of vortex-shedding, which is consistent with what has been known for smooth cylinders in the subcritical regime. The Strouhal number corresponding to the main shedding frequency was found to be 0.205 as shown in Figure 3.

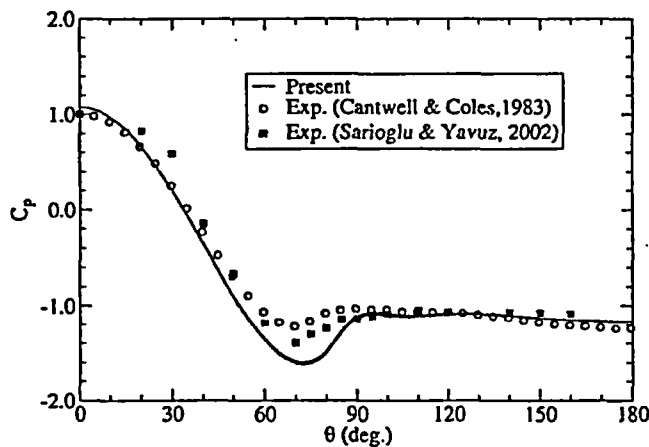


Figure 4. Mean static pressure ( $C_p$ ) distribution on the cylinder surface for  $Re = 1.4 \times 10^5$

The time-averaged pressure distribution on the cylinder surface is shown in Figure 4, along with the experimental data [2, 18] obtained at the same Reynolds number. The negative peak predicted by the present LES is larger than the measured ones. However, the pressure level in the separated region - the plateau after  $\theta = 90$  degrees, and the mean base pressure ( $\bar{C}_{pB}$ ) are all accurately predicted by the present LES.

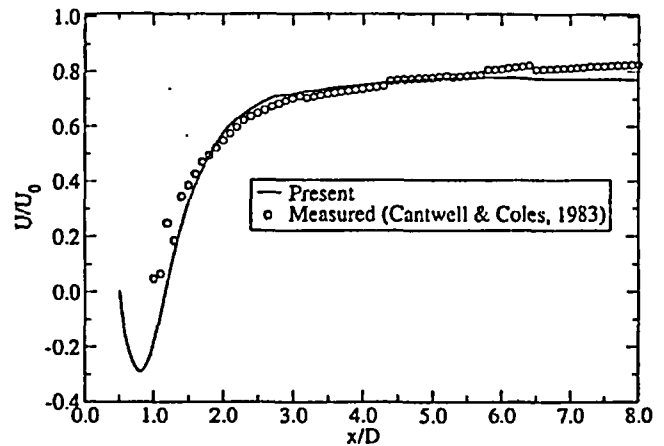


Figure 5. Time-averaged axial velocity profile in the wake predicted by the present LES for  $Re = 1.4 \times 10^5$

Figure 5 depicts the predicted time-averaged axial velocity profile along the wake centerline at the mid-span. The overall agreement between the prediction and the measurement is quite good. The rapid relaxation of the mean axial velocity in  $x/D = 1.0 \sim 3.0$  shown in the measurement is an indication of vigorous mixing of momentum taking place in the near-wake region. That our prediction closely captures the recovery of the mean axial velocity verifies that the dynamics of the large-scale structure in the near-wake is well predicted in the present LES. The length of the time-averaged recirculation bubble (see also Table 2 for  $L_r$ ) from our LES was found to be slightly larger than what Cantwell and Coles [2] reported. Yet the present LES prediction is much closer to the data than the DES predictions. Considering that hot-wire measurements become increasingly difficult and less reliable near the recirculation region, our LES prediction is considered quite good.

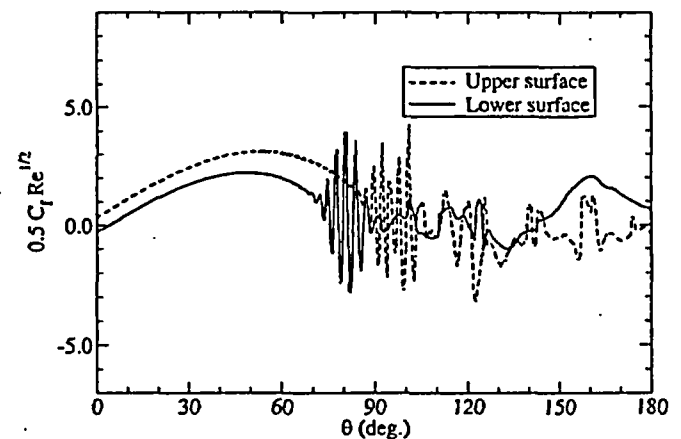


Figure 6. Scaled instantaneous skin-friction coefficient distribution on the cylinder surface at  $Re = 1.4 \times 10^5$

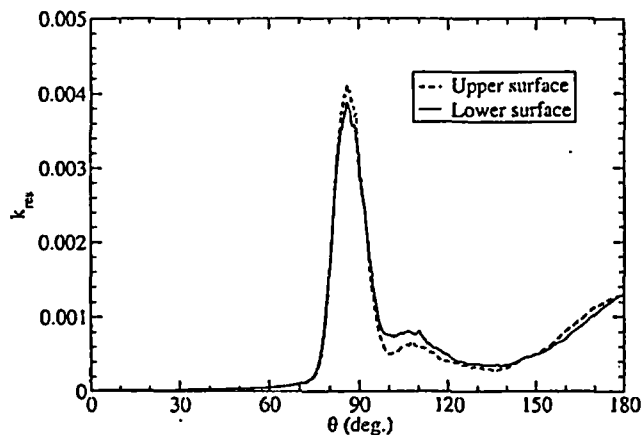


Figure 7. Resolved turbulent kinetic energy distribution at  $0.0001D$  above the cylinder surface, predicted by the present LES at  $Re = 1.4 \times 10^5$

As mentioned earlier, the experimental evidence [19] indicates that, in the subcritical regime, the boundary layer remains laminar until it finally separates from the cylinder surface. Therefore, it would be of much interest to see how closely LES can reproduce the physics associated with the separation and the transition. Figures 6 and 7 depict the circumferential variations of two quantities along the cylinder surface that shed some light on how the LES predicts the separation and transition.

Figure 6 shows a plot of the instantaneous skin-friction coefficient - rescaled to match the non-dimensionalization adopted by Achenbach [19] - against the circumferential angle. First, it is noticeable that the skin-friction distribution exhibits a considerable top-bottom asymmetry. This is a clearly the (upstream) influence of the large-scale, alternate vortex-shedding. What is most interesting in the figure is the appearance of small transient separation bubbles on both upper and lower surface starting as early as 70 - 75 degrees. Interestingly, this range largely coincides with the range of separation angles reported by many others [2, 19] deduced from the inflection point of mean  $C_f$  curve; 77 degree by Cantwell and Coles [2], and 78 degrees by Achenbach [19] at  $Re = 1.0 \times 10^5$ . Although not shown here, the separation angle determined based on the time-averaged velocity field obtained from the present LES was found to be much larger than the ones determined from  $C_f$  distribution, reaching around 98 degree, which was also found by Breuer [1]. Based on the instantaneous skin-friction distribution, we surmise that a transient laminar separation occurs much earlier than the mean separation angle.

The distribution of the resolved turbulent kinetic energy depicted in Figure 7 supports the possibility of an intermittent laminar separation around 70 - 75 degrees, insofar as the turbulent kinetic energy is still quite low there. The complete transition occurs a little downstream as indicated by the rapid increase in the resolved turbulent kinetic energy between 75 and 85 degrees. The magnitude of the skin-friction coefficient predicted by the present LES is also in good agreement with Achenbach's data [19] measured at  $Re = 1.0 \times 10^5$ . Achenbach's data show that the scaled skin-friction coefficient

peaks at 3.0 around  $\theta = 50$  degrees, which is closely reproduced by the present LES.

### Supercritical Reynolds number Case ( $Re = 1.0 \times 10^6$ )



Figure 8. The flow structure behind the circular cylinder at  $Re = 1.0 \times 10^6$  - an iso-surface of the second invariant of velocity deformation tensor, colored by the resolved turbulent kinetic energy

Figure 8 portrays an impression of the instantaneous flow structure. Compared to the flow structure for the subcritical flow shown in Figure 1, the wake is much narrower and more chaotic without any trace of a large-scale alternate vortex shedding, suggesting a delayed turbulent separation. This is typical of the flow in the supercritical regime. The color map on the iso-surface - representing resolved turbulent kinetic energy - also indicates that the laminar boundary layer is sustained farther downstream than the subcritical flow.

Table 3. Summary of the global quantities predicted by LES for  $Re = 1.0 \times 10^6$ , compared with other LES result and the experimental data; CA - Catalano *et al.*[3]; SZ - Szechenyi [20]; SH - Shih *et al.* [21]; ZD - Zdravkovich [16])

	$\bar{C}_D$	$C_L$	$-\bar{C}_m$	$St$
LES (present)	0.27	0.12	0.28	-
LES (CA)	0.31	-	0.32	0.35
Exp.(SZ)	0.25	-	-	-
Exp.(SH)	0.24	-	0.33	-
Exp. (ZD)	0.2/0.4	0.1/0.15	0.2/0.34	0.18/0.5

The global flow parameters predicted by the present LES are summarized in Table 3. Our prediction of the mean drag coefficient ( $\bar{C}_D$ ) closely matches the data of Szechenyi [20] and Shih *et al.* [21] interpolated at the present Reynolds number. We consider their data more reliable than others in view of the sufficiently large spanwise lengths used ( $L/D = 9.3$  and  $8.0$ , respectively), relatively low blockage ratio (7% and 11%, respectively), surface smoothness; and relatively low turbulence intensity of the wind tunnels - 0.08 % for Shih *et al.*'s data [21]. The r.m.s. lift coefficient prediction by the present LES falls within the scatter of the experimental data compiled by Zdravkovich [16]. The base pressure is also seen to be in the range of the experimental data.

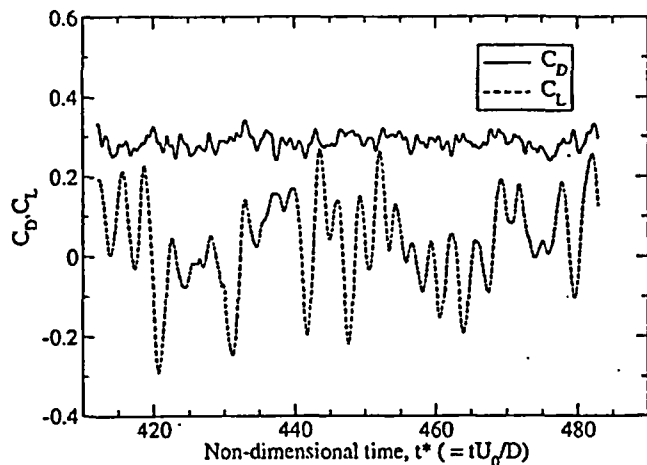


Figure 9. Time histories of drag and lift coefficients for the circular cylinder at  $Re = 1.0 \times 10^6$

The time histories of drag and lift coefficients are shown in Figure 9. Consistent with the flow structure portrayed in Figure 8, the  $C_L$ -history at this supercritical Reynolds number is more random than that for the subcritical flow. Indeed, no single frequency of vortex-shedding could be identified at this Reynolds number, as shown in the plot of the power spectral density of  $C_L$  in Figure 10. This finding is consistent with the others' experimental observations, for instance, Shih *et al.* [21] who found that coherent vortex shedding disappeared on a smooth cylinder beyond  $Re = 4 \times 10^5$ .

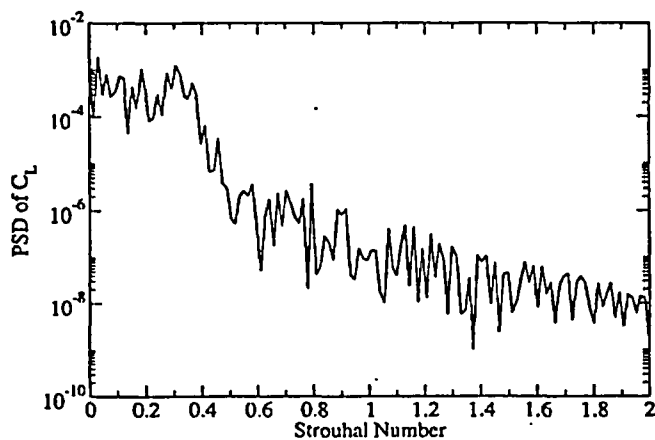


Figure 10. Power spectral density of the lift coefficient ( $C_L$ ) for the critical Reynolds number ( $Re = 1.0 \times 10^6$ )

For a smooth cylinder, the experimental data collected by Zdravkovich [16] and Achenbach's data [19] indicate that, above the Reynolds number of  $1.5 \times 10^6$  referred to as "TrBL4" in [16], transition clearly precedes the boundary layer separation. The exact location of the transition depends on such factors as freestream turbulence level and surface roughness. At  $Re = 1.0 \times 10^6$  falling in the range referred to as "TrBL3", however, both sets of data seem to suggest that transition occurs near the separation.

As before, we plotted the circumferential variations of the instantaneous skin-friction and the resolved turbulent kinetic energy in Figures 11 and 12. The top-bottom asymmetry of the skin-friction distribution is seen to be much less pronounced than for the subcritical flow. Figure 12 suggests that the boundary layer sustains being laminar down to 90 degrees. The separation angle of the time-averaged velocity field from the present LES was found to be around 108 degrees, which is close to 106 degrees estimated by Shih *et al.* [21] using their experimental data on a smooth cylinder at approximately the same Reynolds number. All this taken together, our LES result suggests that the boundary layer undergoes transition starting as early as 90 degrees, before it finally separates – "turbulently" – at around 108 degrees.

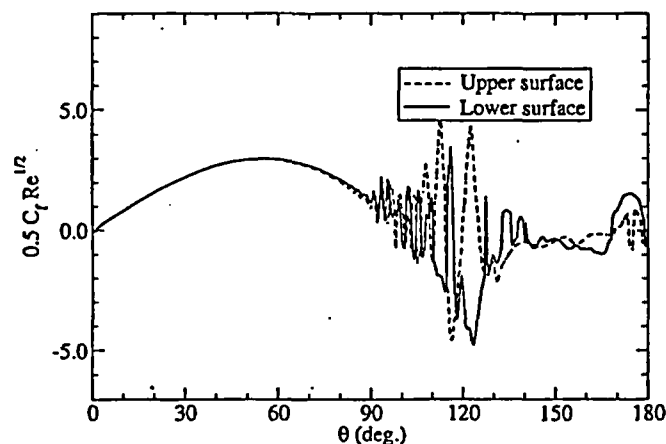


Figure 11. Scaled instantaneous skin-friction coefficient distribution on the cylinder surface at  $Re = 1.0 \times 10^6$

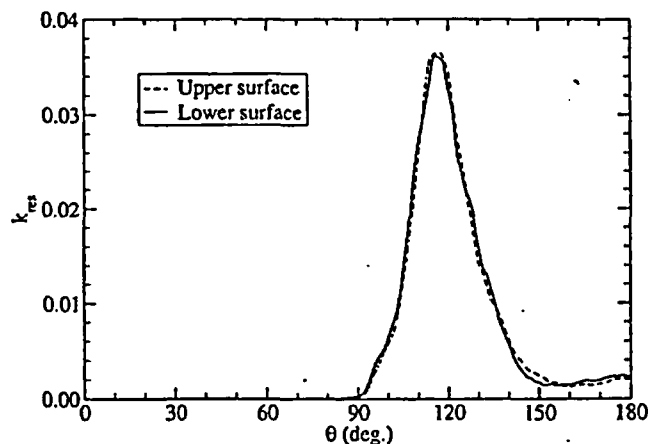


Figure 12. Resolved turbulent kinetic energy distribution at  $0.0001D$  above the cylinder surface, predicted by the present LES at  $Re = 1.0 \times 10^6$

The skin-friction prediction, including the location of the peak and the magnitude, is also in good agreement with the experimental data of Achenbach [19] measured at  $Re = 8.5 \times 10^5$  and  $Re = 3.6 \times 10^6$ . At these two Reynolds numbers,

Achenbach's data show that the scaled skin-friction distributions have the maximum values in the range of 3.5 – 4.0 occurring around  $\theta = 60 - 65$  degrees. As shown in Figure 11, our LES prediction closely matches Achenbach's data. This is in a sharp contrast with the LES prediction by Catalano *et al.* [3], which significantly overpredicted the overall level of the skin-friction on the front half of the cylinder. Contrary to what is suggested by the experimental evidence, their LES seem to yield too early a transition, giving a skin-friction level typical of a turbulent boundary layer from immediately downstream of the front stagnation point. As they pointed out [3], one most likely cause for the discrepancy is the substantially coarser mesh ( $y^+$  around 50) used in their LES predictions.

## SUMMARY AND CONCLUSIONS

Turbulent flow around a smooth fixed circular cylinder was computed using large eddy simulation (LES) at two Reynolds numbers ( $Re = 1.4 \times 10^5, 1.0 \times 10^6$ ). The computations were carried out using a second-order accurate, parallelized finite-volume Navier-Stokes solver capable of handling arbitrary unstructured meshes. An implicit, non-iterative fractional-step method was employed in favor of its high efficiency in LES for incompressible flows.

The LES results for both Reynolds numbers predicted, with a good accuracy, the global flow parameters such as mean drag coefficient, r.m.s. lift coefficient, and the Strouhal number. Furthermore, the salient features of the subcritical and the supercritical flows experimentally observed and measured on a smooth cylinder, such as the separation angle, mean velocity in the wake, length of the recirculation bubble, and transition location, are largely reproduced by the LES. Despite the use of a large number of computational elements (6.8 million cells), the solution turnaround time was quite reasonable.

To summarize what has been achieved through this study:

- The spatial discretization method (finite-volume on unstructured meshes) and the solution algorithm (implicit fractional-step method) employed in this study have been shown to be sufficiently robust and accurate to be used in LES for high Reynolds number flows.
- The dynamic Smagorinsky model adapted to unstructured meshes using a novel test-filter [13] has been shown to work robustly and accurately for complex, high Reynolds number turbulent flows.
- The present LES capability has been shown to predict the salient features of turbulent flow around a smooth circular cylinder at both subcritical and supercritical regimes with a good accuracy and reasonable computational cost.

It is planned to continue this work to include higher Reynolds numbers.

## ACKNOWLEDGEMENT

The authors acknowledge that FLUENT and GAMBIT software were used for this study. The authors are also thankful to Dr. Mustafa Sarioglu at Karadeniz Technical

University in Turkey for kindly allowing me to use his experimental data.

## REFERENCE

- [1] Breuer, M., 2000, "A Challenging Test Case for Large Eddy Simulation: High Reynolds Number Circular Cylinder Flow," *Int'l J. Heat and Fluid Flow*, 21, pp. 648 – 654.
- [2] Cantwell, B. and Coles, D., 1983, "An Experimental Study of Entrainment and Transport in the Turbulent Near-Wake of a Circular Cylinder," *J. Fluid Mech.*, 136, pp. 321 – 374.
- [3] Catalano, P., Wang, M., Iccarino, G. and Moin, P., 2003, "Numerical Simulation of the Flow Around a Circular Cylinder at High Reynolds Numbers," *Int'l J. Heat and Fluid Flow*, 24, pp. 463 – 469.
- [4] Travin, A., Shur, M., Strelets, M. and Spalart, P., 1999, "Detached-Eddy Simulation Past a Circular Cylinder," *Flow, Turbulence and Combustion*, 63, pp. 293 – 313.
- [5] Vatsa, V. N. and Singer, B. A., 2003, "Evaluation of a Second-Order Accurate Navier-Stokes Code for Detached Eddy Simulation Past a Circular Cylinder," AIAA Paper 2003-4085.
- [6] Pandya, M. J., Frink, N. T., Abdol-Hamid, K. S., and Chung, J. J., 2004, "Recent Enhancements to USM3D Unstructured Flow Solver for Unsteady Flows," AIAA Paper 2004-5201.
- [7] Kim, S. E., Makarov, B., and Caraeni, D., 2004, "Multi-Dimensional Reconstruction Scheme for Unstructured Meshes," AIAA Paper 2004-2548.
- [8] Kim, S. E. and Makarov, B., 2005, "An Implicit Fractional-Step Method for Efficient Transient Simulation of Incompressible Flows," To be presented at 17<sup>th</sup> AIAA Computational Fluid Dynamics Conference, June 6 – 9, Toronto, Ontario.
- [9] Park, J., Kwon, K., and Choi, H., 1998, "Numerical Solutions of Flow Past a Circular Cylinder at Reynolds Numbers up to 160," *KSME Int. J.*, 12, pp. 1200 – 1205.
- [10] Norberg, C., 2003, "Fluctuating Lift on a Circular Cylinder: Review and New Measurements," *J. Fluids and Structures*, 17, pp. 57 – 96.
- [11] Williamson, C.H.K., 1989, "Oblique and Parallel Modes of Vortex Shedding in the Wake of a Circular Cylinder at Low Reynolds Numbers," *J. Fluid Mech.*, 206, pp. 579 – 627.
- [12] Germano, M., Piomelli, U., Moin, P., and Cabot, W. H., 1991, "Dynamic Subgrid Scale Eddy Viscosity Model," *Physics of Fluids A*, 3, 19, pp. 1760 – 1765.
- [13] Kim, S. E., 2004, "Large Eddy Simulation Using Unstructured Mesh and Dynamic Subgrid-Scale Turbulence Models," AIAA Paper 2004-2548.
- [14] West, G. S. and Apelt, C. J., 1993, "Measurements of fluctuating Pressures and Forces on a Circular Cylinder in the Reynolds Number Range  $10^4$  to  $2.5 \times 10^5$ ," *J. Fluids and Structures*, 7, pp. 227 – 244.
- [15] Szepessy, S. and Bearman, P. W., 1992, "Aspect Ratio and End Plate Effects on Vortex Shedding from a Circular Cylinder," *J. Fluid Mech.*, 234, pp. 191 – 217.
- [16] Zdravkovich, M. M., 1997, "Flow Around Circular Cylinders, Fundamentals, Vol. 1, Oxford Univ. Press (Chapter 6).



- [17] Roshko, A., 1961, "Experiments on the Flow Past a Circular Cylinder at a Very High Reynolds Number," *J. Fluid Mech.*, 10, No. 3, pp. 345 – 356.
- [18] Sarioglu, M. and Yavuz, T., 2002, "Subcritical Flow Around Bluff Bodies," *AIAA J.* Vol. 40, No. 7, July.
- [19] Achenbach, E., 1968, "Distribution of Local Pressure and Skin-Friction Around a Circular Cylinder in Cross-Flow up to  $Re = 5 \times 10^6$ ," *J. Fluid Mech.*, 34, Part 4, pp. 625 – 639.
- [20] Szechenyi, E., 1975, "Supercritical Reynolds Number Simulation for Two-Dimensional Flow Over Circular Cylinders," *J. Fluid. Mech.*, 70, pp. 529 – 542.
- [21] Shih, W. C. L., Wang, C., Coles, D., and Roshko, A., 1993, "Experiments on Flow Past Rough Circular Cylinders at Large Reynolds Numbers," *J. Wind Eng. And Indus. Aerodynamics*, 49, pp. 351 – 368.

**Exhibit EMEB-B-138-2**

**Vermont Yankee Nuclear Power Station**

**Proposed Technical Specification Change No. 263 – Supplement No. 30**

**Extended Power Uprate**

**Response to Request for Additional Information**

**Large Eddy Simulation of Confined Swirling Coaxial Jets.**

**Total number of pages in this Exhibit  
(excluding this cover sheet) is 10.**

FEDSM 2005-77085

## LARGE EDDY SIMULATION OF CONFINED SWIRLING COAXIAL JETS

Sung-Eun Kim, Fluent Inc.,  
Lebanon, NH 03766, U.S.A.

Xuelei Zhu, Fluent Inc., Lebanon,  
NH 03766, U.S.A.

Stefano Orsino, Fluent Inc.,  
Lebanon, NH 03766, U.S.A.

### ABSTRACT

Large eddy simulations (LES) have been carried out for confined swirling coaxial jets discharged into a suddenly expanded pipe, which was studied experimentally by Roback and Johnson [1, 2]. The computations were made using a parallelized finite-volume-based Navier-Stokes solver that is second-order accurate in time and space, and permits use of unstructured meshes. The computational domain starts from an inlet placed upstream of the swirl generator, which makes the inlet boundary condition easy to specify. Subgrid-scale turbulent stresses were modeled using a dynamic Smagorinsky model applicable to complex three-dimensional flows without any statistically homogeneous directions. Subgrid-scale turbulent scalar flux is modeled using a constant Schmidt number in conjunction with the dynamically computed subgrid-scale turbulent viscosity. The LES predictions were found to closely reproduce the salient features of the flow and the species concentration downstream of the expansion. One of the conclusions was that a good resolution of the mean flow and turbulence in the upstream region is crucial in accurately predicting the mixing downstream of the expansion.

### INTRODUCTION

Confined swirling co-axial jets discharging into a suddenly expanded pipe [1, 2] have been studied numerically by several others using the Reynolds-Averaged Navier-Stokes (RANS) equations [3, 4] and large eddy simulation [6]. The flow in question consists of a non-swirling jet in the center, and an outer annular jet with a swirl imparted by a 8-vane, variable-angle swirl generator, with a swirl number of approximately 0.41.

Earlier numerical studies using RANS-based turbulence models [3, 4] have shown that the mean velocity field in the mixing region - the shear layer between the jets and the inner recirculation region - was predicted with a reasonably good accuracy. However, the predictions of the mean species

concentration were much less satisfactory. The major discrepancy was found in the core region, where the mean species concentration was grossly underpredicted by the RANS computations. Evidently, the RANS model employed gives rise to an excessive mixing. Brankovic *et al.* [3] investigated the sensitivity of their RANS predictions to such parameters as the turbulent Schmidt number and the inlet turbulence level. However, the influence of these parameters was negligibly small. The poor prediction of the species mixing has been attributed to the inability of RANS-based turbulence models to accurately represent the mixing by large-scale turbulent structure (or large eddies).

Playing a major role in mixing, large eddies are also responsible for undesirable yet somewhat subtler phenomena such as combustion instability and acoustic excitation inside combustors. To address these issues properly, one has to turn to high-level turbulent simulation like LES. Akselvoll and Moin [5] used LES to compute the flow and the species concentration in non-swirling coaxial jets. Pierce and Moin [6] attempted LES for the same confined coaxial swirling jet as is considered here. These studies demonstrated that LES can indeed predict the flow and the species concentration in confined coaxial jets with a commendable accuracy. LES also allows one to directly compute r.m.s. velocity fluctuations and r.m.s. species fluctuation which are important quantities in the context of turbulent combustion.

The present study concerns a LES computation for the swirling coaxial jets using a finite-volume solver that permits use of unstructured meshes. Unlike the study of Pierce and Moin [6], however, our computational domain starts from an inlet boundary placed upstream of the swirl generator. Despite the larger solution domain and the implied increase in the computational resource, having the inlet boundary upstream of the swirl generator makes it straightforward to specify the inlet boundary conditions. Meshing the computational domain including the swirl generator, which could become a difficult and time-consuming task with structured meshes, is made easier by the flexibility offered by unstructured mesh allowed by the present finite-volume solver.

This paper is, in many aspects, a progress report about an ongoing study whose ultimate goal is to find an optimal strategy based on the technique of LES for modeling turbulent flow and species mixing in coaxial combustors with or without swirl.

The paper is organized as follows. First, we briefly discuss the numerical method and the subgrid-scale turbulence models for stresses and scalar flux. Special emphasis is laid on a transient algorithm whose efficiency significantly benefits the present study. This is followed by the details of the LES computations regarding the choices of the solution domain, mesh (resolution), boundary conditions, time-step size, and the overall solution strategy. The results are then presented.

## NUMERICAL METHOD

The computation were carried out using the *segregated* solver in FLUENT, a general-purpose CFD software. FLUENT employs a cell-centered finite-volume method based on a multi-dimensional linear reconstruction scheme that permits use of computational elements (cells) with arbitrary polyhedral cell topology including quadrilateral, hexahedral, triangular, tetrahedral, pyramidal, prismatic, and hybrid meshes. The solution gradients at cell centers that are needed to compute convective and diffusive fluxes are obtained by applying Green-Gauss theorem [9]. Diffusive and convective fluxes are discretized using central differencing [8].

An implicit fractional-step method (FSM) [10] in conjunction with a second-order accurate, three-level backward-differencing scheme for time-discretization was employed to advance the solution in time. In this algorithm, the momentum equations are decoupled from the continuity equation applying an approximate factorization of the coupled Navier-Stokes equations. For incompressible flows, the FSM preserves the formal second-order temporal accuracy without having to perform, at each time-step, costly outer iterations to couple velocity-field and pressure. The FSM thus provides a highly efficient algorithm for CPU-intensive transient computations like LES.

Consider the semi-discrete form of the Navier-Stokes equations in "pressure-correction" ( $\delta p^{n+1} = p^{n+1} - p^n$ ) form:

$$\begin{bmatrix} A & G \\ D & 0 \end{bmatrix} \begin{pmatrix} \mathbf{u}^{n+1} \\ \delta p^{n+1} \end{pmatrix} = \begin{pmatrix} \mathbf{r} \\ 0 \end{pmatrix} \quad (1)$$

where  $\mathbf{u}^{n+1}$  and  $\mathbf{r}$  are the velocity vector and the momentum source vector, respectively, and the integer  $n$  is the time level.  $A$  is the coefficient matrix defined in terms of the discrete convective and diffusive operators and the time-advancement scheme chosen, and  $G$  and  $D$  are the discrete gradient and divergence operators, respectively. The coupled system of equations in Equation (1) is extremely difficult to solve as it is, since the matrix  $A$  has to be inverted for every iteration. In the fractional-step method, the original coupled equations in Equation (1) are approximated by

$$\begin{bmatrix} A & 0 \\ D & \Delta t DG \end{bmatrix} \begin{bmatrix} I & \Delta t G \\ 0 & I \end{bmatrix} \begin{pmatrix} \mathbf{u} \\ \delta p^{n+1} \end{pmatrix} = \begin{pmatrix} \mathbf{r} \\ 0 \end{pmatrix} + [O(\Delta t^2)] \quad (2)$$

Factorizing equation (2), we have a series of split operations as

$$\begin{aligned} A\hat{\mathbf{u}} &= -Gp^n + \mathbf{r}^n \\ \Delta t DG\delta p^{n+1} &= D\hat{\mathbf{u}} \\ \mathbf{u}^{n+1} &= \hat{\mathbf{u}} - \Delta t G\delta p^{n+1} \end{aligned} \quad (3)$$

On a per-iteration basis, the series of operations in Equation (3) closely resembles SIMPLEC scheme. The difference is that, in the iterative SIMPLEC scheme, the operations in Equation (3) are repeated in an outer loop until the all the solution variables converge, whereas the FSM needs only one sweep. To preserve second-order accuracy with the FSM, however, sub-iterations are needed for the set of three momentum equations and individual scalar equations to account for the nonlinearity in and coupling among the individual equations and high-order source terms. Yet, non-iterative FSM is takes much less CPU time than iterative SIMPLEC scheme.

The system of discretized governing equations are solved using a point-implicit, Gauss-Seidel relaxation along with algebraic multi-grid (AMG) method to accelerate solution convergence. The N-S solver and the SGS turbulence model are fully parallelized.

## SUBGRID-SCALE TURBULENCE MODELING

For incompressible flows, the filtered Navier-Stokes equations can be written as

$$\frac{\partial \bar{u}_i}{\partial t} + \frac{\partial \bar{u}_i \bar{u}_j}{\partial x_j} = -\frac{1}{\rho} \frac{\partial p}{\partial x_i} - \frac{\partial \tau_{ij}}{\partial x_j} + \frac{\partial}{\partial x_j} \left\{ \nu \frac{\partial \bar{u}_i}{\partial x_j} \right\} \quad (4)$$

where  $\tau_{ij} = \overline{u_i u_j} - \bar{u}_i \bar{u}_j$  is the subgrid-scale turbulent stress. In this study, the subgrid-scale stress is modeled using isotropic eddy-viscosity as

$$\tau_{ij} - \frac{\delta_{ij}}{3} \tau_{kk} = -2C_v \bar{\Delta}^2 |\bar{S}| \bar{S}_{ij} \quad (5)$$

We determined the model constant,  $C_v$ , using the dynamic Smagorinsky model (DSM) originally proposed by Germano *et al.* [7, 8].

The filtered transport equation for a passive scalar is given by

$$\frac{\partial \bar{\varphi}}{\partial t} + \frac{\partial \bar{u}_j \bar{\varphi}}{\partial x_j} = \frac{\partial}{\partial x_j} \left( \alpha \frac{\partial \bar{\varphi}}{\partial x_j} - q_j \right) \quad (6)$$

where  $q_j$  is the subgrid-scale turbulent flux of the species concentration ( $\varphi$ ), and  $\alpha$  the molecular diffusivity. The subgrid-scale flux is modeled using

$$q_j = -\frac{C_s \bar{\Delta}^2 |\bar{S}|}{Sc_c} \frac{\partial \bar{\varphi}}{\partial x_j} \quad (7)$$

where  $Sc_t$  is the subgrid-scale turbulent Schmidt number. In this study, we used a constant value of 0.9.

To implement the dynamic procedure for the present finite-volume solver requires a test-filter applicable to arbitrary unstructured meshes. The test-filter finally adopted for this study is a top-hat filter involving a volume comprising the cell in the center plus the neighboring cells that share the faces with the center cell. To make the dynamic procedure tractable, an approximation was made that is tantamount to a non-varying  $C_v$  over the test-filter volume. Thus, the dynamic procedure employed in this study is "approximately local" in the sense that, despite the *ad hoc* assumption, it does not require an existence of any statistically homogeneous directions, being applicable to complex three-dimensional flows. To avoid numerical instability likely to be caused by a large fluctuation of the model constant, we smoothed the model constant by applying the test-filter on it, and also clipped it so that the effective viscosity remains positive. The additional details of the implementation of the DSM in the framework of an unstructured mesh based finite-volume solver can be found in the reference [8]. The DSM has been validated for a number of wall-bounded flows such as fully-developed channel flows and flows around bluff bodies such as a square cylinder and a sphere.

## DETAILS OF COMPUTATIONS

### Solution domain, swirl vane geometry and meshes

A partial view of the computational domain is depicted in Figure 1, along with the coordinate system. The inlet boundary is placed at  $1.0D$  upstream of the swirl generator, where  $D$  is the downstream pipe diameter ( $D = 122 \text{ mm}$ ). The exit boundary is at  $15D$  downstream of the pipe expansion. The computational domain thus has the swirl generator in it. The entire inlet tube, 8 swirl vanes, and the downstream pipe were modeled without using any periodic boundaries.

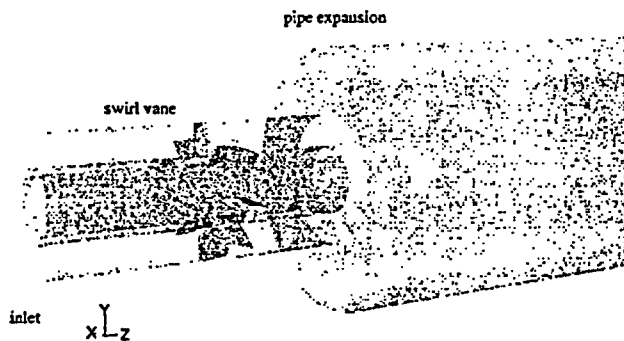


Figure 1. A partial view of the computational domain

The swirl generator consists of 8 identical vanes mounted on the hub with an equal spacing in the azimuthal direction. The blade-section has a camber and a vane-angle that change with the radius. The blade geometry was taken from the design data given in the Ref. [1]. A NURB surface was built based on the digitized surface geometry.

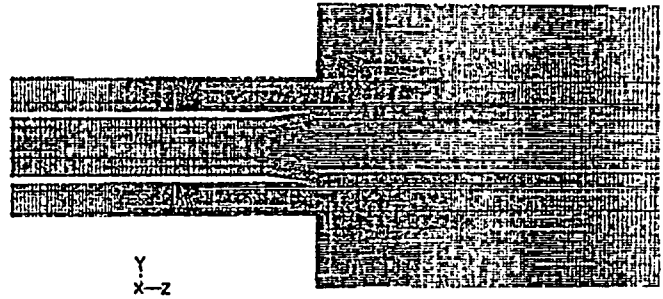


Figure 2. A sectional view of the computational mesh (medium-sized mesh with 2.7 million elements) used in the computations.

The computational meshes were built using Gambit. We used three progressively refined, unstructured hexahedral meshes for the computations. The three meshes have 1.1 million (coarse), 2.7 million (medium), and 4.8 million (fine) elements, respectively. A sectional view of the medium-size mesh is shown in Figure 2. The resolution of the medium-size mesh is such that, in the mixing region, it can resolve the integral length-scale estimated around  $20 \text{ mm}$  based on the experimental observation [1, 2], which is equivalent to  $D/6$ , with approximately 20 elements. It can resolve the smallest observable eddies of a size around  $6 \text{ mm}$ , which were observed in the experiment [1, 2], with 6–7 elements.

It is worth mentioning here that the mesh resolution in and around the inner and the annular tubes and the swirl vanes is too coarse to resolve the energy-containing eddies originating from and transported in that upstream region. We recognize that poor resolution of the turbulent structure in the upstream region will negatively impact the prediction in the downstream, particularly in the shear layers of the mixing region, inasmuch as the energy-carrying eddies from upstream feed the turbulent structure being developed in the downstream mixing region. Furthermore, none of the three meshes are fine enough to accurately resolve the viscous sublayer on the pipe wall downstream of the expansion. This was deemed justifiable in light of a relatively passive role played by the wall downstream of the expansion in the mixing occurring near the central core.

### Boundary conditions, time-step size, and solution strategy

On the annular jet inlet, a uniform axial velocity of  $1.667 \text{ m/s}$  was specified according to the data given by Roback and Johnson [1]. For the velocity boundary condition at the inner jet inlet, we used  $0.797 \text{ m/s}$ , a value derived from the volumetric flow-rate (6.2 gallon per minute) given in Ref. [1], instead of the inlet velocity mentioned in the same report ( $0.52 \text{ m/s}$ ). The inlet velocity of  $0.52 \text{ m/s}$  quoted in the report does not match the given volume flow-rate, and is inconceivably too low considering that the measured axial velocity immediately downstream of the expansion is around  $0.8 \text{ m/s}$ .

On wall boundaries, we employed a blended law-of-the-wall that invokes proper wall-laws depending on the local mesh resolution, namely  $y^+$  at the wall-adjacent cells. The downstream exit boundary was treated as a "pressure-outlet" boundary offered in FLUENT. In essence, the solution

variables are extrapolated in a mass-conserving manner on this boundary.

The influence of the exit boundary condition was discussed at length by Pierce and Moin [6]. They found that the usual convective outflow boundary condition applied on an exit boundary with a cross-section of the downstream pipe yielded a central recirculation zone that is far smaller than what

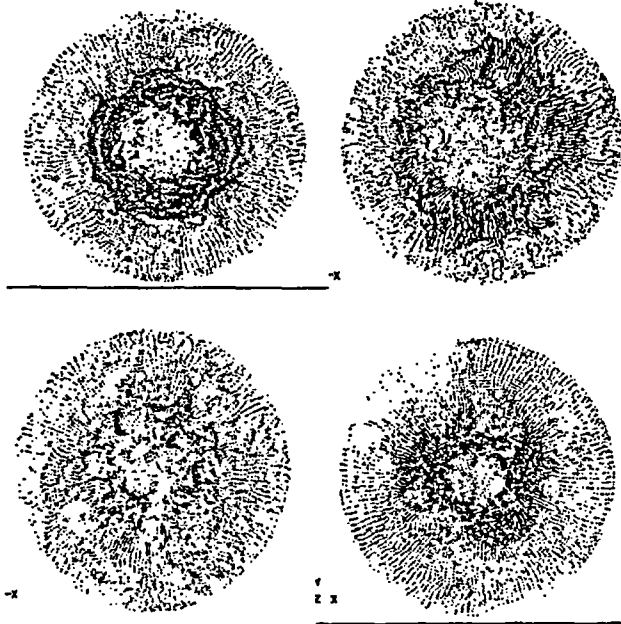


Figure 3. Instantaneous velocity vectors at four axial locations - top-left,  $z = 25 \text{ mm}$ ; top-right,  $z = 51 \text{ mm}$ ; bottom-left,  $z = 102 \text{ mm}$ , bottom-right,  $z = 203 \text{ mm}$

was observed in the experiment. They were able to bring their LES prediction much closer to the experimental data by putting a second expansion before the exit boundary, which was conceived based on an argument that it better represents the settling chamber used in the experiment.

We also investigated the effect of the second expansion, comparing the result to what was obtained without the expansion. However, we could not notice any appreciable difference between the two. The insignificantly small difference found in our computations is perhaps due to the way the solution variables are extrapolated at "pressure-outlet" boundary that could be different from their treatment of the convective boundary.

The time-step size used in the present LES was determined based on the estimated characteristic time-scale of the smallest eddies to be resolved in the LES. We took  $v = 1.0 \text{ m/s}$  and  $l = 0.05D$  ( $D = 0.122 \text{ m}$ ) as the characteristic velocity-scale and length-scale of the smallest eddies. These estimates give an eddy-turnover time of  $\tau = l/v = 0.006 \text{ second}$ . It was finally decided to use a time-step size of  $\Delta t = 0.0002 \text{ second}$ , which will resolve one eddy-turnover time ( $\tau$ ) of the smallest resolved eddies roughly in 30 time steps.

The LES was started using a steady RANS solution as the initial guess. To accelerate the solution to a statistically stationary state, we superimposed a pseudo-random fluctuating velocity-field on the mean velocity field taken from the RANS solution. Before the statistics are collected, the LES computation was run until the initial transients in the solution are completely washed out, which typically took 2 – 3 flow-through times; one flow-through time is taken to be  $L/U_b$ , where  $L$  is the length of the downstream pipe, and  $U_b$  the axial mean bulk velocity.

## RESULTS

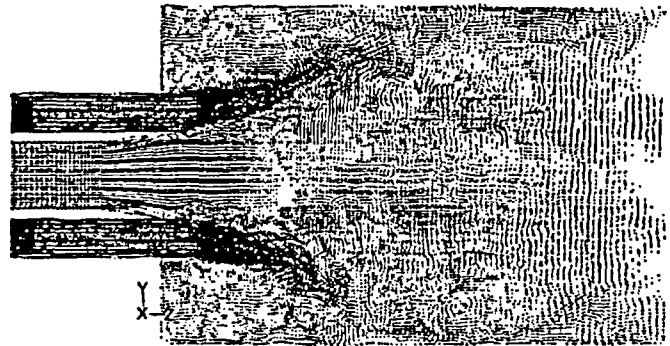


Figure 4. Instantaneous velocity vectors in the  $r$ - $z$  plane

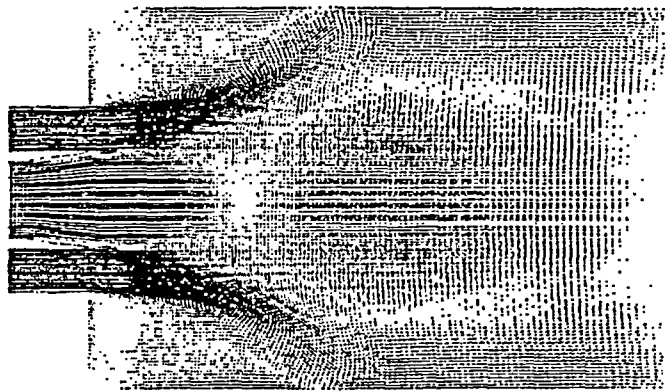


Figure 5. Time-averaged velocity vectors in the  $r$ - $z$  plane

To obtain stable statistics of the solution, the transient computations were continued for a sufficiently long period of time, typically for more than 7 – 8 flow-through times, until the time-averaged velocity and species concentration fields largely recover an axisymmetry.

Regarding the mesh-dependency of the solutions, it was found that the LES results from the medium mesh (2.7 million cells) and the fine mesh (4.8 million cells) showed little difference, while the coarse mesh result deviates a little farther from the other two. Unless stated otherwise, the results presented in this paper are for the medium mesh.

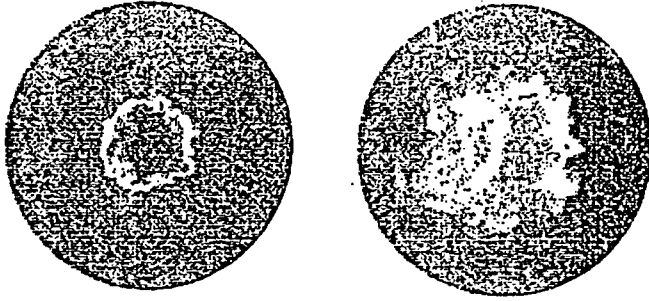


Figure 6. Instantaneous velocity vector plots at two axial locations - left,  $z = 25 \text{ mm}$ ; right,  $z = 51 \text{ mm}$

#### Overall flow structure

Figures 3 and 4 show the instantaneous velocity vectors projected on four crossflow ( $r-\theta$ ) planes and a  $r-z$  plane. The vector plots portray turbulent eddies with widely varying length-scales throughout the mixing region. Small eddies are shown to form in the shear layers between the inner jet and the outer annular jet, growing in size in the downstream direction. At  $z = 25 \text{ mm}$ , small eddies are confined near the shear layer between the inner and the outer annular jets. Yet, larger eddies are also seen to have formed in the annular recirculation region behind the step. One can visually tell from the figure that the smallest structure at  $z = 25 \text{ mm}$  resolved in the LES is roughly  $D/20$  ( $D = 122 \text{ mm}$ ), which is close to the size of the smallest eddy,  $6 \text{ mm}$ , observed by Roback and Johnson [1]. The size of the largest eddy at  $z = 25 \text{ mm}$ , which is about two-thirds of the step-height as shown in the figure, also closely matches the experimentally observed value,  $20 \text{ mm}$ , quoted in ref. [1]. Figure 5 depicts the mean velocity vectors on a  $r-z$  plane.

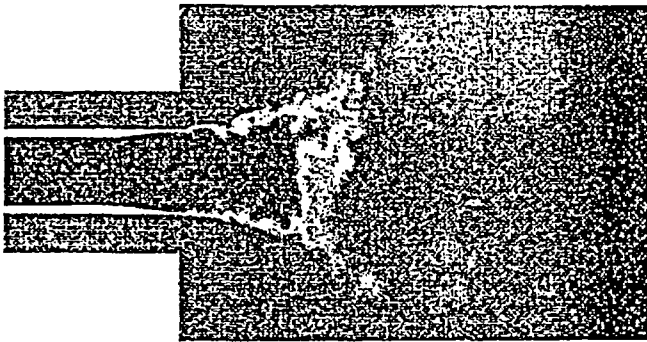


Figure 7. Contours of the instantaneous species concentration in  $r-z$  plane

Figure 6 and 7 depict the contours of the instantaneous species concentration on two crossflow planes and a  $r-z$  plane. The contours on the crossflow planes give an idea of the length-scale of the turbulent structure. The observations from these figures are consistent with those from the instantaneous velocity vector plots discussed earlier. In the experiment [1],

the penetration length of the center jet with high species concentration (colored pink in the figure in Figure 7) was found to be around  $50 \text{ mm}$ , which is closely reproduced by our LES results as shown in Figure 7.

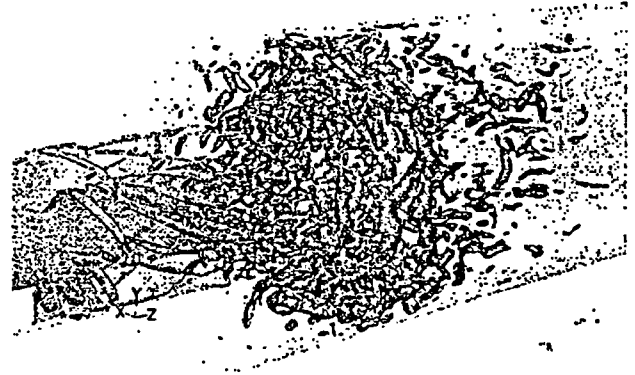


Figure 8. Vortical flow structure in the mixing region visualized by the iso-surface of the second-invariant of the velocity deformation tensor, colored by velocity magnitude.

Figure 8 gives an overall impression of the turbulent vortical structure in the mixing region. This figure indicates that the flow in this coaxial jets are well mixed.

#### Velocity field

Figure 9 shows the mean axial velocity profile along the centerline of the pipe. The LES prediction quite closely reproduces the general trend such as the rapid drop of the mean axial velocity immediately downstream of the expansion and the gradual recovery further downstream. However, the recirculation zone predicted by the present LES appears to be shifted slightly downstream compared to what is indicated by the measurement.

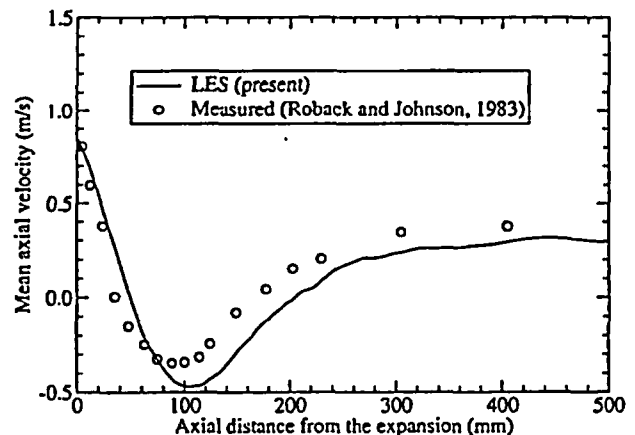


Figure 9. Mean axial velocity along the centerline of the pipe.

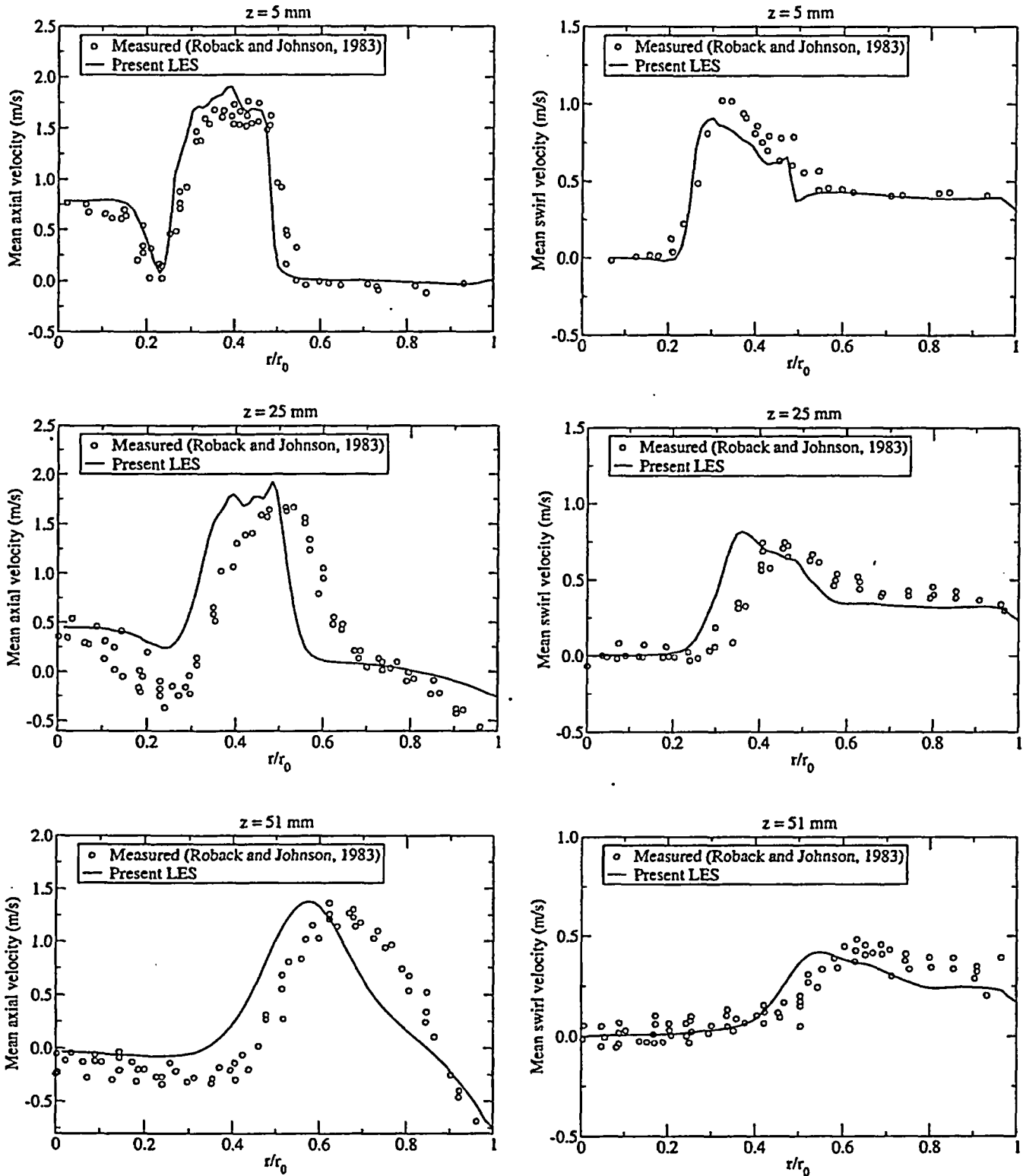


Figure 10. Mean axial and azimuthal velocity profiles at two axial locations ( $z = 25 \text{ mm}$ ,  $z = 51 \text{ mm}$ )

Figure 10 shows the radial profiles of the mean axial and azimuthal velocity components at three axial locations ( $z = 5 \text{ mm}$ ,  $25 \text{ mm}$ ,  $51 \text{ mm}$ ). The profiles shown in the figure were

obtained by averaging the radial profiles taken at four azimuthal locations ( $\theta = 0^\circ, 90^\circ, 180^\circ, 270^\circ$ ). The predictions are seen to capture the overall trends and the peak values of the



velocity components. However, it is clearly noticeable that the locations of the peaks predicted by the LES are generally shifted toward the centerline. This implies that the outer annular jet expands or opens up less than it does in reality. This also means that the annular recirculation zone predicted by the present LES is longer (in the axial direction) than in the experiment. The underprediction of the jet angle is also correlated with the downstream shift of the central recirculation zone discussed earlier.

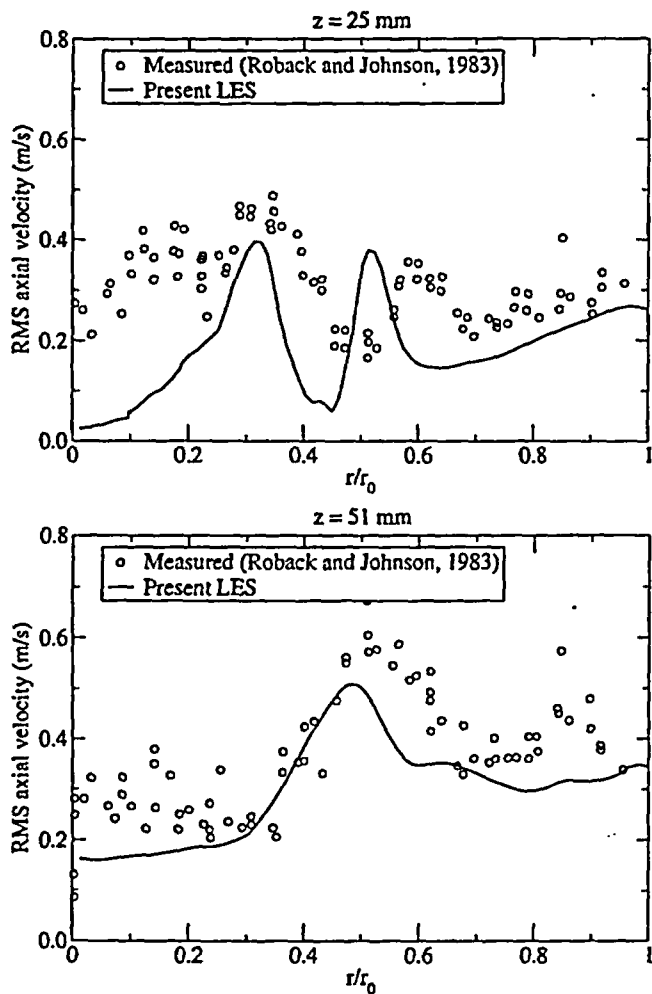


Figure 11. r.m.s. axial velocity fluctuation at two cross-flow planes ( $z = 25 \text{ mm}$ ,  $z = 51 \text{ m}$ )

We surmise that, among others things, the most likely culprit for this discrepancy is the lack of mesh resolution in the region upstream of the expansion, in and around the inner and the outer annular pipes, and the swirl vanes. As mentioned earlier, turbulent eddies coming from the upstream region feed the shear layers developed downstream of the expansion, enhancing the mixing of the momentum and the species concentration in the inner and the annular jets with the surrounding flow, which will lead to an increase in the jet angle. In our LES computations, these energy-feeding eddies are almost missing, since none of the computational meshes

used in this study, including the fine mesh (4.8 million cells), are fine enough to accurately resolve the energy-containing eddies generated in the upstream region.

The r.m.s. axial velocity fluctuation shown in Figure 11 seems to support our reasoning. The r.m.s. axial velocity fluctuation at the centerline ( $r = 0$ ) at  $z = 25 \text{ mm}$  shown in the top-figure, and the one at  $z = 5 \text{ mm}$  (not shown here) are severely underpredicted in the LES computation. As shown in the bottom-figure for  $z = 51 \text{ mm}$ , further downstream of the jet exit, the r.m.s. axial velocity fluctuation catches up with the data, as the turbulent eddies generated in the shear layer become full-fledged.

The impact of the incoming turbulent eddies on the mixing in the downstream as suggested above and the cost implication of using an extremely fine mesh in the upstream region beg a question; what would be the best practice that can be adopted to obtain a sufficiently accurate prediction of the flow and species mixing occurring in a coaxial jet combustor with LES? We will ponder a little upon this question at the very end.

### Species concentration

Figure 12 shows the profile of the mean species concentration along the pipe centerline. The LES prediction closely reproduces the trend - the plunge of the mean species concentration occurring near  $z = 50 \text{ mm}$ . One noticeable discrepancy between the prediction and the measurement is in the length of the inviscid core for the species concentration. The LES yields an inviscid core for the species concentration almost down to  $z = 35 \text{ mm}$ , whereas the experimental data indicates that the mean species concentration starts being diffused away almost immediately after the expansion. We think that this is again, in a major part, due to the poor resolution of the incoming turbulent eddies which would take part in "tearing" the inner jet.

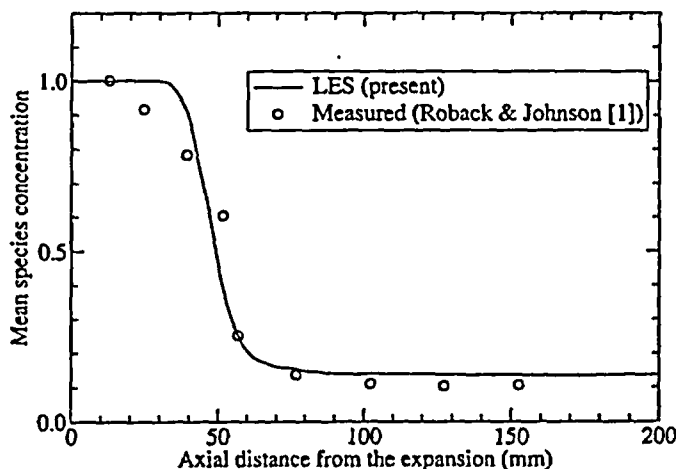


Figure 12. Mean species concentration along the centerline of the pipe

The radial profiles of the mean species concentration at two axial locations are shown in Figure 13. The predictions are in good agreement with the measurements at both locations. The mean species concentration profile at  $z = 25 \text{ mm}$  predicted by the LES computation shows a sign of being "under-diffused", insofar

as it has a fuller profile than the measured one. The prediction at  $z = 51 \text{ mm}$  is somewhat lower than the measurement near the centerline. However, the overall agreement at this location is remarkably good in view of the steep change of the mean species concentration near  $z = 51 \text{ mm}$ , as can be seen in Figure 12. It should be noted, in passing, that the RANS predictions reported in the literature [3] severely under-predicted the mean species concentration at this axial location.

r.m.s. value at  $z = 25 \text{ mm}$ , located in the shear layer between the inner and the outer annular jets, is also considerably underpredicted. Apparently, the LES underpredicts the entrainment of the ambient fluid occurring at this location. At  $z = 51 \text{ mm}$ , the prediction comes much closer to the measurement, as the r.m.s. velocity fluctuation did at the same axial location.

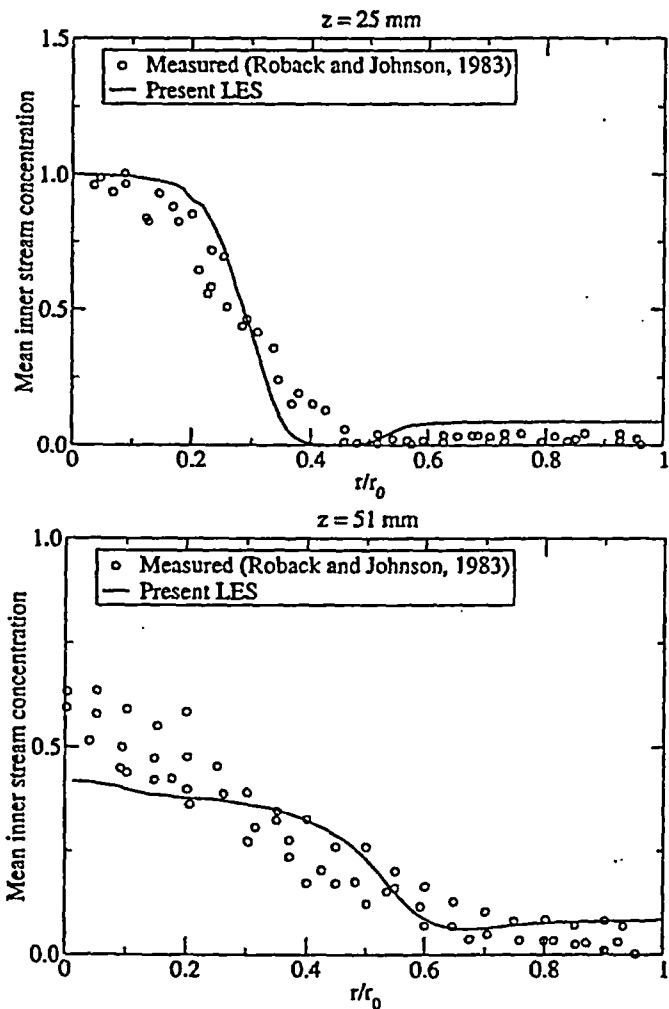


Figure 13. Mean species concentration at two axial locations ( $z = 25 \text{ mm}$ ,  $51 \text{ mm}$ )

Equally important - probably even more important than the mean species concentration in the context of modeling turbulent combustion, is the fluctuation of species concentration. The usual RANS-based turbulence models cannot directly predict the r.m.s. fluctuating species concentration, unless the transport equation for the variance of fluctuating species concentration is explicitly solved. One obvious benefit from LES is that one can directly compute it. Figure 14 depicts the r.m.s. fluctuating species concentration at the two crossflow planes. At  $z = 25 \text{ mm}$ , as in the case of the r.m.s. axial velocity fluctuation, the LES result grossly underpredicts the r.m.s. value in the core region. The peak

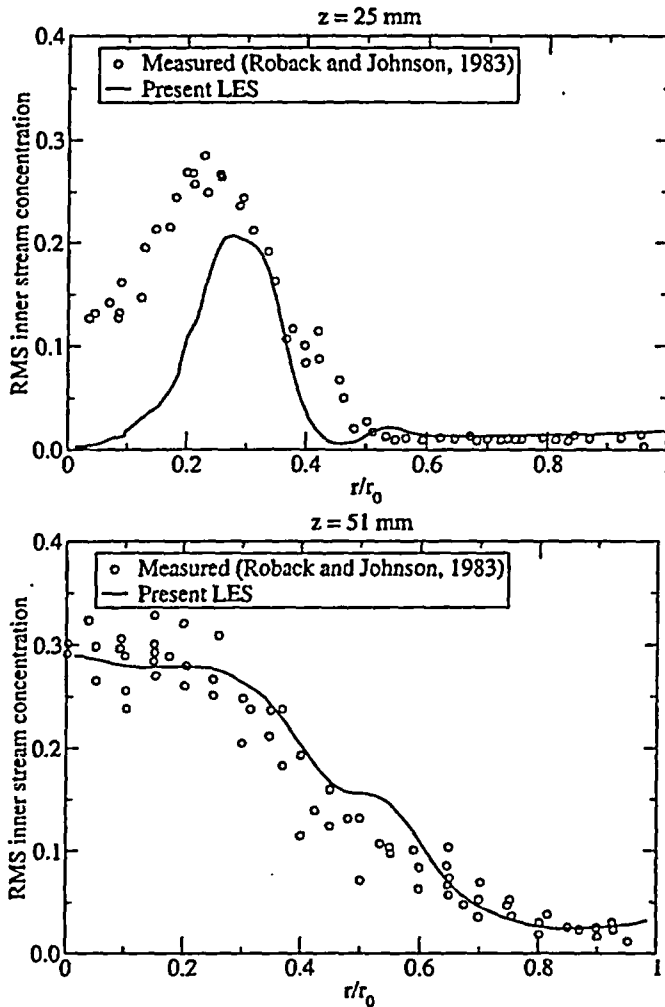


Figure 14. r.m.s. species concentration at two axial locations ( $z = 25 \text{ mm}$ ,  $51 \text{ mm}$ )

The same remarks given regarding what might have caused the discrepancy in the r.m.s. velocity fluctuation (Figure 11) largely apply to the results for the r.m.s. fluctuating species concentration.

#### PRELIMINARY RESULTS WITH LOCALLY REFINED MESHES

The fact that the fine mesh (4.8 million cells) offers a meager improvement over the medium mesh (2.7 million cells) in terms of the mesh resolution (spacing) warrants additional

computations with substantially finer mesh, for instance, by halving the grid spacing in all three (axial, radial, and azimuthal) directions. However, doubling the number of elements in the three directions results in an eight-fold increase in the total cell counts, which becomes unwieldy.

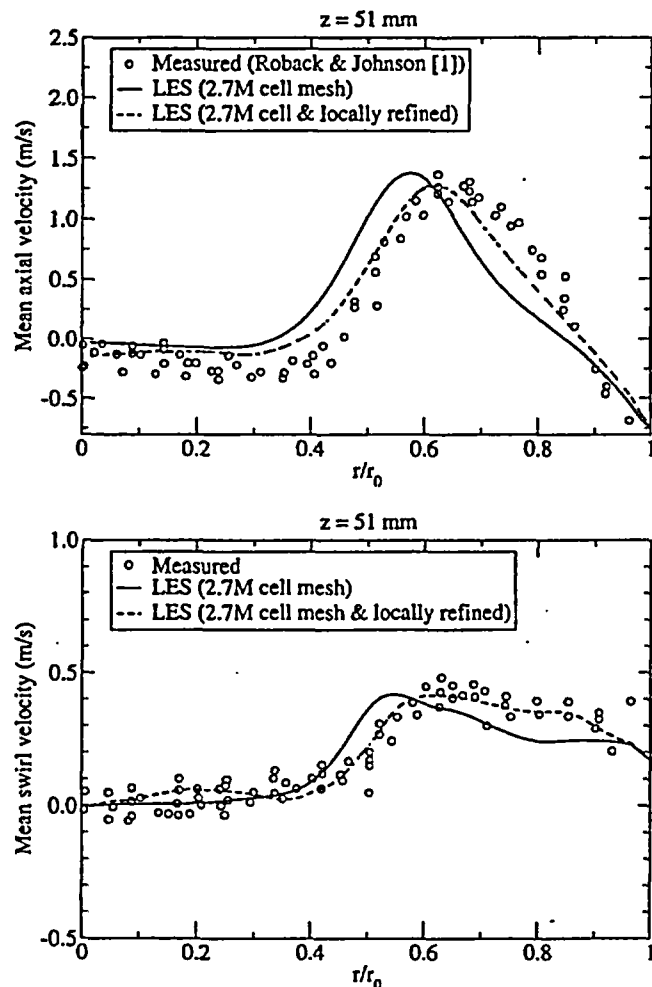


Figure 15. Mean axial and azimuthal velocity profiles at two axial locations - predicted with a locally refined mesh

To keep the mesh size under a tractable limit, the medium mesh was locally refined only in the domain upstream of the expansion. Furthermore, only the cells within a specified distance from the wall, roughly  $0.07D$  in this study, were refined to further save the cell counts. The local refinement resulted in a total of 6.5 million cells. The computation has been carried out on this mesh. The results are shown in Figure 15, being compared with the medium mesh results, for the radial profiles of the mean axial and azimuthal velocity components at  $z = 51 \text{ mm}$ . Clearly, the predictions with the adapted mesh are significantly improved over the predictions with the medium mesh. The overall shift of the velocity peaks is now far smaller than what we saw earlier, and the predictions capture the profiles of the mean velocity components much more closely.

## CONCLUSION

The flow and the species transport in confined swirling coaxial jets were computed using LES. An unstructured mesh-based finite-volume solver was employed for the computations. A highly efficient time-advancement scheme was used in conjunction with second-order accurate temporal and spatial discretization schemes. A dynamic Smagorinsky model adapted to general three-dimensional flows was employed as the subgrid-scale turbulence model.

For LES, it is evidently a bold attempt and a costly proposition to include the upstream components of a combustor like the swirl generator and the upstream tubes in the computational domain. Nevertheless, the present LES computations closely reproduce the salient features of the flow and the species concentration in the mixing region. For an accurate prediction of the mixing in the downstream (e.g., combustion chamber), a good resolution of the mean flow and the turbulence in and around the inner and the outer annular tubes, and the swirl vanes turned out to be more important than originally thought. The numerical evidence found from this study indicates that the three globally refined meshes used in the present study, despite the largest cell counts reaching up to 4.8 million cells, still cannot provide a sufficient resolution of the upstream region. We believe that the lack of mesh resolution is responsible for the discrepancy between the predictions and the measurements, most notably the overall shift of the velocity peaks toward the centerline.

Finally, a preliminary result was presented which was obtained with a new mesh locally refined in the upstream part of the domain. The significant improvement from this locally adapted mesh supports our conclusion, and at the same time, provides us with an avenue to improving the accuracy of LES prediction for the subject flow.

## ACKNOWLEDGEMENT

The authors acknowledge that FLUENT and GAMBIT software were used for this study. The LES-cluster in Fluent Inc. was used for the computations.

## REFERENCES

- [1] Roback, R. and Johnson, B. V., "Mass and Momentum Turbulent Transport Experiments with Confined Swirling Coaxial Jets," NASA CR-168252, 1983.
- [2] Johnson, B. V. and Roback, R., "Mass and Momentum Turbulent Transport Experiments with Confined Swirling Coaxial Jets - Part I," AIAA-84-1380, Presented at AIAA/SAE/ASME 20<sup>th</sup> Joint Propulsion Conference, Cincinnati, OH, June 11 - 13, 1984.
- [3] Brankovic, A., Ryder, Jr. R. C., and Syed, S. A., 1998, "Mixing and Combustion Modeling for Gas Turbine Combustors Using Unstructured CFD Technology," AIAA Paper 98-3854, Presented at 34<sup>th</sup> AIAA/ASME/SAE/ASME Joint Propulsion Conference & Exhibit, July 13 - 15, 1998, Cleveland, OH.

- [4] Lin, C. A., "Modeling a Confined Swirling Coaxial Jet," *Annual Research Brief*, 1998, Center for Turbulence Research., Stanford University, 1998.
- [5] Akselvoll, K. and Moin, P., 1996, "Large-Eddy-Simulation of Turbulent Confined Coaxial Jets," *J. Fluid mech.*, 315, pp.387-411
- [6] Pierce, C. D. and Moin, P., 1998, "Large Eddy Simulation of a Confined Jet with Swirl and Heat Release," AIAA Paper 98-2892.
- [7] Germano, M, Piomelli, U., Moin, P., and Cabot, W. H., 1991, "Dynamic Subgrid Scale Eddy Viscosity Model," *Physics of Fluids A*, 3, 19, pp. 1760 – 1765.
- [8] Kim, S. E., 2004, "Large Eddy Simulation Using Unstructured Mesh and Dynamic Subgrid-Scale Turbulence Models," AIAA Paper 2004-2548.
- [9] Kim, S. E., Makarov, B., and Caraeni, D., 2004, "Multi-Dimensional Reconstruction Scheme for Unstructured Meshes," AIAA Paper 2004-2548.
- [10] Kim, S. E. and Makarov, B., 2005, "An Implicit Fractional-Step Method for Efficient Transient Simulation of Incompressible Flows," To be presented at 17<sup>th</sup> AIAA Computational Fluid Dynamics Conference, June 6 – 9, Toronto, Ontario.

**Exhibit EMEB-B-138-3**

**Vermont Yankee Nuclear Power Station**

**Proposed Technical Specification Change No. 263 – Supplement No. 30**

**Extended Power Uprate**

**Response to Request for Additional Information**

**Large Eddy Simulation Using Unstructured Meshes and Dynamic Subgrid-Scale  
Turbulence Models.**

**Total number of pages in this Exhibit  
(excluding this cover sheet) is 17.**

# Large Eddy Simulation Using Unstructured Meshes and Dynamic Subgrid-Scale Turbulence Models

Sung-Eun Kim\*

*Fluent Inc, Lebanon, New Hampshire, 03766, U.S.A.*

This paper concerns development of a large eddy simulation (LES) capability based on a finite-volume solver that permits use of unstructured meshes. The solver employs a cell-centered scheme along with a multi-dimensional linear reconstruction. Convection and diffusion terms are discretized using a second-order central-differencing scheme. A three-level second-order scheme is used for temporal discretization. Subgrid-scale turbulent stresses are closed using dynamic Smagorinsky model and dynamic turbulent kinetic energy transport model. A test-filter was designed for the dynamic procedure which is applicable to unstructured meshes of arbitrary cell-topology. The dynamic procedure also avails itself to three-dimensional flows without any statistically homogenous directions. Wall boundary conditions are imposed using a wall-function approach that applies appropriate wall-laws depending on near-wall mesh resolution. The LES capability is validated for a wide range of wall-bounded flows. We present here the results for a fully-developed channel flow and two bluff-body flows. The predictions are in good agreement with direct numerical simulation (DNS) results and the experimental data.

## I. Introduction

WE encounter many industrial applications of computational fluid dynamics (CFD) where the flows are dominated by unsteady, large-scale coherent structures. Those large-scale structures impact, to a great extent, various aspects of the flows such as energy consumption, safety, comfort, and noise. The ramification of whether or not one can harness the large-scale structures is therefore quite significant. Attempts to numerically predict such flows using unsteady Reynolds-Averaged Navier-Stokes (URANS) equations have been met with limited success. Some of the better RANS models seem to be capable of capturing the "largest" scale occurring often in the form of alternate vortex-shedding. However, the remaining coherent structures are left largely unresolved.

Large eddy simulation (LES) is fundamentally suited to the task of predicting coherent structures. The major obstacle in using LES for practical high Reynolds-number ( $Re$ ) flows, from the practitioners' standpoint, is its high cost incurred by an unwieldy number of computational elements and painfully long solution time. Yet today's ever-increasing computing power is rapidly making LES feasible. Another difficulty often encountered when attempting LES for industrial applications comes from complex geometry. In CFD, meshing for industrial applications involving complex geometry by itself can become a grand challenge. It is hugely time-consuming or often impossible to generate high-quality structured meshes for complex configurations, which has led industrial CFD practitioners to opt for unstructured meshes. Although unstructured meshes are routinely used today in RANS computations for industrial applications, attempts to conduct LES with unstructured meshes are just starting to appear in the literature.<sup>1-5</sup> As yet the efficacy of unstructured meshes for LES for practical high- $Re$  flows has not been fully established. Among the issues yet to be addressed are numerical accuracy, stability, and subgrid-scale turbulence modeling.

This paper is concerned with evaluating a LES capability developed using a finite-volume solver based on second-order numerics. Permitting use of unstructured meshes, the resulting LES capability can easily handle complex geometries encountered in industrial applications. In addition, it lends itself to local mesh adaptation that can be utilized

\*Principal Engineer, Fluent Inc., Lebanon N.H., Member AIAA.

Copyright © 2004 by Fluent Inc., Published by the American Institute of Aeronautics and Astronautics, Inc. with permission.

to efficiently allocate computational cells, substantially reducing the computational cost. Adequacy of second-order spatial discretization for LES has often been questioned, and there are some misgivings about using it for LES. It will be shown in this paper, however, that the second-order central differencing scheme adopted in the present work yields a commendable accuracy for LES. For subgrid-scale (SGS) turbulence closure, we implemented two dynamic SGS viscosity models in the framework of unstructured meshes, namely, the dynamic Smagorinsky model originally proposed by Germano *et al.*,<sup>6</sup> and Lilly<sup>7</sup> and the dynamic turbulence kinetic energy transport model of Kim and Menon.<sup>8,9</sup> For the dynamic procedure, a test-filter readily applicable to unstructured meshes was designed. The resulting dynamic SGS models can be used for three-dimensional flows without any statistically homogeneous directions.

The paper is organized as follows. We start with a brief description of the two dynamic subgrid-scale turbulence models and the details of their implementations. This will be followed by an overview of the numerical methods and algorithms adopted in this work. Finally, validations will be presented for a selected number of wall-bounded flows ranging from a fully-developed channel flow to a couple of bluff-body flows including one around a square-cylinder with salient edges and another past a smooth sphere.

## II. Filtered Navier-Stokes Equation and Subgrid-Scale Turbulence Modeling

### A. Implicit filter with finite-volume discretization

The governing equations for LES are generally obtained by filtering the Navier-Stokes equations in either Fourier (wave-number) or physical space. In the present work, the filtering operation (denoted by an overbar) is defined as a spatially convoluted integral of the variable in question as

$$\bar{\phi}(\mathbf{x}) = \int_{\mathcal{D}} \phi(\mathbf{y}) G(\mathbf{x}, \mathbf{y}) d\mathbf{y} \quad (1)$$

where  $\mathcal{D}$  is the computational domain,  $\mathbf{y} \in \mathcal{D}$ , and  $G$  is the filter function.

With the cell-centered finite-volume discretization and the linear reconstruction scheme employed in this work, the discrete solution variable at a cell-center ( $c_0$ ) can be written as

$$\phi(c_0) = \frac{1}{V} \int_{\mathcal{V}} \phi(\mathbf{y}) d\mathbf{y}, \quad \mathbf{y} \in \mathcal{V} \quad (2)$$

where  $V$  is the volume of a computational cell.

The definition in Equation (2) of a discrete solution variable at cell center can be interpreted as a filtering operation

$$\bar{\phi}(\mathbf{x}) \equiv \phi(c_0) = \frac{1}{V} \int_{\mathcal{V}} \phi(\mathbf{y}) d\mathbf{y}, \quad \mathbf{y} \in \mathcal{V} \quad (3)$$

The implied filter function,  $G(\mathbf{x}, \mathbf{y})$ , is then a top-hat filter

$$G(\mathbf{x}, \mathbf{y}) = \begin{cases} 1/V & \text{for } |\mathbf{x} - \mathbf{y}| \in \mathcal{V} \\ 0 & \text{otherwise} \end{cases} \quad (4)$$

Using the filtering operation in Equation (3), the filtered Navier-Stokes equations for incompressible flows (assumed for brevity) can be written as

$$\frac{\partial \bar{u}_i}{\partial t} + \frac{\partial \bar{u}_i \bar{u}_j}{\partial x_j} = -\frac{1}{\rho} \frac{\partial \bar{p}}{\partial x_i} - \frac{\partial \tau_{ij}}{\partial x_j} + \frac{\partial}{\partial x_j} \left( \nu \frac{\partial \bar{u}_i}{\partial x_j} \right) \quad (5)$$

$$\frac{\partial \bar{u}_i}{\partial x_i} = 0 \quad (6)$$

where  $\tau_{ij}$  is the subgrid-scale stress defined by;

$$\tau_{ij} \equiv \overline{u_i u_j} - \bar{u}_i \bar{u}_j \quad (7)$$

which is unknown and needs a closure.

Thus, we used in this work grid and finite-volume discretization as an implicit filter.

## B. Subgrid-scale (SGS) stress models

The SGS models based on the concept of isotropic eddy-viscosity compute the SGS turbulent stress from

$$\tau_{ij} - \frac{1}{3}\tau_{kk}\delta_{ij} = -2\nu_t\bar{S}_{ij} \quad (8)$$

where  $\nu_t$  is the SGS eddy-viscosity, and  $\bar{S}_{ij}$  the resolved rate-of-strain tensor defined by

$$\bar{S}_{ij} \equiv \frac{1}{2} \left( \frac{\partial \bar{u}_i}{\partial x_j} + \frac{\partial \bar{u}_j}{\partial x_i} \right)$$

The task of SGS turbulence modeling is to express SGS viscosity,  $\nu_t$ , as a functional of known quantities. In the present work, we employed two dynamic SGS eddy-viscosity models. They are described below.

### 1. Dynamic Smagorinsky Model (DSM)

The underpinning of DSM is the algebraic eddy-viscosity model originally proposed by Smagorinsky.<sup>10</sup> In the original Smagorinsky's model, SGS eddy-viscosity is computed from

$$\nu_t = C_v \bar{\Delta}^2 |\bar{S}| \quad (9)$$

where  $C_v$  is a model constant ( $C_v = 0.1 \sim 0.2$ ),  $|\bar{S}| \equiv \sqrt{2\bar{S}_{ij}\bar{S}_{ij}}$  the modulus of rate-of-strain tensor of the resolved scales, and  $\bar{\Delta} \equiv V^{1/3}$ .

The subgrid-scale stress can then be written as

$$\tau_{ij} - \frac{\delta_{ij}}{3}\tau_{kk} = -2C_v \bar{\Delta}^2 |\bar{S}| \bar{S}_{ij} \quad (10)$$

Despite its simplicity, this model has several shortcomings. The most problematic one, from a practical standpoint, has to do with the model constant,  $C_v$ . There is no single value of the constant which is universally applicable to a wide range of flows. Another serious drawback is that the SGS viscosity model in Equation (9) with a constant value of  $C_v$  is not applicable to transitional flows where the flow in question is laminar either locally or intermittently, since Equation (9) always gives a finite SGS viscosity even in laminar region as long as there is velocity gradient.

Germano *et al.*<sup>6</sup> and subsequently Lilly<sup>7</sup> conceived a procedure that resolves these problems. In this procedure,  $C_v$  is dynamically computed during LES, on-the-fly, using the information provided by the smaller scales of the resolved (known) fields. To separate the smaller scales from the resolved field, the dynamic procedure needs a so-called "test-filter" having a width ( $\bar{\Delta}$ ) that is larger than the grid-filter width ( $\Delta$ ). Denoting the test-filtered variables by a *tilde* and putting the "grid-filtered" Navier-Stokes equations through the test-filter, we obtain "test-filtered" Navier-Stokes equations as

$$\frac{\partial \tilde{u}_i}{\partial t} + \frac{\partial \tilde{u}_i \tilde{u}_j}{\partial x_j} = \frac{1}{\rho} \frac{\partial \tilde{p}}{\partial x_i} - \frac{\partial T_{ij}}{\partial x_j} + \frac{\partial}{\partial x_j} \left( \nu \frac{\partial \tilde{u}_i}{\partial x_j} \right) \quad (11)$$

$$\frac{\partial \tilde{u}_i}{\partial x_i} = 0 \quad (12)$$

where  $T_{ij}$  is now a "subtest-scale" stress defined by

$$T_{ij} \equiv \widetilde{\tilde{u}_i \tilde{u}_j} - \tilde{u}_i \tilde{u}_j \quad (13)$$

The underpinning of the dynamic modeling is a similarity concept that  $T_{ij}$ , the subtest-scale stress, can be written as a functional of the larger resolved scales in a manner similar to  $\tau_{ij}$ ,<sup>6</sup> which leads to



$$T_{ij} - \frac{\delta_{ij}}{3} T_{kk} = -2C_v \bar{\Delta}^2 \left| \bar{S} \right| \bar{S}_{ij} \quad (14)$$

where  $\bar{\Delta}$  is the test-filter width. Note that the same model coefficient,  $C_v$ , is used in the expressions for both  $\tau_{ij}$  and  $T_{ij}$ .

Equation (14) alone is not helpful at all in determining  $C_v$ , because  $T_{ij}$  is not known in LES. The breakthrough came from the realization that  $\tau_{ij}$  and  $T_{ij}$  are related to each other by<sup>6</sup>

$$\begin{aligned} T_{ij} - \tau_{ij} &= \overline{\overline{u_i u_j}} - \overline{\overline{u_i} \overline{u_j}} - \left( \overline{\overline{u_i u_j}} - \overline{\overline{u_i} \overline{u_j}} \right) \\ &= \overline{\overline{u_i u_j}} - \overline{\overline{u_i} \overline{u_j}} \equiv L_{ij} \end{aligned} \quad (15)$$

The stress,  $L_{ij}$ , which might be called subtest-scale Leonard stress, can be interpreted as the stress associated with the smaller resolved scales between the test-filter scale ( $\bar{\Delta}$ ) and the grid-filter scale ( $\bar{\Delta}$ ). Since  $L_{ij}$  can be directly computed from the resolved scales in LES, the identity given by Equation (15) can be used to determine  $C_v$ . Thus, we have

$$L_{ij} - \frac{\delta_{ij}}{3} L_{kk} = \alpha_{ij} C_v - \beta_{ij} \overline{C_v} \quad (16)$$

where

$$\alpha_{ij} = -2\bar{\Delta}^2 \left| \bar{S} \right| \bar{S}_{ij} \quad (17)$$

$$\beta_{ij} = -2\bar{\Delta}^2 \left| \bar{S} \right| \bar{S}_{ij} \quad (18)$$

One predicament that makes it difficult to determine  $C_v$  from Equation (16) is the fact that  $C_v$  in the second term on the right-hand side of the equation is under the test-filtering operator. As it stands, Equation (16) is an integral equation for  $C_v$  as discussed at length by Ghosal *et al.*<sup>11</sup> This difficulty can be avoided by taking out  $C_v$  from the test-filter operation as

$$L_{ij} - \frac{\delta_{ij}}{3} L_{kk} = C_v \left( \alpha_{ij} - \beta_{ij} \right) \quad (19)$$

We followed this rather *ad hoc* approach in this work despite its mathematical inconsistency, which amounts to assuming that  $C_v$  remains constant in the computational cells associated with the test-filter.

Since there are more equations in Equation (19) than the unknowns, the model constant  $C_v$  is obtained by seeking for  $C_v$  which minimizes the error norm defined by

$$E = \left( L_{ij} - \frac{\delta_{ij}}{3} L_{kk} - C_v M_{ij} \right)^2 \quad (20)$$

where

$$M_{ij} \equiv \alpha_{ij} - \beta_{ij} = -2 \left( \bar{\Delta}^2 \left| \bar{S} \right| \bar{S}_{ij} - \bar{\Delta}^2 \left| \bar{S} \right| \bar{S}_{ij} \right)$$

Taking  $\partial E / \partial C_v$  and setting it zero, we obtain

$$C_v = \frac{L_{ij} M_{ij}}{M_{ij} M_{ij}} \quad (21)$$

$C_v$  determined in this way varies with time and space. In fact, it varies in a wide range, often taking either large negative or positive value. Although negative  $C_v$  and consequently negative eddy-viscosity is often interpreted as representing "back-scatter" (flow of energy from smaller to larger scales), too large a negative eddy-viscosity causes numerical instability, ultimately leading to divergence of numerical solutions. The usual remedy for this numerical difficulty is to average  $C_v$  in statistically homogeneous directions. Obviously, this workaround can be exploited only when there are such homogeneous directions, which is a rarity in practical applications. Even if there are any statistically homogeneous directions, the averaging becomes extremely cumbersome with unstructured meshes. In the present

work, we simply “condition” the  $C_v$  computed by Equation (21) by test-filtering it. This simple volume-weighted averaging better preserves the locality of the model constant. To ameliorate the potential numerical difficulty caused by  $C_v$  being negative for an extended period of time, we evaluated two alternative approaches. In one approach, we simply clip  $C_v$  at 0 when it becomes negative. This option therefore rules out any chance for the model to mimic backscatter. In another, effective viscosity ( $\nu + \nu_t$ ) instead of  $C_v$  is clipped at zero, permitting small negative SGS viscosity to happen. As yet we do not have any conclusive evidence that supports superiority of one approach to another in terms of prediction accuracy, except an indication that computations with the first approach appear numerically more robust. For this reason, we used the first approach in the computations presented in this paper.

As mentioned earlier, the dynamic procedure described above requires a test-filter. The most important criterion the test-filter should satisfy specifically for this work is that it should be applicable to unstructured meshes of arbitrary cell topology without incurring unduly high cost. The test-filter finally adopted is a top-hat filter that involves a volume comprising the cell itself plus the neighboring cells that share the cell faces with the center cell. Thus, the test-filter operation amounts to a volume-weighted averaging of the variable in question, which is easily implementable and takes advantage of the data structure of the underlying finite-volume solver. With hexahedral meshes, the ratio of the test-filter to the grid-filter scale ( $\tilde{\Delta}/\Delta$ ) is approximately 2.1 ( $= 9^{1/3}$ ). The ratio for tetrahedra is smaller, being around 1.7 ( $= 5^{1/3}$ ).

## 2. Localized Dynamic Kinetic Energy Model (LDKEM)

The dynamic Smagorinsky’s model described so far is essentially an algebraic model in which subgrid-scale stresses are modeled using the resolved velocity field. A more elaborate SGS stress model would be the one which is directly based on SGS turbulence and can be used to parametrize SGS stresses. The most widely used ones among others are what can be called “one-equation” models in which SGS turbulent kinetic energy,  $k_{sgs} = (\overline{u_k^2} - \overline{u_k}^2)/2$ , is explicitly computed by solving its transport equation.<sup>8,9,11,12</sup>

In the present work, a localized dynamic  $k_{sgs}$ -equation model of Kim and Menon<sup>8,9</sup> was chosen in favor of its overall efficacy.<sup>13,14</sup>

In the LDKEM, the subgrid-scale eddy viscosity,  $\nu_t$ , is computed from

$$\nu_t = C_k k_{sgs}^{1/2} \tilde{\Delta} \quad (22)$$

Consequently, SGS stress is can be written as

$$\tau_{ij} - \frac{2}{3} k_{sgs} \delta_{ij} = -2C_k k_{sgs}^{1/2} \tilde{\Delta} \overline{S}_{ij} \quad (23)$$

$k_{sgs}$  is obtained by solving its transport equation<sup>8,9</sup>

$$\frac{\partial \overline{k}_{sgs}}{\partial t} + \frac{\partial \overline{u_j} \overline{k}_{sgs}}{\partial x_j} = -\tau_{ij} \frac{\partial \overline{u_i}}{\partial x_j} - C_\epsilon \frac{k_{sgs}^{3/2}}{\Delta} + \frac{\partial}{\partial x_j} \left[ \left( \frac{\nu_t}{\sigma_k} + \nu \right) \frac{\partial k_{sgs}}{\partial x_j} \right] \quad (24)$$

The only difference between the original formulation and the present one is that the contribution from the molecular diffusion of  $k_{sgs}$  is included in this work.

As shown above, there are three model parameters appearing in these equations, namely,  $C_k$ ,  $C_\epsilon$ , and  $\sigma_k$ , which need to be specified. In the current implementation of the LDKEM, the first two are determined from the dynamic procedures to be described in the following, whereas  $\sigma_k$  is simply set to a constant value of 1.0. The underpinning of the dynamic procedure employed in the LDKEM is the hypothesis corroborated by the experimental evidence<sup>15,16</sup> that there is a strong correlation between the subgrid scale stress,  $\tau_{ij}$ , and the subtest-scale Leonard’s stress,  $L_{ij}$ . In place of parameterizing  $T_{ij}$  and utilizing the Germano’s identity as was done in the DSM, the LDKEM models  $L_{ij}$  directly as

$$L_{ij} - \frac{\delta_{ij}}{3} L_{kk} = -2C_k \tilde{\Delta} k_{sgs}^{1/2} \tilde{\tilde{S}}_{ij} \quad (25)$$

where  $k_{test}$  is the resolved turbulent kinetic energy associated with the scales between the test-filter ( $\tilde{\Delta}$ ) and the grid-filter ( $\Delta$ ). It can be directly computed from

$$k_{test} = \frac{1}{2} \left( \widetilde{\bar{u}_k \bar{u}_k} - \bar{\bar{u}_k \bar{u}_k} \right) \quad (26)$$

The model parameter,  $C_k$ , can then be determined from Equation (25) by minimizing the error norm as in the DSM. Consequently we have

$$C_k = \frac{L_{ij} M_{ij}}{M_{ij} M_{ij}} \quad (27)$$

with  $M_{ij}$  defined by

$$M_{ij} = -2\tilde{\Delta} k_{test}^{1/2} \bar{S}_{ij} \quad (28)$$

The model parameter,  $C_\epsilon$ , of the dissipation term in Equation (24) is also determined by a dynamic procedure, whose underpinning is the hypothesis that the dissipation-rate of  $k_{test}$  ( $e$ ) can be expressed in the same functional form as the dissipation-rate of  $k_{sgs}$ .

$$e = C_\epsilon \frac{k_{test}^{3/2}}{\Delta} \quad (29)$$

The dissipation-rate of  $k_{test}$  can also be computed from

$$e = (v + v_t) \left( \frac{\partial \bar{u}_i}{\partial x_j} \frac{\partial \bar{u}_i}{\partial x_j} - \frac{\partial \bar{u}_i}{\partial x_j} \frac{\partial \bar{u}_i}{\partial x_j} \right) \quad (30)$$

From Equation (29) and Equation (30),  $C_\epsilon$  is given in a closed form

$$C_\epsilon = \frac{\tilde{\Delta} (v + v_t)}{k_{test}^{3/2}} \left( \frac{\partial \bar{u}_i}{\partial x_j} \frac{\partial \bar{u}_i}{\partial x_j} - \frac{\partial \bar{u}_i}{\partial x_j} \frac{\partial \bar{u}_i}{\partial x_j} \right) \quad (31)$$

The DKEM has several desirable attributes that the DSM lacks. First, as a consequence of parameterizing  $L_{ij}$  directly, the dynamic procedure in the LDKEM does not involve any test-filter operation on the model parameter,  $C_k$ . Thus, unlike the DSM model,  $C_k$  is a genuine, local quantity free from any mathematical inconsistency. Secondly,  $C_k$  in the LDKEM behaves numerically more benignly than  $C_v$  in the DSM, having much less fluctuation. As a small premium, one can even save a small amount of computational effort with the LDKEM, inasmuch as the test-filtering on the SGS stress done on in the DSM is not needed. Lastly and probably most important, the LDKEM enjoys the benefits of a high-order turbulence model. Adopting SGS turbulent kinetic energy to parametrize the SGS stress renders the LDKEM better suited to non-equilibrium flows. By accounting the  $k_{sgs}$ -budget more rigorously, backscatter of kinetic energy is allowed in the LDKEM on a much sounder physical basis than in the DSM.

### III. Boundary conditions

Wall boundaries are the most crucial and yet difficult ones to handle in LES. In LES resolving all the way down to viscous sublayer, no-slip would be clearly the choice for wall boundary condition for the resolved velocity field. However, the cost of such "wall-resolving" LES is prohibitively high for practical flows involving high- $Re$  flows. A practical alternative is to use the law-of-the-wall bridging the wall and the first grid point (cell center) off the wall. The simplest implementation of the wall-law can be done using

$$\bar{u}^+ = \begin{cases} y^+ & \text{for } y^+ < y_v^+ \\ \frac{1}{\kappa} \ln(Ey^+) & \text{for } y^+ \geq y_v^+ \end{cases} \quad (32)$$

where  $E = 9.793$ ,  $\kappa = 0.419$ ,  $y^+ \equiv \bar{u}_\tau y / \nu$ ,  $\bar{u}^+ \equiv \bar{u} / \bar{u}_\tau$ ,  $y_v^+$  is the "cross-over" at which the two wall laws intersect. This demarcation of the entire inner layer into the two distinct layers is apparently a simplification which is at odds with the

presence of a buffer region in reality between the viscous sublayer and the log-layer. However, this is much better than exclusively relying on no-slip condition. One can mimic the presence of the buffer layer by blending the linear and the logarithmic laws using an adequate blending function. The blending has some merits, inasmuch as, besides giving a smooth transition between the two layers (numerically more stable) and representing the mean velocity profile in the buffer layer more accurately, the blending also allows the respective laws in the two regions to be independently modified or extended to take into account other effects such as pressure gradient, surface roughness, and transpiration. In the present work, we employed the blending function suggested by Kader.<sup>17</sup>

In the finite-volume discretization adopted in this work, the blended wall-law is employed to compute wall-shear, essentially diffusion flux at wall. To that end, the wall-law is applied to the parallel components of the resolved velocity at wall-adjacent cells to compute the friction-velocity ( $\bar{u}_\tau$ ) in an iterative manner.

The LDKEM needs a wall boundary condition for  $k_{sgs}$ . To that end, either a Dirichlet-type boundary condition ( $k_{sgs} = 0$ ) or a Neumann boundary condition ( $\partial k_{sgs} / \partial n = 0$ , in view of  $k_{sgs} \sim y^2$ ) is conceivable. In the present work, we simply set the diffusion flux of  $k_{sgs}$  at walls to zero, which is essentially equivalent to the Neumann boundary condition.

#### IV. Flow solver

The present work was carried out using FLUENT, a general-purpose CFD code. FLUENT employs a cell-centered finite-volume method based on a multi-dimensional linear reconstruction scheme, which permits use of computational elements (cells) with arbitrary polyhedral topology, including quadrilateral, hexahedral, triangular, tetrahedral, pyramidal, prismatic, and hybrid meshes. There are several choices of the solver algorithms in FLUENT including coupled explicit, coupled implicit, and segregated solvers. For the computations presented in this paper, we used the segregated solver exclusively.

In the segregated solver, the governing equations are solved sequentially. Several different solution algorithms are offered including SIMPLE, SIMPLEC, PISO, and fractional-step method (FSM). The temporal discretization in the segregated solver employs a fully-implicit, three-level second-order scheme. Time-accurate solutions can be obtained using either iterative time-advancement (ITA) scheme or non-iterative time-advancement (NITA) scheme. The NITA scheme greatly saves CPU time, since the costly outer iterations are not needed. Unless stated otherwise, we used the fractional-step method in conjunction with the NITA scheme in this study.

Accurate spatial discretization is crucial in LES. The spatial discretization schemes employed in this work are based on a multi-dimensional linear reconstruction scheme.<sup>18-20</sup> Diffusive fluxes are discretized using central differencing. Discretization of convective fluxes requires caution in LES. Upwind-biased schemes such as second-order upwind, QUICK, and third-order MUSCL schemes have been most widely used for RANS computations. Unfortunately, numerical diffusion introduced by upwind schemes, which might be acceptable in RANS computations for high Reynolds-number flows, is detrimental to LES. This is because, in LES, numerical diffusion, however small it is, can easily overwhelm physical diffusion. This is the case even with high-order upwind schemes. For this reason, for LES, central-differencing schemes have been preferred for their meritoriously low - or zero in ideal conditions - numerical diffusion. Thus we added a second-order central differencing (CD) scheme for discretization of convective terms specifically for LES.<sup>21</sup> Unfortunately, any pure CD schemes are susceptible to producing unphysical oscillations in the solution fields, which becomes especially pervasive in high Peclet-number situations - low diffusivity and coarse mesh which is almost a norm in LES for industrial applications. The usual remedy is to add a modicum of numerical dissipation, either explicitly or implicitly, to suppress the oscillations at the price of sacrificing spatial accuracy. In our implementation of CD, however, no numerical dissipation was explicitly added. And, unless stated otherwise, the CD scheme was used in this work. To back up the CD scheme in case it fails, we also developed what may be called a bounded central differencing (BCD) scheme that essentially detects in the solution fields any wiggles with a wave length of  $2\Delta x$  or less ( $\lambda \leq 2\Delta x$ ) and suppress them by switching to upwind schemes of varying orders depending on the severity of the wiggles, while retaining the CD elsewhere. It should be emphasized that the BCD scheme significantly differs from the often-employed hybrid schemes blending central differencing and upwind schemes with a fixed ratio. The BCD scheme is reserved for industrial applications involving high-Reynolds number flows and less-than-ideal

meshes.

The discretized algebraic equations are solved using a point-wise Gauss-Seidel iterative algorithm. An algebraic multi-grid (AMG) method is employed to accelerate solution convergence. The solver is fully parallelized, which is crucial in LES for industrial applications.

## V. Validations

The LES capability described so far has been validated for a wide range of wall-bounded flows from simple to complex ones. In this paper, we present the results of a fully-developed channel flow and two bluff-body flows. The channel flow case is a fundamentally important case whose subtlety offers an opportunity to critically evaluate various aspects of SGS turbulence modeling such as the dynamic procedure used to determine the model constants.

The bluff-body flows include the one around a cylinder with square cross-section at a moderately high Reynolds number and the one around a sphere at two Reynolds numbers. Deliberately chosen, both involve large-scale, coherent structures around the bodies and in the wake, representing typical bluff-body flows encountered in industrial applications.

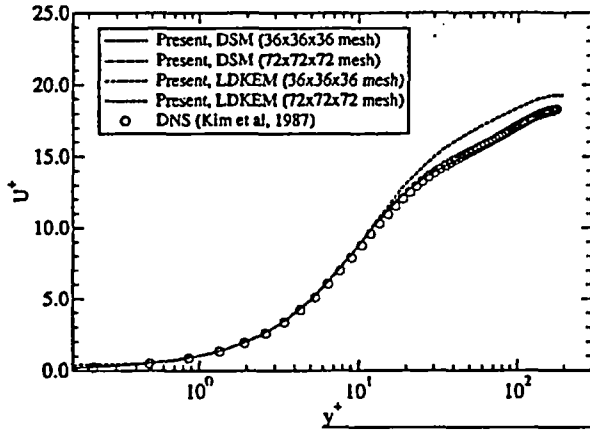
### A. Fully-developed channel flow at $Re_\tau = 180$

A fully-developed channel flow was computed for the Reynolds number of  $Re_\tau = 180$  ( $Re_H = 3,300$ ) using the two dynamic models. The computational domain is a box of the size  $[2\pi H \times 2H \times \pi H]$  in the axial, normal, and spanwise directions, respectively. The computational domain is bounded by two walls on the bottom and the top of the channel, two pairs of periodic boundaries in the axial and the spanwise directions. The computations were carried out using two hexahedral grids; a coarse grid with  $36 \times 36 \times 36$  cells and a globally refined mesh with  $72 \times 72 \times 72$  cells. The resolutions of the meshes are such that, with the coarser mesh,  $y^+$  value at the wall-adjacent cells is approximately 0.6, and the cell size is  $\Delta y^+ = 27$  near the channel centerplane. The channel walls are treated effectively as no-slip boundaries due to sufficiently low  $y^+$  values at the wall-neighboring cells. On the pair of periodic boundaries in the axial direction, a pressure-drop across the pair derived using the given wall-shear ( $\tau_w = \rho u_\tau^2$ ) was specified, with the flow-rate determined as a part of the solution. The time-step size of  $\Delta t^+ = 0.3$  was used, where  $\Delta t^+ \equiv \Delta t u_\tau^2 / \nu$ . The CD scheme was used for the discretization of convection terms.

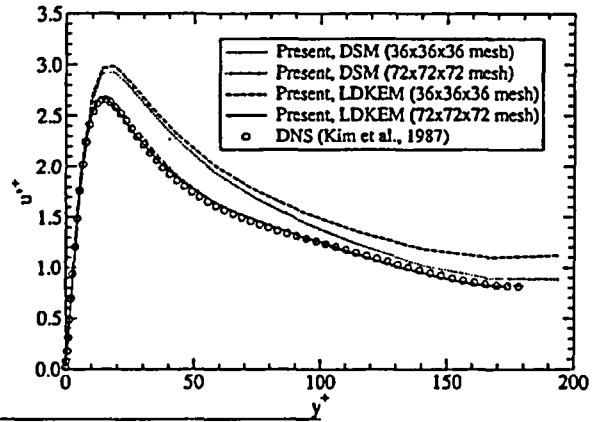
The mean axial velocity ( $U^+$ ) and the three r.m.s. velocity components ( $u'^+, v'^+, w'^+$ ) predicted using the two dynamic models are shown in Figure 1 on the following page along with the DNS results of Kim *et al.*<sup>22</sup> The predictions with the coarse mesh are seen to overpredict  $U^+$  by about 8 ~ 12% near the center of the channel. The peak in the  $u'^+$  profile is also overpredicted with the coarse mesh, whereas the peaks in the profiles of  $v'^+$  and  $w'^+$  are underpredicted. Our results with the coarse mesh show largely the same trends as found by others who employed grids of somewhat finer resolutions ( $32 \times 64 \times 32$  mesh,<sup>23</sup>  $65 \times 65 \times 65$  mesh<sup>1</sup>), yet closely matching their predictions despite the coarser mesh employed in this work. However, our predictions of the r.m.s. velocity components near the channel center is relatively poor. We surmise that the much larger grid spacing near the channel center ( $\Delta y^+ = 27$ ) is responsible for that.

The predictions improve greatly with the fine mesh. Both dynamic models reproduce the DNS results remarkably well. The mean axial velocity and the r.m.s. fluctuating velocity components are accurately predicted throughout the entire range of  $y^+$ . Particularly noteworthy is the excellent agreement with the DNS data in terms of the peaks values and their locations of the r.m.s. fluctuating velocity components. Overall, the results obtained with the fine mesh compare favorably with other results mentioned earlier.<sup>1,23</sup> For instance, our predictions are substantially closer to the DNS data than the results of Haworth and Jansen<sup>1</sup> who computed the same channel flow using LES on a  $65 \times 65 \times 65$  node mesh using the Lagrangian dynamic Smagorinsky's model.

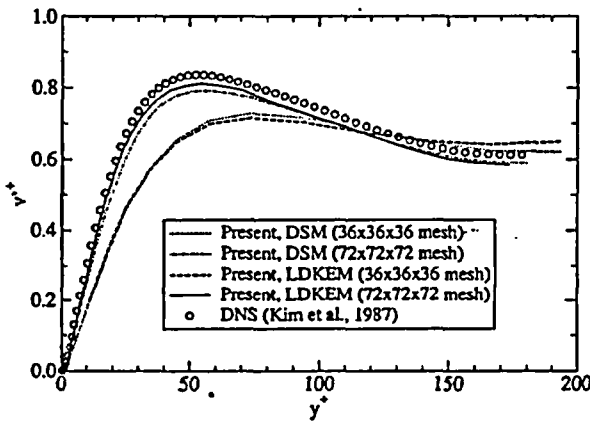
The present results are promising, inasmuch as they demonstrate that the second-order CD scheme in conjunction with the dynamic models is able to accurately predict this fundamentally important wall-bounded flow carrying an intricate near-wall physics. Regarding the impact of SGS modeling, we did not find any significant difference between the results from the two dynamic models. This should not come as a big surprise, however, since the fully-developed channel flow is near equilibrium in the mean.



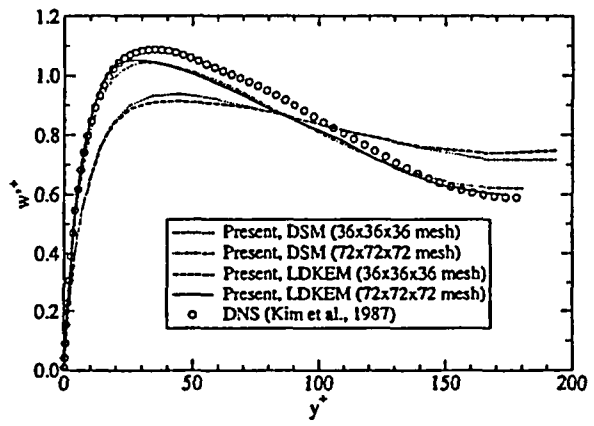
(a) Mean velocity ( $U^+$ ) predictions



(b) r.m.s. velocity ( $u'^+$ ) predictions



(c) r.m.s. velocity ( $v'^+$ ) predictions



(d) r.m.s. velocity ( $w'^+$ ) predictions

Figure 1. The results of LES using two dynamic SGS turbulence models for  $Re_\tau = 180$

## B. Flow around a square cylinder

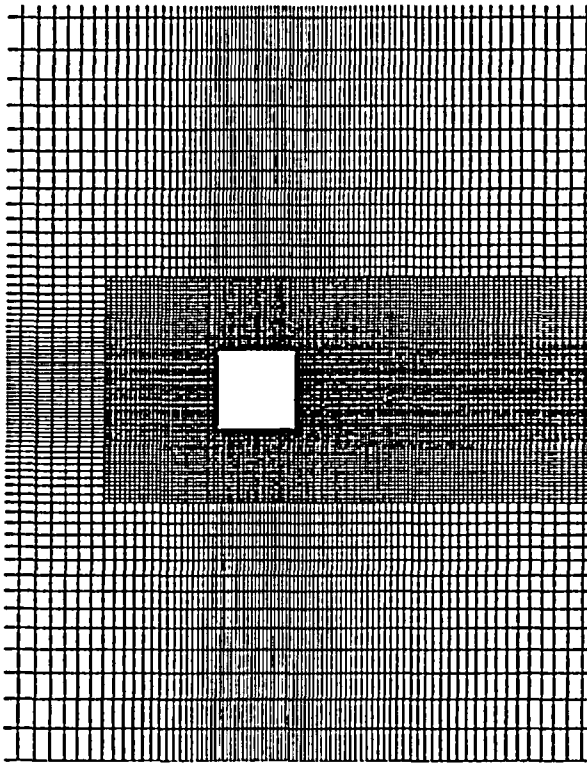
The flow past a square cylinder measured by Lyn *et al.*<sup>24</sup> was considered. The Reynolds number based on the freestream velocity ( $U_0$ ) and the width of the cylinder ( $H$ ) is 22,000. The subject flow is featured by a massive flow separation accompanied by unsteady large-scale structures of widely varying length scales. As such, it aptly represents turbulent flows around bluff bodies with sharp edges. Some others have also tackled this flow using LES.<sup>13,25</sup>

The domain size and the mesh resolution were chosen in reference to the earlier studies by others.<sup>13,25</sup> A more comprehensive study using different mesh resolutions and domain sizes (spanwise in particular) is deferred for a future study. Our objective here is to evaluate the efficacy of the present LES capability by comparing the predictions with other results based on meshes with comparable resolution. The computational domain is bounded by an upstream inlet boundary, top and bottom boundaries located  $7.0H$  from the center of the cylinder, and an exit boundary at  $20H$  from the cylinder axis. Freestream conditions were specified at the inlet. The top and the bottom boundaries were treated as symmetry planes (frictionless walls). The exit boundary was modeled as a pressure boundary where the solution variables are extrapolated in a mass-conserving manner. A pair of periodic boundaries separated with a span of  $3.0H$  were used in the spanwise direction. The computational domain is filled with a hexahedral mesh with 660,000 elements. We took advantage of our unstructured mesh capability, embedding a block of locally refined mesh around the cylinder to better resolve the near-wall and wake regions as depicted in Figure 2 on the next page. The averaged wall-distance at the wall-adjacent cells is  $0.012H$ . The time-step size ( $\Delta t$ ) used for the present computations is 0.02 time unit ( $H/U_0$ ) which is comparable to that used by others.<sup>13</sup> The CD scheme was used for the discretization of convective terms. The statistics were obtained during the LES for a sufficiently long period of time, typically for more than several scores of time units.

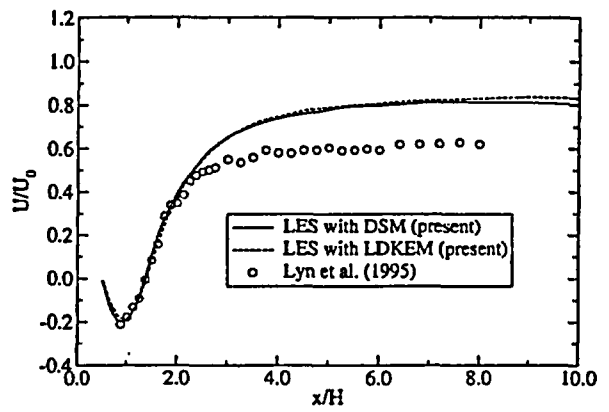
Figure 2 on the following page shows the profiles of the mean axial velocity ( $U/U_0$ ) and the r.m.s. velocity fluctuations ( $u'$  and  $v'$ ) along the centerplane ( $y=0$ ) in the wake predicted using the two dynamic models. The time-averaged axial velocity distributions show that the length of the recirculation bubble behind the cylinder is predicted by the two dynamic models to be around  $L_r = 0.9$  which agrees remarkably well with the experimental value ( $L_r \approx 0.9$ ). The negative peak and the recovery of the mean velocity in the near-wake are also captured very closely. However, the predictions start to deviate from the measurement for  $x/H > 2.0$ , reaching  $0.8U_0$  asymptotically in the far-wake. As shown in the figure, this value is considerably larger than what the measurement indicates ( $0.62U_0$ ).<sup>24</sup> Interestingly, others who computed the same flow<sup>13,25</sup> also have grossly overpredicted the recovery of the axial mean velocity. Our LES predictions of the mean axial velocity in the far-wake with both dynamic models were found to be largely comparable to the prediction by Sohankar *et al.*<sup>13</sup> based on their dynamic one-equation model denoted by "OEDSMA" in their paper. However, the present LES predictions reproduce the mean velocity profile in the recirculation bubble more accurately than others. Particularly noteworthy is that our DSM yields somehow a much better prediction than the DSM model used by Sohankar *et al.* in terms of the recirculation bubble size and the asymptotic value of the axial mean velocity in the far-wake, which begs a question of what could possibly contribute to this sizable difference. One possible cause is the effectively finer mesh used in the present computations which was made possible by the embedded region of fine mesh around the cylinder. It is also quite likely that the differences in the details of the DSM implementation is responsible. In this regard, it should be noted that Sohankar *et al.* average  $C_v$  in the spanwise (homogeneous) direction, whereas the DSM used here does not.

The r.m.s. fluctuating velocity components are also predicted with a reasonable accuracy by the present LES. The peak values are appreciably underpredicted. However, the locations of the peaks are closely captured. Another observation worthy of mentioning is that  $v'$  is relatively poorly predicted by both dynamic models.

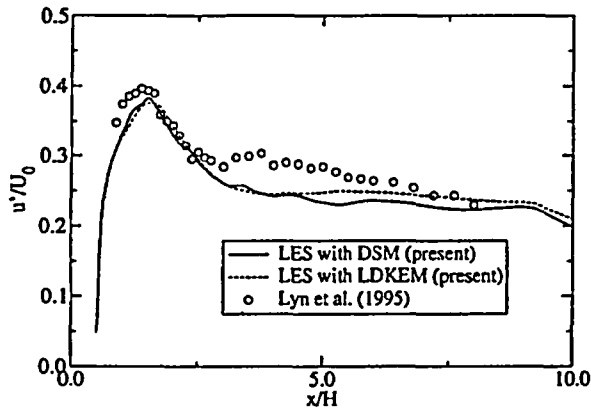
Table 1 on page 12 summarizes other global parameters predicted by the present computations, along with the results predicted by others.<sup>13,25</sup> Our LES predictions of the mean drag coefficient, Strouhal number, and r.m.s. lift coefficient well match the measurements and the predictions by others.



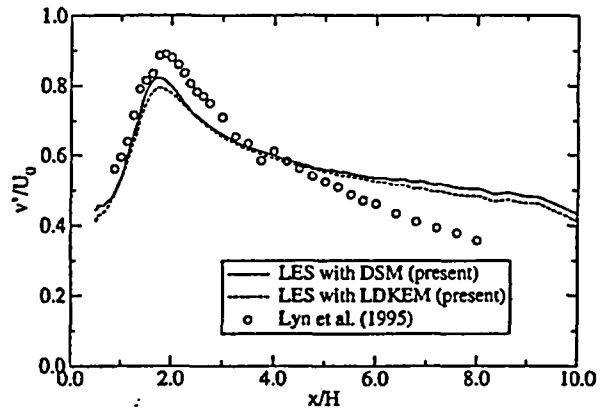
(a) Mesh with an embedded fine mesh



(b) Axial mean velocity



(c) r.m.s. axial fluctuating velocity



(d) r.m.s. vertical fluctuating velocity

Figure 2. Mesh used for the flow around a square cylinder and the mean axial velocity and normal stress distributions along the wake centerline



Table 1. Summary of the LES predictions of the global quantities for the square-cylinder case ( $Re_H = 22,000$ )

Methods	$L_r$	$St$	$C_D$	$C_L^*$
DSM (present)	0.9	0.133	2.19	1.19
DSM (Sohankar <i>et al.</i> <sup>13</sup> )	$\approx 0.6$	0.126	2.03	1.23
DSM (Fureby <i>et al.</i> <sup>25</sup> )	0.83	0.132	2.0	1.34
LDKEM (present)	0.9	0.131	2.14	1.17
OEDSM (Sohankar <i>et al.</i> <sup>13</sup> )	$\approx 0.6$	0.132	2.32	1.54
LDKEM (Fureby <i>et al.</i> <sup>25</sup> )	0.74	0.130	2.10	1.32
Measured (Lyn <i>et al.</i> <sup>24</sup> )	$\approx 0.9$	$\approx 0.13$	$\approx 2.1$	1.2

### C. Flow around a sphere

#### 1. Direct simulation for $Re_D = 300$

Before tackling the turbulent flow cases, laminar flow at  $Re_D = 300$  was computed on a hybrid unstructured mesh using direct numerical simulation. At this Reynolds number, the flow exhibits a weak unsteadiness leading to oscillations in drag and lift forces. The hybrid mesh has a total of 860,000 cells, consisting of prismatic cells in the near-wall region grown from the surface triangles on the body surface and tetrahedral cells filling the rest of the solution domain. The time-step size of  $0.04 D/U$  was used. Several others have computed this flow to validate their numerics.<sup>26-28</sup>

Table 2. Summary of the prediction for the laminar flow over a sphere ( $Re_D = 300$ )

Methods	$St$	$C_D$
Present	0.133	0.667
Tomboulides <i>et al.</i> <sup>27</sup>	0.136	0.671
Johnson and Patel <sup>26</sup>	0.137	0.656
Measured <sup>29</sup>	0.15 – 0.16	0.629

The results are summarized in Table 2 along with others' predictions.<sup>26-28</sup> Tomboulides *et al.*<sup>27</sup> and Johnson and Patel<sup>26</sup> used, respectively, a high-order spectral element method and a second-order upwind finite difference scheme on high-quality structured meshes. As shown, our predictions agree well with others' results, which is remarkable considering that a hybrid unstructured mesh was used in this work in conjunction with the second-order discretization scheme.

#### 2. Turbulent flows

We considered two Reynolds numbers ( $Re_D = 1.0 \times 10^4, 1.14 \times 10^6$ ), one being in sub-critical and the other in super-critical regime. The subcritical flow case has been numerically studied by several others,<sup>28,30</sup> while the supercritical case was studied experimentally by Achenbach.<sup>31</sup>

In this work, a hybrid unstructured mesh was deliberately used for both  $Re$  cases. The hybrid mesh has in total 2.46 million cells, consisting of 0.6 million prismatic cells in the near-wall region and tetrahedral cells filling the rest of the solution domain, with a large fraction of the total cell counts clustered in the near-wake region (see Figure 3). The mesh quality is not exceptionally high and yet quite reasonable, except the rapid expansion of cell size around the

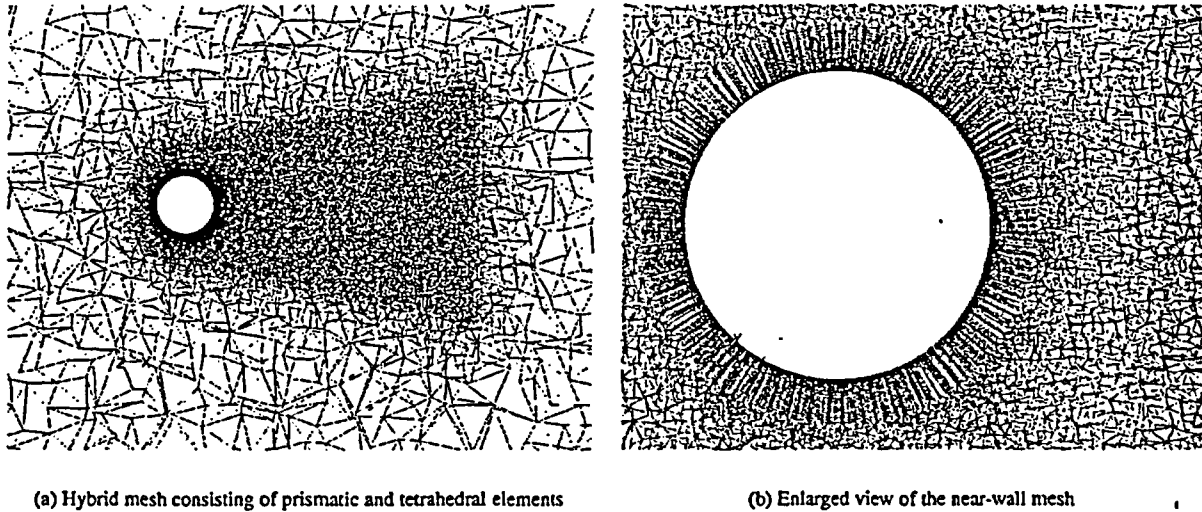


Figure 3. Hybrid unstructured mesh used for the flow around a sphere

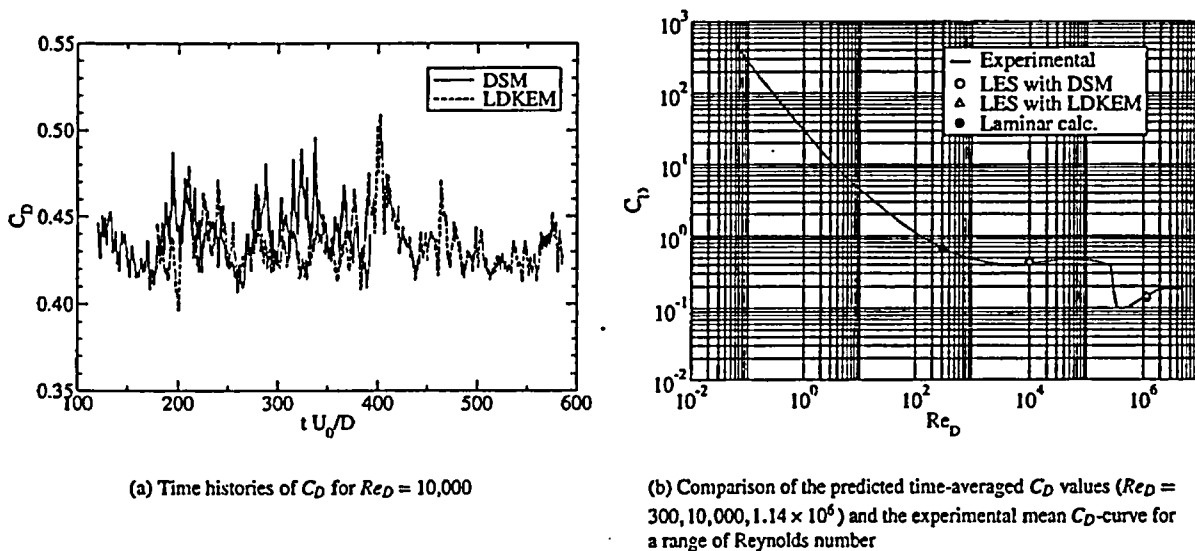
cell-clustered region. The average distance from the wall at the wall-adjacent cells is around  $1.1 \times 10^{-3} D$ . For the lower- $Re$  case, the near-wall mesh is sufficiently fine to resolve the boundary layer, with the  $y^+$  values at the wall cells below  $y^+ = 1.0$  for most part of the wall. For the higher- $Re$  case, however, the near-wall mesh is far from being fine enough to accurately resolve the boundary layer which is much thinner than the lower- $Re$  case, and the  $y^+$  values at the wall cells increase by almost two orders of magnitude. Thus, the wall adjacent cells are most likely to penetrate the fully turbulent region (log-layer) on a significant portion of the wall, especially near  $\theta = 90^\circ$  where the skin-friction reaches a maximum. The mesh being not ideal, the higher- $Re$  case offers a good opportunity to assess the wall-function based approach adopted in this work. Partial views of the mesh are shown in Figure 3.

Attempts to use the pure CD scheme have not been successful for this case. Numerical oscillations were observed sporadically in a few spots rather remote from the body where the cell size increases rapidly, being accompanied by abnormally large velocity magnitude. Although the oscillations were not catastrophic and affected the global quantities very little, the subsequent computations were carried out using the BCD scheme discussed earlier. A time-step size of  $0.02D/U$  was used for both Reynolds numbers. The data were collected for more than hundreds of time units. Figure 4 shows the time-histories of  $C_D$  for the lower- $Re$  case recorded during the LES using the two dynamic models.

Table 3. Summary of the LES prediction for turbulent flow past a sphere ( $Re_D = 10,000$ )

Methods	$C_D$	$St$	$\phi_s$	$\phi_t$
LES with DSM (present)	0.438	0.182	86 - 87	86 - 88
LES with LDKEM (present)	0.433	0.185	86 - 87	86 - 88
DES (Pelaez <i>et al.</i> ) <sup>30</sup>	0.430	—	—	—
DES (Constantinescu <i>et al.</i> ) <sup>28</sup>	0.397	0.200	84 - 87	93 - 108
LES (Constantinescu <i>et al.</i> ) <sup>28</sup>	0.393	0.195	84 - 86	86 - 88
Measured <sup>31,32</sup>	$\approx 0.40$	0.185 - 0.19	—	—
Correlation <sup>33</sup>	$\approx 0.46$	—	—	—

The global quantities predicted for the lower  $Re$  case are summarized in Table 3 on the page before along with others' results. The predicted  $C_D$  values (0.438 and 0.433 for the DSM and LDKEM, respectively) are in fair agreement with the often-quoted experimental value of 0.4 measured in 1920's<sup>34</sup> and other predictions. Constantinescu *et al.*<sup>28</sup> predicted  $C_D$  at around 0.4 using LES and detached eddy simulation (DES) on a structured hexahedral mesh having 450,000 nodes. Our predictions are closer to the value obtained by Pelaez *et al.*<sup>30</sup> ( $C_D \approx 0.43$ ) who carried out a DES on an unstructured mesh with 770,000 nodes. The Strouhal numbers predicted by the two dynamic models came out very close to each other, matching the measured one quite closely in view of the scatter in the experimental data. The data of Achenbach<sup>31</sup> and Kim and Durbin<sup>35</sup> favor lower Strouhal number around  $St = 0.15$ , whereas Sakamoto's data<sup>32</sup> suggests a higher value between 0.18 and 0.19. The locations of flow separation ( $\phi_s$ ) predicted by the two dynamic models are nearly identical and were found in  $86^\circ \sim 87^\circ$ . The locations of laminar-to-turbulent transition ( $\phi_t$ ), which were obtained in this work by reading off the angle beyond which  $v_t$  or  $k_{sg}$  increases rapidly, were found in  $86^\circ \sim 88^\circ$  for both dynamic models, which compare well with the LES predictions by Constantinescu *et al.*<sup>28</sup>



(a) Time histories of  $C_D$  for  $Re_D = 10,000$

(b) Comparison of the predicted time-averaged  $C_D$  values ( $Re_D = 300, 10,000, 1.14 \times 10^6$ ) and the experimental mean  $C_D$ -curve for a range of Reynolds number

Figure 4. Time histories of drag coefficient ( $C_D$ ) and the predicted mean drag coefficients for the sphere

With the higher- $Re$  case, the flow in reality has already undergone the "drag crisis", and the flow structure has changed drastically from those of subcritical regime. The change in the flow structure can be seen from Figure 5 and Figure 6. Depicted in these figures are the iso-contours of the second-invariant of the deformation tensor,  $(\Omega_{ij}\Omega_{ij} - S_{ij}S_{ij})/2$ . Both figures aptly portray the hairpin-like vortical structures in the wake observed in experiments. The wake for the higher- $Re$  case (Figure 6) is much narrower than in Figure 5, which is the consequence of the delayed onset of flow separation. The  $C_D$  values predicted by the DSM and the LDKEM are 0.139 and 0.142, respectively. These values are fairly close to the range of values ( $C_D = 0.12 \sim 0.14$ ) measured by Achenbach.<sup>31</sup>

For the higher- $Re$  case, the predictions of the locations of the separation and the onset of transition were much less satisfactory. At  $Re = 1.14 \times 10^6$ , the experimental results<sup>31</sup> show that the transition occurs near  $97^\circ \sim 98^\circ$  well before the separation occurring near  $120^\circ$ . The present predictions failed to reproduce this experimental finding. The present results exhibit too early a separation at around  $100^\circ$  and a delayed transition. This discrepancy is most likely due to the use of too coarse a mesh in this work to resolve the very thin boundary layer for the high- $Re$  case.

The drag coefficients predicted in this study for the three Reynolds numbers are plotted in Figure 4 along with the mean experimental curve.



Figure 5. Vortical structure in the near-wake of the sphere for  $Re_D = 10,000$  - visualized using the iso-contour of the second-invariant of the velocity deformation tensor



Figure 6. Vortical structure in the near-wake of the sphere for  $Re_D = 1.14 \times 10^6$  - visualized using the iso-contour of the second-invariant of the velocity deformation tensor

## VI. Summary and Conclusion

A large eddy simulation capability based on a finite-volume solver has been developed and validated for a number of wall-bounded flows. The finite-volume solver employs second-order numerics and permits use of unstructured meshes, thus being able to easily handle industrial applications involving complex geometry. Turbulence closure for subgrid-scale stresses is effected using two dynamic subgrid-scale viscosity models, namely, the dynamic Smagorinsky model (DSM) and the localized dynamic  $k$ -equation model (LDKEM). These two dynamic models allow one to compute arbitrary three-dimensional flows without any statistically homogeneous directions. The validations demonstrated that the present LES capability is capable of predicting the wall-bounded flows of varying complexity with a commendable accuracy, having a potential to provide a practical tool for high-level simulation of turbulent flows encountered in industrial applications.

## VII. Acknowledgments

The author gratefully acknowledges use of Fluent Inc.'s software and thanks the members of the development group at Fluent Inc. Special thanks go to Sunil Vijay Unaune at the Fluent India who contributed the mesh used for the computation of the flow past a sphere.

## References

- <sup>1</sup>Haworth, D. C. and Jansen, K., "Large-Eddy Simulation on Unstructured Deforming Meshes: Towards reciprocating IC Engines," *Computers Fluids*, Vol. 29, 2000, pp. 493-524.
- <sup>2</sup>K. Mahesh, G. Constantinescu, P. M., "Large Eddy Simulation of Gas Turbine Combustors," *Annual Reserach Briefs*, Center for Turbulence Research, NASA Ames/Stanford University, 2000, pp. 219-229.
- <sup>3</sup>Urbin, G. and Knight, D., "Large Eddy Simulation of a Supersonic Boundary Layer Using an Unstructured Grid," *AIAA Journal*, Vol. 39, No. 7, July 2001, pp. 927-935.
- <sup>4</sup>K. Jansen, T. M. and Reba, R., "Finite-Element Based Large-Eddy Simulation of the Near-Nozzle Region of a Compressible Round Jet," Aiaa paper 2002-2358, 2002.
- <sup>5</sup>S. Benhamadouche, K. M. and Constantinescu, G., "Colocated Finite-Volume Schemes for Large Eddy Simulation on Unstructured Grids," *Proceedings of the Summer Program*, Center for Turbulence Research, NASA Aames/Stanford University, 2002, pp. 143-154.
- <sup>6</sup>M. Germano, U. Piomelli, P. M. and Cabot, W. H., "Dynamic Subgrid Scale Eddy Viscosity Model," *Physics of Fluids A*, Vol. 3, 1991, pp. 1760-1765.
- <sup>7</sup>Lilly, D. K., "A Proposed Modification of the Germano Subgrid Scale Closure Method," *Physics of Fluids A*, Vol. 4, No. 3, 1992, pp. 633-635.
- <sup>8</sup>Kim, W.-W. and Menon, S., "A New Dynamic One-Equation Sub-Grid Scale Model for Large Eddy Simulations," Aiaa paper 95-0356, 1995.
- <sup>9</sup>Kim, W.-W. and Menon, S., "Application of the Localized Dynamic Subgrid-Scale Model to Turbulent Wall-Bounded Flows," Aiaa paper 97-0210, 1997.
- <sup>10</sup>Smagorinsky, J., "General Circulation Experiments with the Primitive Equations, part I : The Basic Experiment," *Monthly Weather Review*, Vol. 91, 1963, pp. 99-165.
- <sup>11</sup>S. Ghosal, T. Lund, P. M. and Akselvoll, K., "A Dynamic Localization Model for Large Eddy Simulation of Turbulent Flows," *Journal of Fluid Mechanics*, Vol. 286, 1995, pp. 229-255.
- <sup>12</sup>Davidson, L., "Large Eddy Simulation : A Dynamic One-Equatio Subgrid Model for Three Dimensional Recirculating Flow," *Proceedings of the 11th International Symposium Turbulent Shear Flows*, Vol. 3, 1997, pp. 26.1-26.6.
- <sup>13</sup>A. Sohankar, L. D. and Norberg, C., "Large Eddy Simulation of Flow Past a Square Cylinder: Comparison of Different Subgrid Scale Models," *Journal of Fluids Engineering*, Vol. 122, No. 1, 2000, pp. 376-404.
- <sup>14</sup>Krajnovic, S. and Davidson, L., "Large Eddy Simulation of the Flow Around a Bluff Body," *AIAA Journal*, Vol. 40, No. 5, May 2002, pp. 927-935.
- <sup>15</sup>S. Liu, C. M. and Katz, J., "On the Properties of Similarity SUBgrid-Scale Models as Deduced from Measurements in a Turbulent Jet," *Journal of Fluid Mechanics*, Vol. 275, 1994, pp. 83-119.
- <sup>16</sup>S. Liu, C. M. and Katz, J., *Experimental Study of Similarity Subgrid-Scale Models of Turbulence in the Far-Field of a Jet, Direct and Large Eddy Simulation*, Kluwer, 1994.
- <sup>17</sup>Kader, B. A., "Temperature and Concentration Profiles in Fully Turbulent Boundary Layers," *Int. J. Heat Mass Transfer*, Vol. 24, No. 9, 1981, pp. 1541-1544.
- <sup>18</sup>Mathur, S. R. and Murthy, J. Y., "A Pressure-Based Method for Unstructured Meshes," *Numerical Heat Transfer*, Vol. 31, 1997, pp. 195-215.

- <sup>19</sup>S.-E. Kim, S. R. Mathur, J. Y. M. and Choudhury, D., "A Reynolds-Averaged Navier-Stokes Solver Using Unstructured Mesh-Based Finite-Volume Scheme," Aiaa paper 98-0231, 1998.
- <sup>20</sup>S.-E. Kim, B. M. and Caraeni, D., "A Multidimensional Linear Reconstruction Scheme for Arbitrary Unstructured Grids," Aiaa paper 2003-3990, Jan. 2003.
- <sup>21</sup>L. Davidson, D. Cokljat, J. F. M. A. L. C. M. W. R., "LESFOIL: Large Eddy Simulation of Flow Around a High Lift Airfoil," *Notes on Numerical Fluid Mechanics and Multidisciplinary Design - Volume 83*, Springer, 2002.
- <sup>22</sup>J. Kim, P. M. and Moser, R., "Turbulent Statistics in Fully Developed Channel Flow at Low Reynolds Number," *Journal of Fluid Mechanics*, Vol. 177, 1987, pp. 133-166.
- <sup>23</sup>D. Choi, D. Prasad, M. W. and Pierce, C., "Evaluation of an Industrial CFD code for LES Applications," *Proceedings of the 2000 Summer Program*, Center for Turbulence Research, NASA Ames/Stanford University, 2000, pp. 221-228.
- <sup>24</sup>D. A. Lyn, S. Einav, W. R. and Park, J. H., "A Laser Doppler Velocimetry Study of Ensemble Averaged Characteristics of the Turbulent Near-Wake of a Square Cylinder," *Journal of Fluid Mechanics*, Vol. 304, 1995, pp. 285-319.
- <sup>25</sup>C. Fureby, G. Tabor, H. G. W. and Gosman, A. D., "Large Eddy Simulation of the Flow Around a Square Prism," *AIAA Journal*, Vol. 38, No. 3, May 2000, pp. 442-452.
- <sup>26</sup>Johnson, T. A. and Patel, V. C., "Flow Past a Sphere up to a Reynolds Number of 300," *Journal of Fluid Mechanics*, Vol. 378, 1999, pp. 19-70.
- <sup>27</sup>A. G. Tomboulides, S. A. Orszag, G. A. K., "Direct and Large-Eddy Simulations of Axisymmetric Wakes," Aiaa paper 93-0546, Jan. 1993.
- <sup>28</sup>G. Constantinescu, M. C. and Squires, K., "Turbulence Modeling Applied to Flow over a Sphere," *AIAA Journal*, Vol. 41, No. 9, 2003, pp. 1733-1742.
- <sup>29</sup>Roos, F. W. and Williams, W. W., "Some Experimental Results on Sphere and Disk Drag," *AIAA Journal*, Vol. 9, No. 2, 1971, pp. 285-291.
- <sup>30</sup>J. Pelaez, D. J. M. and Kandil, O., "Unsteady Analysis of Separated Aerodynamic Flows Using an Unstructured Multigrid Algorithm," Aiaa paper 2001-0860, Jan. 2001.
- <sup>31</sup>Achenbach, E., "Experiments on the Flow past Spheres at Very High Reynolds Numbers," *Journal of Fluid Mechanics*, Vol. 54, No. 3, 1972, pp. 565-575.
- <sup>32</sup>Sakamoto, H. and Haniu, H., "A Study on Vortex Shedding from Spheres in a Uniform Flow," *Journal of Fluids Engineering*, Vol. 112, 1990, pp. 386-393.
- <sup>33</sup>White, F. M., *Viscous Fluid Flow*, McGraw-Hill, 1974.
- <sup>34</sup>Schlichting, H., *Boundary-Layer Theory*, McGraw-Hill, 1979.
- <sup>35</sup>Kim, K. J. and Durbin, P. A., "Observation of the Frequencies in a Sphere Wake and Drag Increase by Acoustic Excitation," *Physics of Fluids*, Vol. 31, No. 11, 1988, pp. 3260-3265.